DEVELOPMENT OF FABRIC REINFORCED CONCRETE FOR FLEXURAL STRENGTHENING OF RC BEAMS

A THESIS

SUBMITTED BY

SMITHA GOPINATH

for the award of the degree

of

DOCTOR OF PHILOSOPHY

BUILDING TECHNOLOGY AND CONSTRUCTION MANAGEMENT DIVISION
DEPARTMENT OF CIVIL ENGINEERING
INDIAN INSTITUTE OF TECHNOLOGY MADRAS
CHENNAI 600036

MARCH 2017

THESIS CERTIFICATE

This is to certify that the thesis titled **DEVELOPMENT OF FABRIC REINFORCED CONCRETE FOR FLEXURAL STRENGTHENING OF RC BEAMS**, submitted by **Smitha Gopinath** to the Indian Institute of Technology Madras, Chennai for the award of the degree of **Doctor of Philosophy**, is a bonafide record of the research work done by her under our supervision. The contents of this thesis, in full or in parts, have not been submitted to any other Institute or University for the award of any degree or diploma.

Prof. Ravindra Gettu
Research Guide
Professor
Dept. of Civil Engineering
IIT Madras, Chennai- 600 036

Prof. Nagesh R. Iyer
Research Guide
Former Director, CSIR-SERC &
Distinguished Emeritus Professor, AcSIR
Chennai- 600 113

Place: Chennai

Date:

ACKNOWLEDGEMENTS

Passion and Dedication Towards a Work Can Be Unlimited, So Are The Opportunities. Proper Blend of Passion and Dedication To Address Tough Challenges and Thrilling Opportunities Always Brings The Best Out Of You!

(Smitha Gopinath)

ABSTRACT

There is a staggering demand for construction materials all over the world, which performs better than conventional materials. Moreover, the development of novel and innovative materials are instrumental at every stage of societal development leading to the overall development of the country. In today's construction scenario, repair and retrofitting is a major challenge and availability of materials to meet this demand is scanty. In such situations, it is necessary to develop cement based binders and new material combinations with the available materials, and characterize and apply them in appropriate construction practices. However, developing and selecting materials for strengthening of structures requires proper understanding of the material behavior, and this thesis addresses one such situation.

The present thesis focuses on the development of one type of textile reinforced concrete or fabric reinforced concrete, designated as *FABcrete,* and its application for the flexural strengthening of RC beams. A cementitious matrix is developed as the binder for *FABcrete* and its characterization is done to determine the mechanical properties and durability aspects. Two types of alkali resistant glass textiles are considered, and uniaxial tensile characterization is carried out towards finding their suitability as reinforcement in *FABcrete*. Most textiles have waviness of yarns due to the manufacturing process, which leads to delayed activation during the loading and affect the composite performance negatively. To overcome this, a mechanical stretching mechanism has been developed for straightening the textile while casting *FABcrete*. This has been scaled up for practical on-site applications. The bond of the binder with the textile is examined microscopically and the integrity of *FABcrete* with old concrete substrate has been investigated. Considering the absence of a generalized uniaxial tensile characterization methodology for textile reinforced concrete as of today, the thesis also focuses on the development of a uniaxial tension test configuration for *FABcrete*. A detailed study has been carried out to determine the tensile behaviour of *FABcrete,* and the influence of the type and amount of textile in *FABcrete*. The results obtained are further used in the development of mathematical models and as design parameters. A qualitative analysis using X-ray computed tomography has been carried out to understand the various failure mechanisms in *FABcrete*. In addition, image analysis has been carried out for the quantitative determination of defects.

From the application point of view, *FABcrete* is investigated for its capability to address the demand for thin cementitious composites with better compatibility with the base concrete structural member towards retrofitting and restoration applications. Experimental investigations have been carried out on cracked and un-cracked RC beams strengthened with *FABcrete*. The proposed system avoids the use of custom anchoring methods while strengthening. The structural performance of the strengthened beam is mainly evaluated for ultimate load carrying capacity and ductility. Monitoring using a non-contact video gauge has been attempted to measure strains at various locations in *FABcrete* strengthened beams and is found to be a better option for capturing strains than conventional methods. The practical applicability of *FABcrete* for strengthening of an existing RC beam was demonstrated on-site using a cast-in-place strategy; and a method has been developed for this purpose.

Mathematical models have been developed to predict the response of RC beams strengthened with *FABcrete*. Numerical simulation has been carried out by conducting nonlinear finite element analysis by giving due considerations to the geometrical modelling, material modelling, and interaction between various materials. The response of the numerical model is validated with the experimental results. In addition, a non-iterative analytical model has been developed using material parameters from experimental characterization. The model is simple and is found to predict the load and displacement characteristics satisfactorily and recommended for design practice. Further, a simplified design guideline is proposed for the flexural strengthening of RC beams with *FABcrete*.

Keywords: Textile Reinforced Concrete; Glass Textile; Flexural Strengthening; X-ray Computed Tomography.

TABLE OF CONTENTS

LIST OF TABLES

LIST OF FIGURES

ABBREVIATIONS

Abbreviation	Expansion
FABcrete	Fabric reinforced concrete dealt with in the present work
TRC	Textile reinforced concrete
FRCM	Fabric reinforced cementitious mortar
RC	Reinforced concrete
HPFRCC	Fiber reinforced cementitious concrete
FABmix	Cementitious matrix for *FABcrete*
GFRC	Glass fiber reinforced concrete
PE	Polyethelene
PP	Polypropylene
AR	Alkali resistant
SEM	Scanning electron microscopy
X-ray CT	X-ray computed tomography
SP	Superplasticizer
RCPT	Rapid chloride permeability
LVDT	Linear variable differential transducer
FEA	Finite element analysis
2D	Two-dimensional
3D	Three-dimensional
CoV	Coefficient of variation

NOTATIONS

Symbol	Explanation
w/b	Water-binder ratio
f_c	Compressive strength
E_c	Young's modulus of concrete
ν	Poisson's ratio
ε_c	Concrete compressive strain
ε_{cu}	Ultimate compressive strain
f_{ct}	Tensile strength
V_f	Volume fraction of textile
A_c	Cross-sectional area of specimen
A_f	Cross-sectional area of textile
ε_{cr}	First cracking strain of *FABcrete*
β	Normalized strain parameter
η	Normalized stiffness parameter
$E_{cracked}$	Cracked modulus of *FABcrete*
$E_{uncracked}$	Un-cracked modulus
f_{cr}	First cracking stress
$E_f{}^*$	Elastic modulus of textile in un-cracked state of specimen
E_f	Elastic modulus of textile in cracked state of specimen
ε_{fu}	Ultimate textile strain
σ_{fu}	Peak textile stress
σ_{ft}	Transition stress of textile
ε_{ft}	Transition strain of textile
$\emptyset$	Curvature
EI	Bending stiffness
M	Bending moment
P	Applied load
a	distance between the first loading point and support
d	Effective depth upto steel reinforcement

h	Cross section height
b	Cross-section width
L	Clear span
I_g	Gross moment of inertia
f_c'	Characteristic compressive strength of concrete
ε_{cmax}	Maximum compressive strain in concrete
A_s	Cross-sectional area of steel reinforcement
f_y	Yield strength of steel
E_c	Modulus of elasticity of concrete
E_s	Modulus of elasticity of steel
ε_{sy}	Yield strain
n	Modular ratio
N_{lay}	Number of layers of textile
h_{new}	Neutral axis depth
ε_{con}	Strain at a particular level in concrete
β_1	Concrete stress block factor
α_1	Concrete stress block factor
T_s	Tensile force in steel
T_f	Tensile force in textile
C	Compressive force
ε_{fib}	Effective tensile strain level in *FABcrete*
M_s	Moment due to steel
M_f	Moment due to FABcrete
M_n	Nominal moment
Mu	Ultimate moment
$\varnothing_m$	Reduction factor for moment
Δ	Midspan deflection
f_{co}	Peak compressive strength
ε_{co}	Peak compressive strain
G	Elastic shear modulus
E_{comp}	Composite stiffness
V_m	Volume fraction of the matrix

E_m	Elastic modulus of the matrix
σ_{mu}	Matrix failure stress
λ	Normalized compressive strain at top fiber, $\frac{\varepsilon_c}{\varepsilon_{cr}}$
η	Normalized postcrack tensile modulus, $\frac{E_{cr}}{E}$;
ω	Normalized strain when concrete yields , $\frac{\varepsilon_{cy}}{\varepsilon_{cr}}$;
γ	Normalized compressive modulus, $\frac{E_c}{E}$
n	Normalized steel modulus, $\frac{E_s}{E_{cr}}$
ρ_g	Reinforcement ratio per cross sectiona area, $\frac{A_s}{bh}$
κ	Normalized strain when steel yields, $\frac{\varepsilon_{sy}}{\varepsilon_{cr}}$
ρ_t	Normalized depth of textile reinforcement, $\frac{t}{h}$
β	Normalized tensile strain at bottom fiber, $\frac{\varepsilon_f}{\varepsilon_{cr}}$
α	Normalized depth of steel reinforcement, $\frac{d}{h}$
ε_f	Tensile strain in *FABcrete*
ε_{fe}	Effective tensile stress in *FABcrete* at failure
f_{fe}	Effective tensile stress level in *FABcrete* at failure
ε_{nt}	Net tensile strain in extreme tensile steel reinforcement
I_{cr}	Cracked moment of inertia
c_{cr}	Factor for neutral axis depth at cracking
C_y	Factor for neutral axis depth at yield
c_u	Factor for neutral axis depth at ultimate load
P_u	Ultimate load
d_u	Deflection at ultimte load
P_{cr}	Cracking load
d_{cr}	Deflection at cracking load
E	Tensile modulus of *FABcrete*

f_{cy}	Compressive yield stress of concrete
f_{sy}	Yield stress of steel
ε_{cy}	Compressive yield strain
t	Thickness of *FABcrete*
f_s	Stress in steel
χ	Normalized steel strain before yield
ε_t	Tensile strain in *FABcrete*

CHAPTER 1

INTRODUCTION

1.1 BACKGROUND

Innovative construction materials and practices are becoming globally competitive and continuously in demand. Infrastructure loss caused by premature deterioration of reinforced concrete (RC) structural members has led to crucial problems in civil engineering. Replacement or retrofit of deficient structural members incur a huge amount of money and time. In this situation, thin composites are needed, especially in the area of repair and retrofitting, to provide cost-effective and sustainable solutions.

One possible course of action aiming at providing external reinforcement for retrofitting of RC members would be the use of composites with cement-based mortars. Upgrading civil structures with cement-based bonding agents and high performance fiber materials could be an efficient strategy. A recent development, along these lines, is textile reinforced concrete (TRC). The use of a textile mainly made of alkali resistant glass, when placed in the main stress direction of the composite, leads to high effectiveness. In order to address the demand for thin cementitious composites towards retrofitting applications, especially for flexural strengthening of reinforced concrete structures, TRC is developed in this thesis and called as *FABcrete* (for Fabric Reinforced Concrete). *FABcrete* has a fine grained mortar as matrix and an alkali resistant glass textile as reinforcement.

1.2 OBJECTIVES

The main objective of this study is to develop a thin cementitious composite *FABcrete*, which can be used as an overlay for existing structural members. The specific objectives set to develop this material and to prove its applicability in flexural strengthening of RC beams are as follows:

- To develop a suitable fine grained binder for *FABcrete* and to characterize the relevant material characteristics in compression and tension.

- To characterize the uniaxial stress-strain behaviour of *FABcrete* and to study the behaviour of *FABcrete* with respect to the volume fraction and type of glass textile.

- To carry out investigations on cracked and un-cracked reinforced concrete beams for the evaluation of the suitability, applicability and performance of *FABcrete* towards flexural strengthening.

- To develop mathematical models for the structural response of strengthened concrete beams with *FABcrete*.

1.3 SCOPE

Two types of glass textiles from Saint Gobain Adfors and a glass textile from Kera Koll are considered for the investigations. These are materials that are available in the Indian market and have the potential for being used in strengthening applications in India.

1.4 ORGANIZATION OF THE THESIS

Chapter 1 gives a general overview about the thesis. The importance of developing *FABcrete* for future construction scenario is brought out. The scope and objectives of the present study are also reported.

A detailed review is carried out in Chapter 2 to identify critical research needs, which affect the implementation of *FABcrete* in construction. A brief background of the constituent materials, the various production methodologies, micro-structural characterization, mechanical characteristics, analytical and numerical modeling techniques, durability aspects, and the possible applications are covered in detail. Further, different cement-based strengthening systems used for strengthening of concrete members are also reviewed. Also, this chapter describes the methodologies followed for developing *FABcrete* towards flexural strengthening based on the properties reported in previous works.

The development of *FABcrete* is discussed in Chapter 3. The materials used, its mechanical characteristics, effect of loading rate, bond of textile in cementitious binder, integrity of *FABcrete* with existing concrete are the various aspects discussed in this chapter.

Chapter 4 presents the methodology proposed for characterizing the uniaxial tensile behavior for *FABcrete*. The step-by-step methodology followed to arrive at the final test configuration, such as the geometry of specimen, type of gripping mechanism, development of a mechanism to stretch the glass textiles, and the rate of loading for conducting uniaxial tensile test is explained. Detailed experimental investigations on uniaxial tensile behaviour of *FABcrete* to find the effect of type of textile, volume fraction, cracking details, and failure pattern are also discussed in this chapter. Evaluation of various failure mechanisms in *FABcrete* using X-ray tomography and image analysis is also discussed.

Chapter 5 deals with the experimental investigations carried out to evaluate the feasibility and applicability of *FABcrete* for flexural strengthening. The details of the investigations related to the flexural behaviour of un-strengthened RC beam, and cracked and un-cracked RC beam strengthened with *FABcrete* are reported. An instrumentation technique using non-contact video gauge and its applicability for measuring strain in strengthened beams is also discussed. This chapter also provides details of the development of mathematical models to predict the load and displacement of RC beam strengthened with *FABcrete*.

An on-site illustartion of TRC based strengthening of beams and walls is reported in Chapter 6. The details about the apparatus and methodology developed to perform strengthening with TRC is elaborated.

The conclusions of the study along with the future scope for the work are presented in Chapter 7. Finally, the references and appendices consisting of information's about details of binder, textile and TRC in various applications from literature, response of *FABcrete* specimens with manually and mechanically stretched textiles, working principle of non-contact video gauge, flowchart for the determination of load and deflection behaviour of *FABcrete* strengthened RC beams using ACI method and development of finite element modelling methodology for RC beams strengthened with *FABcrete* is given.

CHAPTER 2

LITERATURE REVIEW AND RESEARCH METHODOLOGY

2.1 INTRODUCTION

The present chapter attempts to summarise the state-of-the-art in the use of textile reinforced concrete (TRC), also known as fabric reinforced cementitious mortar (FRCM). TRC is a composite material with a non-metallic textile/fabric reinforcement embedded in fine grained cementitious binding matrix. To use the full potential of this composite, fundamental questions regarding the failure and damage evolution, durability aspects, production processes, and possible applications have to be well understood. Also, it is important to identify the individual characteristics and behaviour of components that benefit TRC. A concise review has been carried out to identify critical research needs that affect the implementation of TRC in construction. Some emerging and novel applications for TRC in infrastructure development have been discussed. Further, the experimental characterization, numerical models developed and durability aspects addressed for TRC have been reviewed. More extensive reviews are available in the books/reports by Brameshuber (2006), Mobasher (2011) and ACI Committee 549 (2013).

Based on the literature review, the research methodology to be used in this work is described, covering the necessity to develop different cement based binders, new combinations of TRC, and to investigate their compatibility and composite performance.

In this chapter, a brief background of textile reinforced concrete (TRC) has been first provided, along with the definition of TRC and its constituent components. Various production methodologies used for producing TRC structural components have also been described, followed by a description of analytical and numerical modeling techniques for TRC. The durability aspects of TRC have been covered in separate section. Further, possible applications of TRC in infrastructure development have been listed. A separate review on TRC based strengthening systems has been reported, followed by a description of the scope for TRC in present and future structural applications, and the areas that lack information in this regard. Finally, with specific reference to the strengthening of reinforced concrete beams the research methodology to be followed and the targets for the material and structural performance are discussed in detail.

2.2 TRC - A COMPOSITE MATERIAL

Textile reinforced concrete (TRC) is a relatively new construction material that offers a vast scope for design and application. It is composed of a fine grained cementitious binding matrix and non-metallic textile/fabric as reinforcement. Various fibers of glass, carbon, polypropylene or aramid are used to manufacture textile (Peled et al. 1998, 1999, Peled & Bentur 2000, Hegger et al. 2004, Kruger et al. 2003, Reinhardt & Kruger 2004, Mayer & Vinkler 2003, Peled & Mobasher 2005, Peled et al. 2004a, 2004b, Mobasher et al. 2004a, 2004b). Both strength and toughness of TRC is related to the mechanical anchoring provided by the fabric structure and the matrix-reinforcement bond (Bentur et al. 1997, Peled et al. 1998, Peled & Mobasher 2003). TRC is also considered as a pseudo-ductile concrete since it overcomes the brittle nature of the cementitious matrix through the incorporation of an appropriate textile. In direct tension, TRC can have a tensile straining capacity of 2% to 5% depending upon the type and amount of textile and can be about 250 times more deformable than typical concrete. Another advantage of TRC is their custom making ability of material properties for particular loading situations by modifying the textile architecture and material combinations. Promising results (e.g., in Figure 2.1) show the superior tensile behaviour of this new class of cementitious composite over other composites made up of discrete fibers (Peled & Mobasher 2005, Brameshuber 2006). In Figure 2.1, the tensile behavior of the various cement-based composites with different fabrics tested by Peled & Mobasher (2005) are compared with conventional glass fiber reinforced concrete (GFRC) having 5% volume fraction (V_f) of glass fibers. The response with two different bonded fabrics made from alkali resistant (AR) and E-glass fibers with 2 and 8 yarns/cm, respectively, in both directions of the fabric have been examined. A woven fabric made from monofilament polyethelene (PE) with 22 yarns/cm in the reinforcing direction (warp yarns) and 5 yarns/cm in the perpendicular direction (fill yarns) was also studied. The AR glass fibers have tensile strength of 1270 to 2450 MPa, elasticity modulus of 78000 MPa, bundle diameter of 800 microns and filament diameter of 13.5 microns. The PE fibers had a tensile strength of 260 MPa, modulus of elasticity of 1760 MPa and 0.25 mm diameter. The E-glass meshes had fiber bundles with diameter of 400 microns. Both the AR and E-glass were coated with epoxy during fabric production. A cementitious mixture with silica fume and Class-F fly ash, as well as a high-range water-reducing admixture, was used as the matrix for all the cement-based composites. The use

of the different fabrics (PE with low modulus, E-glass with intermediate, and AR glass with high modulus) with different mesh openings resulted in different stiffness. When comparing the tensile behavior, strain hardening behavior is clearly seen in all cases, even though the polyethylene fabrics are made from low modulus fibres. It was observed that the improvement in tensile behavior of the AR glass composite is more than four times that of the matrix and twice that of the GFRC. The highest tensile strength is observed for the AR glass fabric, at 18 to 20 MPa, compared to only 12 MPa for the E-glass and the PE fabric. The better performance of the AR glass fabric composites can be attributed to the higher modulus of elasticity of the glass fabric (78 GPa) and the excellent bonding of the fabric due to appropriate sizing. The relatively low tensile performance of the PE fabric composite is attributed to the lower stiffness of the yarns; however, the strain capacity of the composites is well over 3%. Hence, it can be concluded that, among different cement-based composites, AR glass fabric along with cementitious binder shows good tensile performance in terms of strength and ductility.
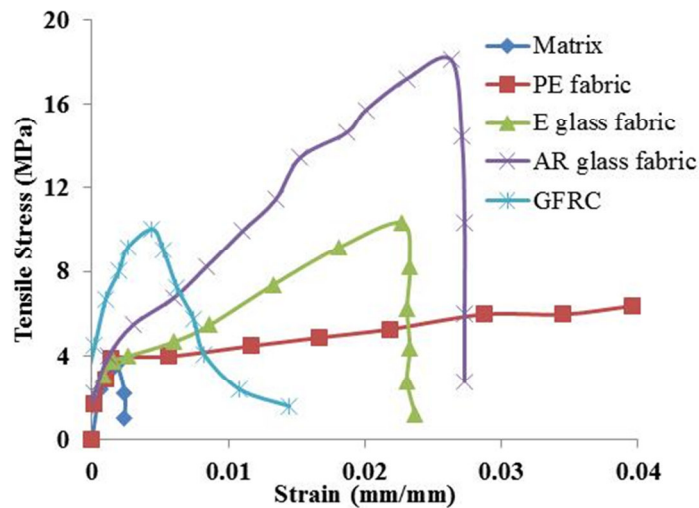
Figure 2.1 Tensile behaviour of different cement-based composites (Peled & Mobasher 2005)

2.2.1 Textiles/Fabrics

The textile used in cement-based composites is frequently made from multifilament yarns. These yarns can be made up of different fiber materials, e.g., alkali-resistant glass, carbon, aramid or polymeric fibers, depending on the intended application of TRC. The yarns have different geometrical structures, such as crimped or straight; the geometry of the yarn and the nature of

connecting points in the textile affect the bond and the composite properties. The multifilament nature of yarns and the degree of cement penetrability in between their filaments can lead to differences in tensile behaviour. The tensile response under different loading rates with carbon, AR glass and PE fabrics were reported by Mobasher (2011); and it was observed that the highest load carrying capacity was exhibited by carbon fabric composites.

There are different textiles available such as woven, bonded, or knitted textiles with stitches. The explanation of fabric/textile terminology and other technical terms related to textile reinforced concrete can be found in Brameshuber (2006). Generally, the basic mechanical properties of AR-glass textile vary depending on the yarn fineness; it has a tensile strength upto 1400 MPa, a linear elongation up to 2% with a modulus of elasticity varying between 70 to 80 GPa. The most important criterion for using glass textile as reinforcement for concrete is the possibility to create open structures with high displacement stability. Currently, there are 2D and 3D textiles available in the market; typical 2D and 3D textiles are seen in Figure 2.2. As an illustration, the specifications of typical 2D and 3D textiles manufactured by Saint Gobain Adfors are given in Table 2.1. It is observed that the tensile strength of the 2D alkali-resistant glass textiles ranges between 600 to 900 N per 50 mm width whereas that of 3D textile ranges between 1900 to 3740 N per 50 mm width. Further, in the case of the 2D textile, the half leno weave is used whereas for the 3D textile, the leno weave is used; in a leno weave, the warp yarns are twisted together in pairs between the weft to produce open mesh.
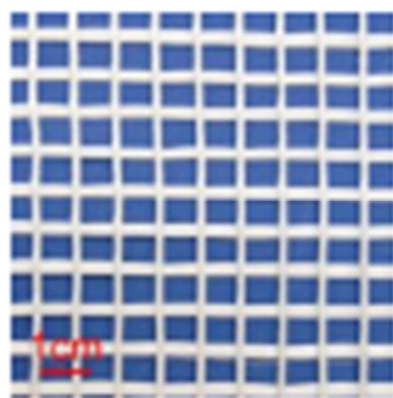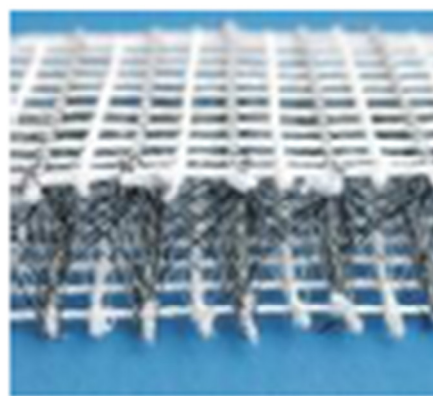
2D Textile   3D Textile

Figure 2.2 Different textile geometries (Peled and Mobasher, 2010)

Table 2.1 Comparison between typical 2D and 3D glass fabrics

Fabric Mesh	2D fabric Type 1	2D fabric Type 2	3D mesh Type 1	3D mesh Type 2
Weave	half leno	half leno	leno	leno
Fabric weight (g/m^2)	125.5	225	147	300
Dimension (mm)	12.7×12.7	25×25	20×10	20×10
Tensile strength (N/50 mm width)	600	900	1900	3740

In most TRC applications, two-dimensional textiles are predominantly used. Composites using 2D-textiles have excellent in-plane behaviour due to the fiber arrangement whereas the properties in the through-thickness direction are dominated by its matrix and fiber-matrix strength. Recent developments in the field of 3D-reinforced cementitious composite materials can be considered very promising; 3D textiles can enhance the through-thickness properties, such as inter-laminar shear and normal strength, damage tolerance and fracture toughness. Presence of reinforcement in three orthogonal directions in the 3D textile can also limit failure by delamination and is, therefore, expected to improve the mechanical properties of cement composites, especially under dynamic and impact loads (Peled et al. 2012). Owing to the wide variety of structure and geometry, and the different textile production processes, a standardized and general classification of 2D and 3D textile is not possible.

In the 2D-warp knitted textile sketched in Figure 2.3, the yarns in the warp (lengthwise) and the yarns in the weft (crosswise) are connected together by stitches (loops). In the woven textiles sketched in Figure 2.4, the warp and fill (weft) yarns pass over and under each other, resulting in a crimped shape of the yarn in the textile, and hence, the reinforcing yarns are not straight. In woven textiles, yarns are not as tightly held as in knitted fabrics, and hence allow better cement matrix penetration. In bonded textiles, perpendicular sets of yarns (i.e., warp and weft) are glued together at the junction points, resulting in straight yarns in both directions. The secondary yarns (in the weft direction) have significant influence on the composite behaviour, as they enhance bonding due to the cement penetration in the mesh opening in the textile, as well as between the

filaments of the yarn, leading to improved mechanical performance, even when low-modulus yarns are used (Peled et al. 1999, 2004b).
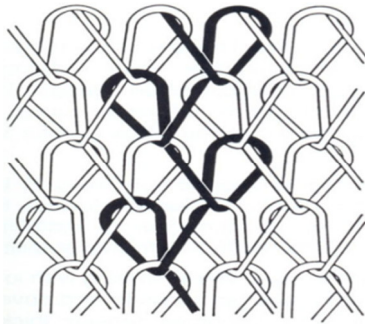
Figure 2.3 Warp knitted textile   Figure 2.4 Woven textile
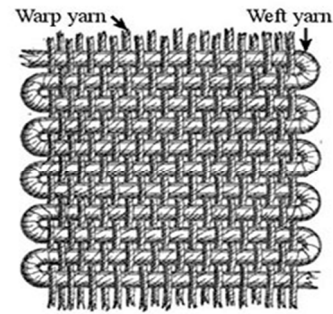
The bond with the matrix in a textile is mainly influenced by the physical nature of the yarn, in terms of being monofilament, multifilament or film. In general, high-strength high-moduli yarns increase the strength and toughness of the cementitious composite, providing strain-hardening behaviour, whereas low-moduli yarns mainly enhance the ductility of the cement composite, resulting in strain-softening or elastic-plastic behaviour. However, if the yarns have a complex configuration, strain-hardening behaviour may also be obtained with textiles having low moduli yarns. Further, the penetration of the matrix into the multifilament will govern the composite performance in terms of strength, toughness and durability (Leonard & Bentur 1984, Zhu & Bartos 1997, Trtik & Bartos 1999, Hegger et al. 2004, Banholzer & Brameshuber 2004, Peled et al. 2004b). There is a variation of 0.5 to 3 for efficiency factors of flexural strength for different fabrics (Peled & Bentur 2003), where the efficiency factor is defined as the ratio of flexural strength of the composite to the tensile strength of fabric.

Various types of textile production methods such as weaving, knitting, braiding and non-woven, give a high level of flexibility in the textile design (Brameshuber 2006). In 2D textiles, bundles of alkali-resistant glass fibers are combined in a biaxial layout by warp knitting threads. The warp knitting threads are laid into loops to fix the single layers of alkali-resistant glass bundles. The loop length of the warp knitting threads influences both the inner friction of the straight glass roving and cementitious binder penetration ability. In the case of 3D textiles, the production process, involving 3D weaving, multi-layer weft knitting, circular warp knitting with weft insertion etc., facilitates the direct production of 3D textiles in a single process step. Figure

2.5 shows textiles produced through different methodologies (Peled & Mobasher 2010). The possibility of using different production methods provide the opportunity of tailoring the textile to specific needs of different cement-based composite products by appropriate design of the textile geometry, yarn geometry and orientation of yarns, and combination of yarn material. The optimal choice can even be arrived for the particular application and the anticipated loading. Nevertheless, different failure mechanisms of textiles needs to be understood to explore their optimization according to product requirements.

Tensile test was conducted to investigate the bonding quality with cement matrix for warp knitted fabrics (Peled et al. 2008). It was observed that the best bond with cement matrix was developed by the fabrics with combinations of a small bundle diameter and a large loop size. Moreover it was concluded that the shape of the yarn in the fabric affects the bonding characteristics. Even it is possible to enable a strain-hardening behaviour for low modulus yarn fabrics by the proper choice of shape of yarn (Peled et al. 2003).
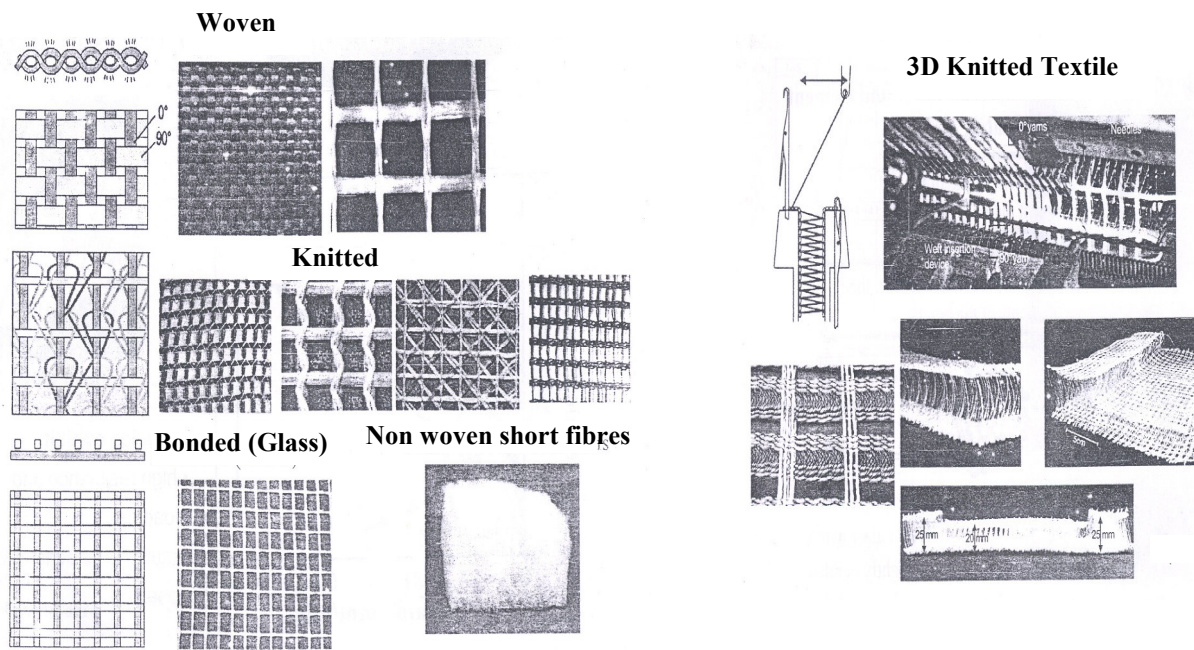
Figure 2.5 Different types of textile geometries from various production process
(Peled & Mobasher 2010)

2.2.2 Matrices for the TRC

The binding matrix in the TRC generally consists of cement, mineral admixtures, superplasticizer, water and aggregates having a size less than 1 mm (Banholzer et al. 2006, Ortlepp et al. 2009). The particle morphology of mineral admixtures affects the rheology of fresh mix while the pozzolanic reactions reduce the calcium hydroxide content to enhance strength and durability of the composites. For perfect bonding of the matrix with the fabric, it has to be a slurry in the fresh state with a high level of fluidity and moderate cohesion. The high fluidity is required to ensure the penetration through the filaments and filling up of the spaces within the yarn. On the other hand, insufficient cohesion in the matrix leads to non-uniformity in the penetration and segregation of the components during the casting of the composite. The increase in fluidity that is desired in the matrix can be obtained with the use of superplasticizers. However, the compatibility between the superplasticizer and cement has to be studied and ensured (Ramachandran et al. 1998, Roncero et al. 2002, Jayasree & Gettu 2012). The cohesiveness of the matrix can be optimized by using fine fillers, such as fly ash and quarry dust. It may also be necessary to introduce an optimal dosage of a viscosity modifying agent (Rixom & Mailvaganam 1999) for ensuring segregation resistance and robustness.

The degree of penetration of the matrix into the fabric significantly influences the mechanical properties of the composite by controlling the bond strength. In this context, microstructural features, such as matrix penetration through the opening of the fabrics and the filaments, size and distribution of flaws and pores, and yarn damage are relevant and need to be evaluated. Scanning electron microscopy (SEM) is one of the methods used to examine the microstructural properties of cementitious composites and fiber-matrix interface (Peled et al. 1998, 2008, Peled & Mobasher 2003). The impregnation of multi-filament yarns by a cementitious matrix was studied by Hana et al. (2010). By making use of SEM observations, they were able to link the physical properties measured to the level of impregnation of the yarns. The cementitious matrix impregnation were also correlated with the flow rates; it was observed that higher flow rates result in better impregnation of the yarns and reduction in the pore volume within the yarns.

Studies have been conducted to find the influence of different cementitious matrices on the tensile behavior of TRC. It was observed that the nature of multiple cracking and the resulting stress–strain curve, toughness and strength of the composite are dependent on the properties of

the textile and the matrix, as well as the bond at the textile–matrix interface (Peled & Bentur 2000, Colombo et al. 2013). The details related to different mixes used for TRC construction can be seen in Brameshuber (2006). Table 2.2 shows some compositions and parameters of matrices from the literature (Brockmann 2007, Brameshuber 2006).

Table 2.2 Composition of mixtures and dimensioning parameters for fine grained cementitious matrix (Brockmann 2007, Brameshuber 2006)

Materials / Characteristic parameters	Mix 1	Mix 2	Mix 3
Cement (kg/m^3)	490	210	980
Fly ash (kg/m^3)	175	455	210
Silica fume (kg/m^3)	35	35	210
Water (w) (kg/m^3)	280	280	350
w/b	0.41	0.40	0.27
Superplasticiser (polycarboxylate), % of binder	1.50	0.90	2.45
Siliceous fines 0-0.25 mm (kg/m^3)	500	470	118
Silicious sand 0.2-0.6 mm (kg/m^3)	715	670	168
Flow f_{10min} (mm)	340	266	320
Flow f_{30min} (mm)	340	263	305
Flow time t_{10min} (sec)	6.5	4.4	7.0
Flow time t_{30min} (sec)	7.2	4.8	9.0
Compressive strength, f_c (MPa)	86	40	135
Young's modulus, E_c (GPa)	32.0	22.0	28.5
Poisson's ratio, ν	0.21	0.21	0.25
Compressive strain at ultimate load, ε_{ci} (mm/m)	4.5	3.5	5.0
Ultimate compressive strain, ε_{cu} (mm/m)	5.5	4.5	6.3
Tensile strength, f_{ct} (MPa)	4.0	3.0	5.0
Flexural strength, f_{cf} (MPa)	5.0	3.4	5.8
Fracture energy (N/m)	42	26	16

In the mixes reported in Table 2.2, the desired flow properties are achieved by using sand with a maximum grain size of 0.6 mm, high binder content, and different pozzolanic admixtures and plasticizers (Brameshuber 2006). These matrices have been designed to increase the stability of

AR-glass rovings. For reasons of workability, the amount of silica fume added is limited to moderate quantities, lower than 10% by mass of total binder content. In order to determine the workability, the flow and flow time were determined according to German standards. Mix 1 shows better flowability compared to other mixes. In the case of Mix 2, the quantity of fly ash added is more compared to Mixes 1 and 3. Mix 3 was developed for higher mechanical performance that not only required high tensile strength but also good compressive strength. Due to the high cement content of Mix 3 and a low water-binder ratio (w/b), it offers a more dense structure and high strength. It is observed that the compressive strength of the mixes varies between 40 to 135 MPa. Further, the fracture energy of the mixes varies between 16 to 42 N/m.

In general, the composition of the matrix used for TRC differs considerably from that of conventional concrete. It is mainly because of the small gaps of only a few millimetres between the layers of the reinforcement textiles in TRC that necessitates the use of relatively small aggregates with maximum size about 1 mm. This enables the penetration of the matrix into the textiles; for better penetration, the consistency of the matrix has to be adjusted for the properties of the textile, geometry of specimen and production process. Further, thermal and chemical compatibility of fabrics and the substrate is essential to ensure durability.

Tensile tests of TRC have shown that the addition of short fibers along with textile reinforcement leads to an enhancement in loading capacity and fracture resistance (Brameshuber 2006); higher compressive and tensile strengths were obtained when short AR-glass fibers were incorporated in the matrix.

2.3 PRODUCTION TECHNOLOGIES FOR TRC

Identification of a suitable production technology is essential to control the quality and variability in the mechanical behaviour of TRC. Depending on the design, form and size of the structure and the application, different production processes can be feasible. Premix and spray methods, which are commonly used for short fiber reinforced matrices, can be used for the production of TRC. Cement-based composite laminates prepared with continuous fibers allow the full potential of the fibers to be used because the manufacturing technique is fully controlled and the composite laminates can be designed for specific service loads. Some of these processes include high energy mixing (Fraay et al. 1989), extrusion (Mallick 1988), filament winding

(Mobasher et al. 1997), compression molding, cross-ply and sandwich lamination techniques (Mobasher & Pivacek 1998).

Towards improving the composite material performance, pre-stressing of textile is often done with a clamping device, during casting, to overcome the initial waviness of the textile during the casting-in-place production of TRC (Brameshuber 2006). However, it has been reported that the outer filaments in a yarn that are in direct contact with the clamping device do not transfer load to the inner filaments due to low friction, and consequently pre-stressing with clamping is very difficult. A better method is to use a clamping device, where the single filaments do not slip within the yarns, especially for impregnated yarns. Yet another type of pre-stressing device consists of a rectangular rigid frame with hydraulic pistons, which generate a maximum force of 3.5 kN each with an oil pressure of 12 MPa. Nevertheless, in this case a large number of difficulties had to be overcome to anchor a sufficiently large number of yarns to apply a useful pre-stress force. When pre-stressing is done with gluing using epoxy resin, the ends of the yarns are inserted in a slit between two toothed metal sheets and a pre-stressing force of up to 4 kN is applied. In all the methods, it is obvious that a homogeneous pre-stressing will be obtained if the textile fabrication and concrete element production is combined to one continuous production line. Importantly, the bond stress is higher if textiles are pre-stressed. In such cases, the bond stress-slip behaviour consists of a linear elastic behaviour up to a peak and then a decay until a friction-type response; the initial part is due to the tight embedment of the fabric in the concrete. It has also been shown that there is an influence of the type of yarn and pre-stressing on the bond-slip behaviour (Brameshuber 2006). A peak pull-out force of 20N/mm to 60N/mm is reported in literature for different types of AR-glass yarns, along with a relatively high residual pull out force.

A production method known as the pultrusion process has been developed for fabric cement composites (Peled & Mobasher 2003, 2005, Mobasher et al. 2004a, 2004b, Peled et al. 2004a, 2004b). In this process, a continuous fabric is impregnated with the fresh cementitious binder and then pulled through a set of rotating cylinders, which apply pressure, remove excess binder and form the composite laminates. The setup for the pultrusion process used by Peled & Mobasher (2003) is shown in Figure 2.6.
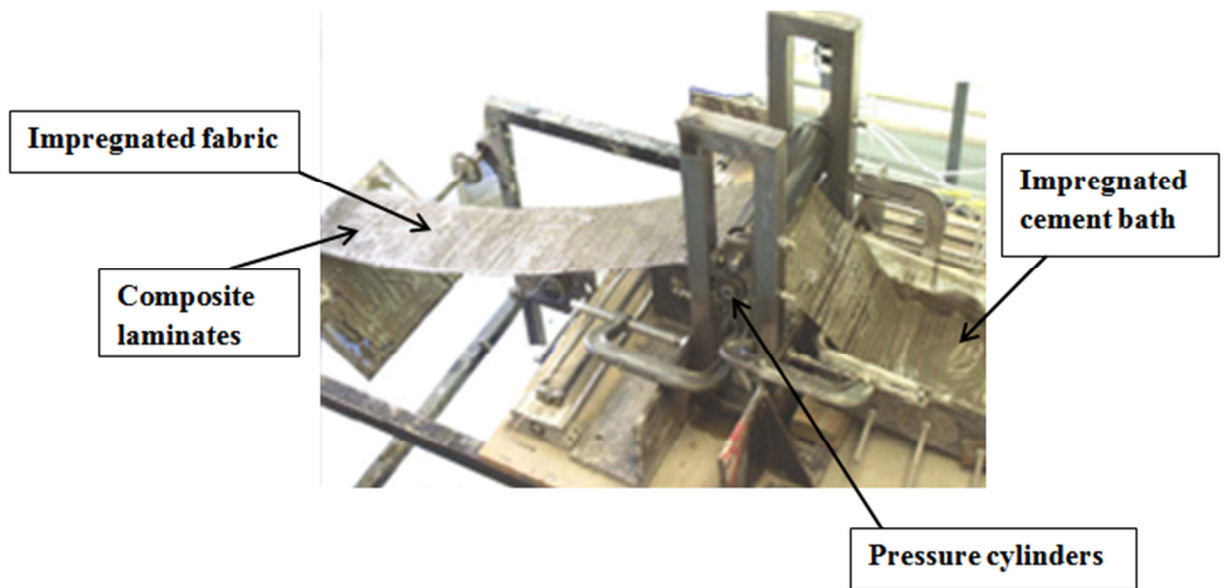
Figure 2.6 Set-up for the pultrusion process (Peled & Mobasher 2003)

It has been observed that pultruded products exhibit superior tensile and flexure behaviour compared to cast-in-place specimens because of the better alignment of fabric (i.e., positioning of the fabric) and product uniformity (Peled & Mobasher 2005, Sueki et al. 2007). The pultrusion process improves matrix penetration both into the fabric openings and multifilament bundles, leading to better matrix-fabric bonding characteristics (Peled et al. 2006). By means of pultrusion, it is possible to enhance the mechanical behavior of the cementitious composite and thus achieving strain-hardening behavior even for fabrics with low modulus of elasticity. A relative comparison of the pullout load versus slip response in pultruded and cast-in place cementitous composites with polypropylene (PP) fabric as reinforcement is shown in Figure 2.7. It is observed that the pullout resistance in the pultruded system is much greater than that in the cast systems. The impregnation process incorporated in pultrusion process helps to fill the spaces between the filaments of the bundled yarns of the fabrics, as well as in the the loops of the stitches with cement matrix. This leads to improvement in mechanical anchoring and bonding in cementitious composite.
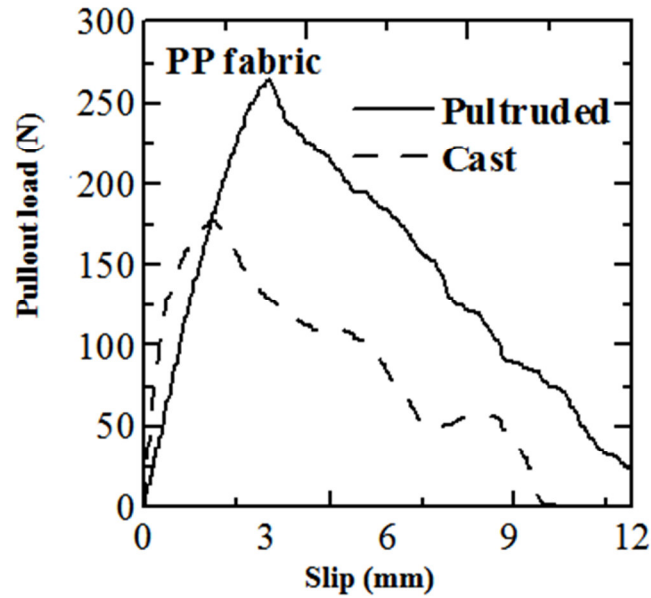
Figure 2.7 Pullout behaviour of PP fabric in pultruded and cast composites (Sueki et al. 2004)

Structural components made up of pultruded fabric cement composites such as sandwich composites that combine different layers of single fabric types; and hybrid composites, made from several yarn types within the same fabric have been investigated by Peled et al. (2009). Low-modulus fabrics of polyethylene (PE), polypropylene (PP) and high-modulus AR glass/aramid fabrics were prepared as hybrid combinations by the pultrusion process and tested. It was observed that composites with brittle and relatively strong fabrics (e.g. glass) at the mid-section and ductile fabrics (e.g. PE) near the surfaces of the composite performed better in tension than composites with the opposite arrangement. It can be concluded that the combination of various fabrics, cementitious binders and the pultrusion process will lead to better performing textile/fabric reinforced concrete. However, pultrusion requires special equipment, which uses an efficient mortar impregnation methodology and an efficient fabric pulling unit for the production of TRC.

2.4 ANALYTICAL/NUMERICAL MODELLING OF TRC

Modelling of structural components is extremely important to improve the understanding and design aspects, and validate the performance. In TRC, the accuracy of response predictions and the ability to represent the failure phenomena mainly depend on the geometrical representation

and material modelling of cementitious matrix, textile reinforcement and bond between matrix and textile. Analytical models such as the ACK Model (Aveston et al. 1971), the AK Model (Aveston and Kelly 1973) and the OH Model (Ohno and Hannant 1994) have been used to predict the stress-strain response of TRC. In these models, the material parameters have been described in a deterministic manner; a detailed evaluation of these models was given by Jesse (2004). Bond characteristics between textile and cement based matrix have been considered to develop analytical models for TRC (Richter 2005, Brameshuber 2006) through a representation of the pullout behavior of the textile strand to arrive at load carrying capacity and failure mechanisms. Models have also been developed to represent explicit crack formation by considering the stress redistribution between matrix and reinforcement (Hegger et al. 2006, Brockmann 2007); in the two-subroving model, the multi-filament yarn in the textile is divided into the sleeve and core, and both are considered to be directly linked to the matrix. This may be appropriate for the subdivision into subrovings but may not be physically meaningful for representing the behaviour of the multi-filament yarns. A finer discretisation of the reinforcement and the consideration of the interaction with the concrete are done in the Strand Pull-Out Model (Banholzer et al. 2004), in which the yarn is represented by a layered model with an arbitrary number of layers and the force-displacement relations for the layers are established using a cohesive interface.

The structural response of TRC is highly dependent on the spatial and temporal variations of the material and geometric data of the constituents. To address this, generalized uncertainty modelling of material and geometric parameters using fuzzy random functions are used (Graf et al. 2007). The uncertainty model, on the other hand, based on stochastic methods, may be applied if sufficiently large data is available. One such approach is based on the ACK model together with the stochastic distribution of the concrete tensile strength (Cuypers & Wastiels 2006).

Multi-scale model frameworks with different micro, meso and macro concepts related to the behaviour of TRC have been implemented with the help of finite element analysis by several researchers (Holler et al. 2002, Kruger 2004, Konrad & Chudoba 2004, Mobasher 2011; Hegger et al. 2006, 2007, Lepenies 2007). Within the multi-scale framework, a laminate theory was used by Mobasher (2003) for predicting the behaviour of TRC. In this model, the property of each

layer was specified based on the fiber and matrix constituents, in addition to the orientation as well as the stacking sequence of fabrics, and was able to predict the stress-strain behaviour of TRC very well. The main basis for development of this model was the consideration of stiffness reductions for each strain increment, as a function of a scalar damage parameter that was derived from experimental results.

2.5 DURABILITY ASPECTS

In order to have widespread acceptability of TRC, durability needs to be given due importance. An overview of the current knowledge on the durability of textile-reinforced concrete (TRC) was given by Mechtcherine (2012). Based on the review, transport properties in the cracked state, long term strain capacity, and resistance to aggressive environments can be identified as critical parameters for TRC. The microstructure of the fiber/matrix interface can also be affected by aging and environmental conditions (Mumenya et al. 2008). In addition to the parameters that correspond to the attacking medium, the composition of the fiber material when used as reinforcement is of crucial importance (Czymai 1995). Among the most commonly used textile reinforcements, the performance and durability differ. For example, carbon and aramid textiles generally do not degrade within the concrete, due to the highly alkaline environment, whereas the glass textile looses some of its strength due to long-term deterioration (Orlowsky & Raupach 2006). On the other hand, there is significantly enhanced resistance in AR glass (compared to conventional glass) due to the addition of 16–20% zirconium dioxide, by mass (Majumdar et al. 1977, Paul 1977). In the case of non-alkali resistant glass textiles used as reinforcement, there may be a loss in roving volume causing a reduction in strength. To tackle such situations and to improve the alkali resistance of glass textiles, sizing and coatings are employed. However, the sizing and coating could also affect the mechanical properties (Scheffler et al. 2009).

From accelerated ageing tests, it has been concluded that fibre impregnation has the greatest impact on the improvement of strength and durability (Raupach and Brockmann 2001, Mumenya et al. 2008, Scheffler et al. 2009, Brockmann & Raupach 2002, Brockmann & Brameshuber 2005, Butler et al. 2009, Hegger et al. 2010). The durability aspects related to water absorption, gas and water permeability for TRC with coated and uncoated yarns revealed that if the fabric is uncoated, there is an increase in the fineness of the yarns as well as the residual strain leading to

a considerable increase in water absorption (Mechtcherine and Lieboldt, 2011). Tests on samples aged in hot water without any load and while loaded upto 70% of failure load showed that there was appreciable macro-stress degradation (Orlowsky and Raupach, 2003). Nevertheless, in more recent studies of time-dependent modelling, it was found that AR glass could also have a 30% strength loss over a service life of 50 years, without considering the effects of concrete carbonation and fibre impregnation (Hegger & Kulas 2010).

As of today, with TRC, detailed information is lacking on the long-term performance, and in order to properly utilize the superior qualities of this material, it will be necessary to develop realistic and reliable performance-based design concepts to further optimize the usablity of TRC (Mechtcherine 2012).

2.6 APPLICATIONS OF TRC

Different structural applications were realized using TRC with various textile reinforcements. The ability to place the textile in the main tensile stress direction according to various product application of TRC opens up the field for new innovative designs. The uniformity in the placement of textile in TRC provide better cracking resistance. The higher strength-to-weight ratio, ductility and energy absorption of textile enables possibilities for TRC thin walled constructions. TRC is capable of yielding slender, light-weight, modular, free-form structures without any risk of corrosion (Brameshuber, 2006). For example, a segmented and pre-stressed pedestrian bridge was realized in TRC, which weighed only 20% of that of a comparable reinforced concrete structure, in Germany (Curbach et al. 2006, Schneider & Bergmann 2008, Hegger et al. 2011). The individual segments in this type of construction were advantageous in terms of transport and assembly.

Industrial sized applications of lightweight and thin self-supporting sandwich elements, as well as large-sized ventilated façade elements with TRC has been implemented in Germany (Brameshuber, 2006, Insu-Shell-Projekt LIFE, 2009, Hegger et al. 2011, Tomoscheit et al. 2011). In such applications, there was about 70% less CO_2 emission from TRC elements compared with conventional concrete elements. Other benefits of TRC included better frost resistance, longer life and better fire protection (Fydro, 2012).

Another set of applications of TRC is in roofing. Shell roofs with minimal thickness, in the range of 10-30 mm, have been constructed, differing in form and load bearing behaviour from conventional structures (Guldentops et al. 2009). Different and complex shapes/forms can be realized for roofing with TRC, such as planar, single-folded and curved or double-curved shells adapted to the practices of the construction industry (Ramm & Schunck, 2002, Schneider et al. 2006, Hausding et al. 2006, Verbruggen et al. 2013).

TRC has also been used in other applications, such as thin-structured elements, three-dimensional structural profiles and hybrid pipe systems (Brockmann & Brameshuber 2005). In general, TRC has been considered to be a low-cost construction material when used for light weight and space saving applications along with other construction materials (Holschemacher et al. 2006, Lieboldt 2006).

As an impact resistant material, TRC performs better than many conventional materials and it can also be used to protect existing concrete components (Zhu et al. 2009, Padaki et al. 2010, Peled et al. 2012). This is due to the capability to dissipate the imparted energy through several interacting damage modes and fiber breakage. Hence, when existing concrete panels are protected by TRC, scabbing of concrete from the back face of the structural component can considerably be reduced.

Apart from the above mentioned applications, TRC has also proven to be an adequate strengthening material for reinforced concrete and masonry structures in a variety of applications (Papanicolaou et al. 2006, Tommaso et al. 2007, Ortlepp et al. 2009, Triantafillou 2010, Ombres 2011). A detailed review of the effectiveness of TRC as a strengthening material is reported in the next section.

A consolidated graphical representation about various structural applications of TRC reported in the literature is given in Figure 2.8. Appendix-A provides more details on the applications given in some of the research publications reviewed.
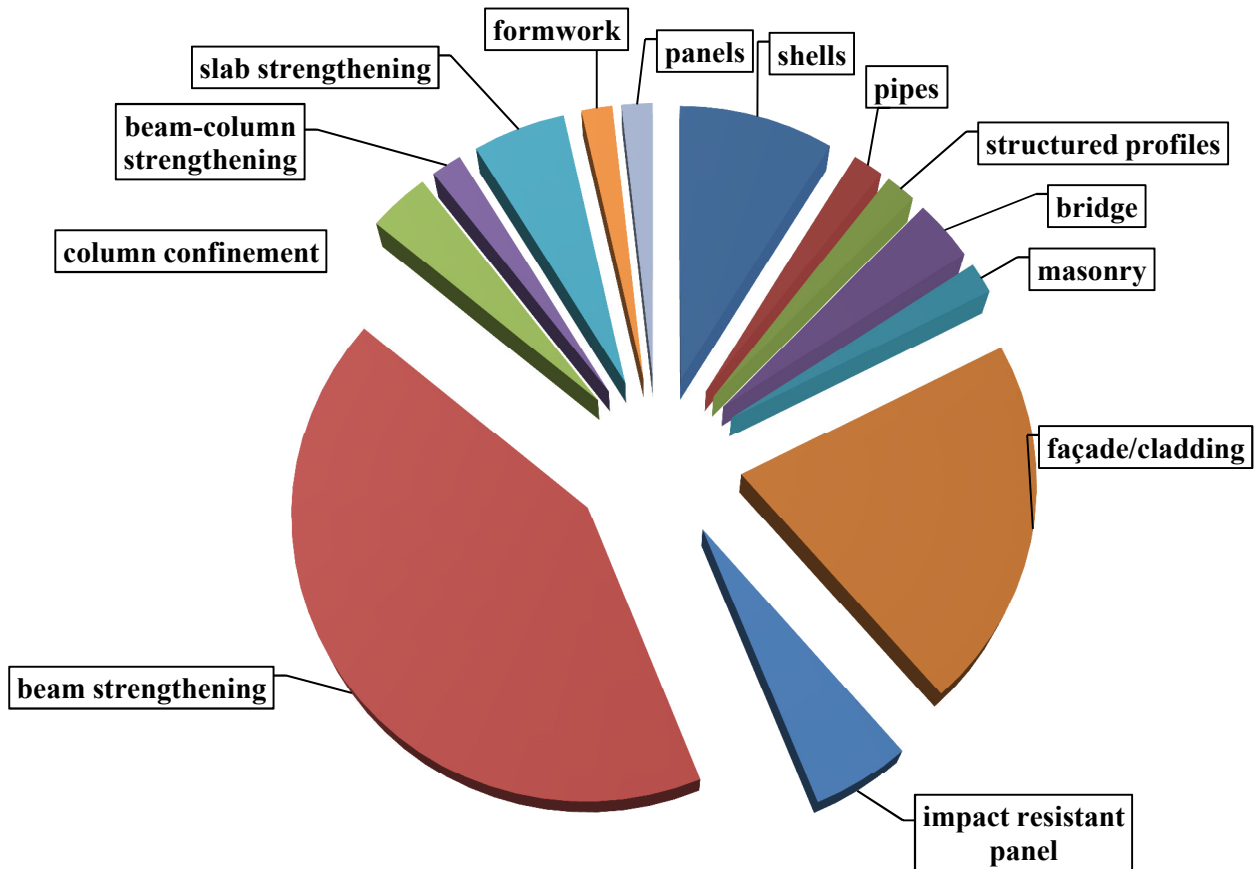
Figure 2.8 Different structural applications of TRC

2.7 REVIEW OF TRC BASED STRUCTURAL STRENGTHENING

In the development of TRC as a cement based composite for the strengthening of concrete members, two approaches have been used. One approach is finding the most suitable combination of a textile reinforcement and an existing mortar, and the other one is to modify the mortar with different short fibres or involve existing ductile mortars that yield improved textile-mortar interaction and cracking characteristics.

The use of TRC in structural strengthening applications is gaining interest (Triantafillou and Papanicolaou 2005, Bruckner et al. 2006, Bruckner et al. 2008, Larbi et al. 2010a, Larbi et al. 2010b, Angaleo and Focacci 2011, Al-Salloum et al. 2012, D'Ambrisi et al. 2012, Contamine et al. 2013, Babaeidarabad et al. 2014), especially for flexural and shear strengthening of RC beams.

TRC offers a viable solution that consists of a high strength flowable mortar and either carbon, polypara-phenylene benzobisoxazole (PBO) or AR-glass textile as reinforcement (Triantafillou et al. 2006, Triantafillou & Papanicolau 2005, Bruckner et al. 2005& 2008, Blansksvard et al. 2009, Larbi et al. 2012 & 2013, Babaeidarabad et al. 2014). Further, closed TRC jackets used for strengthening of RC beams can provide a substantial gain in the shear capacity. When TRC was used as a shear strengthening material, even two layers of mortar-impregnated textile reinforcement could prevent sudden shear failure and allowed the activation of flexural yielding. It was observed that the binding matrix, the number of layers and the placement of layers of textile affect the enhancement of ultimate beam capacity, which varied from 10% to 100%. The ductile behaviour of a TRC strengthened beam mainly depends on the nature of final failure of the system. There could be decrease of 30-50% in ultimate deflection compared to the unstrengthened beam due to debonding of strengthening layer from existing concrete. It is mainly because the final failure of the strengthened beam depends on the tensile strength and bond strength of the binder. Generally, it is seen that a load increase in the range of 15 to 20% can be achieved with 2 to 4 layers of glass textile without anchorage to the compressive zone. In all studies reported in literature, strengthening methods using TRC result in lower crack widths in the service phase, when compared with other methods.

It can also be concluded that the fiber arrangement in the textile used, such as the type of mesh, ratio between free spaces and roving dimensions, is of great importance for strengthening (Curbach et al. 2006, Ortlepp et al. 2006), along with the bonding between fibers and matrix, and the fineness of matrix particles. The incorporation of higher fibre amounts in the textile grid leads to an increase of the load bearing capacity, possible through the effective use of multiaxial grids. Moreover, when TRC is used as a strengthening material for slabs, a significant increase in load-bearing capacity and reduction in deflection have been observed (Papanicolaou et al. 2009, Schladitz et al. 2012).

To improve the ductility of concrete columns in earthquake resistant structures, TRC jacketing has been found to be viable (Triantafillou and Papanicolaou 2005, Triantafillou et al. 2006, Ortlepp et al. 2009). Depending on the type of mortar and the number of confining layers used, the enhancement due to confinement can be upto 80% for strength and 50% for ultimate strain. TRC has also been proven to enhance the ductile behaviour of beam-column joints (Mobasher

2011). Yet another application of TRC as a strengthening material is for brick masonry (Papanicolaou et al., 2006).

Recently, design and construction recommendations of externally bonded FRCM systems for concrete and masonry repair and strengthening have been established by ACI 549 (2013). According to these recommendations, the maximum force provided by the TRC should be designed not to exceed 50% of the capacity of the unstrengthened beam. In addition, the strength reduction factor follows the philosophy of ACI 318 (ACI 2011), in which an element with low ductility should be compensated with a higher reserve of strength. However, it needs to be kept in mind that the experimental database on the use of different textile reinforcements considered for structural strengthening to develop ACI recommendations is not extensive, and the applicability and limitations for the proposed recommendations are not yet fully been examined.

2.8 SUMMARY OF THE LITERATURE REVIEW

The potential of TRC as a construction material is explored in the previous sections of this chapter. The various aspects such as the ingredient materials, mechanical characteristics, production technologies, analytical models and durability issues were reviewed. Applicability of TRC in various civil engineering applications were also reported. It was observed that the research related to the TRC is gaining popularity towards practical applications and scope is vast. The benefits of the research in this area will mainly depends on the optimization of the matrix and fabric materials considering mechanical performance, environmental impact and cost. This would lead to low cost solutions that could be used for housing, retrofitting, impact-resistant design, water supply, and many more.

Studies of TRC strengthening consisting of cement based composites and textile grids that yield a highly ductile failure are limited in literature. Also, when using a cement based material as the binder, further investigation is needed to understand on whether, and to what extent, the direct tensile contribution from the matrix improves the load capacity. Information related to the influence on the bond in the transition zone, between textile composite and binder, due to the increase in the fibre amount in the textile grids is also lacking. In TRC, if the bond is significantly weak, there is a limitation on the number of textile layers that can be used effectively, without anchorage problems and debonding. This also limits the maximum fibre

amount applicable in a certain direction and, therefore, the maximum strengthening effect achievable in a TRC system. The penetration of the textile component by the matrix has been a problematic issue in several systems. Non-impregnated sheets, grids or textiles could generate larger slip and inferior effective strain over the roving cross-section, with possibly overloaded yarns. The use of impregnated fibres needs to be checked for more effective strain distribution in the textile grids.

2.9 MOTIVATION FOR THE PRESENT RESEARCH

Developing and selecting alternate materials for strengthening of structures requires proper understanding of the material behavior. High strength, corrosion resistance, ease and speed of application at minimal change of cross section, moisture compatibility, applicability at low temperatures, fire resistance and compatibility with the substrate materials are some of the main challenges to be addressed for a strengthening material. Based on the review carried out for TRC, it is observed that most of the research and practical applications of TRC is in the area of structural strengthening and that TRC has a good potential for flexural strengthening of RC beams. However, there are a lot of varying results reported with respect to the efficiency of TRC systems, which depends on the performance of binder, textile and composite as a whole.

Considering the overall scenario of developments with TRC, it can be noticed that in India there is no industrial scale application reported till date with TRC, even though its applications are significant in many other countries, such as Germany, Israel, Brazil, Italy, France and USA. Moreover, there are very limited varieties of textiles available to develop TRC in India. Hence as an alternate construction material, India needs more use and popularization of TRC. In such a situation, it is necessary to develop cement based binders and new combinations of TRC with the available materials, and characterize and apply them in appropriate construction practices. It is important to demonstrate the compatibility and composite performance of TRC for flexural strengthening of RC beams, with new combination of materials, to prove its efficiency in terms of load-carrying capacity and ductility.

2.10 DETAILED RESEARCH METHODOLOGY

The primary highlight of this thesis is to develop and demonstrate the feasibility and applicability of a type TRC, called in the work as *FABcrete*, towards flexural strengthening. Essentially, *FABcrete* should contain a cementitious binder and a textile reinforcement, and should yield a strain hardening behaviour. To establish this material and to demonstrate the feasibility and structural performance for strengthening of RC beams, the methodology proposed is shown in flowchart in Figure 2.9.

This type of study should start with the development of cementitious binder and mechanical properties of fresh and hardened state should be evaluated. Choosing the appropriate textile and characterizing its tensile behaviour should be the next step. Most textiles have waviness of yarns due to the manufacturing process, which may lead to delayed activation during the loading and affect the composite performance negatively. Hence, there should be a process to take care of this aspect while casting *FABcrete* specimens. After finalizing the binder and textile, the tensile performance of *FABcrete* should be characterized as it is important for determining the effect of volume fraction and the appropriate combination of textile.

Yet another aspect is that when *FABcrete* is used for strengthening or retrofitting, the strain compatibility of *FABcrete* with base concrete should be evaluated. Also, it is important to understand the conclusive failure mechanism of *FABcrete* strengthened concrete elements.

After development of *FABcrete*, investigations needs to be focussed on flexural strengthening by studying both un-cracked and cracked RC beams. The structural performance of the strengthened system should mainly be evaluated for ultimate load carrying capacity and ductility. In order to use *FABcrete* in structural applications, an efficient mathematical modelling procedure must be developed and validated through comparisons with the experimentally obtained behaviour. The various tasks planned in the thesis are given in the following sections, and their sequence and interrelations are given in the flowchart of Figure 2.9.

Flexural Strengthening of RC beams with *FABcrete*

Development of *FABcrete*

Matrix for *FABcrete*

Glass Textile

Fresh properties

Mix proportioning, Workability

Ultimate strength, Ultimate strain, Load vs. strain response

Hardened properties

Compressive strength, Uniaxial tensile strength, E, Poisson's Ratio

Requirements of *FABcrete* to be used in flexural strengthening

Stiffness, Ductility, Tensile strength, Bond strength, Compatibility between existing concrete and *FABcrete*

Investigation of *FABcrete* strengthened un-cracked and cracked RC beams for load carrying capacity and ductility

Methods of strengthening

Wet lay-up process

Demonstration of techniques

Modelling approach

Development of models for numerical and analytical simulation

Figure 2.9 Flow chart for the methodology followed

2.10.1 Requirements for Fresh Properties of Matrix of *FABcrete*

In the matrix design, the requirements such as mechanical parameters and bonding behaviour, as well as durability, need to be fulfilled. While using different ingredients for the development of binder, arriving at a specific mix for a particular targeted structural application could be a challenge in TRC. A variety of mix designs can be seen in the literature with the above stated aspects. The cementitious matrix used in *FABcrete* has to yield highly flowable consistency that can offer good penetration and suitable bond with the textile. Hence, it will be appropriate to combine cement, water, sand, and mineral and chemical admixture as ingredients of the binder for a homogeneous and fine structure. Nevertheless, to ensure matrix penetration between textiles, the maximum grain size of the sand used should not be more than 1mm. Further, considering the fact that the end application envisioned for *FABcrete* in this thesis is in flexural strengthening, it is important that the matrix has have sufficient workability till the strengthening process is completed, say over one hour.

2.10.2 Requirements for Characterizing Tensile Behaviour of the Textile

An open grid textile is the better option to use in *FABcrete* as reinforcement along with cementitious binder since it can permit good permeability and envelope completely with the binder. Two types of glass textiles, available in the Indian market, having two different size of mesh opening (25mm and 10mm) have been used in the investigation. In order to determine the ultimate tensile strength and ultimate tensile strain of the textiles and to determine the load vs. strain behaviour, experimental studies are needed. Such information about the mechanical characteristics, including the failure pattern, is required for both materials engineering, as well as for the development models for TRC applications. For proper experimental studies, there should be an objective method for specimen preparation, as well. Further, an efficient test setup should be designed, where there is no slipping and breakage of the textile at the grip, and direct measurement of elongation and good reproducibility of test results are possible.

2.10.3 Requirements for Hardened Properties of *FABcrete*

When a material is used for structural strengthening, it is not desirable to have large differences in the moduli of elasticity of the adherent materials, as this can create stress concentrations

during loading. To avoid this, the elastic modulus of the strengthening material should be in the same range as that of the substrate material. In such situations, determining the material behaviour under compression, tension and evaluation of the Young's modulus and Poisson's ratio is important. The application of *FABcrete* is usually based on very thin elements with a thickness of about 12mm, which is low compared to the dimensions of ordinary concrete structures. Hence, testing equipment and specimen sizes used for ordinary concrete are not suitable for the determination of the mechanical characteristics of such slender elements. Even though test methods for panels and other slender elements are not new, in principle, enhanced or modified test setups have to be developed for specimens of *FABcrete*.

Moreover, while characterizing the tensile behaviour of TRC, there should be a reliable test setup since tensile strength is a crucial property for the dimensioning of such elements. A number of setups have been developed by various researchers and research groups that differ in many details, such as specimen dimension, loading rate, measurement device, load application, etc. For a final answer to the question as to which test setup should be preferred for the determination of the strength of TRC, more aspects have to be considered, such as reinforcement ratio and size of stressed fiber surface. Towards this, a testing methodology should be validated to characterize the uniaxial tensile behaviour of *FABcrete*.

There are many unavoidable aspects of material behaviour that are consequences of production constraints. Sometimes, these will not allow the utilization of the full potential of the material. In *FABcrete*, this situation arises due to the initial waviness the textile. Towards improving the efficiency of the composite, pre-stressing or, in other words, stretching is a viable solution. The mechanism developed should be capable of stretching a number of layers of textile while casting *FABcrete* elements.

In the hardened state, perfect bond is essential for the composite behaviour as it governs the strength and ductility of the material. In a textile yarn, outer filaments are in direct contact with the matrix and have better bond with the matrix than the inner filaments, which consequently get stressed only indirectly. So, in addition to the bond between outer filament and matrix, the bonding of filaments is also important. By examining the bond at the micro-level, it can be seen how much the inner and outer portions of yarn transfer the force between concrete and yarn. It also gives an idea of the friction between single filaments and the voids inside the yarn.

2.10.4 Requirements for the Strengthening of RC beams with *FABcrete*

Several studies reported in Section 2.7 of this chapter, which use cement based strengthening materials, report increases in ultimate load for strengthened RC beams under flexure. However, in most investigations, one of the drawbacks reported is the loss of ductility to an extent of 30 to 50% for the strengthened member. Another adverse effect is the debonding of the strengthened material from the existing concrete, due to which the effectiveness of the strengthening material is not fully utilized. In *FABcrete* strengthening, it is aimed that the binder itself will act as the adhesive with the concrete. Hence, the matrix has to serve the purpose of transferring the stresses between the filaments of the fabric, protecting the filaments from damage and also bonding with the substrate material. In this scenario, there is a need to develop *FABcrete* in such a way that it provides an increase in ultimate load carrying capacity, without a loss of ductility after strengthening.

2.10.5 Requirements for the Modelling

For simulating RC beams strengthened with FABcrete, there is a prerequisite for appropriate models wherein the structural behaviour can be predicted over the entire range of load application. From the literature review, it is observed that finite element modelling is a viable option for such kind of problems for which appropriate material models should be developed based on the experimental database of *FABcrete*. Further, it is also noticed that a non-iterative simple analytical method is lacking for TRC strengthened beams, which can be used for design practices.

CHAPTER 3

DEVELOPMENT OF *FABcrete*

3.1. INTRODUCTION

For satisfying the requirements arrived at for developing and establishing *FABcrete* as a viable TRC, the matrix, textiles and the composite as a whole need to be characterized in order to assess the workability of the matrix, mechanical properties of the textile, bonding between textile and matrix, as well as the tensile response of the *FABcrete*.

The studies carried out towards the development of *FABcrete* are reported in this chapter, including details about the cementitious binder and its mechanical characterization. The testing of two types of alkali resistant glass textiles is described in Section 3.3. The microscopic examination carried out to assess the bond between textile and cementitious matrix is reported in Section 3.4. The investigations on the bonding capability of *FABcrete* with concrete is also discussed in detail in Section 3.4.

3.2. DEVELOPMENT OF THE CEMENTITIOUS BINDER

A fine grained cementitious binder, consisting of portland cement, fly ash, silica fume, quartz sand, quartz powder, polycarboxylate based superplasticizer (SP) and water was developed. The mix was designed in such a way that the required properties are achieved by incorporating a high binder content, pozzolanic admixtures, aggregates with a maximum size of 0.6mm, and a high-range superplasticizer. To provide good stability for the glass textile in *FABcrete*, the binder was developed by substituting cement partially with flyash and silica fume (Brameshuber, 2006). In order to achieve satisfactory workability, the silica fume dosage was limited to 10%, by mass, of total binder content. Further, the selection of aggregates was such that the penetration of binder into the opening of glass textiles, into the filaments and in between number of layers of textiles (a maximum of 1mm) is not obstructed. For this reason, quartz sand with a maximum aggregate size of 0.6mm was used. Moreover, it is seen in the literature that the aggregate of size less than 1mm yield better fiber holding capacity in TRC. In the absence of a well-established method for the design of TRC matrices, the binder mix was arrived at, with input from the literature, to get

the desired strength and workability, after several trials. The main objective was to achieve a splitting tensile strength above 4MPa and cube compressive strength above 40MPa, as already justified in Section 2.10. Also, the workability retention of the mix (over 60 minutes) was given importance. The details and mix proportions are given in Table 3.1; this mix is designated as *FABmix* throughout the study.

The mixes were prepared in a Hobart mixer of 15litre capacity shown in Figure 3.1. While preparing the mix, the dry ingredients were poured to the mixer and mixed for 4 minutes, at low speed. Subsequently three-quarters of the required water was incorporated, followed by the remaining water to which the SP was added, and the mixing continued for 4 more minutes, at medium speed. Finally, the speed of the mixer was increased and the mixing process was continued for about two more minutes. The total mixing time was 10 minutes.

Figure 3.1 Hobart mixer

To determine the workability retention of the mix, the flow was measured after 1 hour of mix preparation, using the flow table apparatus, shown in Figure 3.2. The cone shaped mold used in the flow table apparatus has a top diameter 70mm, bottom diameter 100mm and height 50mm, as given in ASTM C 1437 (2001). The mix is poured into the cone, the cone is lifted and the vibrating table is dropped 25 times in 15 seconds. After 25 drops, the flow is measured and reported as the percentage increase in the spread diameter over the base diameter of the mold. For the mix proportions reported in Table 3.1, it was able to achieve an initial flow of more than 150% and 80% flow after one hour.

Figure 3.2 Flow table test

Table 3.1 Mix proportions for *FABmix* ingredients by weight ratio and its properties

Materials/Characteristic parameters	Cementitious Binder (FABmix)
Cement	1.0
Fly ash	0.357
Silica fume	0.071
Quartz sand	1.020
Quartz powder	0.612
Water	0.571
Water/binder ratio	0.4
Superplasticizer dosage (% weight of binders)	0.50
Flow after 1 hr (%)	80
Cube compressive strength (MPa) - mean and coefficient of variation	44.5 (±4.2%)
Cylinder compressive strength (MPa) - mean and coefficient of variation	34.0 (±3.2%)
Splitting tensile Strength (MPa) - mean and coefficient of variation	4.50 (±0.8%)
Uniaxial tensile Strength (MPa)	2.50
Young's modulus (GPa)	28.0
Poisson's ratio	0.20
Bond strength (MPa)	2.35 (±8.7%)
Charge passed in the RCPT (Coulomb) - mean and coefficient of variation	1250 (±6.7%)

3.2.1 Mechanical and Durability-Related Properties of *FABmix*

Mechanical characterization was carried out on *FABmix* to determine the cube compressive, cylinder compressive, splitting tensile and uniaxial tensile strengths, with cubes of 70mm, cylinders of 50×100mm and panels of 500×60×8mm. In addition, the rapid chloride penetration test was also performed to get a measure of the permeability of the *FABmix*. The procedures used for their determination are discussed in the following paragraphs and the properties of the mix are given in Table 3.1.

3.2.1.1 Compression

After casting cubes and cylinders with *FABmix*, the specimens were demoulded after 24 hours and immersed in water till the test date. Cube specimens of 70×70×70mm were tested after 28 days to get the compressive strength, according to IS-516 (1959). A UTM of 100 Tonne capacity was used for testing the *FABmix* specimens. The specimens were placed in the machine in such a manner that the load is applied on two cast parallel surfaces of the cubes. The mean compressive strength and the coefficient of variation are given in Table 3.1.

In order to determine the stress-strain characteristics, *FABmix* cylinders of 50×100mm were tested under compression. The size of the specimen was limited to 50×100mm considering that this will be representative of the applications of *FABcrete*. Strain gauges of 30mm length were bonded at mid-height of the specimen in axial and longitudinal directions. Figure 3.3 shows the typical stress-strain curve obtained from three *FABmix* specimens. It is observed that the maximum axial stress obtained was around 34MPa.
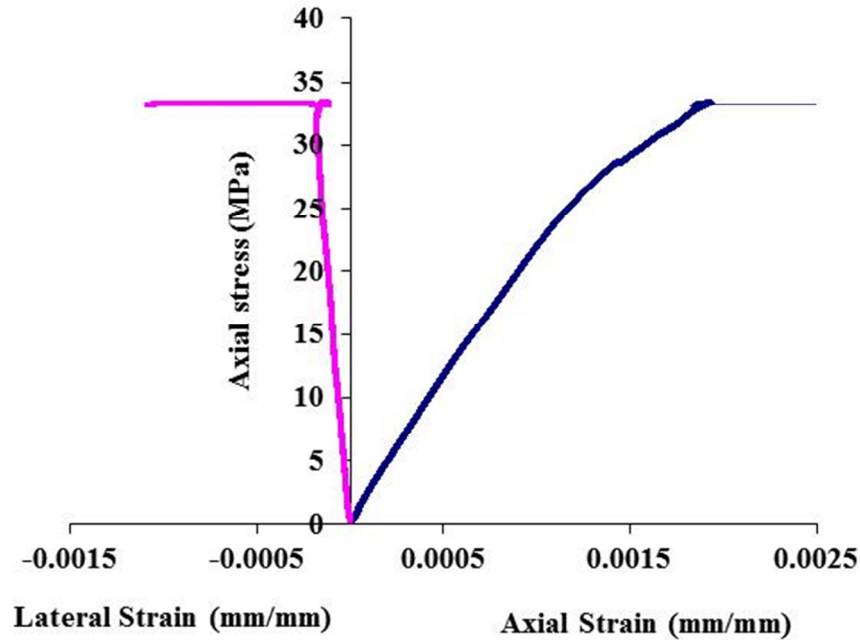
Figure 3.3 Typical stress-strain behaviour of *FABmix* in compression

3.2.1.2 Splitting-tension

FABmix cylinders of 50×100mm were tested at the age of 28 days to find the tensile strength, according to IS-516 (1959). This method measures the splitting tensile strength by the application of a diametric compressive force on a cylindrical specimen placed with its axis horizontal between the platens of a testing machine. Plywood strips were used so that the load was applied uniformly along the length of the cylinder. The spiltting tensile strength obtained is 4.5MPa (±0.8%).

3.2.1.3 Uniaxial tension

Uniaxial tensile behaviour is expected to give a realistic representation of the stress-strain and fracture behaviour of a cementitious matrix. However, there are many experimental difficulties that are encountered for gripping, aligning and controlling while conducting such tests. In this work, uniaxial tests were conducted on *FABmix* specimens to find the relation between uniaxial tensile and splitting tensile strengths. Moreover, it is essential to know the contribution of cementitious matrix alone, in order to optimize the efficiency of the textile in the composite.

The uniaxial tensile behavior of *FABmix* was studied on panels of 500×60×8mm. The ends of the specimen was strengthened by using a woven roving glass textile glued with a resin over 125 mm of the specimen at both ends. Then, the specimen was gripped in the 25Tonne servo hydraulic INSTRON machine and load was applied at a rate of 0.1mm/min. The typical stress-strain behaviour of *FABmix* under uniaxial tension is shown in Figure 3.4, where the nominal strain has been calculated from the piston displacement of the machine divided by the free length of the specimen (i.e., 350mm). After reaching peak stress, the specimen showed an abrupt failure. It is observed that the uniaxial tensile strength of *FABmix* is 2.5MPa (±8.7%), which is 0.56 times the split tensile strength and the elastic modulus in tension is around 28GPa. The splitting test gives higher values than a uniaxial tensile test, which may be due to the influence of size of the specimen and the width of plywood strip used (Rocco et al., 1999a; Rocco et al., 1999b) .
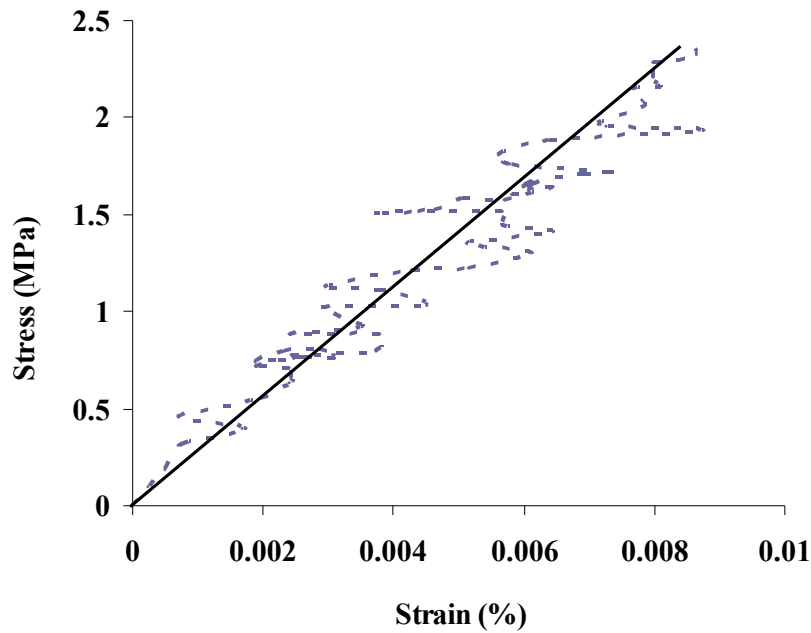
Figure 3.4 Stress-strain behaviour of *FABmix* under uniaxial tension

3.2.1.4 Chloride ion penetrability

To evaluate the chloride ion penetrability that could be decisive in repair and rehabilitation, the rapid chloride permeability test (RCPT) was performed on 3 *FABmix* specimens, following the standardized procedures as per ASTM-C1202. An electrical current was passed through a cylindrical specimen of 50mm thickness and 100mm diameter for 6 hours. A voltage of 60V DC

is maintained across the sample, throughout the test. In the test setup, one face of the specimen is immersed in a sodium chloride (NaCl) solution (0.5N) and the other in a sodium hydroxide (NaOH) solution (0.3N). Current was recorded for every 30 min interval for 6 hours. From the current readings, total charge passed (Q) was calculated using the Equation 3.1.

$$Q = 900(I_0 + I_{360} + 2(I_{30} + I_{60} + \ldots\ldots\ldots + I_{300} + I_{330})) \qquad (3.1)$$

where, Q – Charge passed (Coulomb), I_0 – current (ampere) immediately after voltage is adapted, and I_{360} – current (ampere) at 360min after voltage is applied.

The amount of charge passed through the specimen was then used to rate the concrete according to the rating system of ASTM-C1202 (1997). The average charge passed for *FABmix* was obtained as 1250Coulombs (±6.7%), which indicates that *FABmix* can be considered as a low chloride penetrability matrix. This could have implications for the use of *FABmix* as the binder in *FABcrete* for structural retrofitting.

3.3 CHARACTERIZATION OF THE GLASS TEXTILES

In the present study, two types of glass textiles, shown in Figure 3.5(a), with registered trademarks SRG-45 from Saint Gobain Adfors and AR1 from Kerakoll were used for the investigations. SRG-45 has an acrylic coating (black in color) in order to prevent alkali silica reaction in cementitious composites. The details of the textiles, as provided by the manufacturers, are given in Table 3.2.

In the case of SRG-45, there are two available yarn arrangements in the warp direction: one in which there are two yarns per line in warp direction and another in which there is only one yarn per line, as shown in Figure 3.5(b). The bundle diameter of each yarn of SRG-45 that has one yarn per line is more compared to that of the textile having two yarns per line; the diameter of each yarn, as measured with a vernier calipers, is about 1mm in the former whereas it is about 0.7mm in the latter. Considering the fact that the textile behaviour depends on the yarn configuration, it was decided to evaluate the tensile performance of both the yarn arrangements of SRG-45 to decide on the configuration that would be more appropriate. The diameter of the glass filament used in both the SRG-45 yarn arrangements is 14µm, as given by the

manufacturer, actual diameter of the coated filament was measured to be 20 μm. When two yarns are used in each warp line, the yarn contains 1600 filaments and in the textile with one yarn per line it consists of 3200 filaments (as indicated by the manufacturer). The mesh size in both arrangements of SRG-45 is 25×25mm and the weight per unit area is 225g/m^2. Further, it was also indicated by the manufacturer that the weight of fibers in SRG-45 is 180g/m^2 and the density of glass fiber used is 2.68g/cm^3.

Two yarns per line   One yarn per line
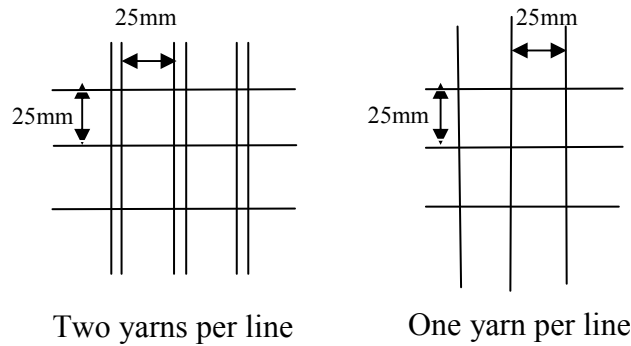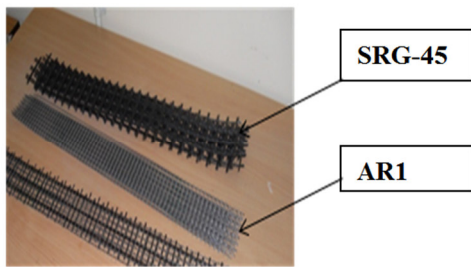
Figure 3.5 (a) Glass textiles used   Figure 3.5 (b) Yarn configurations in SRG-45

The other type of glass textile, AR1, has a smaller mesh size of 10×10mm. The weight per unit area of this textile is 110g/m^2 and that of fibers used in the textile is 90g/m^2. In the case of AR1 also, the density of glass fiber used is 2.68g/cm^3. Further, the glass used contains about 15% by mass of zirconium dioxide (ZrO_2) in order to impart alkali resistance. Each yarn in this textile consists of approximately 600 filaments of 12μm diameter each (as indicated by the manufacturer).

Table 3.2 Details of the glass textiles provided by manufacturer

Textile	Max. extension	Mass/unit area (g/m^2)	Roll length (m)	Roll width (m)	Grid size (mm)	Tensile strength
SRG-45 (both with 1 and 2 yarns per line)	<3%	225	45.7	0.91	25×25	45kN/m (across warp)
						45kN/m (across weft)
AR1	<3%	110	50	1	10×10	29kN/m (both across warp & weft)

To assess the warp and weft yarns in both the textiles, stereo microscopic investigations were carried out at 6.3X magnification with the setup shown in Figure 3.6. Microscopy images of the warp and weft junctions in SRG-45 and for AR1 textiles are shown in Figures 3.7 and 3.8, respectively, where the interlacing of warp yarns with weft yarns can be observed in both cases. This indicates that the type of textile production method used gave a half leno weave. Further, in both textiles, it is observed that the warp yarns are bundled and twisted whereas the weft yarns are not twisted. Moreover, the warp yarns pass over the weft yarns, whereas the weft yarns are straight and not woven.

Figure 3.6 Stereo microscope
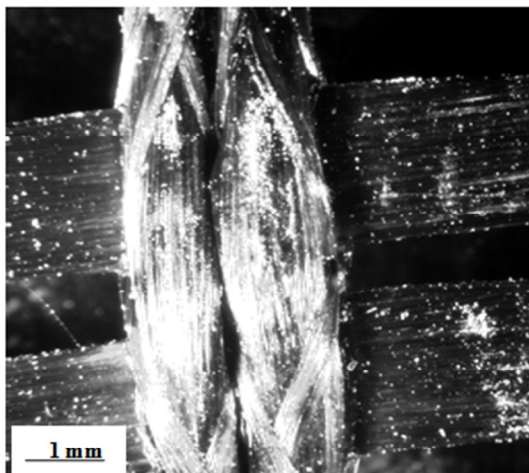
Figure 3.7 Microscopic view of SRG-45   Figure 3.8 Microscopic view of AR1
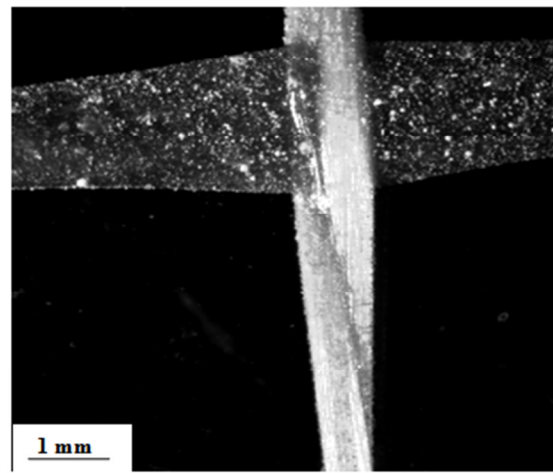
3.3.1 Tensile characterization of the yarns

To find the load carrying capacity of a yarn line of SRG-45, uniaxial tensile tests were attempted. Single yarn lines were obtained by removing the warp yarns from the textile. The sample ends were glued to steel plates of 2mm thickness and hydraulically gripped in an INSTRON machine of 25T capacity, leaving a free length of 325mm. Tests were conducted under displacement controlled loading at 0.1mm/min. The test setup is shown in Figure 3.9.
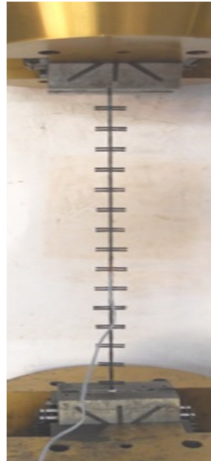
Figure 3.9 Setup for testing a yarn line

The resulting load versus nominal strain behaviour of the yarn lines of both varieties of SRG-45 is shown in Figure 3.10, where the nominal strain is taken as the piston displacement divided by the free length 325mm. It is observed that the maximum load taken by a yarn line of SRG-45 with one yarn per line is 0.55kN corresponding to a strain of 1.56%, whereas for the yarn line of the textile with two yarns per line, the load taken is 0.45kN and corresponding strain is 0.9%. When two yarns are used together in a line, only one of them ruptures, resulting in a lower peak load and earlier failure compared to those of the yarn line with a single yarn. Nevertheless, the failure of the yarn was due to rupture with filament separation, in both the varieties. Moreover, it is seen that the yarn line with a single yarn exhibited higher elongating ability, which can be due to the activation of more number of filaments. In addition, it was also observed that there is an initial nonlinearity in the load versus strain behaviour in both varieties, attributed to the waviness of the yarns, which is more prominent in the case of SRG-45 specimen with one yarn per line because there is are more filaments that need to be stretched to overcome the waviness. The nonlinearity observed is upto a strain of 0.6% for the specimen with one yarn per line and 0.15% in the case of the specimen with 2 yarns per line. It gives an indication that when more filaments

are bundled and twisted to make a yarn, there is more waviness, resulting in a higher frictional force between the filaments and subsequently more force is required to straighten the yarn.
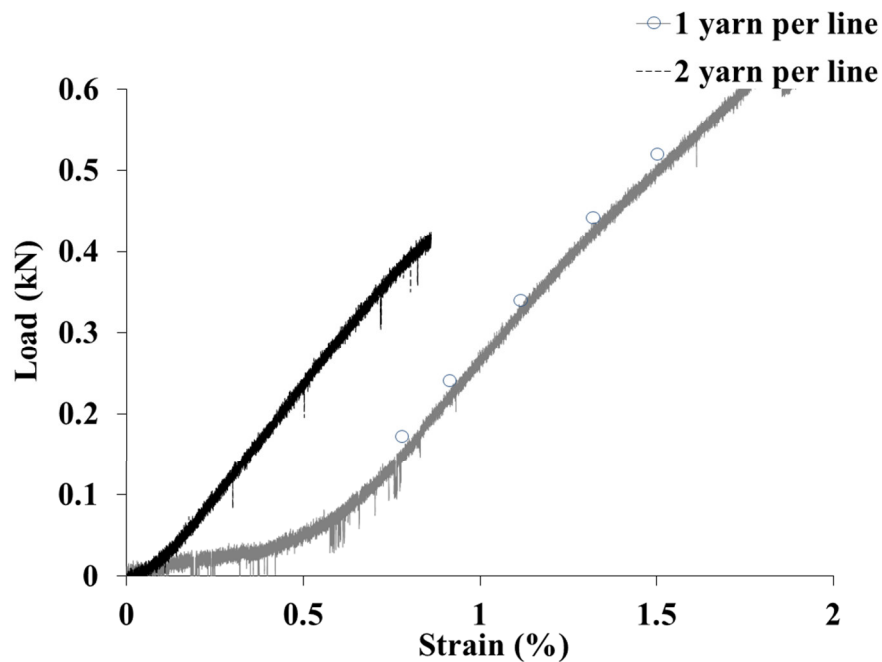
Figure 3.10 Typical load versus nominal strain for yarn lines of SRG-45

3.3.2 Tensile characterization of the textiles

To perform uniaxial tensile characterization of textiles, a methodology that is along the lines of the wide-strip test for geogrids, as prescribed in ASTM D6637-01 (2007), was used. Accordingly, the test specimen should consist of at least three junctions in length and the width should be such that the behaviour is representative. Here, the specimen dimensions are 475mm long and 50mm wide, and the strip of textile is gripped across its entire width in a tensile machine, leaving a free length of 325mm. The loading rate was chosen in the range used in previous works on glass textiles (e.g., Peng and Cao, 2005): displacement rates of 0.1, 0.2 and 0.4mm/min were used corresponding to nominal strain rates 5×10^{-6}/s, 1×10^{-5}/s and 2×10^{-5}/s, respectively, where the nominal strain is obtained by dividing the piston displacement by the free length 325mm. Further, three specimens are tested in each case.

3.3.2.1 Uniaxial tensile behaviour of AR1

The typical load versus nominal strain curves obtained for the AR1 samples are shown in Figure 3.11. In the tests conducted at the loading rates of 0.1 and 0.2mm/min, the failure was away from

the grip whereas at 0.4mm/min loading rate the specimens failed at the grip and so the data from those tests are not reported. The final failure in all the cases was due to abrupt rupture of warp yarns without any filament separation, indicating that the filaments are well bonded. Mesh distorsion in both longitudinal and transverse directions was observed, as seen in Figure 3.12. Further, there was more distorsion in the edge yarns indicating that there could be a shear lag effect due to the nonlinear displacement distribution across the textile.

From the data reported in Table 3.3, it can be seen that the maximum load is about 29.5kN/m (±1.2%) and 30kN/m (±1.5%) for 0.1 and 0.2mm/min loading rates, respectively. Further, the secant stiffness for the textile is calculated as the ratio of change in load per unit width to a prescribed value of strain. A strain value of 1% and strain corresponding to maximum load was considered for the calculations. At a rate of loading of 0.1mm/min, the secant stiffness for 1% strain is 1375N/mm (±1.1%) and is 1324N/mm (±1.2%) at maximum load. Similarly, at a rate of loading of 0.2mm/min, the secant stiffness at 1% strain is 1350N/mm (±0.8%) and at maximum load is 1304N/mm (±1.2%). It is noticed that that there is no significant effect of rate of loading on the stiffness for AR1. It is also seen that the deformation (strain) capacity at the maximum load is about 2.50%.
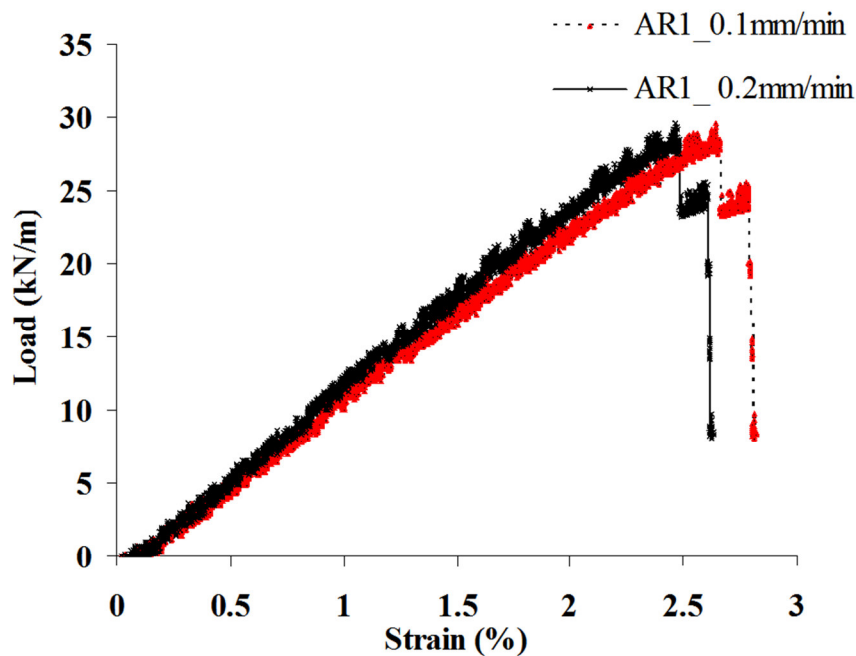
Figure 3.11 Typical load versus nominal strain for AR1   Figure 3.12 Failure pattern of AR1
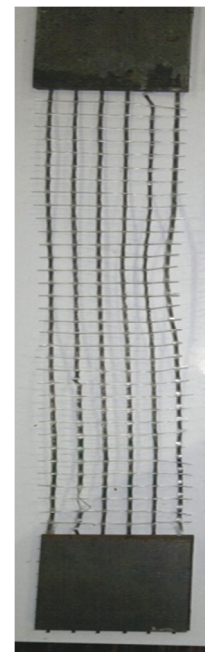
Table 3.3 Properties of the Textiles *(mean values and coefficients of variation)*

Textile	AR1		SRG-45				
			Textile with 1 yarn per line		Textile with 2 yarns per line		
Rate of Loading (mm/min)	0.1	0.2	0.2	0.4	0.1	0.2	0.4
Tensile load capacity (kN/m)	29.5 (±1.2%)	30.0 (±1.5%)	26.0 (±4.5%)	44.0 (±6.5%)	48.0 (±5.5%)	44.0 (±6.5%)	36.0 (±4.5%)
Strain at Maximum Load (%)	2.50 (±2.6%)	2.65 (±3.2%)	1.80 (±6.4%)	1.82 (±4.4%)	1.60 (±1.4%)	1.40 (±2.4%)	1.30 (±4.8%)
Secant Stiffness at 1% strain (N/mm)	1375 (±1.1%)	1350 (±0.8%)	2727 (±2.8%)	2714 (±2.6%)	3111 (±1.8%)	3444 (±2.7%)	3375 (±3.8%)
Secant Stiffness at Maximum Load (N/mm)	1324 (±1.2%)	1304 (±1.2%)	1677 (±5.8%)	2470 (±4.7%)	2705 (±3.2%)	3230 (±3.8%)	3090 (±5.8%)

3.3.2.2 Uniaxial tensile behaviour of SRG-45

The uniaxial behaviour of the configurations with one and two yarns per line of SRG-45 was investigated. The sample specimens and test setup are shown in Figures 3.13 and 3.14, respectively.
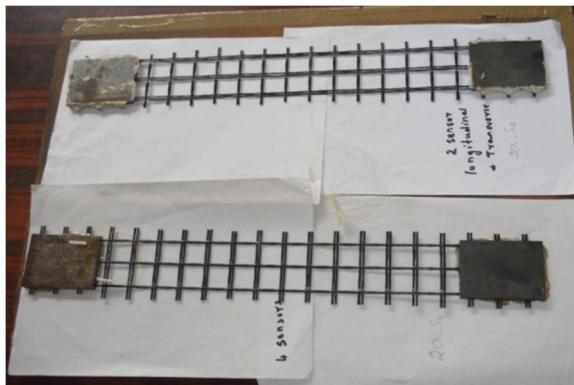
Figure 3.13 Specimens of textile for uniaxial tensile test   Figure 3.14 Test setup

3.3.2.2.1 Behaviour of SRG-45 with one yarn per line

The typical load versus nominal strain curves obtained for SRG-45 with one yarn per line are shown in Figure 3.15 for different loading rates, where the nominal strain is obtained by dividing the piston displacement by the free length 325mm. When the rate of loading was 0.1mm/min, the specimens failed near the grip and hence the corresponding data are not considered for further discussions.
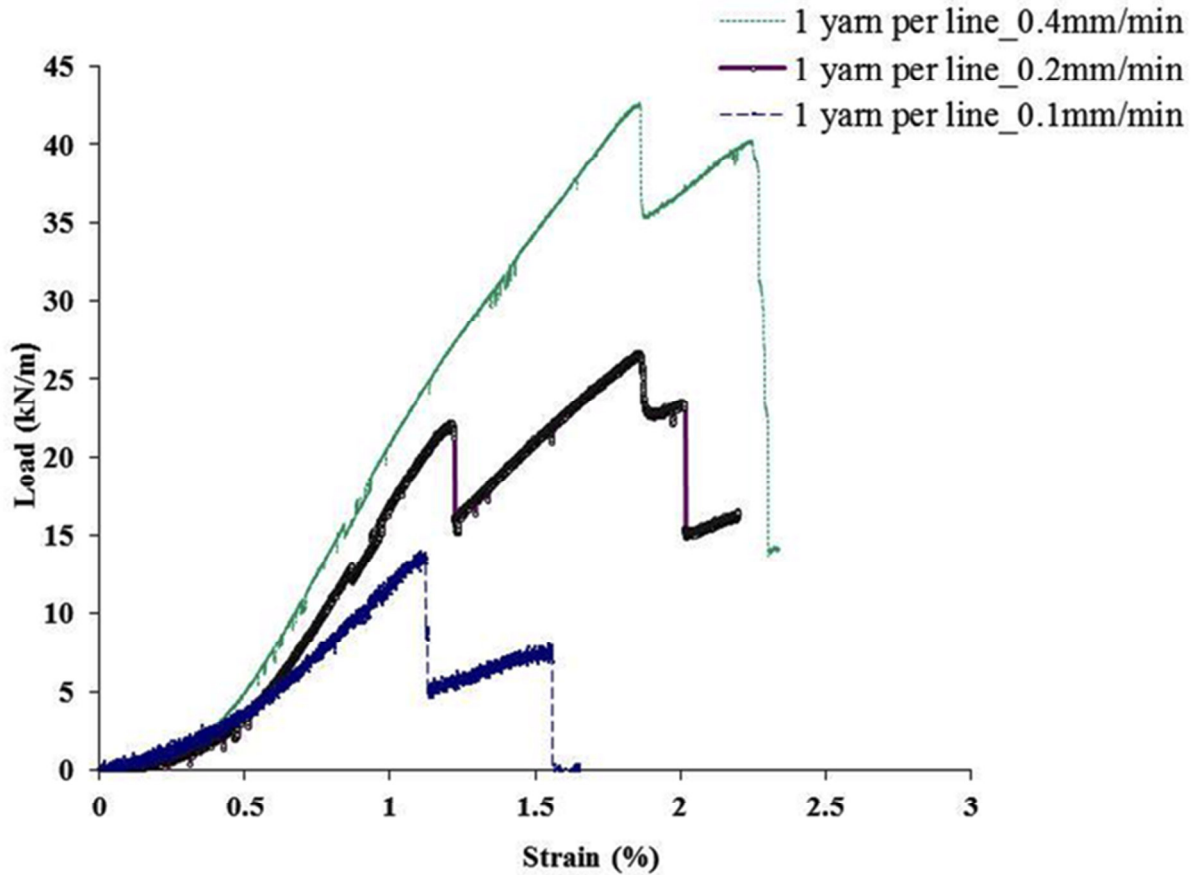
Figure 3.15 Typical load versus nominal strain curves of SRG-45 with one yarn per line

It is seen that there is an initial nonlinearity with an increase in stiffness, reflecting the stretching of the wavy warp yarns in the textile. The lag in stiffness is observed upto a strain of 0.6%. Similar slack was also seen in the yarn test. Hence, it is clear from Figure 3.15 that a certain load (around 7 to 10kN/m) has to be applied to straighten the waviness of the textile so that the initial lag in stiffness can be avoided. Once the stiffness lag is overcome, the response is linear until a peak followed by a rapid loss in load carrying capacity due to multiple filament rupturing and separation.

44

While examining the failure, it is seen that the telescopic rupture of the filaments leading to strain localization was significant at the warp-weft junctions. Moreover, there was a significant filament rupture and separation seen at a few warp-weft junctions. This indicates that once the filament ruptures, only those filaments in the vicinity share the load, leading to further filament rupturing at that specific location.

At the rate of loading of 0.2mm/min, the textile exhibited a maximum load of 26kN/m (±4.5%) and at 0.4mm/min, the maximum load was 44kN/m (±6.5%). The test results show that there is significant variability in the maximum load for different rates of loading though the strain at maximum load remains almost the same. Only few filaments rupture and separate before the first peak, which is followed by a sudden drop in load and subsequent increase due to load redistribution among the adjacent filaments. However, it was observed that as the rate of loading increases, more filaments separate due to which more load is redistributed across adjacent filaments, more filaments carry the load, resulting in an increase of load carrying capacity as the rupture strain of yarn governs the failure. Such load sharing may be attributed to the degree of twist per yarn and efficiency of leno weave provided in SRG-45 to hold the filaments together during production process.

The data from the tests of SRG-45 textiles with one yarn per line are reported in Table 3.3. The secant stiffness at the rate of loading of 0.2mm/min corresponding to 1% strain is 2727N/mm (±2.8%) and 1677N/mm (±5.8%) at maximum load. Similarly, at the rate of loading of 0.4mm/min, the secant stiffness at 1% strain is 2714N/mm (±2.6%) and the corresponding value at maximum load is 2470N/mm (±4.7%). It is observed that for the rate of loading of 0.2mm/min, there is about 38% loss of stiffness between 1% strain and strain corresponding to maximum load, whereas the difference is only 8% for rate of loading of 0.4mm/min. However, the rate of loading does not show any significant effect on stiffness till 1% strain.

3.3.2.2.2 Behaviour of SRG-45 with two yarns per line

The typical load versus nominal strain behaviour SRG-45 with two yarns per line is shown in Figure 3.16. At the rates of loading of 0.1, 0.2 and 0.4mm/min, the maximum load exhibited by the textile was 48kN/m (±5.5%); 44kN/m (±6.5%)and 36kN/m (±4.5%), respectively. The test results shows that there is no trend in the variability in the maximum load as the rate of loading

changes. Even though the number of filaments is the same in both configurations of SRG-45, the number of individual yarns for the textile with two yarns per line is more (i.e, 6 yarns per 50mm width as opposed to 3 yarns per 50mm width in the textile with one yarn per line). Further, it appears that the load is redistributed more uniformly across all the yarns, which may be attributed to the degree of twist per yarn and the efficiency of the leno weave of SRG-45 at the warp-weft junctions to hold the filaments together. Since there was no filament rupture seen before reaching the maximum load, the production method of SRG-45 with two yarn per line seems to be more efficient.

The data from the tests for SRG-45 with two yarns per line are reported in Table 3.3. At the rate of loading of 0.1mm/min, the secant stiffness for 1% strain is 3111N/mm ($\pm$1.8%) and the value is 2705N/mm ($\pm$3.2%) at the maximum load. Similarly, at the rate of loading of 0.2mm/min, the secant stiffness at 1% strain is 3444N/mm ($\pm$2.7%) and the corresponding value at maximum load is 3230N/mm ($\pm$3.8%). Further, at the rate of loading of 0.4mm/min, the secant stiffness at 1% strain is 3375N/mm ($\pm$3.8%) and the corresponding value is 3090N/mm ($\pm$5.8%) at maximum load.
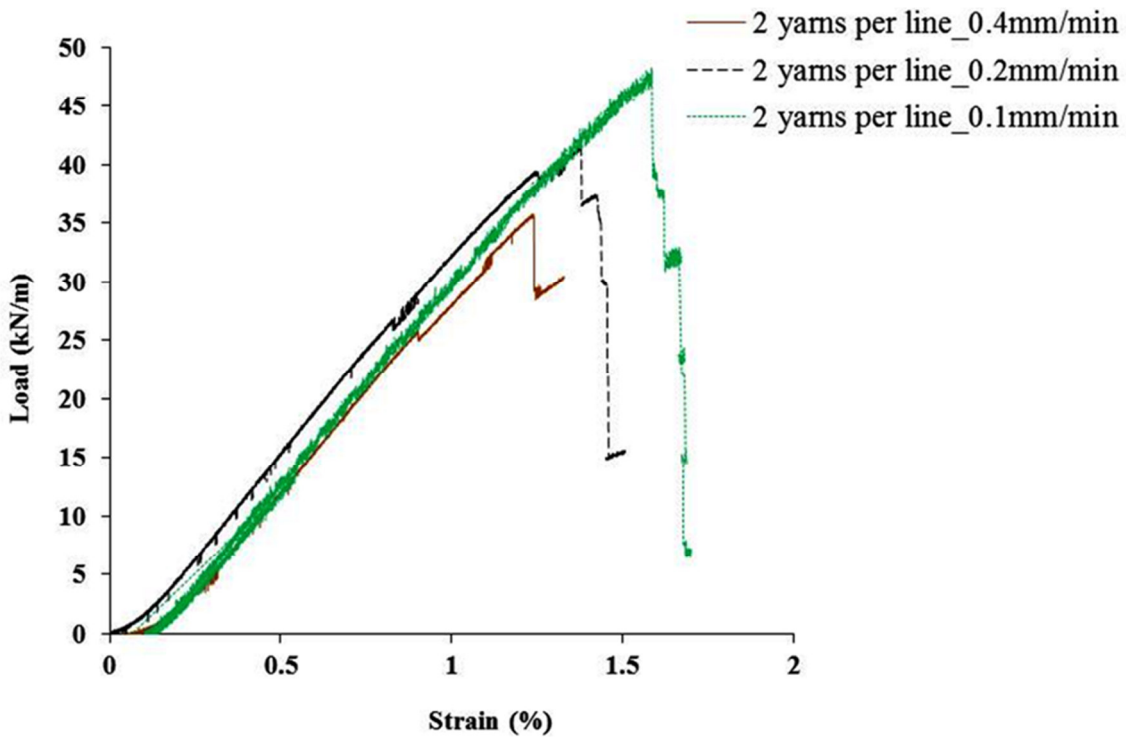
Figure 3.16 Typical load versus nominal strain curves of SRG-45 with two yarns per line

While examining the failure of two yarn per line SRG-45 textile, it is seen that the filament rupturing was more predominant at the warp-weft junctions. In this case, more number of warp-weft junctions showed filament rupture; however, the number of ruptured filaments was less compared to the textile with one yarn per line. This indicates that once filament rupture occurs in the textile with two yarns per line, the released load is shared almost equally by all remaining filaments. Moreover, if load is distributed throughout the filaments in the yarn, it will cause additional filament failure, leading to an unstable process of subsequent filament failure and finally the rupture of entire yarn. The failure pattern of SRG-45 with two yarns per line is seen in Figure 3.17.

filament rupture and separation
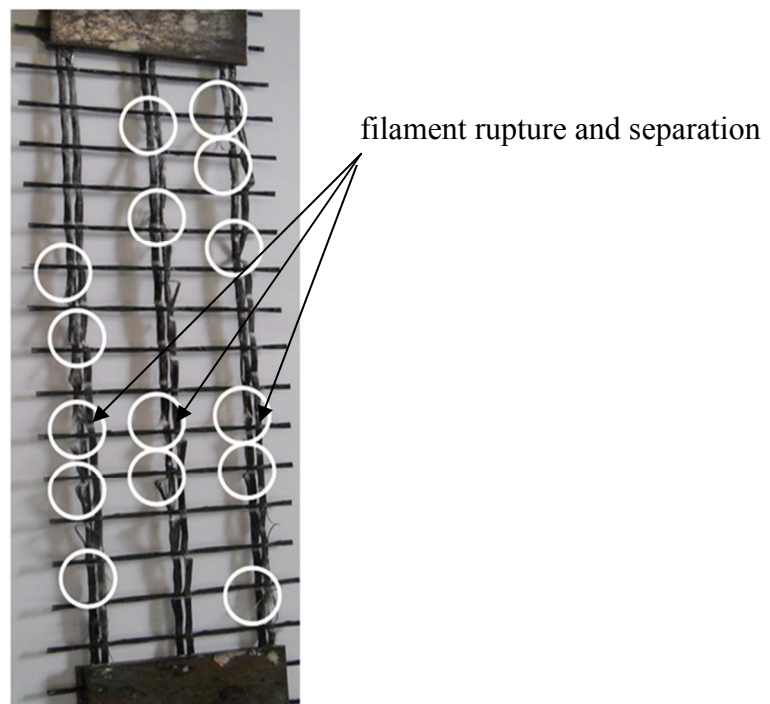
Figure 3.17 Failure pattern in SRG-45

From the investigations on the variability in load versus strain behaviour, it is noted that for SRG-45 with two yarns per line, there is more uniform distribution of load and localization of strain at the junction of warp and weft yarns, whereas in the textile with one yarn per line, the stress redistribution is more local. For 1 yarn per line textile, the maximum load increases as rate of loading increases. It is mainly due to the activation of more number of filaments in the whole bundle of yarn for higher loading rate, which enables local load distribution in the adjacent

filaments in the yarn. When rate of loading is low, the activation rate of filaments is less and there are more chances for filament separation locally, which can lead to reduction in maximum load carrying ability. In this type, as soon as the specimen is loaded and as test progresses local distribution of force to adjacent filaments governs the load carrying ability. However, for 2 yarns per line textile, the maximum load decreases as rate of load increases. It should be noted that there is a small gap between two yarns in a line. Hence progressive filament rupture in any one yarn per line can lead to decrease in load carrying ability. In this case, a slow rate of loading allows smooth load transfer (uniform global load transfer) and its equal distribution to all filaments leading to increases in load compared to higher rate of loading. The textile with one yarn per line is capable of elongating more due to the loosening of more filaments in a yarn; however, the weft yarns hold the filaments of warp yarn at the warp-weft junctions for the textile with two yarns per line more effectively.

Moreover, the dependence of the stiffness on the rate of loading is not significant for the SRG-45 with two yarns per line. Further, the initial nonlinearity observed was more in the case of one yarn per line, which may delay the activation of the textile in the TRC. Consequently, it was decided to use the SRG-45 with two yarns per line for further studies and subsequent discussion is on this type of textile alone. Furthermore, the total contact area between the binder of *FABcrete* and the outer filaments (sleeve filaments) of the yarns in the case of the textile with two yarns per line will be more than in the case of the textile with one yarn per line, leading to better bond and deposition of hydration products between the core filaments.

To understand the effect of the number of meshes perpendicular to the loading direction on the load versus strain response, tests were carried out on SRG-45 with two and three meshes. The typical results are given in Figure 3.18, where the specimen with two meshes in the transverse direction is denoted as 2A whereas the specimens with three meshes is denoted as 3A. It is observed from Figure 3.18 that increasing the number of meshes in the transverse direction from 2 to 3 resulted in an decrease in the maximum load from 47kN/m (±4.5%) to 38kN/m (±8.5%). This could be attributed to the higher possibility of defects as the number of yarns increases, resulting in the reduction in maximum load. Further, it is seen that the strain corresponding to maximum load is slightly lower in the case of the specimen with 3 meshes but there is no

significant effect of the number of meshes on the rupture strain of yarn indicating that most of the filaments are equally strained.
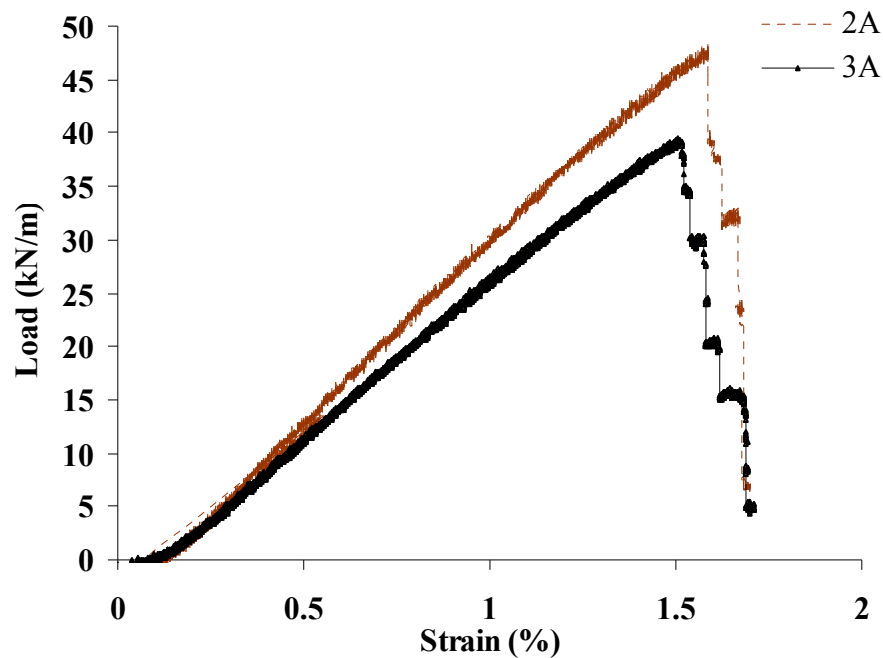
Figure 3.18 Effect of number of mesh on load vs strain response of textile

The tensile characterization studies reported are further used to establish a correlation between textile behaviour and the composite *FABcrete* in Chapter 4. From the present investigation, it is seen that the yarn behaviour cannot be extrapolated to textile behaviour and there is a need to characterize each independently.

3.4 INVESTIGATION OF THE BOND CHARACTERISTICS OF *FABcrete*

Studies were carried out to examine the bond characteristics between *FABmix* and the SRG-45 to develop *FABcrete*. Microscopic examination was carried out on a *FABcrete* specimens before and after tensile loading to assess the degree of bonding of filaments in the textile and the penetration of *FABmix* between the filaments. Further, the bond strength of *FABmix* with the textile and a concrete base was evaluated by performing pull-off tests. Finally, the integrity of *FABcrete* with concrete was investigated using a concrete specimen confined with *FABcrete*.

3.4.1 Microscopic Examination

Microscopic investigations were carried out on *FABcrete* specimens using a stereo microscope at 6.3X magnification. Observations on a virgin *FABcrete* specimen showed good bonding between the matrix and the textile yarns. In Figure 3.19, a surface cut parallel to the weft direction in the specimen with two layers of SRG-45 textile with two yarns per line shows the space between the closely spaced yarns (of the same line) filled with binder. This reflects the efficiency of binder penetration, and bonding between textile and matrix.
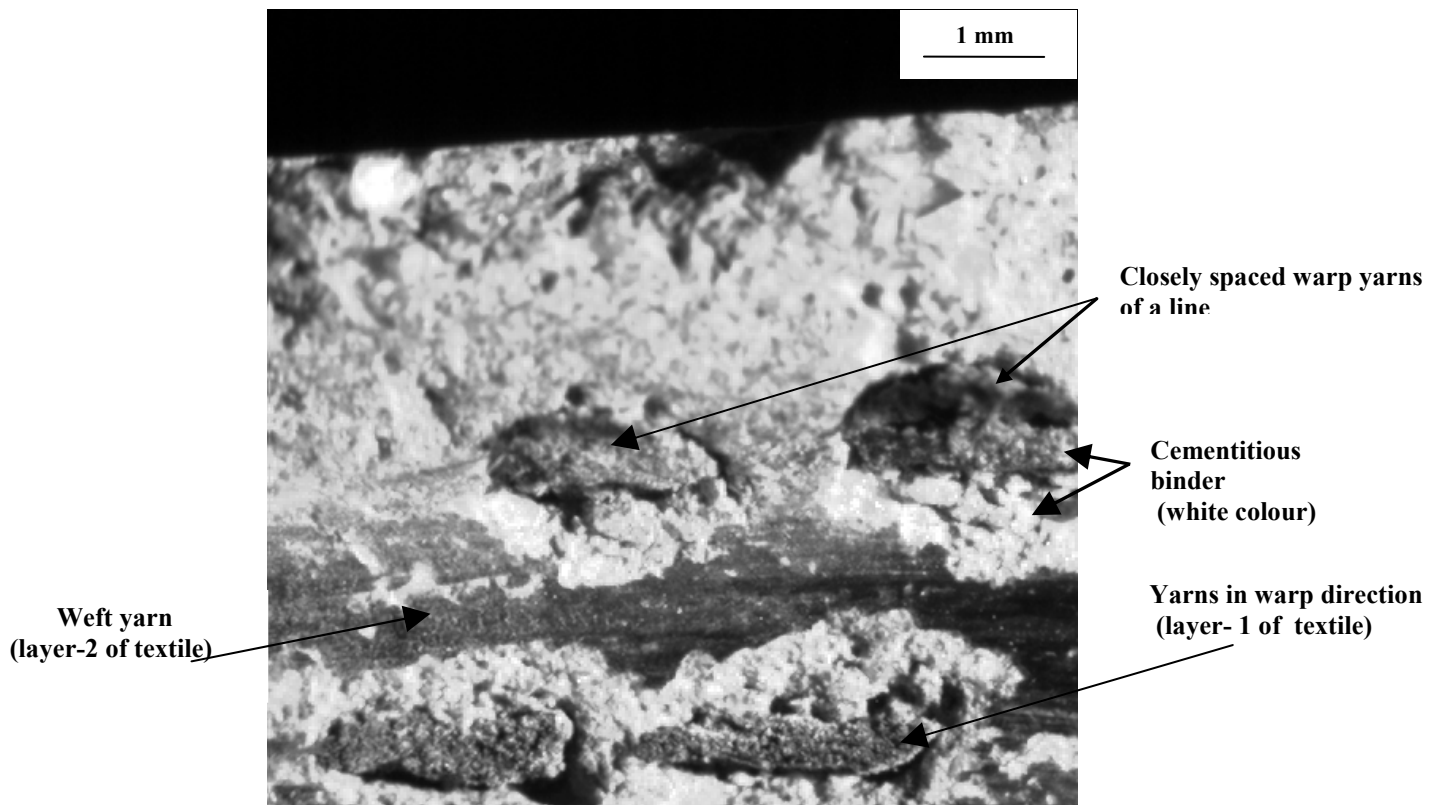
Figure 3.19 Image of surface cut parallel to the weft yarns of glass textile in virgin specimen

Observations on a sample cut from a tensile test specimen (see Figure 3.20), whose details are reported in Chapter 4, indicated that the matrix retains its integrity under load.
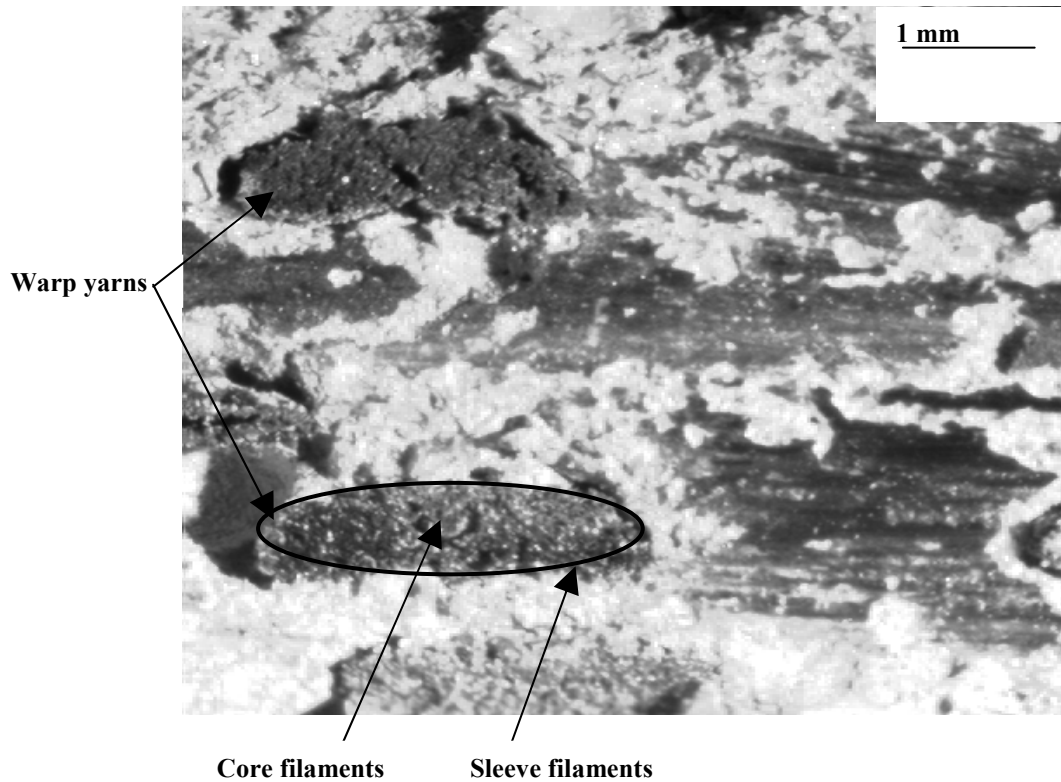
Figure 3.20 Image of surface cut parallel to weft yarns of glass textile in tested specimen

3.4.2 Pull-off Test

In order to determine the bond strength and assess the compatibility of *FABmix* with substrate concrete, pull-off tests were performed as per ASTM C1583 (2004). Concrete specimens of 100mm diameter and 25mm thickness were cast with a mix having the proportions of cement: fine aggregate: coarse aggregate as 1:2.12: 2.23, by weight, with a water-cement ratio of 0.45. A 5mm thick layer of *FABmix* was applied on top of the concrete specimens after curing them under water for 28 days. To conduct the pull-off test, a circular notch of 15mm depth and 50mm diameter was cut on the concrete surface. A metal disc matching the core area was glued using an epoxy resin and subsequently a ball head screw was then fixed onto the disc. The pull-off instrument used had a load capacity of 16kN. In all the tests, the failure occurred in the substrate concrete. The nominal bond strength, calculated by dividing the failure load with area of core, was 2.35MPa (±8.7%), which is close to uniaxial tensile strength of *FABmix*.

Further, to assess the bonding of *FABcrete* with concrete, cubes of 150×150×150mm were cast with concrete having the proportions of cement: fine aggregate: coarse aggregate as 1:2.12: 2.23,

51

by weight, with a water-cement ratio of 0.45. A 10mm thick layer of *FABcrete* with five layers of SRG-45 was adhered to the top of the cube. A circular notch of 15mm depth and 50mm diameter was cut on the surface. As before, the pull-off load was determined and the bond strength was calculated. The test set-up used for the investigation is shown in Figure 3.21. In all the tests, the failure occurred within the *FABcrete* layer, along the third textile layer (from the top); the nominal bond strength obtained was 1.92MPa (±4.4%).

Figure 3.21 Pull-off test on *FABcrete*

3.4.3 Test for Integrity Between Old Concrete and *FABcrete*

When *FABcrete* is used as a strengthening material, the cementitious binder itself acts as an adhesive to existing concrete. In order to check the integrity of *FABcrete* with concrete and to examine the final failure pattern, a limited study on concrete specimens jacketed with *FABcrete* was carried out. Concrete cylinders of 150mm diameter and 300mm height were cast with mix proportions of cement: fine aggregate: coarse aggregate as 1: 2.12: 2.23, by weight, with a water-cement ratio of 0.45. The cylinders were demoulded after 24 hours and were wrapped with a 8-10 mm thick layer of *FABcrete* consisting of 1 layer of SRG-45 (without any special surface preparation). The *FABcrete* jacketing was done on the cylinder by first applying a layer of *FABmix,* then wrapping the layer of the SRG-45 textile and finally applying an exterior layer of

FABmix. Later, the specimens were air cured for 24 hours and then immersed in water for 28 days.

Sulphur capping was done to ensure the uniform load transfer to the specimens. A servo-controlled UTM machine was used to test the specimens under uniaxial compression with a constant piston displacement rate of 0.5mm/min till final failure. Nominal axial strain was taken to be piston displacement divided by the specimen height. Figure 3.22 gives a typical stress versus nominal axial strain curve for cylinders, with and without the *FABcrete* jacket. The peak stress exhibited by *FABcrete* jacketed specimen is around 41.5MPa (±4.5%) and corresponding nominal strain is 0.004 (±9.12%). In the case of unjacketed specimens, the peak stress is 38MPa (±6.1%) and corresponding strain is 0.002 (±10.34%). The values indicate that the jacketed specimen exhibits higher peak stress and strain compared to unjacketed specimen. As loading progressed, it was observed that the specimen confined with *FABcrete* acted integrally, with failure occurring with a vertical splitting crack, as seen in Figure 3.23. There was no debonding of *FABcrete* from the concrete surface throughout the test and the failure of all specimens were in a controlled manner. Even in other tests on jacketed cylinders with 2 and 5 layers of textile, no debonding failure was observed.
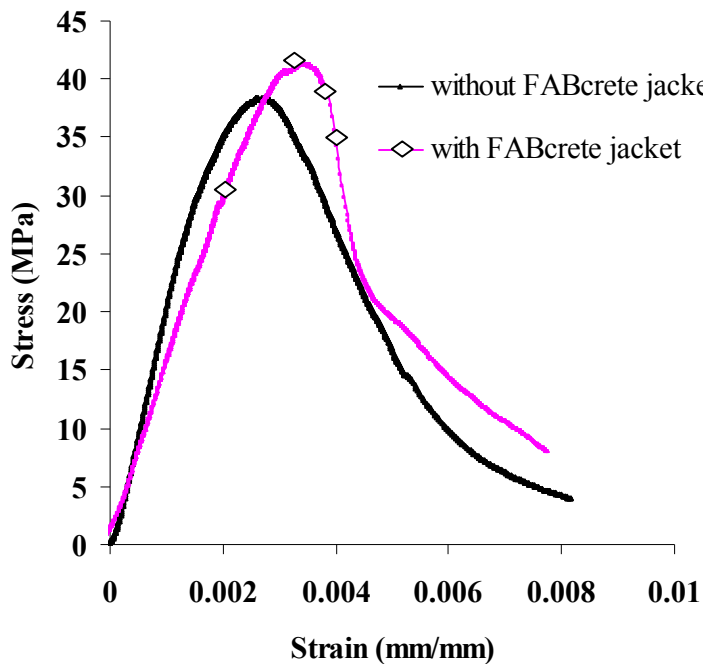
Figure 3.22 Stress versus axial strain curves

Figure 3.23 Typical failure of F*ABcrete* jacketed specimen

3.5 SUMMARY

In this chapter, the development of *FABcrete* with the cementitious binder and alkali-resistant glass textiles have been discussed. The details of the cementitious binder (*FABmix*) with required workability and mechanical properties have been reported. The applicability of two types of glass textiles have been investigated and performance evaluation has been done to find the suitability as a reinforcement in *FABcrete*. Bonding of FABcrete with concrete was also investigated and the integrity of *FABcrete* with existing concrete (without using any anchoring) has been shown.

CHAPTER 4

UNIAXIAL TENSILE CHARACTERIZATION OF *FABcrete*

4.1. INTRODUCTION

Generally, for the design and dimensioning of TRC components, the constitutive behaviour in tension needs to be obtained from appropriate tests. The methodology should be such that the data can be accurately reproduced with low effort and preferably low cost. Detailed tensile characterization is necessary to understand and utilize the full potential of TRC when different textiles or combination of textiles are used. This often necessitates modification of existing or development of new test setup to determine the mechanical properties.

The investigations carried out to develop a uniaxial tensile test methodology for *FABcrete* followed by a study of the tensile behaviour are reported in this chapter. The design of the uniaxial tensile test setup is explained in Section 4.2. The specimens used in the investigations were reinforced with textiles in two ways, one in which the textiles were placed by manual stretching and the other by mechanical stretching of the textiles during casting. Elaborate studies on tensile behaviour of *FABcrete* with SRG-45 and AR1 textiles, and their combinations are reported in Sections 4.3. The stress-strain characteristics and related parameters for design are discussed in detail in Section 4.4. In addition, Section 4.5 reports the investigations related to damage assessment in *FABcrete* using X-ray computed tomography.

4.2. DEVELOPMENT OF THE TEST SETUP

Different types of uniaxial tension test setup have been used by researchers in the study and development of TRC (Dugas et al. 1998, Jesse 2004, Brockmann and Raupach 2002, Orlowsky and Raupach 2006, Molter 2005, Brameshuber et al. 2010, Hartig et al. 2012). There is difference in the specimen geometry, dimensions and the way the load is applied in most of the test set-ups. Some of these have been described in detail by Hartig et al. (2012); see Figure 4.1. Usually, the TRC specimens used are either rectangular or dumbell in shape with a thickness of 5mm to 20mm, width of 30mm to 100mm, and length less than 1m (Hartig et al. 2010). While examining the details reported by Hartig et al. (2012), it is observed that the basic specimens are

panels (Figures 4.1 a,b), which can be prepared with the least effort. The dumbbell specimens, shown in Figures 4.1 c&d, require more effort in specimen preparation, mainly due to the embedding of the textile. The most complicated specimen with regard to preparation is that shown in Figure 4.1e, where the specimen is thicker at the ends to reduce the stress concentration at the grip and ensure failure within the free length. A drawback of such specimens is that they often crack in the offset zones, leading to an influence of the specimen geometry on the tensile response.
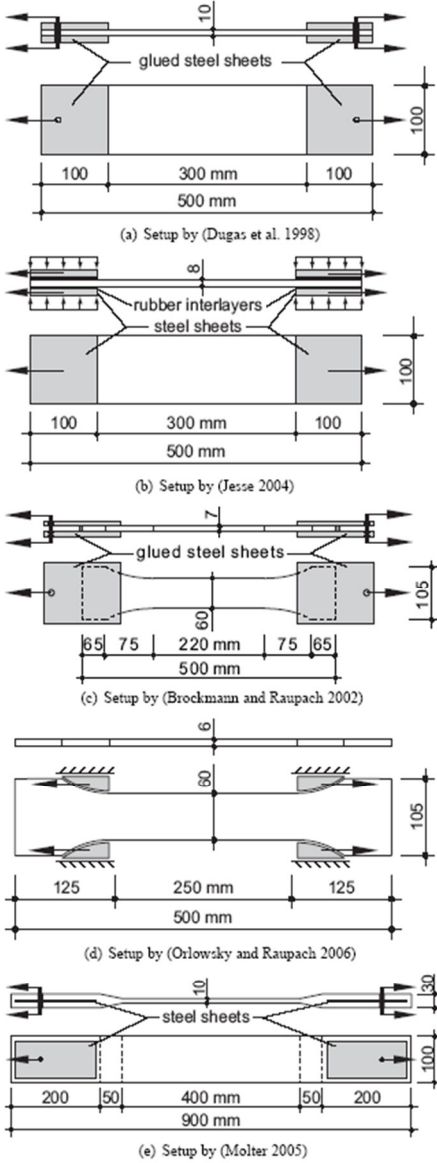
Figure 4.1 Different setups used for uniaxial tensile characterization of TRC (Hartig et al. 2012)

Different grip configurations are used to connect the specimen to the testing machine (Figure 4.1). A common technique is to adhere steel sheets to the specimen as, e.g., shown in Figures 4.1(a&c). This leads to the stiffening of the supported parts of the specimen and suppression of cracking. One such setup, which allows some cracking within the supported part of the specimen is shown in Figure 4.1(b), here the specimen is gripped through rubber layers placed between the specimen and steel plates to prevent local stress concentration. Thus, the load is primarily applied by friction. Another clamping technique used in the setup shown in Figure 4.1(d), where steel flanges fitting to the waist of the specimen is used for load application. This technique supposedly leads to multi-axial stress states in the specimen, at least in the vicinity of load application, which is undesirable. A different technique used in the setup where the load is applied by means of bolts is shown in Figure 4.1(e). In this case, perforated steel sheets are embedded at the ends of the specimen to distribute the concentrated load.

As far as the type of load application is concerned, it can be generally categorized into two types. One is by adhesion (Type A) and another one is by Coulomb friction (Type B). For Type A load application, steel plates are glued to the specimen (Figures 4.2 a&c) or a steel sheet is placed inside the specimen (Figures 4.2e). In these cases, no slip should take place between the steel sheets and the specimen. For Type B load application by soft clamping (Figure 4.2 b), the concrete cracks in the supported parts of the specimen can occur and slip can also occur between specimen and grip. Recently, Hartig et al. (2012) examined the differences in the apparent load-bearing capacity of the TRC with Type-A and Type-B load application. From their studies, it was concluded that there is a dependency of the load application type on the ultimate load and final crack location in the specimen. Tests with Type-A gripping showed lower ultimate loads and frequent failure of the specimens adjacent to the transition between the gripped and free parts of the specimens. In contrast, tests with Type-B gripping had higher ultimate loads and final cracking mainly within the free part of the specimen.

It is observed that various configurations have been developed and used in the literature and there has been no agreement on the standard configuration that would be acceptable. Hence, preliminary investigations were carried out to arrive at a configuration for the tensile characterization of *FABcrete*. The objectives set are the determination of the geometry of specimen to be used; development of a stretching mechanism for textiles in *FABcrete* in the

specimen fabrication and determination of type of gripping configuration to arrive at a suitable test configuration for *FABcrete*. Detailed discussions on each of these aspects are given in the subsequent sections.

4.2.1 Specimen Preparation

Two types of *FABcrete* specimens are prepared in the present investigation. In one type, the textiles are placed in the mould by providing a light manual stretching during casting of the specimen. In the second type, a mechanical force was applied to the textiles using a special mechanism during casting. The details of both the type of specimen preparations are discussed in the following Sections.

4.2.1.1 *FABcrete* with manually stretched textile

In the present study, the rectangular geometry was considered, and specimens of 500 (length) ×60 (width) × 11 to 12 (thickness) mm were cast; see details in Figure 4.2. The specimens were prepared in steel moulds using a hand lay-up technique with the following sequence: a layer of cementitious binder (*FABmix*) was cast followed by placement of the required number of textile layers by manually stretching and finally one more layer of *FABmix* was cast; see Figure 4.3. The placement of layers of textiles in between layers of cementitious matrix is as shown schematically in Figure 4.4. The overall thickness of the specimen was controlled by using edge strips of appropriate thickness. After one day, the specimens were removed from the moulds and cured under water for 28 days. After the curing period, the specimens were maintained in the laboratory environment until testing.
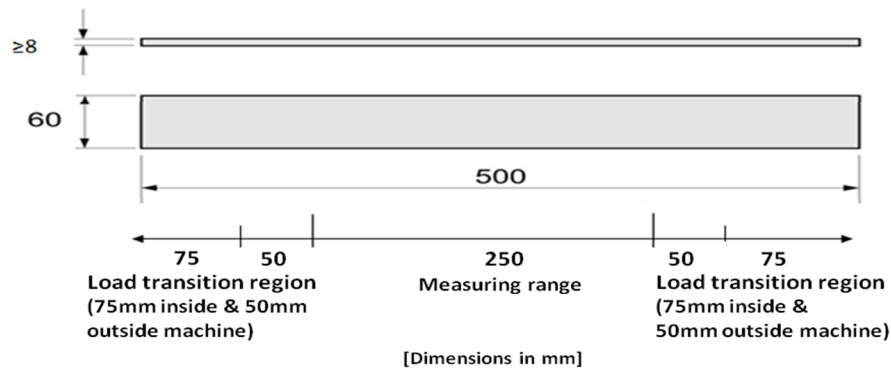
Figure 4.2 Geometry of the test specimen

Figure 4.3 Casting of specimens
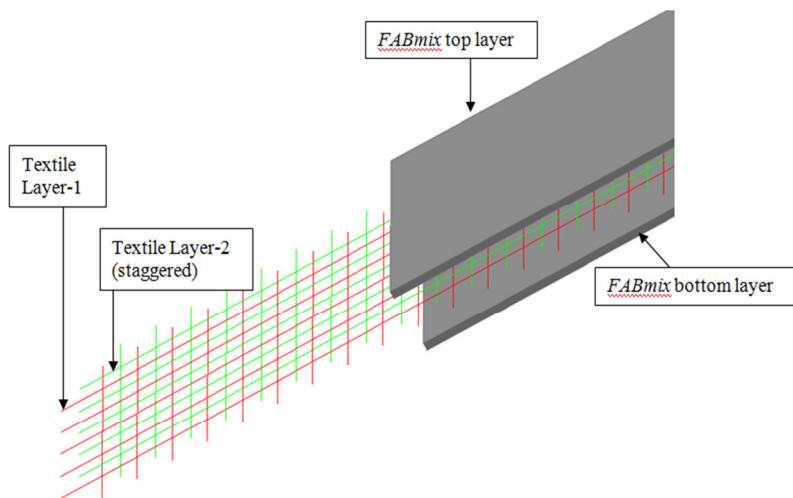
Figure 4.4 Schematic representation of placement of textiles and matrix

4.2.1.2 *FABcrete* with mechanically stretched textile

The mould used for casting rectangular *FABcrete* specimen was designed such that it has a mechanism to stretch the textile, as shown in Figures 4.5(a) and 4.5(b). The moulds had adjustable edge strips for varying the specimen thickness while casting and also for the placement of textiles at the desired level. For casting the *FABcrete* specimen, after deciding the position and number of layers of textile, the bottom-most strips are fixed at all edges. On top of

that, at one end, the required number of layers is fixed and steel strips are bolted; and at the other end, certain extra length of textile is allowed to project beyond the specimen length and the end strip is bolted. There are two angle-section connected by bolts at the stretching side and there is a fixed angle-section at the other end. While tightening the two bolts on the angle-section, the textile undergoes stretching with one full rotation of the bolt giving 1mm extension of the textile. Once, the tightening is completed, visual examination was carried out to ensure that most of the yarns in the textile are straight. Here, the textile is stretched only in the longitudinal direction since only these yarns are subjected to tensile load. Figure 4.5(b) shows the textiles in stretched position for casting *FABcrete*.
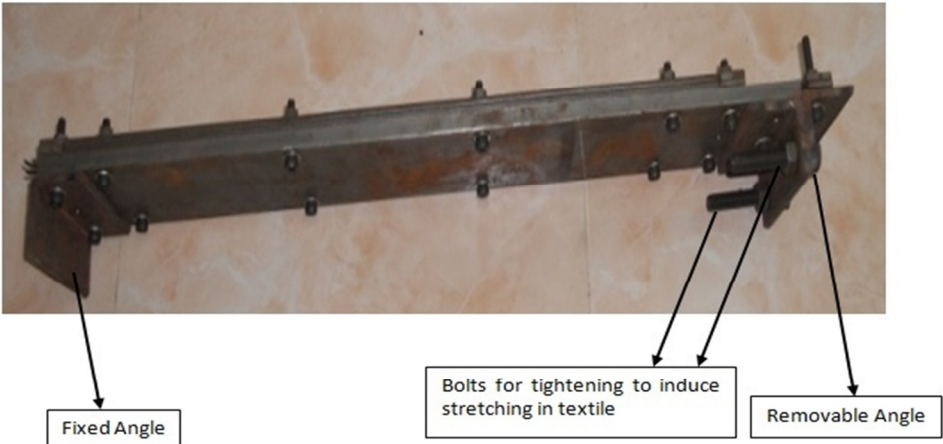
(a)
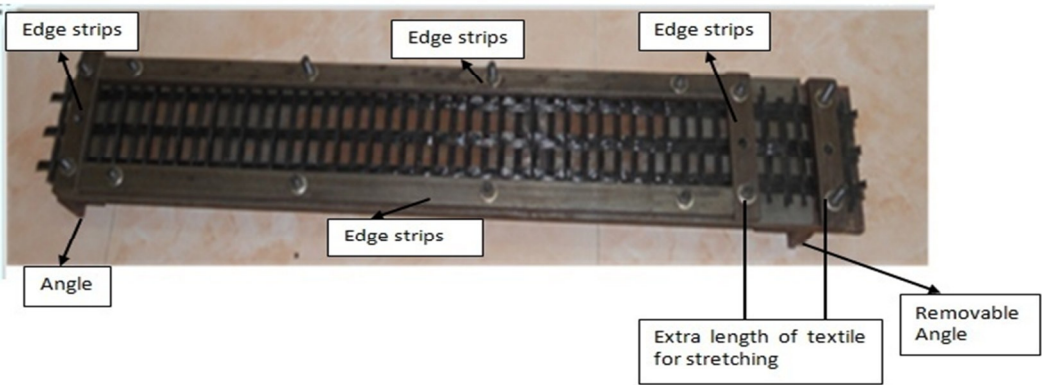
(b)

Figure 4.5 Mould with stretching mechanism - (a) Sectional view and (b) Textiles in stretched position

Rectangular specimens of 60mm×8mm cross section with a length of 500mm were cast to investigate the tensile behaviour of *FABcrete* with textiles in stretched position. The layers of stretched textiles were placed between layers of cementitious matrix, as shown schematically earlier in Figure 4.4. A hand lay-up method is used for casting the *FABcrete* specimens. At the bottom of the mould, a 2mm thick gap is left and above that the required number of textiles are placed in direct contact with each other in a staggered manner. Subsequently, textiles are stretched using the mechanism described above. In all cases, the warp yarns are kept parallel to the length of the specimen. After placing the textiles in stretched position, *FABmix* is poured into the mould till a final thickness of 8mm is achieved. The textiles are kept in the stretched position till demoulding of specimen on the next day. After demoulding, the specimens are cured under water for 28 days, after which they were maintained in the laboratory environment until testing.

4.2.2 Gripping configurations

Two types of load transfer mechanisms were considered for *FABcrete* specimens, one by Coulomb friction and another by adhesion. In both cases, the gripping pressure exerted from the machine was kept at 0.6MPa to avoid any local crushing of the specimen at the gripping portion. Another objective of designing the grips was to ensure that the failure of the specimen does not occur near the gripping portion.

To transfer load by means of Coulomb friction, a soft clamping technique was used (see Figure 4.6). The *FABcrete* specimen was first bolted in between steel plates of 125mm length but this resulted in cracking within the gripped part of the specimen and slip between specimen and clamping. To improve the friction, rubber sheets were placed in between the specimen and steel plates but even then there was slip and cracking. Even gluing the rubber sheets to the specimen did not eliminate these problems. Since the failure was always in the grip portion, this method was not used further in the investigations.

For achieving load transfer by adhesion, three materials (steel plates, woven glass fabric and carbon fiber reinforced polymer (Carbodur) plates) that are all stiffer than *FABcrete* were tried. In the first trial, the ends of the specimen were glued to rubber layers and then to stiff steel plates by means of adhesive (Araldite) on both the sides and mounted in the hydraulic grip of the

testing machine. The gripped part of the specimen had a length of 125mm, at each end. There was slip in the specimen from the grips and the test could not proceed further. In the next trial, woven glass fabric is wrapped and glued around the ends of the specimen using resin in order to transfer load. In this case, the woven roving ruptured and the failure was again within the grip. Finally, Carbodur plates were glued to the ends of the specimen with a resin for gripping the specimen. While using Carbodur plates, two configurations were considered, as shown in Figure 4.7. In one case a square cut Carbodur plate with a length of 125mm and width equal to that of the specimen (i.e., 60mm) is glued to either side of the specimen end. In the other case, the Carbodur plate has 60mm width upto 75mm and then tapers from 60mm width to 30mm over a length of 50mm. The tapering was done to avoid sudden transition of load in the gripping region. When Carbodur plates were glued to the specimen, no slip was observed. There was no grip failure in either configuration. However, in the specimens with square cut Carbodur plates, the final failure was by rupturing near the transition region while, in the specimens with tapered Carbodur plates, the textile rupture was much within the free length. Hence, tapered Carbodur plate were glued in the specimens during the remaining investigations.

(dimensions in mm)
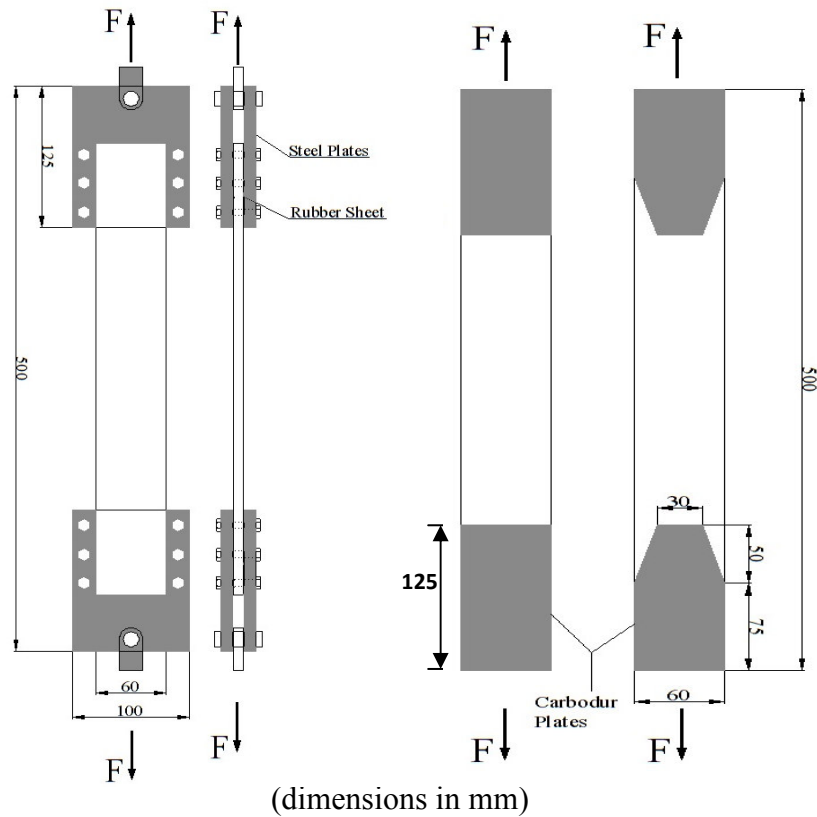
Figure 4.6 Soft clamping   Figure 4.7 Carbodur plate adhesion

4.2.3 Test setup and instrumentation

The tests were conducted in a closed-loop servohydraulic INSTRON 8802 system with a capacity of 250kN, with hydraulic grips. The load and displacements were monitored and recorded using the INSTRON Bluehill software. To define the nominal strain, displacements were obtained using two LVDT measurements. When LVDTs were used, a HBM Catman professional data logger was used to acquire the displacement data at 10 Hz. The specimens were fixed in the testing machine, leaving a platen to platen distance of 350mm and a LVDT gauge length of 250mm. To measure the displacement, two LVDTs were placed along the central line in either side of the specimen. The average of both LVDT outputs (displacements) was used to calculate the strain. The load was measured directly from the load cell attached to the cross head. The setup of a typical instrumented specimen is shown in Figure 4.8. Tests were conducted using a displacement controlled loading rate of 0.5mm/min. A crack width measuring microscope was used to determine the maximum crack width at peak load.

(a) Side view   (b) Front view
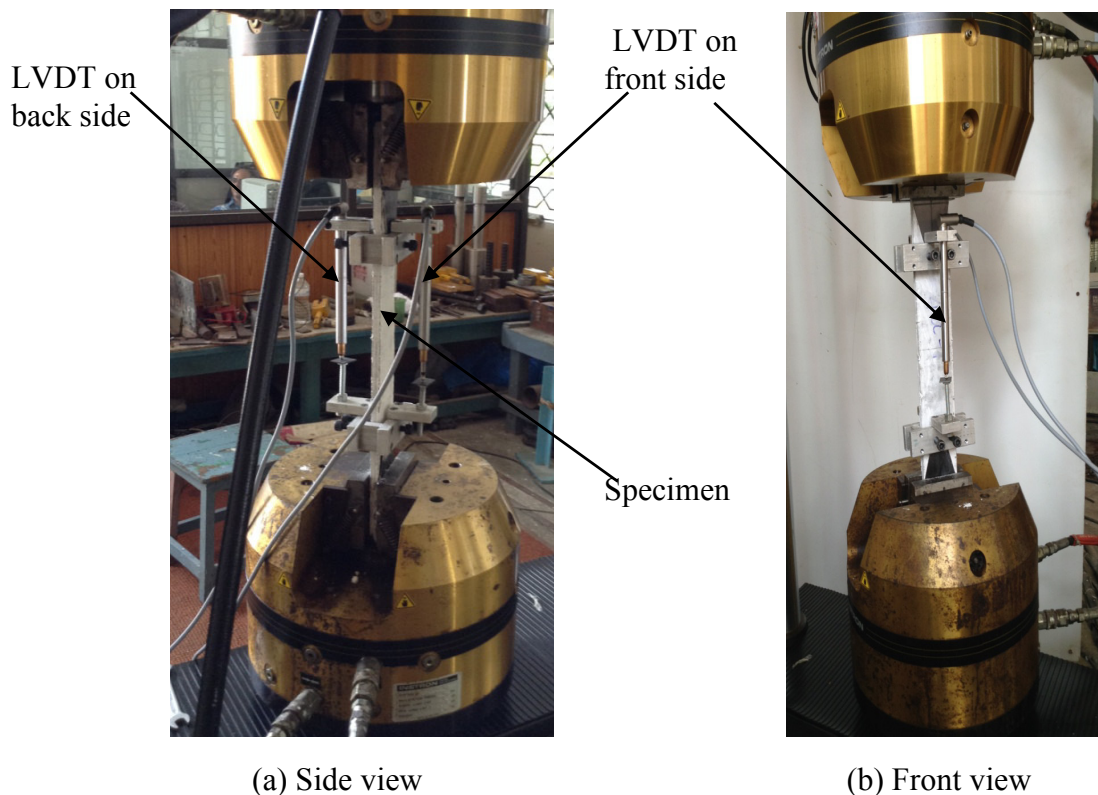
Figure 4.8 Typical setup and instrumented specimen

4.3. STUDIES OF UNIAXIAL TENSILE BEHAVIOUR OF *FABcrete*

Uniaxial tensile tests were carried out on *FABcrete* specimens reinforced with textiles in two ways, one in which the textiles were placed by manual stretching and the other by mechanically stretching the textiles during casting. A detailed characterization programme is reported here for the determination of the stress versus strain behaviour of *FABcrete* to subsequently arrive at appropriate parameters for design. The performance of different glass textiles and the influence of number of layers (volume fraction of textile) in *FABcrete* were the main parameters in the study.

4.3.1 Specimen details for *FABcrete* with manually stretched textile

Three types of rectangular specimens (500mm length and 60mm width) of *FABcrete* with the manually stretched textiles SRG-45 and AR1, and combinations of SRG-45 and AR1 were considered; see details in Table 4.1. The thickness of specimen is 11mm when the number of layers are less than 5, and 12mm for the remaining specimens (see Table 4.1). This difference was mainly because of the difficulty faced during placing more number of textile layers.

Based on the cross sectional dimensions and the area of number of layers of textile, the volume fraction of glass textile (V_f) in each specimen is calculated as:

$$V_f = 100 \times A_f/A_c$$

where A_f and A_c are the cross-sectional areas of the textile and specimen, respectively. The area of textile was calculated using the uncoated textile weight per unit area and the density of glass fiber that are reported in Section 3.3 of Chapter 3. Based on the calculations, the cross-sectional area per unit width for SRG-45 is obtained as 33.58mm^2/m and for AR1 as 16.8mm^2/m. These details are used to arrive at the textile volume fraction (V_f) reported in Table 4.1.

In the tests, 3, 4 and 6 layers of SRG-45 were used, giving textile volume fractions of 0.89%, 1.19% and 1.62% respectively. For 3, 5 and 6 layers of AR1, the textile volume fractions are 0.45%, 0.66% and 0.84%, respectively. In the combinations of SRG-45 and AR1, 3 layers each of SRG-45 and AR1 with a total volume fraction of 1.27% were used. In Table 4.1, the notation 3a corresponds to *FABcrete* containing 3 layers of SRG-45 textile. The specimen containing 3

layers of AR1 textile is denoted as 3b and specimen containing the combination of 3 layers each of SRG-45 and AR1 is denoted as 3c. Similar notations have been used for the other cases.

Table 4.1 Details of *FABcrete* specimens with manually stretched textile

Type of textile	Specimen ID	Number of layers of textile used	Thickness of specimen (mm)	Volume fraction, V_f (%)
SRG-45	3MT_3a	3	11	0.89
	4MT_4a	4	11	1.19
	6MT_6a	6	12	1.62
AR1	3MT_3b	3	11	0.45
	5MT_5b	5	12	0.66
	6MT_6b	6	12	0.84
Combination of SRG-45 & AR1	3MT_3c	3 layers of SRG-45 & 3 layers of AR1	12	1.27

4.3.2 Load versus displacement for *FABcrete* with manually stretched textile

Manually stretched *FABcrete* specimens were tested under a displacement rate of 0.5mm/min. Three specimens were tested in each category that is reported in Table 4.1. The average displacement is obtained by using the data captured by both LVDTs placed at the centre line of the specimen on either side covering a gauge length of 250mm. The load versus displacement curves for individual specimens are given in Appendix-B.

It is to be noted that in some of the specimens, the individual measurements of LVDTs located at front and back side vary significantly. Such differences can be attributed to the non-symmetric crack propagation in the matrix at either face of the specimen. In some specimens it is seen that they were not perfectly loaded in uniaxial tension and there is eccentricity due to the initial loss in planarity. In this case the LVDT located on the one side of the specimen recorded compressive strains and the other side the tensile strains. However, the flexure is vanished upon crack development. Based on the investigations carried out, it is recommended to capture the displacement always by using LVDTs on either side of the specimen and use the average value for further calculations and interpretations of results.

4.3.2.1 *FABcrete* with SRG-45

Typical load versus average LVDT displacement is shown in Figure 4.9(a) for *FABcrete* reinforced with SRG-45. It is noticed that there is a linear portion of the load versus displacement curve up to first crack (see zoomed view, when there is a major change in slope). The first cracking load is almost same in all type of specimens irrespective of the increases in number of layers. Beyond first cracking, the load versus displacement curve shows a lower slope, due to the occurence of multiple cracking. As the number of layers increase from 3 to 6, the peak load, initial slope and slope after cracking increase, whereas the displacement corresponding to peak load decreases. The peak load increase is around 66% and 104% as the layers increase from 3 to 4 and 3 to 6. The displacement recorded by the LVDT unloaded when the peak load (maximum load) is reached in most of the specimens, which indicates that the LVDT could not capture the subsequent specimen displacement as the major crack widening occured outside the gauge length. However, no specimen failure or textile rupture was noticed at the peak load.
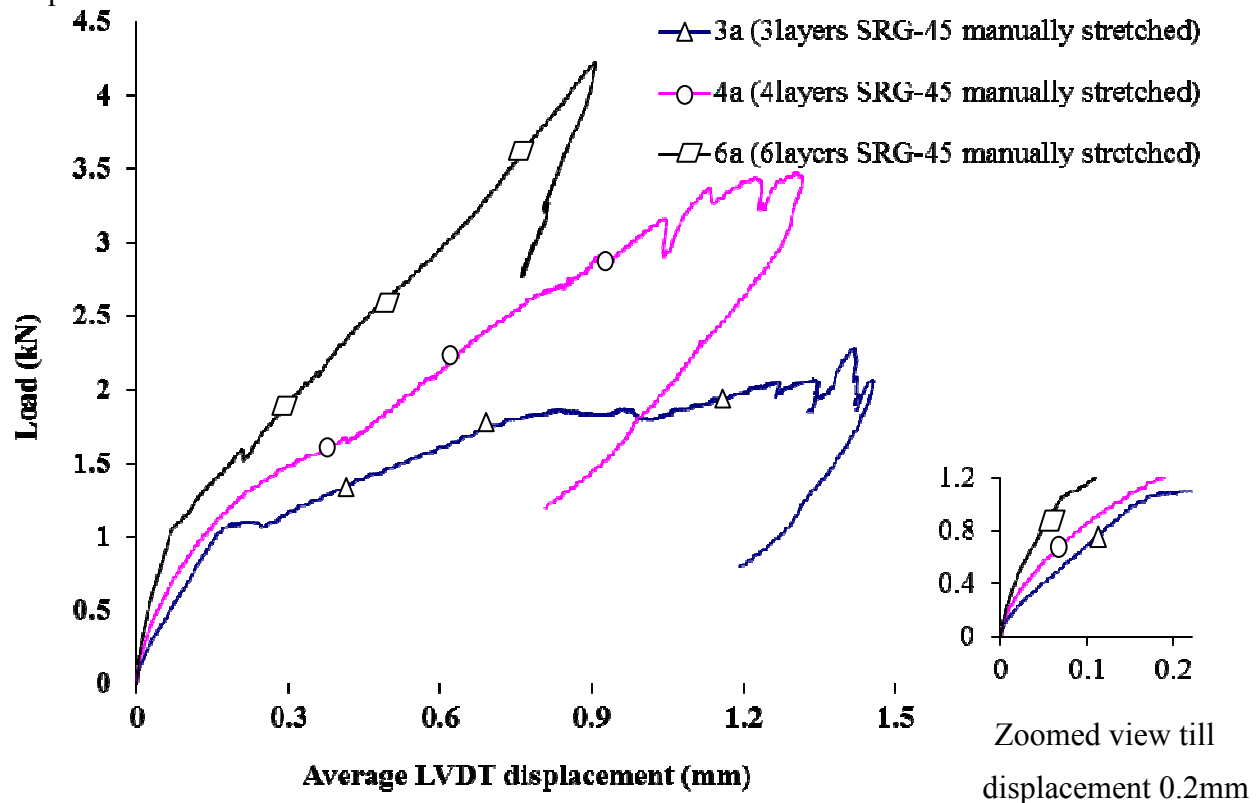
Figure 4.9(a) Typical load versus LVDT displacement curves for *FABcrete* with manually stretched SRG-45

The load versus actuator displacement curve is shown in Figure 4.9(b) for better understanding of the specimen behaviour till the failure of the specimen. From the curve, it is seen that the material possesses significant elongating ability. Since, the displacement captured by the LVDTs are more reliable for material characterization compared to actuator displacement; only the load versus LVDT displacements are considered in the remaining sections.
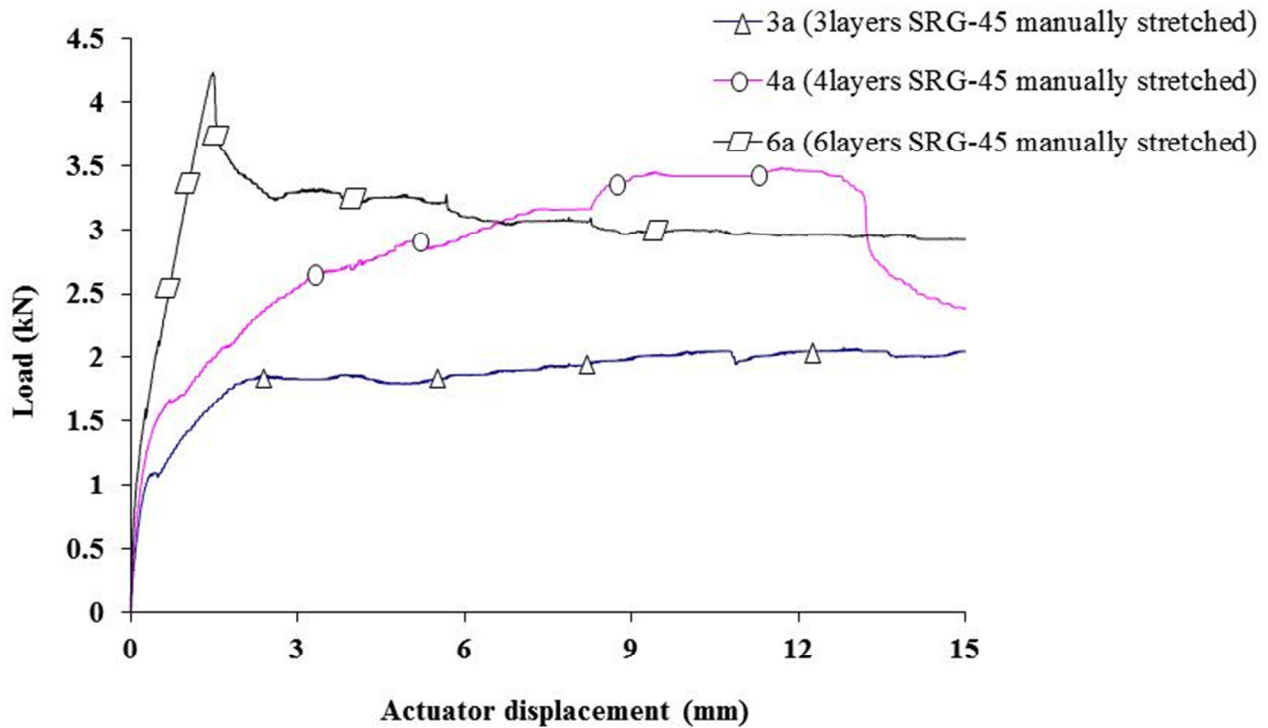
Figure 4.9(b) Typical load versus actuator displacement curves for *FABcrete* with manually stretched SRG-45

4.3.2.2 *FABcrete* with AR1

Typical load versus average LVDT displacement curves are shown in Figure 4.10 for *FABcrete* reinforced with AR1. It is observed that, as the number of layers increases from 3 to 6, the peak load and the displacement increase. Softening is observed for all the AR1 reinforced specimens. In this specimen, as the number of layers increased from 3 to 5, there is 53% increase in peak load, whereas the increase in peak load is 87% when the number of layers changes from 3 to 6. It was further noted that both 5 layer and 6 layer specimens have the same elongating ability (i.e.,

the final displacement at failure is same in both specimens). In all cases, the LVDTs could capture the displacement till the failure of specimen.
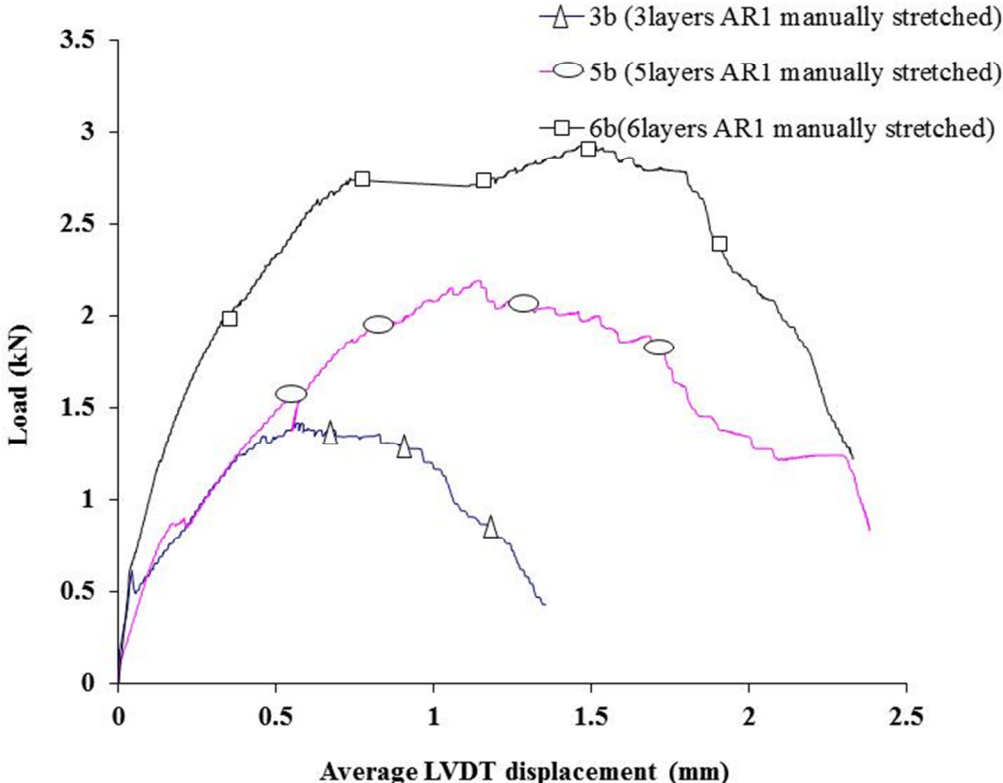
Figure 4.10 Typical load versus displacement curves for *FABcrete* with manually stretched AR1

4.3.2.3 *FABcrete* with combination of SRG-45 and AR1

When a combination of 3 layers each of SRG-45 and AR1 is used in *FABcrete,* the typical load versus average LVDT displacement curve is as shown in Figure 4.11. Since the major crack widening happened outside the LVDT gauge length, it was not able to capture elongation beyond the peak. It is noticed that by combining 3 layers each of SRG-45 and AR1 resulted in superior performance in terms of maximum load carrying ability (41% higher) compared to the sum of the maximum load carrying ability of *FABcrete* with individually reinforced 3 layers of SRG-45 and AR1.
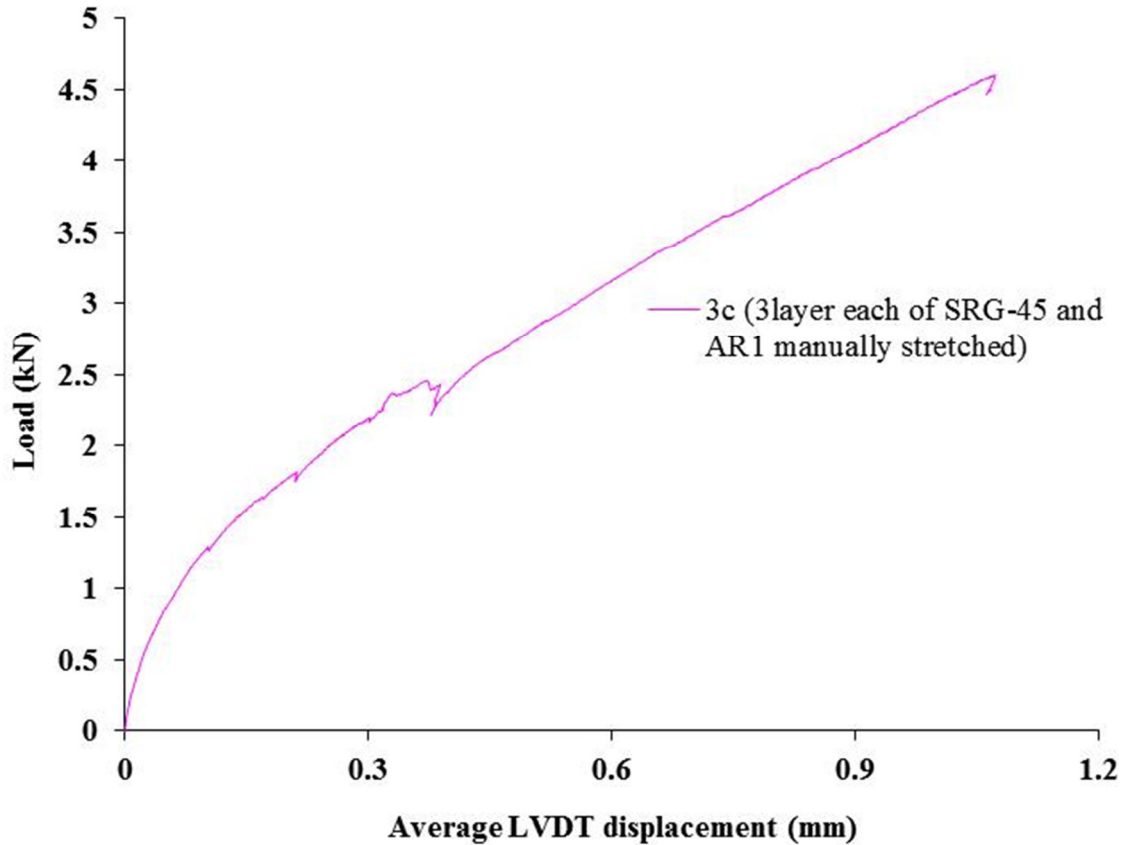
Figure 4.11 Typical load versus displacement curve for *FABcrete* with manually stretched
SRG-45 and AR1

4.3.3 Specimen details for *FABcrete* with mechanically stretched textile

In the tests for *FABcrete* with textiles placed in a mechanically stretched manner (as shown in Figure 4.5), 2, 3, 4 and 6 layers of SRG-45 were used, giving textile volume fractions of 0.84%, 1.26%, 1.68% and 2.5%, respectively. For 2, 3, 4 and 6 layers of AR1, the textile volume fractions were 0.42%, 0.63%, 0.84% and 1.26%, respectively. In the combinations of SRG-45 and AR1, 2 layers each of SRG-45 and AR1 with a total volume fraction of 1.26%, and 3 layers each of SRG-45 and AR1 with a volume fraction of 1.89% were used. Further details about the specimens are reported in Table 4.2. The notation 2a corresponds to *FABcrete* containing 2 layers of SRG-45 textile. The specimen containing 2 layers of AR1 textile is denoted as 2b and specimen containing the combination of 2 layers each of SRG-45 and AR1 is denoted as 2c. Similar notations have been used for the other cases.

69

Table 4.2 Details of *FABcrete* specimens

Type of textile	Specimen ID	Number of layers of textile used	Thickness of specimen (mm)	Volume fraction, V_f (%)
SRG-45	2ST_2a	2	8	0.84
	3ST_3a	3	8	1.26
	4ST_4a	4	8	1.68
	6ST_6a	6	8	2.50
AR1	2ST_2b	2	8	0.42
	3ST_3b	3	8	0.63
	4ST_4b	4	8	0.84
	6ST_6b	6	8	1.26
Combination of SRG-45 & AR1	2ST_2c	2 layers of SRG-45 & 2 layers of AR1	8	1.26
	3ST_3c	3 layers of SRG-45 & 3 layers of AR1	8	1.89

4.3.4 Load versus displacement of *FABcrete* with mechanically stretched textile

FABcrete specimens with textiles placed in a mechanically stretched manner were tested under a displacement rate of 0.5mm/min. Four to six numbers of specimens were tested in various categories as reported in Table 4.2. The average displacement is obtained by using the data captured by both LVDTs placed at the centre line of the specimen at front and back side covering a gauge length of 250mm. Only the typical load versus displacement curves for various specimens are shown for interpretations in this section. The load versus displacement curves for individual specimens are given in Appendix B.

4.3.4.1 *FABcrete* with SRG-45

Typical load versus average LVDT displacement curves are shown in Figure 4.12 for *FABcrete* with SRG-45. The results indicate that the initial slope and the slope after cracking increase as the layers increase from 2 to 6 (see zoomed view in Figure 4.12). In some of the specimens, the LVDTs could not capture beyond peak load since the major crack widens outside the gauge length. All specimens exhibit increasing load as displacement increases with more layers. The increase in peak load is 143% , 213% and 314 % as the number of layers of SRG-45 increases

70

from 2 to 3, 2 to 4 and 2 to 6. Similarly, the increase in displacement at peak load is 2, 3 and 4 times as the number of layers of SRG-45 increases from 2 to 3, 2 to 4 and 2 to 6 and the increase in displacement at failure is 25%, 75% and 150%.

From the overall behaviour, it is noticed that there is a linear portion of the load versus displacement curve up to first crack. Beyond first cracking, the curve shows less slope due to the occurence of multiple cracking. In this state, there were more cracks formed in the specimen followed by equal widening of most of them in the stabilized state. Subsequently, one major crack widened near the peak load and final failure was by rupture of the textile at this crack. Similar behaviour was seen in all cases reported in Figure 4.12.

Zoomed view till
displacement 0.5mm
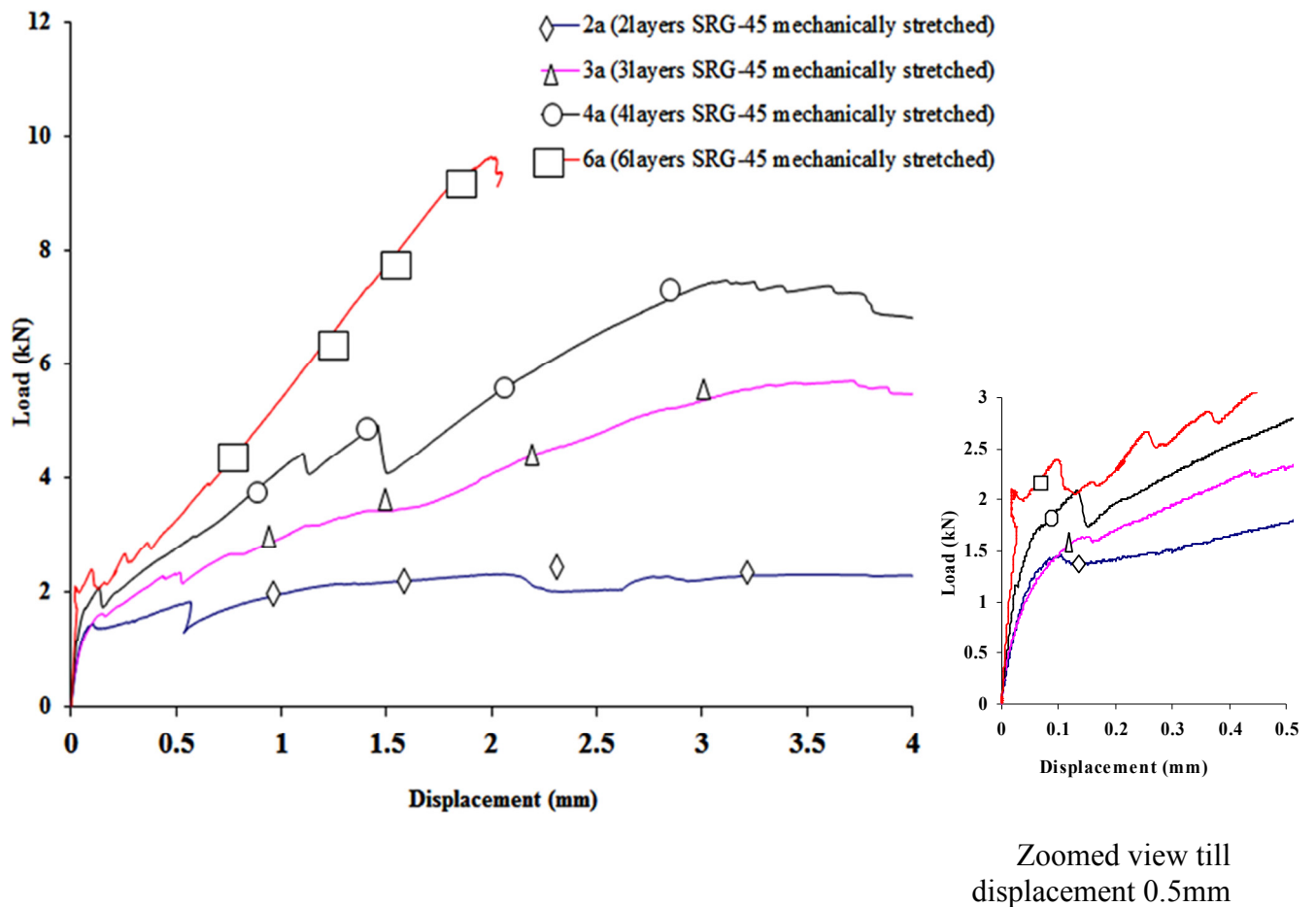
Figure 4.12 Load versus displacement curves for *FABcrete* with mechanically stretched SRG-45

4.3.4.2 *FABcrete* with AR1

For *FABcrete* specimens with AR1 as reinforcement, the typical load versus average LVDT displacement is shown in Figure 4.13. It is observed that as the number of layer increases from 2 to 6, there is an increase in the peak load and corresponding displacement. The initial slope of all the specimen is same in this case (see zoomed view in Figure 4.13). It is observed that as the number of layers of AR1 increases from 2 to 3, 2 to 4 and 2 to 6, the increase in peak load is 43%, 118%, 184% respectively. The displacement corresponding to peak load is almost same in the 2, 3 and 4 layer specimens whereas there is 350% increase in displacement for 6 layer reinforced specimen compared to 2 layer specimen. It is noted that stress transfer between textile and binding matrix after cracking is more effective for the 6 layer reinforced specimens, leading to multiple cracking and strain-hardening. In this case the release of energy at the onset of cracking was small compared to other specimens and allowed strain-hardening type behaviour. However, in the case of the 2, 3 and 4 layer AR1 reinforced specimens, the volume fraction was not sufficient to exhibit strain hardening. The displacement at rupture of 2 layer reinforced specimen is more (i.e., 2.5mm) compared to other specimens, and it is almost the same for 3 and 4 layer reinforced specimens. This indicates that the rupture of textile would have taken place for 3 and 4 layer reinforced specimens soon after reaching the peak load, whereas in the 2 layer reinforced specimen there is possibly pullout followed by rupture in the post peak region.

Zoomed view till displacement 0.5mm
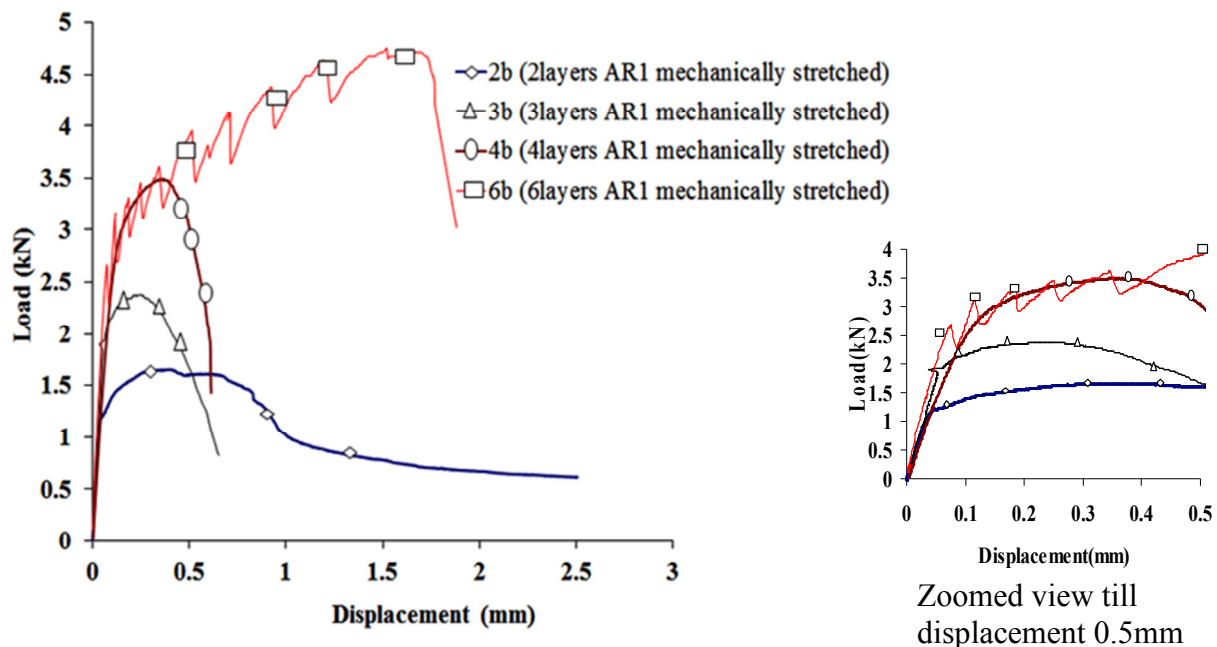
Figure 4.13 Load versus displacement curves for *FABcrete* with mechanically stretched AR1

72

4.3.4.3 *FABcrete* with combination of SRG-45 and AR1

Typical load versus average LVDT displacement curves for *FABcrete* specimens with each 2 layers SRG-45 & AR1 and 3 layers each of SRG-45 & AR1 are shown in Figure 4.14. It is observed that there is only a 22% increase in peak load by adding 1 layer each of SRG-45 and AR1.The peak load obtained by adding 2 layers each of SRG-45 and AR1 is more than sum of peak loads obtained for individual specimens. However, for the specimen with 3 layers each of SRG-45 and AR1, the peak load is less than the sum of peak loads obtained for individual configurations. In these specimens, there was unloading at peak load and major crack widening outside LVDT gauge length. Hence, the further elongation was not captured.
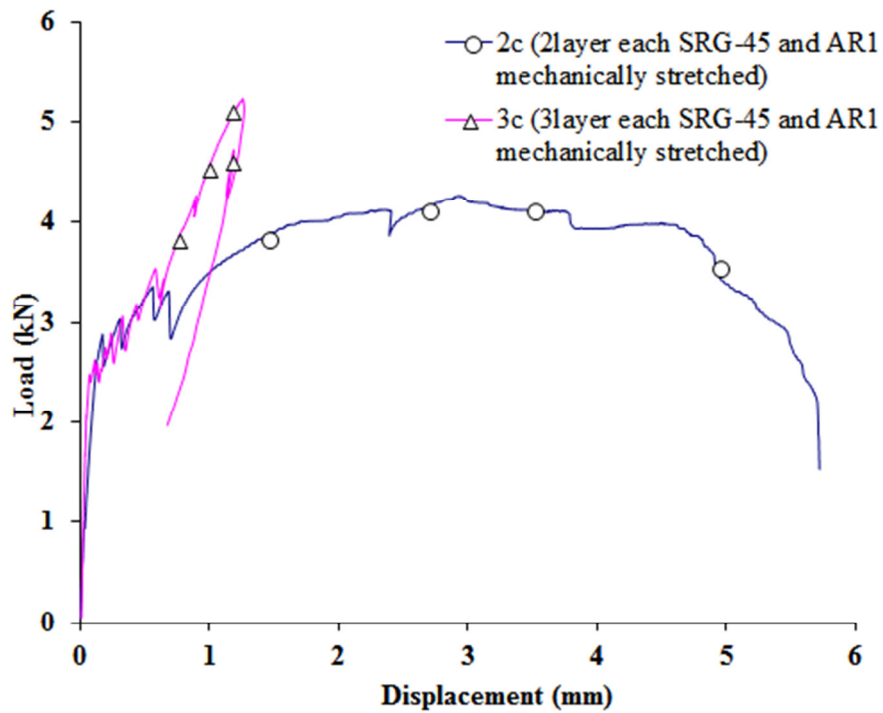
Figure 4.14 Load versus displacement curves for *FABcrete* with mechanically stretched SRG-45and AR1

4.3.5 Cracking and failure pattern

The details about the cracking in various specimens are given in Table 4.3. It is seen that for both manually and mechanically stretched specimens, the number of cracks increased as the number of layers in *FABcrete* increases. For SRG-45 reinforced specimens, in both cases, the average crack spacing reduced as the number of layer increases. In the case of manually stretched AR1

reinforced specimens, there was not much decrease in the average crack spacing as the number of layers increased. However, the average crack spacing reduction was significant in the case of mechanically stretched specimens due to the uniform load transfer from textile to matrix and leading to more number of cracks. The crack width was measured using a microscope just after the maximum load (peak load). It was noticed that there is considerable decrease in crack width as the number of layers increases in specimens with mechanically stretched textile. Figure 4.15 shows the typical failure pattern of *FABcrete* specimens wherein the textiles were manually stretched. It was noted that in all the specimens, the rupture of textile was not seen, which indicates that the yarn pullout or delamination of textile layer from matrix or combination of these would have caused the failure. This was further verified by conducting X-ray computed topographic analysis, which is reported later on in Section 4.5. It can be concluded that the elongating ability of the textiles was underutilized in this case. Figure 4.16 shows the typical specimen failures in *FABcrete* with mechanically stretched textiles. In this type of specimens, the final failure was by the rupture of textile.

Table 4. 3 Crack details

Specimen with Manually Stretched Textile				*Specimen with Mechanically Stretched Textile*			
Specimen id	*No: of cracks*	*Average crack spacing (mm)*	*Crack width at peak load (mm)*	*Specimen id*	*No: of cracks*	*Average crack spacing (mm)*	*Crack width at peak load (mm)*
2MT_2a	Not available			2ST_2a	2	125	0.50
3MT_3a	3	83	0.40	3ST_3a	4	62	0.40
4MT_4a	5	50	0.35	4ST_4a	6	41	0.30
6MT_6a	10	25	0.30	6ST_6a	8	31	0.10
2MT_2b	Not available			2ST_2b	1		0.40
3MT_3b	2	125	0.40	3ST_3b	1	-	0.40
4MT_4b	Not available			4ST_4b	2	125	0.40
5MT_5b	3	83	0.35	5ST_5b	Not available		
6MT_6b	3	83	0.30	6ST_6b	5	50	0.40
2MT_2c	Not available			2ST_2c	6	41	0.30
3MT_3c	10	25	0.25	3ST_3c	8	31	0.10

With SRG-45 textile (Type-a)   **With AR1 textile (Type-b)**   **With SRG-45 & AR1 textiles (Type-c)**

Figure 4.15 Typical failed specimens of *FABcrete* with manually stretched textile
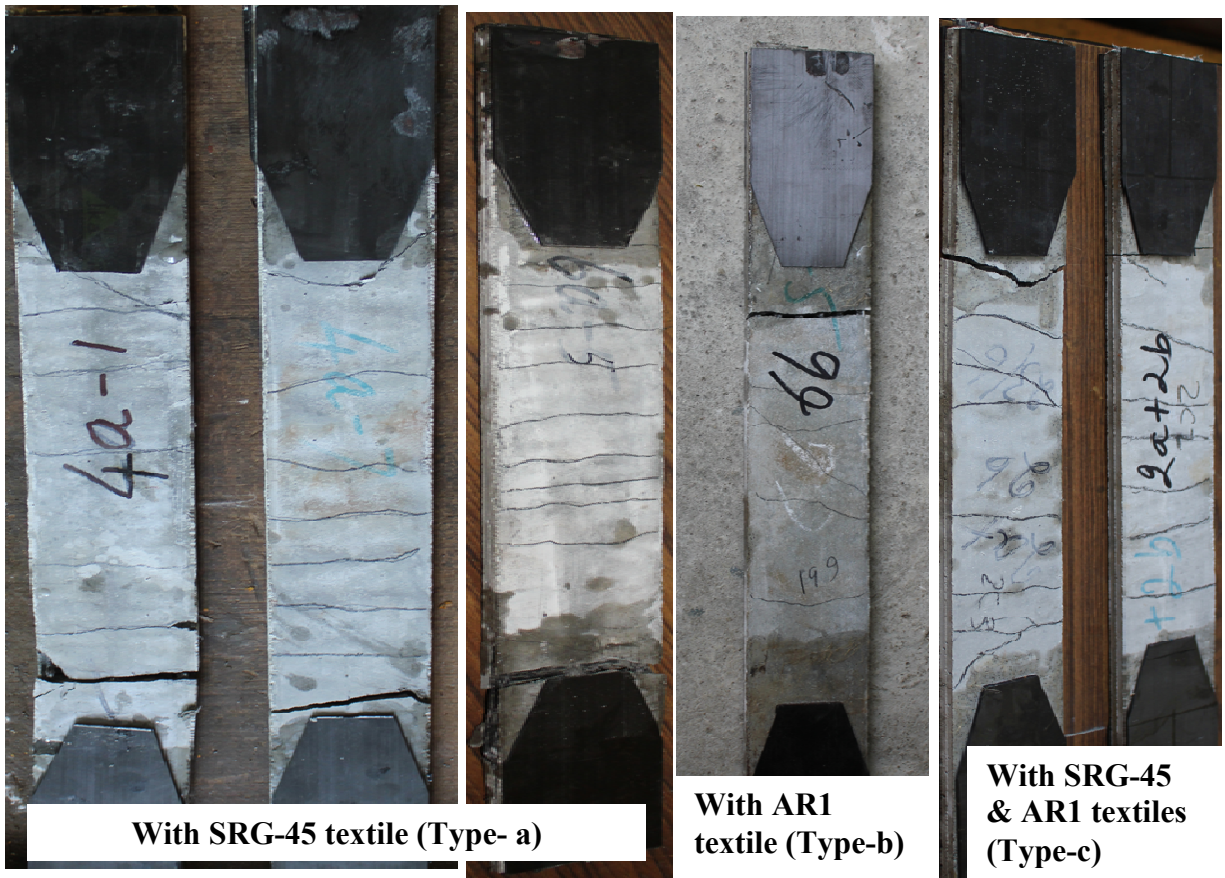
With SRG-45 textile (Type- a)   **With AR1 textile (Type-b)**   **With SRG-45 & AR1 textiles (Type-c)**

Figure 4.16 Typical failed specimens of *FABcrete* with mechanically stretched textile

4.3.6 Summary of the study of the effect of mechanical stretching in *FABcrete*

Based on the investigations reported in earlier sections, it can be concluded that the *FABcrete* with mechanically stretched textile shows better performance compared to specimens with manually stretched textile in terms of higher load carrying ability. However, the strength improvement is not significant in specimens with manually stretched textiles as the number of layers increases, indicating the under utilization of the textile. Hence, it can be concluded that the *FABcrete* with manually stretched textiles can be used in construction, which require more ductility without collapse of the structural member. For specimens with mechanically stretched textiles, even though there is considerable increase in load carrying as the number of layers increases, there is a decrease in the final elongation due to stretching compared to manually stretched specimens. In this type of specimen, both the strength and elongation can be tailored according to the structural requirement by placing specific number of layers and using various combination of textiles. However, the design should be supported by characterization of *FABcrete* for each application.

The variation in peak load (failure load) with an increase in volume fraction and with respect to textile type for *FABcrete,* with manually and mechanically stretched specimens, is shown in Figure 4.17. A relative comparison of the effect of stretching for peak load is seen in Table 4.4(a) and 4.4(b). It can be seen that for lower volume fractions (2 layer specimens with V_f around 0.85%), there is no considerable improvement in the peak load for SRG-45 reinforced specimens. However, as the number of layers increases (3 to 6 layers corresponding to V_f of 1 to 2.5%), there is a significant increase in the peak load. When the volume fraction is around 1.64%, there is almost 50% increase in the peak load for the mechanically stretched specimen. In the case of AR1 reinforced specimens and for combination of AR1 and SRG-45 reinforced specimens, there is no considerable improvement in the peak load between manually and mechanically stretched specimens (see Figure 4.17). Hence, it can be concluded that *FABcrete* with mechanically stretched SRG-45 will be more suitable for structural applications where enhanced tensile strength is required.
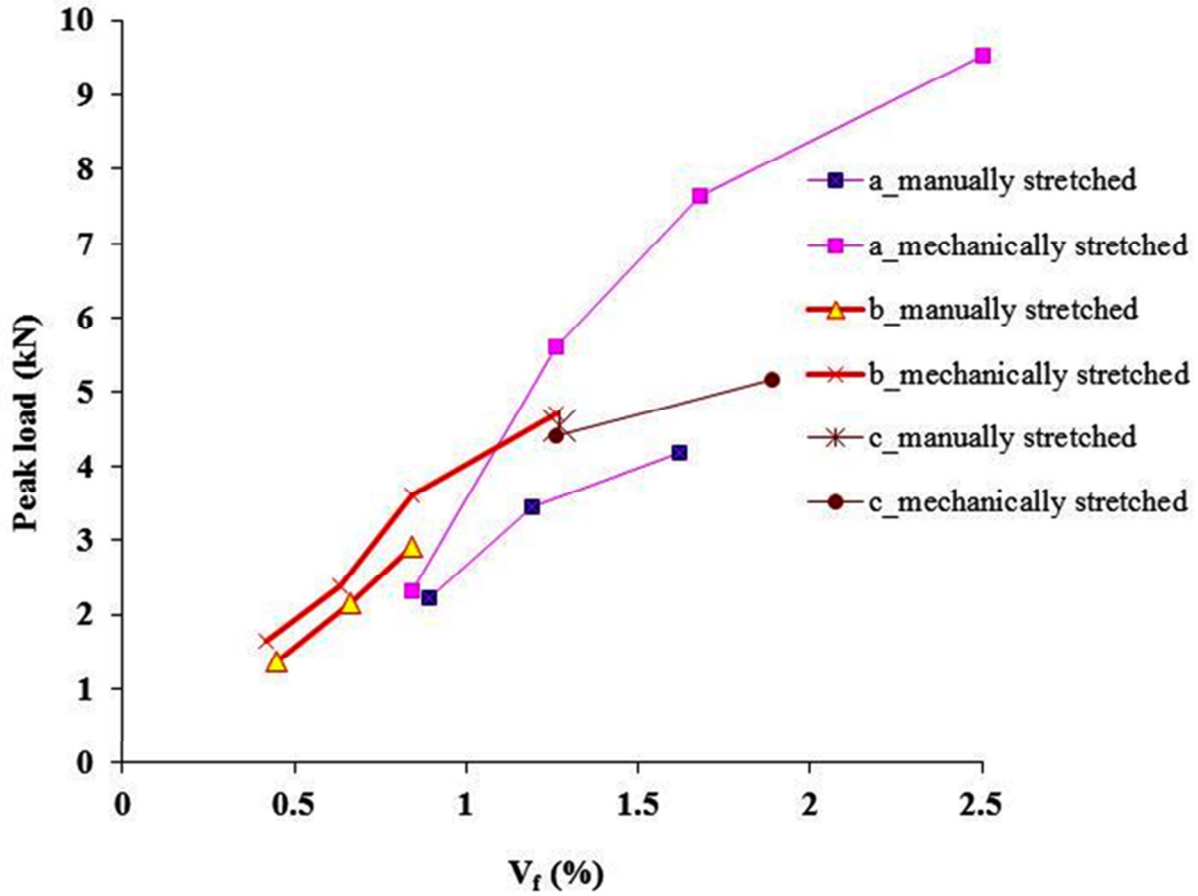
Figure 4.17 Effect of mechanical stretching on peak load

Table 4.4(a) Influential parameters for *FABcrete* with manually stretched textiles

Parameter	SRG-45 (Type-a)			AR1 (Type-b)			SRG-45 & AR1 each (Type-c)
No. of layers of textile	3	4	6	3	5	6	3
Peak load (kN)	2.23	3.43	4.18	1.37	2.15	2.92	4.55
Efficiency (%)	0.31	0.36	0.29	0.25	0.24	0.27	0.36

Table 4.4(b) Influential parameters for *FABcrete* with mechanically stretched textiles

Parameter	SRG-45 (Type-a)				AR1 (Type-b)				SRG-45 &AR1 each (Type-c)	
No. of layers of textile	*2*	*3*	*4*	*6*	*2*	*3*	*4*	*6*	*2*	*3*
Peak load (kN)	2.30	5.60	7.64	9.52	1.65	2.37	3.60	4.7	4.24	5.18
Efficiency (%)	0.48	0.78	0.80	0.66	0.46	0.44	0.50	0.44	0.50	0.41

In order to find out whether the textile is under, over or optimally utilized in *FABcrete*, an efficiency factor is defined as the maximum load carried by *FABcrete* in kN/m divided by the tensile strength of textile in kN/m. The tensile strength of SRG-45 and AR1 textiles is taken from the results of the characterization studies reported in Chapter 3; 40kN/m for SRG-45; 30kN/m for AR1 and 35kN/m for combination of SRG-45 and AR1. The efficiency of various textiles in various specimens with respect to the volume fraction is shown in Figure 4.18. A relative comparison of the effect of stretching on the efficiency of textiles SRG-45, AR1 and their combination can be seen from Table 4.4 (a) and 4.4 (b) as well. It is observed that the efficiency factor of SRG-45 for manually stretched textiles in *FABcrete* is around 0.35 whereas it can be enhanced upto 0.8 by mechanically stretching SRG-45 while placing 6 layers of textile. Hence, it can be concluded that the potential of SRG-45 is underutilized if *FABcrete* specimens are cast with manually stretched textiles. Similarly it can be noted that the efficiency of AR1 specimens and combination of SRG-45 and AR1 is improved from 0.35 to 0.5 by mechanical stretching.
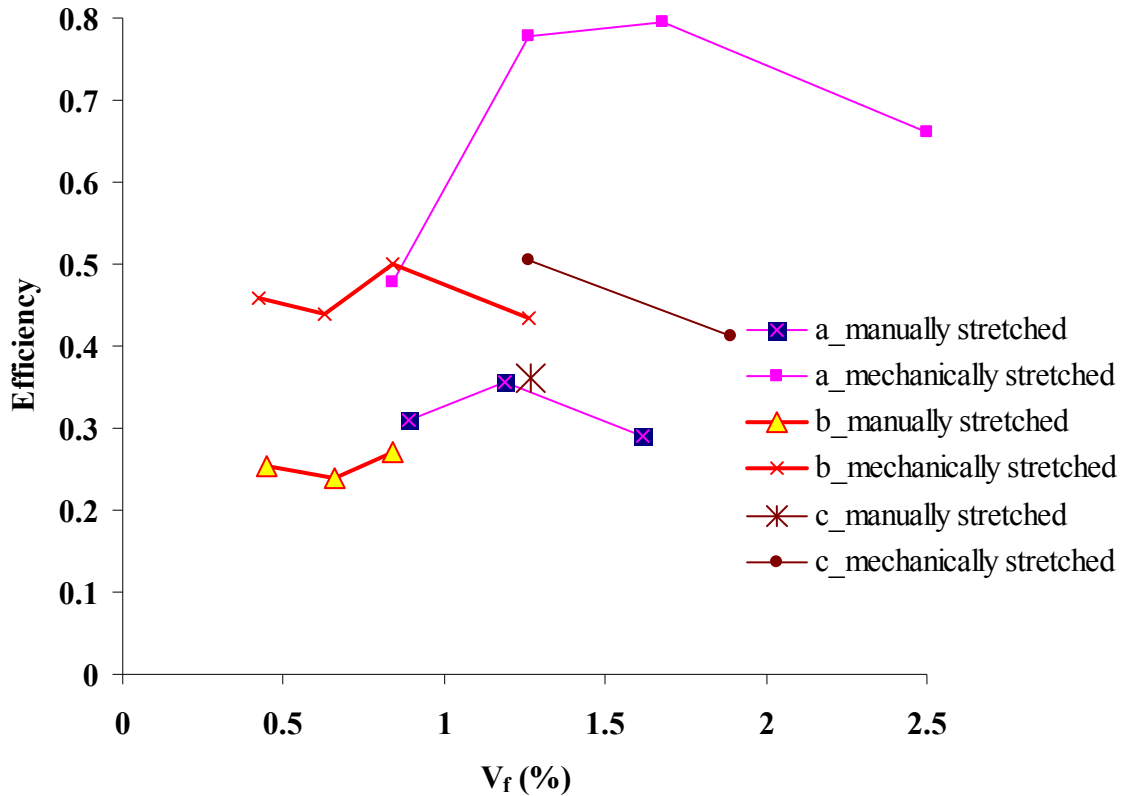
Figure 4.18 Effect of mechanical stretching on efficiency of textile

The effect of mechanical stretching on average crack spacing and crack width corresponding to maximum load (peak load) is shown in Figures 4.19 and 4.20, respectively. It is seen from Figure 4.19 that the average crack spacing is marginally higher for mechanically stretched specimens. For specimens with AR1 textiles placed by mechanical stretching, it can be seen that there is only one crack for the 2 and 3 layer reinforced specimens due to which the average crack spacing is same. However, above 3 layers, there are more number of cracks formed leading to a reduction in average crack spacing. From Figure 4.20, it is noticed that the crack width is less in all type of mechanically stretched cases compared to manually stretched cases except for specimens with AR1 textile, where the crack width at peak load is almost constant irrespective of the volume fraction.
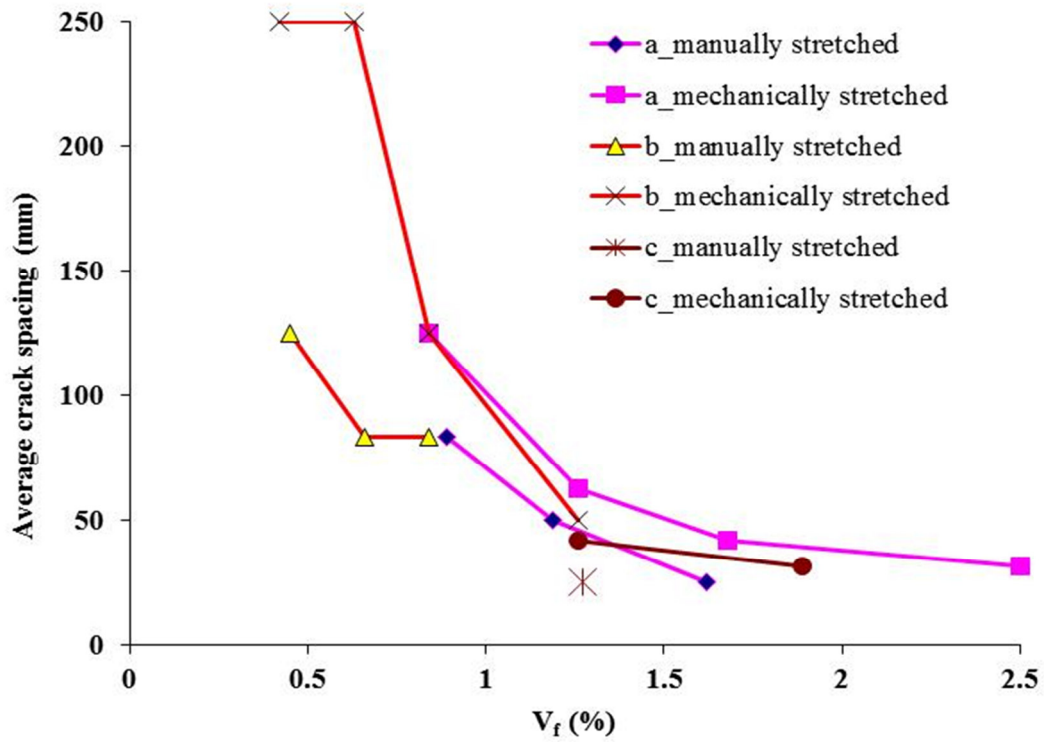
Figure 4.19 Effect of mechanical stretching on crack spacing
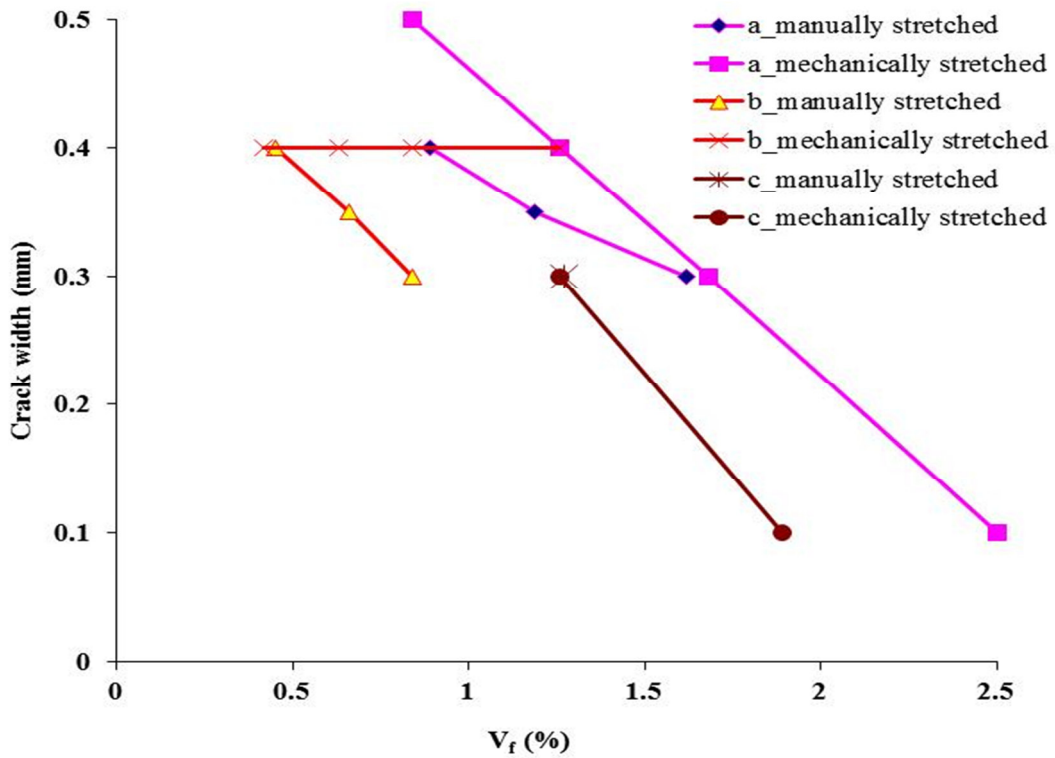
Figure 4.20 Effect of mechanical stretching on crack width

Considering the performance of *FABcrete* specimens with textiles placed in manually and mechanically stretched manner, it was concluded that the mechanical stretching helps to achieve enhanced structural performance. Henceforth, the results of further investigations on uniaxial tensile behaviour reported in Section 4.4 are related to *FABcrete* with textiles placed by mechanical stretching only.

4.4 STRESS-STRAIN BEHAVIOUR

The nominal stress versus nominal strain for *FABcrete* was calculated based on the load versus displacement characteristics that were determined experimentally in Section 4.3. In all cases, the nominal strain is arrived by dividing the average LVDT displacement by the gauge length (i.e., 250mm) of the specimen. For obtaining the nominal stress, the applied force is divided by the cross-section of the specimen A_c (i.e., 60mm×8mm).

4.4.1 *FABcrete* with SRG-45 as textile

In order to assess the scatter in the nominal stress versus strain behaviour between various specimens, a minimum of four *FABcrete* specimens of size 500×60×8mm consisting of various number of layers of SRG-45 were tested. All specimens were tested under a displacement rate of 0.5mm/min. The typical nominal stress versus nominal strain for *FABcrete* with 0.84%, 1.26%, 1.68% and 2.5% volume fractions of SRG-45 (2ST_2a, 3ST_3a, 4ST_4a, 6ST_6a) is shown in Figure 4.21. This figure closely resembles the idealized representation of TRC behaviour given by Mechtcherine (2013) and shown in Figure 4.22, consisting of the crack-free state, multiple crack formation state and stabilized crack formation state with crack widening. It can be seen in the zoomed view of Figure 4.21 that the trend shown in state I and in IIa is similar in all specimens as the number of layers of SRG-45 increases. However, the state IIb is predominant in specimens with more number of layers. The individual data for all the specimens are reported in Appendix-B.
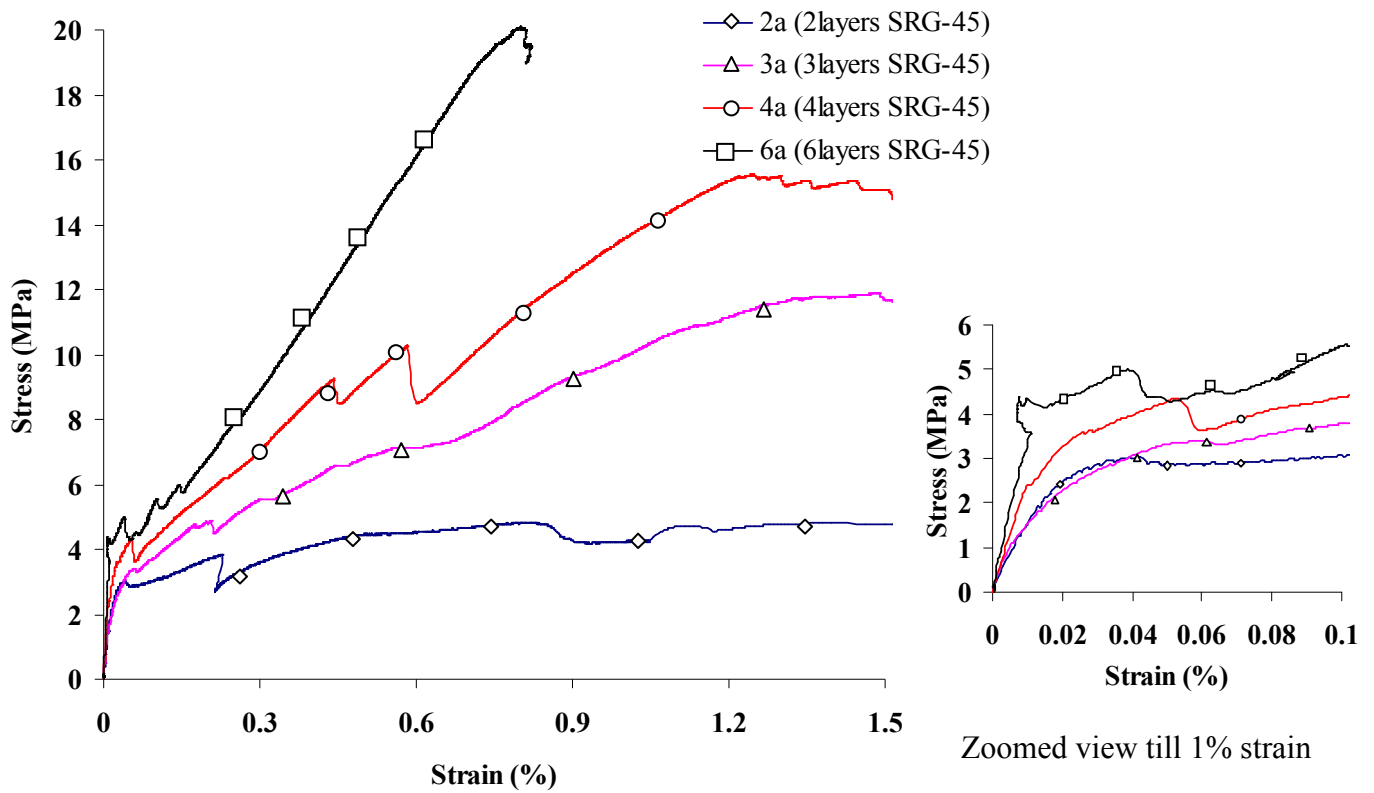
Figure 4.21 Typical stress-strain for *FABcrete* with SRG-45 mechanically stretched
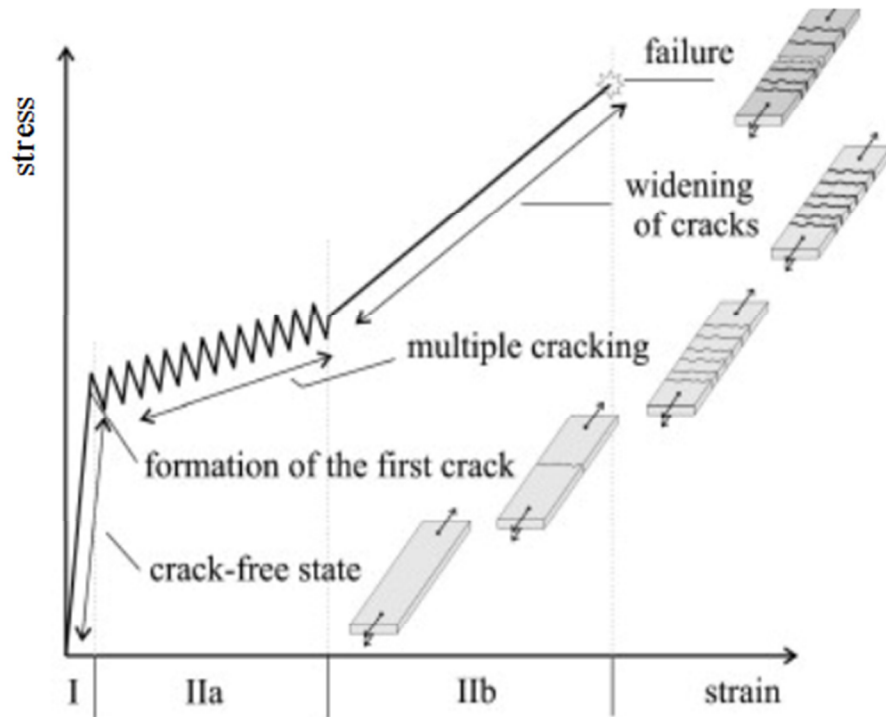
Figure 4.22 Idealized TRC tensile stress-strain behaviour (Mechtcherine 2013)

The results obtained are further used to arrive at parameters of the idealized bilinear stress versus strain curve and the design parameters of *FABcrete* that are mentioned in ACI 449 (2013). The slope of the initial phase of the bilinear curve ($E_{uncracked}$), the slope of the second linear phase of the bilinear curve ($E_{cracked}$), maximum stress (σ_u), the strain corresponding to the maximum stress (ε_u) and the stress (σ_{cr}) and strain (ε_{cr}) corresponding to the first cracking point were determined from the experimental behaviour. The values obtained are reported as mean and standard deviation in Table 4.5.

Two normalized parameters derived from the tension test have been proposed in this work, which is further used in the analytical modelling of *FABcrete* in Chapter 5. The normalized strain parameter (β) is taken as the ratio of 0.6% strain to cracking strain and the normalized stiffness parameter (η) is the ratio of tensile modulus of cracked specimen to the tensile modulus of uncracked specimen. The tensile modulus of uncracked specimen is defined as the initial slope of stress versus strain and the tensile modulus of cracked specimen is the slope between the points corresponding to 0.6% strain and cracking strain. The main reason for considering 0.6% strain is that the LVDTs in all specimens captured the displacement till 1.5mm (corresponding to strain of 0.6%) without unloading. It indicates that there would not have been any failures such as delamination between textile and matrix or the filament pullout in the yarn of textile; the matrix cracking in *FABcrete* alone governs the behaviour till 0.6% strain (which is the state IIa in Figure 4.22), and will lead to conservative design practices.

The results reported in Table 4.5 indicate that there is an influence of volume fraction on the cracking stress. It is noticed that there is around 50% increase in cracking stress as the volume fraction increases from 0.84% to 2.5%. This may be due to the effectiveness of mechanical stretching of the textiles, which delays the crack formation in matrix. In addition, a reduction in the maximum strain (corresponding to the maximum stress) and increase in the tensile modulus is seen as the volume fraction increases. In the uncracked state, the tensile modulus increase is due to the participation of more number of filaments in the textile in the composite action. In the cracked state, the tensile modulus of the cracked specimen until 0.6% strain increases as the number of layers increases, which is due to the enhanced tension stiffening effect as number of layer increases. However, it is noticed that there is around 200% increase in the maximum stress

as volume fraction increases from 0.84% to 2.5% indicating the effective stress distribution between textile and matrix.

Table 4.5 Parameters for *FABcrete* with SRG-45 (Mean & standard deviation)

FABcrete property	Symbol	FABcrete with SRG-45			
		2a (V_f=0.84%)	3a (V_f=1.26%)	4a (V_f=1.68%)	6a (V_f=2.5%)
Cracking stress (MPa)	σ_{cr}	3.04 (±0.12)	3.70 (±0.08)	4.36 (±0.66)	4.63 (±0.83)
Cracking strain (%)	ε_{cr}	0.05 (±0.002)	0.05 (±0.012)	0.03 (±0.01)	0.02 (±0.012)
Maximum tensile stress (MPa)	σ_u	5.80 (±0.73)	11.31 (±1.17)	14.95 (±1.48)	17.53 (±2.14)
Tensile strain corresponding to maximum stress (%)	ε_u	1.46 (±0.17)	1.74 (±0.22)	1.012 (±0.28)	0.82 (±0.17)
Tensile modulus of uncracked specimen (MPa)	$E_{uncracked}$	23550 (±3030)	24855 (±3927)	27665 (±5165)	28695 (±4131)
Tensile modulus of the cracked specimen till 0.6% strain (MPa)	$E_{cracked}$	667 (±1662)	933 (±1250)	1416 (±398)	2833 (±610)
Normalized strain parameter for design ($\beta=\frac{\varepsilon_{0.6\%}}{\varepsilon cr}$)	β	11.10	12.80	20.00	26.96
Normalized stiffness parameter for design ($\eta = \frac{E_{cracked}}{E_{uncracked}}$)	η	0.01	0.01	0.02	0.07

4.4.2 *FABcrete* with AR1 as textile

The typical nominal stress versus nominal strain curves of *FABcrete* with 0.42%, 0.63%, 0.84% and 1.26% volume fractions of AR1 (2ST_2b, 3ST_3b, 4ST_4b, 6ST_6b) are shown in Figure 4.23. At least four specimens were tested in each category and the corresponding stress versus strain curves are presented in Appendix-B. It is noted that except for the 6 layer specimen (with V_f=1.26%), no other specimen exhibits the strain hardening behaviour over a longer strain range.

84

The overall behaviour indicates that there is a linear portion of the stress versus strain curve up to the first cracking and following this, additional cracks occur. The number of cracks formed at this state depend on the volume fraction of textile. Soon after the multiple crack formation, one of the crack widens and specimen fails by the rupture of the textile. It is noticed that the stabilized state wherein all cracks widen equally in a particular straining range is specifically absent here. The various parameters obtained from the test data are given in Table 4.6 as mean and standard deviation values.
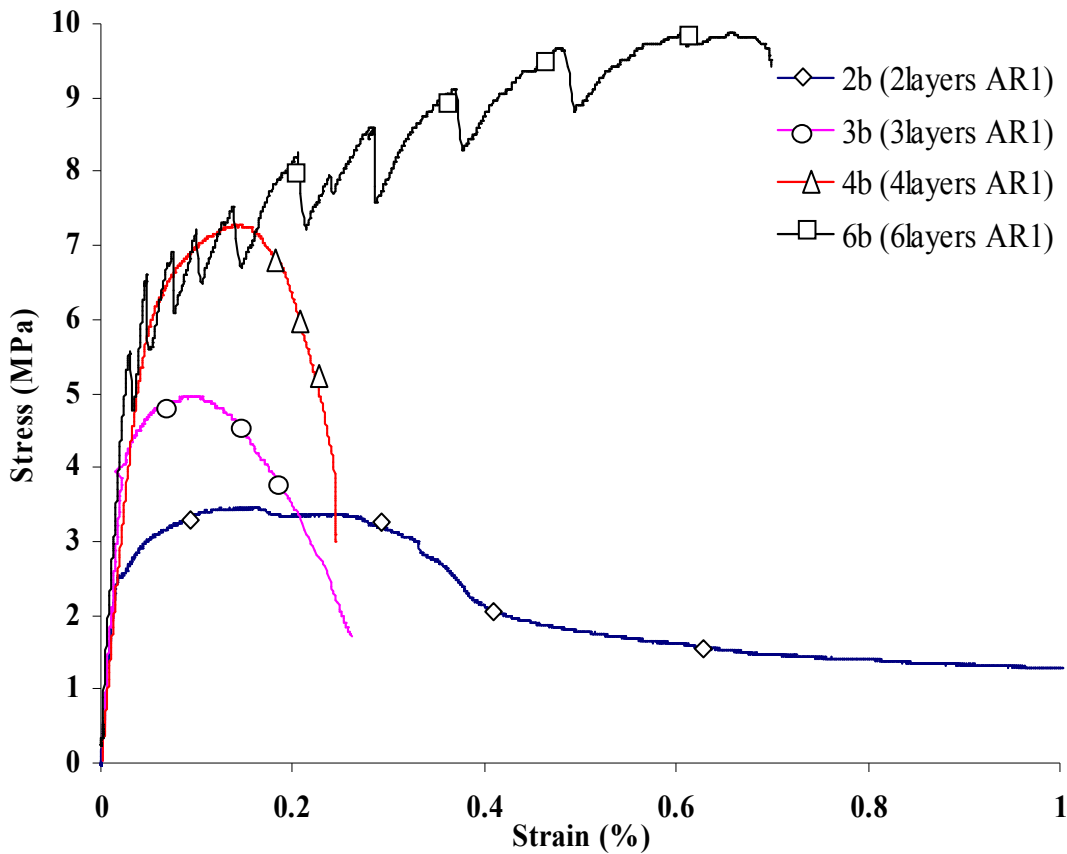
Figure 4.23 Typical stress-strain for *FABcrete* with AR1

From Table 4.6, it is seen that there is a significant increase in the first cracking stress as the volume fraction increases (three-fold increase as the volume fraction increases from 0.42% to 1.26%). The tensile modulus before cracking also shows an increase as the volume fraction increases. This may be due to the paticipation of more filaments in the mechanically stretched AR1 as the number of layers increases, which delays crack formation. After cracking, there is an

increase in the tensile modulus as volume fraction increases, which reflects the enhanced tension stiffening, leading to strain hardening behaviour. Further, the strain at failure is around 1% for specimens with 0.42% AR1 and it is around 0.8% for specimens with 1.26% AR1. It is noticed that in the specimen with 0.42% AR1, there is a softening branch after peak stress, indicating that pullout of textile has occured. Moreover, in all specimens, the final failure was by rupture of textile.

Table 4.6 Parameters for *FABcrete* with AR1 textile (Mean & standard deviation)

FABcrete property	Symbol	FABcrete with AR1			
		2b $(V_f=0.42\%)$	3b $(V_f=0.63\%)$	4b $(V_f=0.84\%)$	6b $(V_f=1.26\%)$
Cracking stress (MPa)	σ_{cr}	1.25 ($\pm$0.04)	2.48 ($\pm$0.31)	4.2 0 ($\pm$0.10)	4.70 ($\pm$0.54)
Cracking strain (%)	ε_{cr}	0.06 ($\pm$0.006)	0.02 ($\pm$0.008)	0.03 ($\pm$0.002)	0.16 ($\pm$0.003)
Maximum tensile stress (MPa)	σ_u	1.65 ($\pm$0.08)	4.92 ($\pm$0.28)	6.82 ($\pm$0.61)	9.91 ($\pm$0.37)
Tensile strain corresponding to maximum stress (%)	ε_u	0.33 ($\pm$0.03)	0.12 ($\pm$0.02)	0.16 ($\pm$0.01)	0.56 ($\pm$0.09)
Tensile modulus of the uncracked specimen (MPa)	$E_{uncracked}$	21835 ($\pm$2330)	22425 ($\pm$2780)	23925 ($\pm$3074)	26780 ($\pm$3160)
Tensile modulus of the cracked specimen till 0.6% strain (MPa)	$E_{cracked}$	275 ($\pm$15)	821 ($\pm$355)	1137 ($\pm$645)	1651 ($\pm$215)
Normalized strain parameter for design ($\beta=\frac{\varepsilon_{0.6\%}}{\varepsilon cr}$)	β	-	-	-	37.67
Normalized stiffness parameter for design ($\eta=\frac{E_{cracked}}{E_{uncracked}}$)	η	-	-	-	0.03

The normalized strain and stiffness parameters have been calculated only for the 6layer reinforced specimens that showed the typical characteristics of TRC of strain hardening behaviour. The values are reported in Table 4.6 and it is observed that the normalized strain parameter is around 37 in *FABcrete* with 1.26% of AR1, indicating the enhanced straining ability and better utilization of the textile.

4.4.3 *FABcrete* with combination of SRG-45 and AR1 as textile

Investigations were carried out to find the feasibility of using a combination of SRG-45 and AR1 textile in *FABcrete*. Two different volume fractions 1.26% (2ST_2c, with 2 layers of SRG-45 and 2 layers of AR1 each) and 1.89% (3ST_3c, with 3 layers of SRG-45 and 3 layers of AR1 each) were considered for the study. The typical nominal stress versus nominal strain (based on average LVDT values) is shown in Figure 4.24. At least four specimens were tested in each category and the corresponding stress versus strain response for each specimen is presented in Appendix-B. The various parameters obtained from the tests is reported in Table 4.7. The results indicate that the cracking stress and cracking strain are almost same in both 2ST_2c and 3ST_3c and are independent of the volume fraction. This may be due to the difference in amount of stretching required for two different varieties of glass textile that has undergone different manufacturing processes leading to different waviness of the yarns. The results indicates that there is an increase in the maximum stress, and a decrease in the maximum strain, as more textile layers are combined. It is noted that there is no change in the final elongation ability if a combination of SRG-45 and AR1 is used in *FABcrete* compared to the independently reinforced cases. Moreover, there is an increase in load carrying capacity as the number of combined layer increases. The results obtained are further used to arrive at an idealized bilinear stress versus strain curve and design parameters of *FABcrete* for the combination of SRG-45 and AR1, as reported in Table 4.7. The tensile moduli before and after cracking also increase as the volume fraction increases by combining textiles. Similarly, there is an increase in the normalized strain and stiffness parameters as more layers are combined.
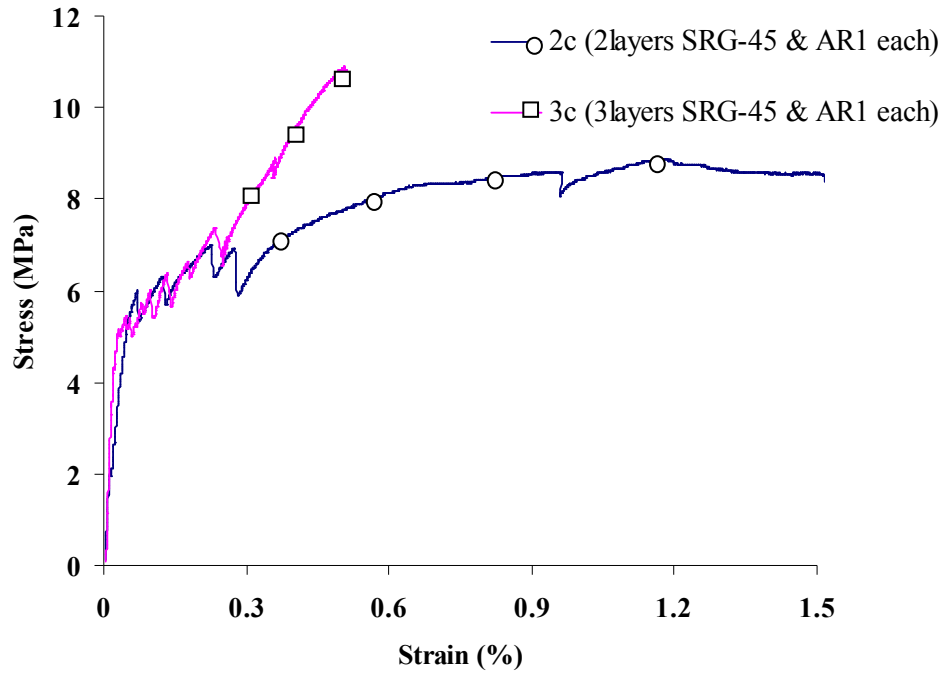
Figure 4.24 Stress-strain for *FABcrete* with combination of SRG-45 and AR1

Table 4.7 Parameters for *FABcrete* with SRG-45 & AR1 (Mean & standard deviation)

FABcrete property	Symbol	FABcrete with SRG-45 & AR1	
		2c (V$_f$=1.26%)	3c (V$_f$=1.89%)
Cracking stress (MPa)	σ$_{cr}$	3.92 (±0.34)	3.90 (±0.50)
Cracking strain (%)	ε$_{cr}$	0.03 (±0.015)	0.02 (±0.002)
Maximum tensile stress (MPa)	σ$_u$	8.65 (±0.20)	11.15 (±0.14)
Tensile strain corresponding to maximum stress (%)	ε$_u$	0.80 (±0.25)	0.53 (±0.04)
Tensile modulusof the uncracked specimen (MPa)	E$_{uncracked}$	22105 (±3463)	24605 (±2903)
Tensile modulus of the cracked specimen till 0.6% strain (MPa)	E$_{cracked}$	1300 (±1217)	1860 (±313)
Normalized strain parameter for design ($\beta = \frac{\varepsilon_{0.6\%}}{\varepsilon_{cr}}$)	β	20.51	25.00
Normalized stiffness parameter for design ($\eta = \frac{E_{cracked}}{E_{uncracked}}$)	η	0.03	0.05

88

The normalized strain and stiffness parameters are also calculated for the specimens and reported in Table 4.7. The non-dimensional strain parameter is around 20 to 25 while combining the textiles, indicating that the textiles can accommodate strain to a greater extent after cracking.

4.4.4 Influential parameters for stress-strain behaviour of *FABcrete*

The various parameters that affect the uniaxial tensile behaviour of *FABcrete* are reported in this section. Figure 4.25 shows the variation of first cracking stress with respect to the volume fraction and type of textile. For SRG-45 reinforced specimens, there is a substantial increase in the first cracking stress as the volume fraction increases from 0.84 to 1.68% and thereafter the increase is less. A similar trend is seen with the AR1 reinforced specimens between volume fractions of 0.42% to 0.84%, beyond which the increase is not significant.
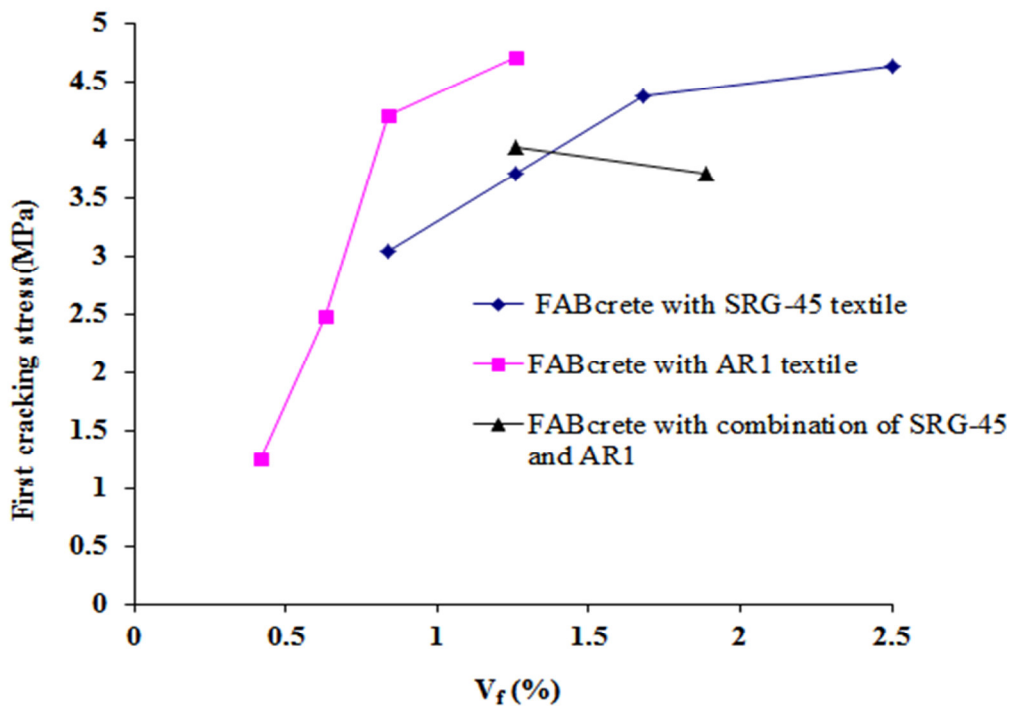
Figure 4.25 Influence of volume fraction and type of textile on first cracking stress

The influence of volume fraction and type of textile on the peak stress is given in Figure 4.26. It is seen that there is significant increase in the peak stress as the volume fraction increases while using the textiles independently or by combining them. It can be concluded that beyond 1% volume fraction, it is better to use SRG-45 to achieve an enhanced peak stress.
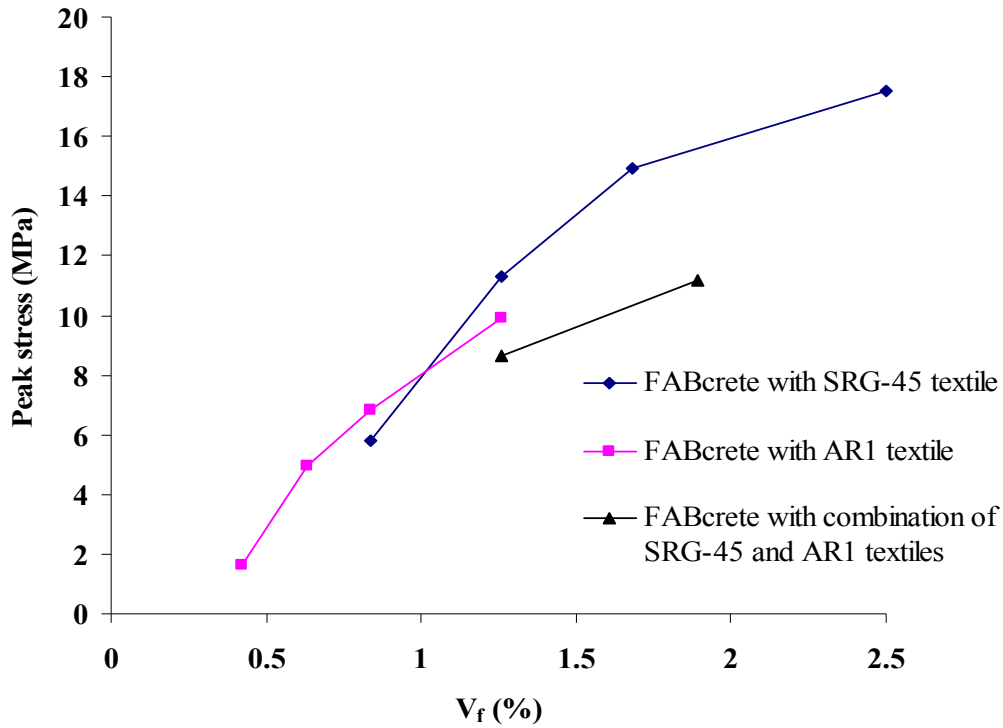
Figure 4.26 Influence of volume fraction and type of textile on peak stress

For the analysis and design of *FABcrete* components, it is possible to use the non-dimensionalized strain and stiffness from the characterization. Towards this aim, the data is presented showing the influence of volume fraction and type of textile. Figure 4.27 gives an indication of how the normalized strain (β) varies with textile and volume fraction. It is seen that for SRG-45 reinforced specimens, there is a continuous increases in β from 11 to 26 as the volume fraction increases from 0.84% to 2.5%. In the case of AR1 specimens, the β value is around 35 when the volume fraction is 1.26%. While combining SRG-45 and AR1, β shows a continuous increase from 20 to 25 when the volume fraction increases from 1.26% to 1.89%. Also, by extrapolating the trend of variation of β with respect to V_f to lower volume fractions, it is noted that combining SRG-45 and AR1 leads to more straining ability for the *FABcrete* (for 1% volume fraction of SRG-45 and AR1 independently, $\beta=12$, whereas for combinations of SRG-45 and AR1, $\beta=19$).
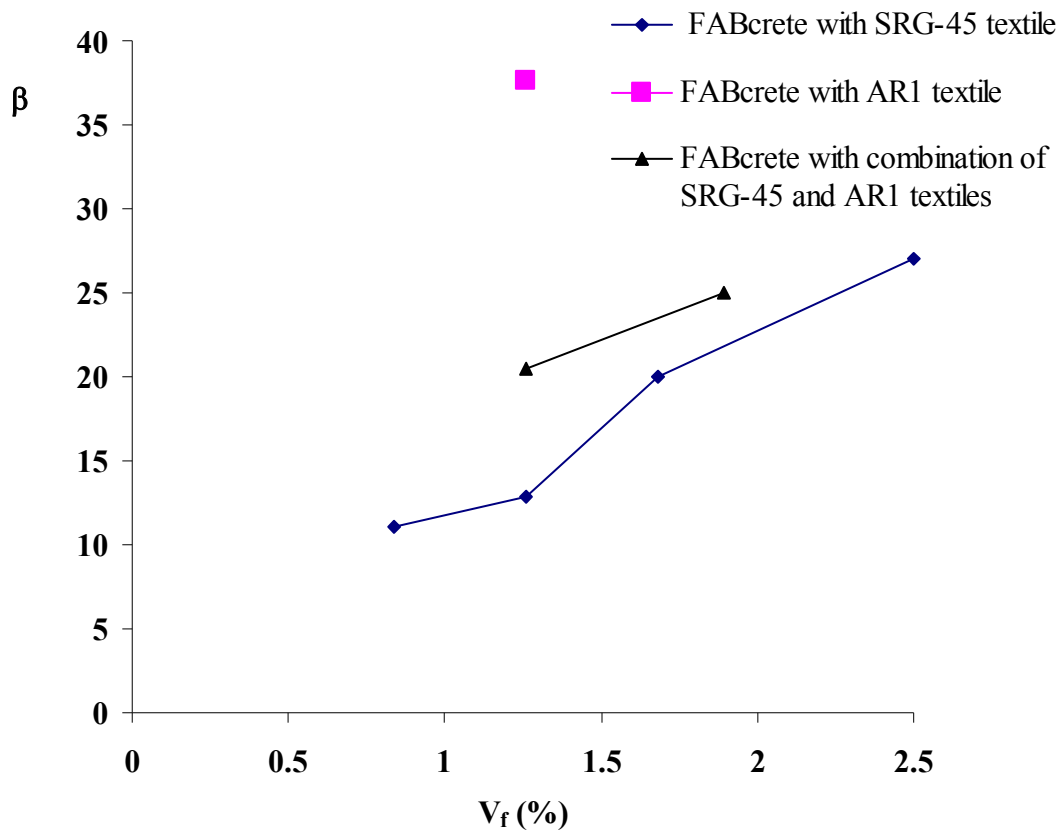
Figure 4.27 Normalized strain parameter versus volume fraction for design

Normalized stiffness parameter (η), which is the ratio of cracked modulus to uncracked modulus, can be considered as a design parameter. Figure 4.28 shows the variation of 'η' with respect to the volume fraction and type of textile. In the case of SRG-45 reinforced specimens, there is a continuous increase in η from 0.007 to 0.07 as the volume fraction increases from 0.84% to 2.5%. While combining SRG-45 and AR1, η also shows an increasing trend as the volume fraction increases.
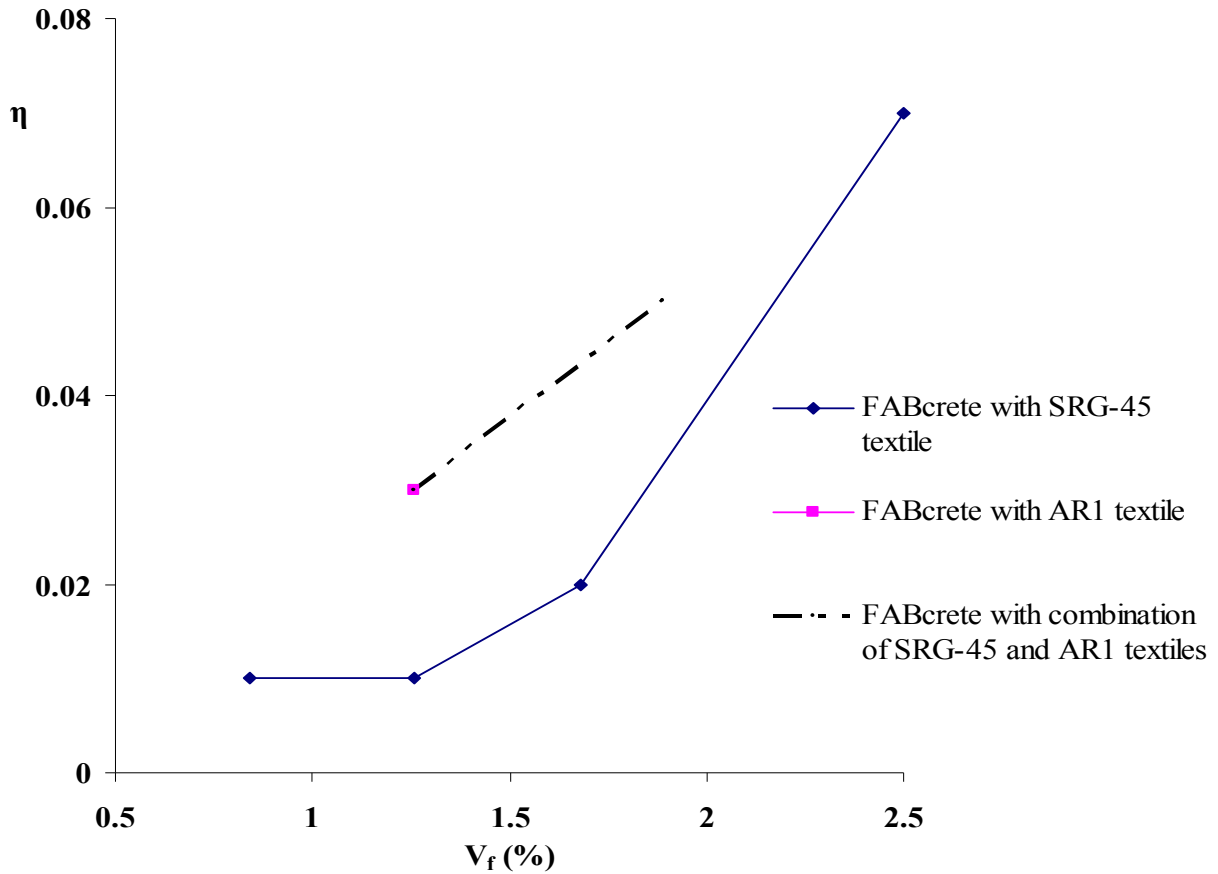
Figure 4.28 Normalized stiffness parameter versus volume fraction for design

4.4.5 Textile based parameters

To determine the textile contribution in *FABcrete*, the nominal stress has been obtained by dividing the applied force by the textile reinforcement cross-section A_f. The area of textile was calculated using the uncoated textile weight per unit area and the density of glass fiber reported in Section 3.3 of Chapter 3. Based on the calculations, the cross-sectional area per unit width for one layer of SRG-45 is obtained as 33.58mm^2/m and AR1 as 16.8mm^2/m. The parameters of textiles that can be useful in the design of *FABcrete* are reported in Table 4.8. It is noted that the maximum stress experienced by 2 layer SRG-45 reinforced specimen is lower compared to 3, 4 and 6 layer reinforced specimens. The maximum stress experienced when 3 and 4 layers of SRG-45 are used in *FABcrete* indicates that an efficiency of around 70% is achieved for these textiles compared to their tensile strength of 1280 MPa.

Table 4.8 Parameters for textiles in *FABcrete* (Mean & standard deviation)

Type of textile	No: of layers	Maximum stress (MPa)
SRG-45	2	560 (±5)
	3	930 (±70)
	4	930 (±60)
	6	800 (±20)
AR1	3	800 (±40)
	4	850 (±70)
	6	750 (±30)
SRG-45 & AR1	2 each	700 (±15)
	3 each	590 (±7)

4.5 DAMAGE EVALUATION IN *FABcrete* USING X-RAY CT

Based on the tensile characteristics of *FABcrete*, it can be concluded that the evolution of damage in *FABcrete* is a complex phenomenon. Hence it is advantageous to have an insight towards the possible damage that occurs during failure. This can also help correlate the mechanical behaviour of composite with the internal mechanisms. To investigate this, a non-destructive imaging technique known as X-ray computed tomography (CT) was used for the damage evaluation of *FABcrete*. Detailed investigation with X-ray CT were conducted for *FABcrete* reinforced with SRG-45 at the Centre for Nondestructive Evaluation at IIT Madras.

The possible failures in *FABcrete* can be due to delamination of matrix from textile, pullout of internal filaments from external filaments or by rupture of filaments in the yarns. Moreover, the final failure can be due to any one of these or due to the combination of more than one mechanism. The objective of the X-ray CT study was mainly to identify various failure phenomenon in *FABcrete*, to understand the effect of mechanical stretching of textiles compared to manual stretching, to examine the bond between textile and matrix in tested (under uniaxial

tension) and un-tested specimens, and to find the influence of number of layers in *FABcrete* on these factors.

4.5.1 X-ray CT

X-ray CT is a method of digitally visualizing a physical object to reveal its interior details, and can be used to reconstruct full three-dimensional images by collecting two-dimensional slices. In principle, collecting images with X-ray CT requires three main components. These are: (1) an X-ray source and its configuration, (2) a specimen to be imaged, and (3) a detector. X-rays are aimed at a specific location on the specimen and those penetrated through the specimen are collected using a high resolution detector. The amount of X-ray energy penetrating the specimen is converted to scalar, grey-scale values (roughly proportional to the material density) that are assigned to each spatial location within the specimen. When a high resolution CT scan is made on a specimen object, hundreds of two-dimensional radiographic images are produced. These images are referred to as "slices" which reveals the interior of the object as if it has been sliced open along the image plane. The difference in density within each element of the object is the main factor that creates a difference in X-ray absorptivity that allows for a level of contrast in the image. Therefore, X-ray absorption is a function of the elemental composition of the object, which is directly related to the microstructure of the material.

To capture the tomography image, the sample is placed on a rotating platform capable of full rotations. The X-ray emitting source is held fixed while the platform is rotated at small angular increments repeating the intensity measurements on each turn. This allows the X-rays to penetrate the sample along several different paths in several different directions. A slice is complete only after the intensity measurements of a full rotation of the platform is collected. In this manner, two-dimensional images are taken at many levels and assembled to create a 3D image. CT creates cross section images by projecting X-rays through an object from defined angle positions. X-rays transmitted around the object at different directions are collected on the detector and visualized, creating a complete reconstruction of the scanned CT image. Lambert-Beer's Law (Oesch, 2015) is used to relate the intensity of transmitted radiation to the intensity of incident radiation, the objects linear attenuation coefficient and the distance travelled through the object. The transmitted X-ray beams have a modulated intensity dependent on the overall linear

attenuation characteristic of the intervening material. The brighter region corresponds to higher values of the attenuation coefficient and darker region to lower ones. A detailed description about the working principle of X-ray CT can be found elsewhere (Oesch, 2015).

4.5.2 Description of the X-ray CT scanner

Tomography scans on *FABcrete* samples were performed using a General Electric/Phoenix VtomexS CT system. The setup used for the investigation is shown in Figure 4.29. It has a 240kV micro-focus source and 180kV nano focus beam transmission heads. The detector is a flat panel detector with a pixel density of 200microns. Since the cone beam has a magnification of 2.6 times, the effective voxel size is 75 microns. All scans were performed with X-ray peak energy at 110kV and current at 190Micro Amps. Each scan consisted of 1000 projections, with an acquisition time of 4 sec per projection. The specimens were exposed to 360º angle to take the images. A filtered back propagation algorithm was applied for reconstruction based on direct Fourier reconstruction methods using GE Phoenix Datosx Reconstruction software. For the experiment described in the following section, 1000 images were acquired and reconstructed to form a 3D view. The vertical separation between each slice of the specimen was 0.6mm.
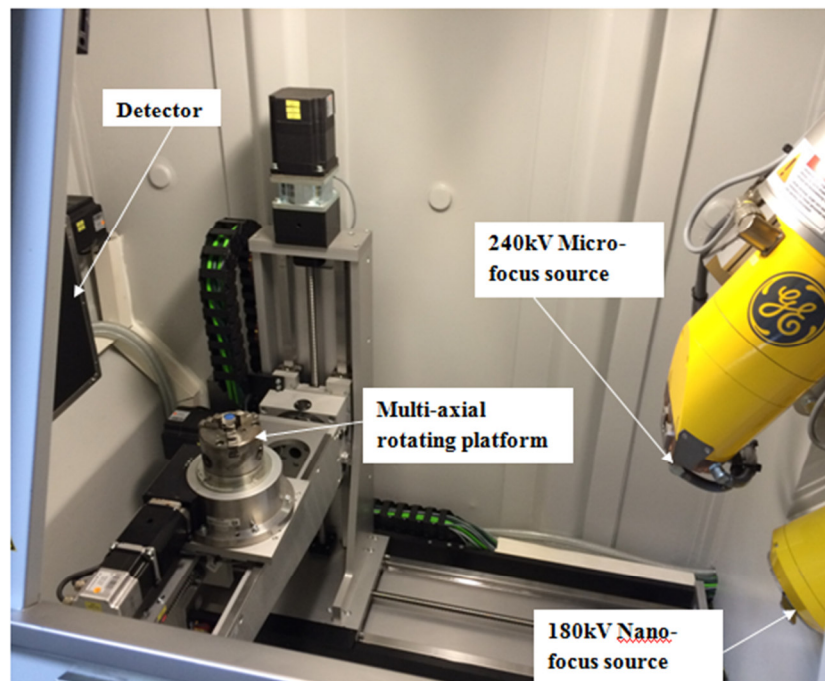
Figure 4.29 Setup used for X-ray CT

4.5.3 Specimen details

Specimens with 3, 4 and 6 layers of SRG-45 were used to understand the interior details about *FABcrete*. To conduct the X-ray CT, samples of size 60 mm length was cut from the *FABcrete* specimens that were virgin and tested. The dimensions were chosen in a such a way that at least 2 meshes were incorporated along the length of the specimen. The details of various specimens used for the X-ray CT are given in Table 4.9 (see Table 4.1 and 4.2 also). In the specimen id, the letter "M" stands for manually stretched, "S" for mechanically stretched, "T" for tested and "U" for un-tested. The number denotes the number of layers used in the specimen.

Table 4.9 Details of specimens examined using X-ray CT

Specimen id	Description of specimen	Purpose of X-ray CT
3MU_3a	Un-tested *FABcrete* specimen with 3 layers of manually stretched textile	To examine the bond between textile and matrix with manually stretched textile
3SU_3a	Un-tested *FABcrete* specimen with 3 layers of mechanically stretched textile	To examine the bond between textile and matrix with mechanically stretched textile
3MT_3a	Tested *FABcrete* specimen with 3 layers of manually stretched textile	To compare the effects of manual stretching of textiles with mechanical stretching
3ST_3a	Tested *FABcrete* specimen with 3 layers of mechanically stretched textile	To examine the effects of mechanical stretching
4ST_4a	Tested *FABcrete* specimen with 4 layers of mechanically stretched textile	To determine various failure phenomena in *FABcrete*
6ST_6a	Tested *FABcrete* specimen with 6 layers of mechanically stretched textile	To examine the failure in *FABcrete*

A typical sample used for the X-ray CT scan is shown in Figure 4.30. In this case the sample corresponds to specimen 4ST_4a. The visualization of the X-ray CT image of the *FABcrete* specimen (4ST) is shown in Figure 4.31. The CT images across thickness and also in-plane were analyzed.

96
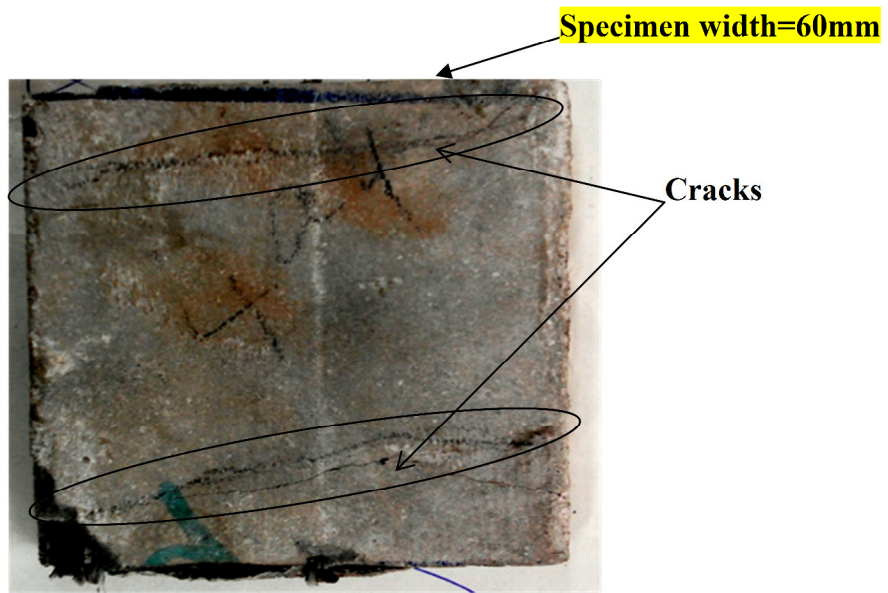
Figure 4.30 Sample of *FABcrete* specimen considered for X-ray CT analysis
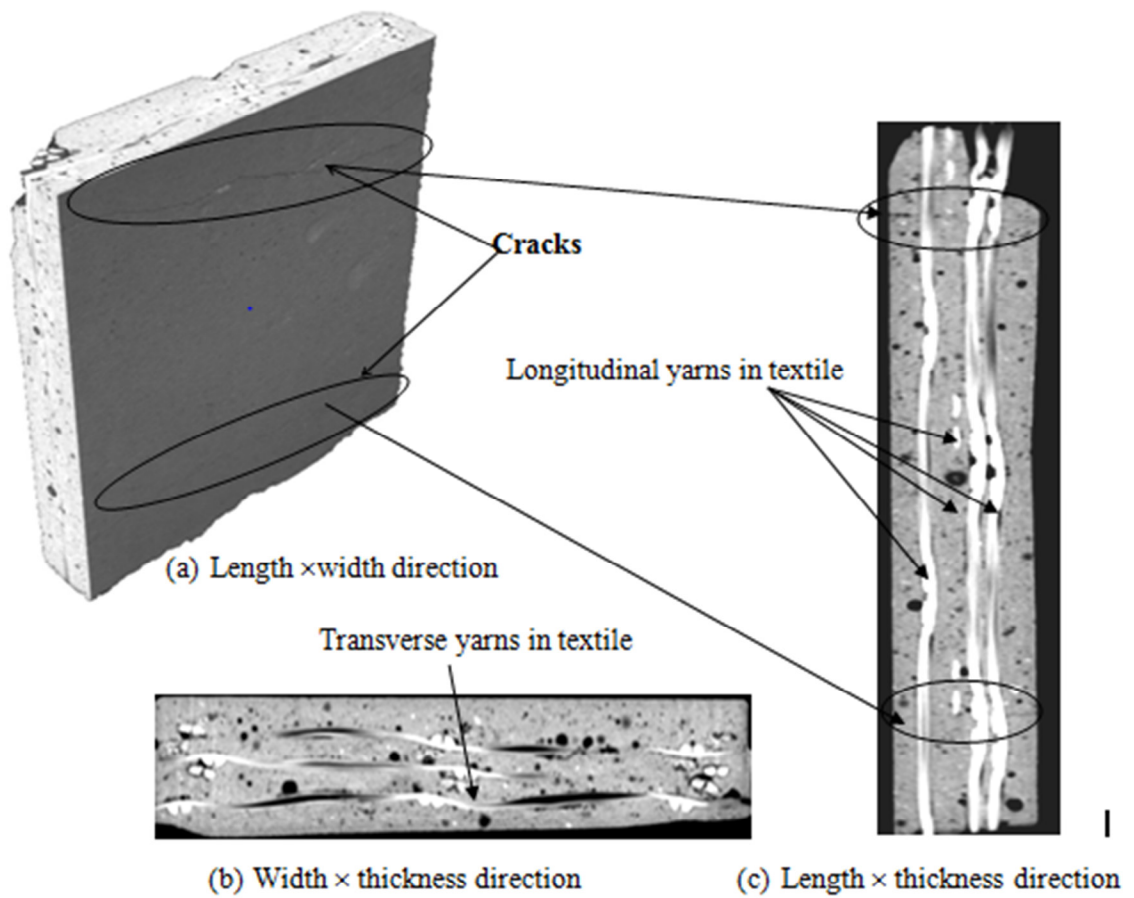
Figure 4.31 X-ray CT 3D-image of *FABcrete* specimen

In Figure 4.32(a), the 3D image of textile in the sample from 4ST_4a is shown and the matrix image is omitted to allow an unobstructed view of the textile yarn locations. In X-ray CT, the denser the material, it will be more whitish; in *FABcrete* glass is relatively most dense and shows up more whitish. In Figure 4.32(b), the stretching done to the layers of textile is clearly visible. Further, the successive slices of textile stacked one over the other demonstrated that the stacked layers have gaps for the matrix penetration. Compared to the longitudinal yarns, the filaments in the transverse yarns appears to be loose, which indicates that they were not stretched, whereas the longitudinal yarns appears more straight, stretched and waviness is not seen in them.
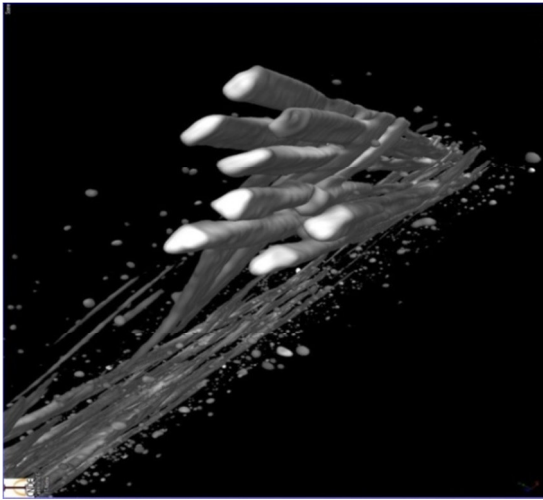
Figure 4.32(a) 3D-image of textile across the thickness
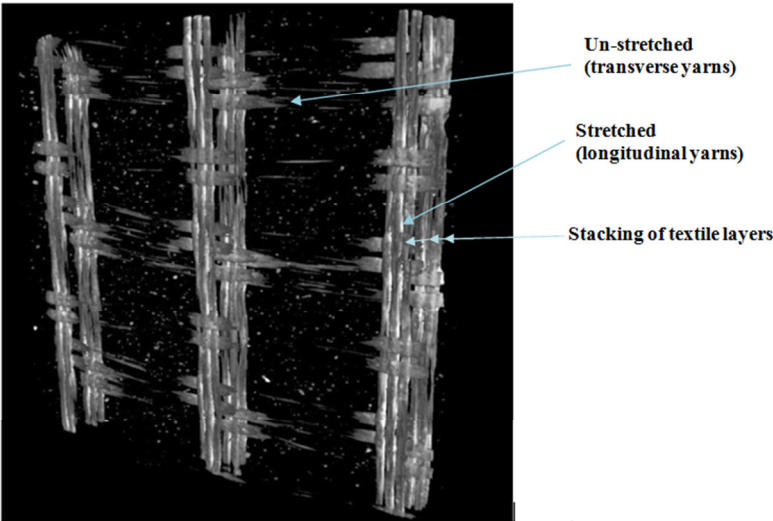
Figure 4.32(b) Isometric view of 3D image of textile

4.5.4 Bond between textile and matrix in tested and untested specimens

The specimens 3MT_3a, 3MU_3a and 3ST_3a & 3SU_3a were used to compare the bond between tested and untested *FABcrete* with manually and mechanically stretched textiles. The X-ray CT images of these specimens are shown in Figure 4.33. In the image, the hydration products are grey; and the voids and cracks are black in color.

While comparing the tomography images of un-tested specimens, it is noticed that the size of voids are larger in manually stretched specimens compared to mechanically stretched specimens (see Figure 4.33(a)). The larger voids are present at the locations where yarns are meeting the matrix. Further, the loosening of filaments in the yarns is lower in the mechanically stretched specimens (3SU). It can be concluded that the bond is significantly lost between textile layers and matrix in the manually stretched untested specimens compared to that of mechanically stretched untested specimens.
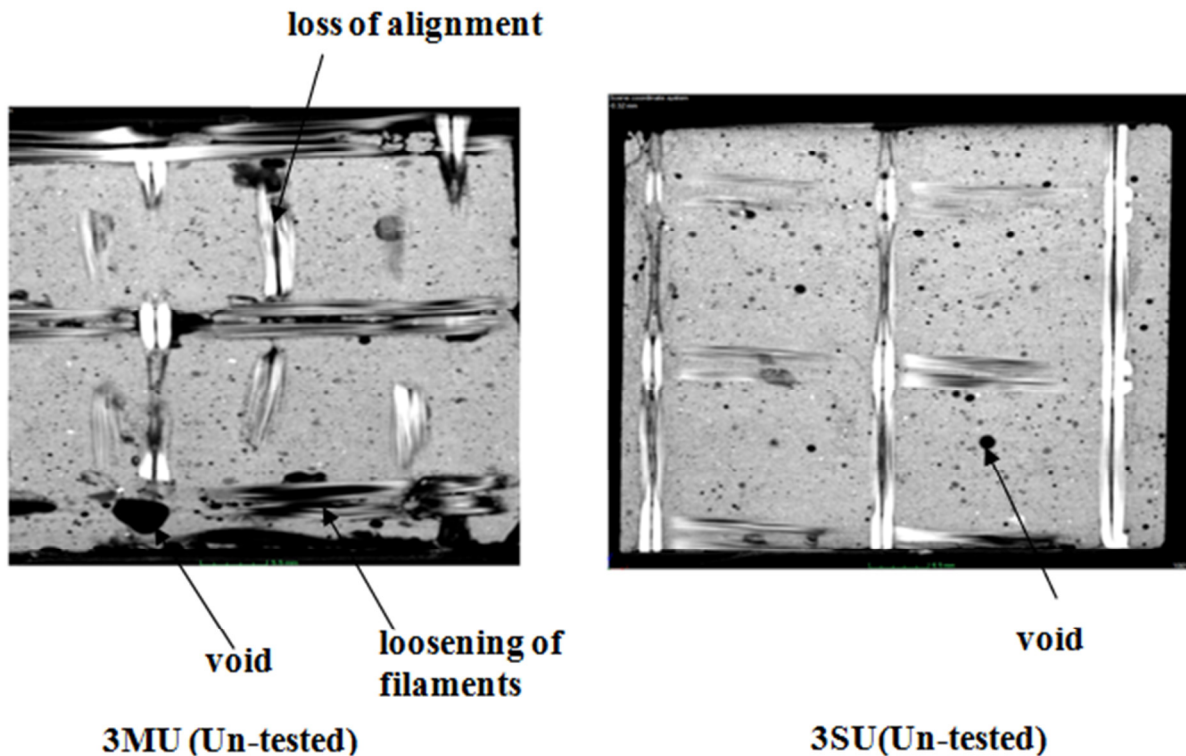
Figure 4.33(a) Comparison of X-ray CT images for bond evaluation in un-tested *FABcrete* specimens of manually and mechanically stretched textiles

While comparing the tomography images of manually (3MT) and mechanically (3ST) stretched specimens in Figure 4.33(b), it is seen that bond is significantly lost between the textile layers and matrix in manually stretched specimens. This indicates that the pull-out of external filaments in textiles can be more in these type of specimens, which makes them under utilized in the composite performance. However, the tomography images of mechanically stretched and tested (3ST) specimens show a better bonded condition in the specimens, and pull-out is not the cause of failure in these specimens. Similar observations was made in the uniaxial tensile characterization reported in Section 4.3.6.
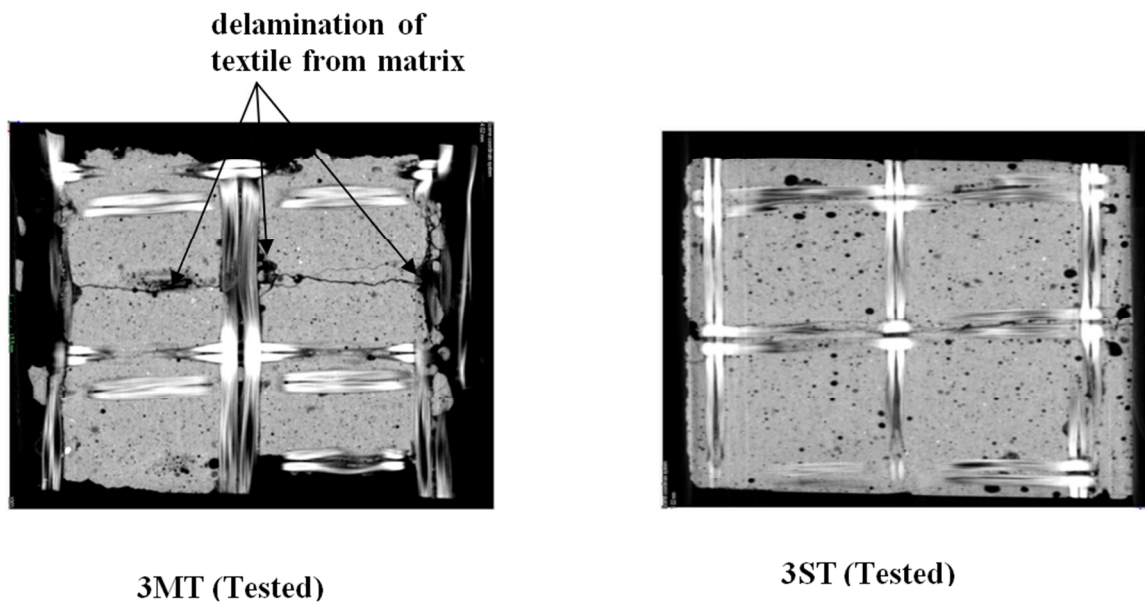
Figure 4.33(b) Comparison of X-ray CT images for bond evaluation in tested *FABcrete* specimens of manually and mechanically stretched textiles

4.5.5 Examination of failure phenomena

The sample 4ST_4a was used to examine the failure of mechanically stretched specimen elaborately; the sample had 2 surface cracks as seen in Figure 4.34(a). These specimen is examined through the thickness, and the visualization in various slices, wherever there the textile layer is present, is shown in Figures 4.34(b) to (f).

It can be noted from Figures 4.34(b) to 4.34 (e) that, there is good penetration of binder in the yarn as well as between the layers of textile. Since there are two yarns per line in the textile, the gap between the yarns allows more penetration of textile by the binder in some layers. The hydration products are coated well in the longitudinal yarns. It is also noticed that there is some loosening of filaments in the transverse yarns compared to longitudinal yarns. Since the longitudinal filaments are mechanically stretched, there is better bonding of external filaments with the matrix and also in between the internal filaments compared to transverse yarns, which are not stretched. This further reveals the importance of stretching to avoid the waviness in yarns for better binder penetration and stability of yarns in *FABcrete*.

Across the thickness, the images further show better bonding of the textile with the binder in between layers (see Figure 4.35). The delamination of the matrix from the internal filaments in the yarns of textile is seen in the 4th layer (see Figure 4.35).
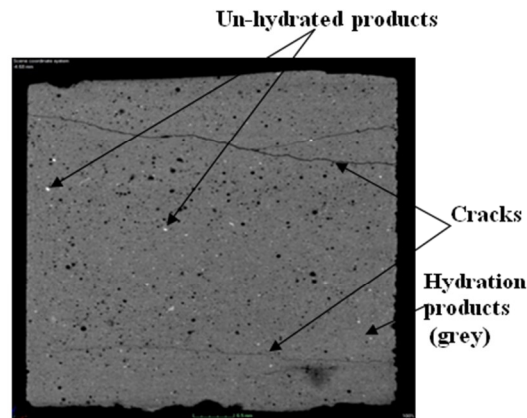
(a) External surface (front side)
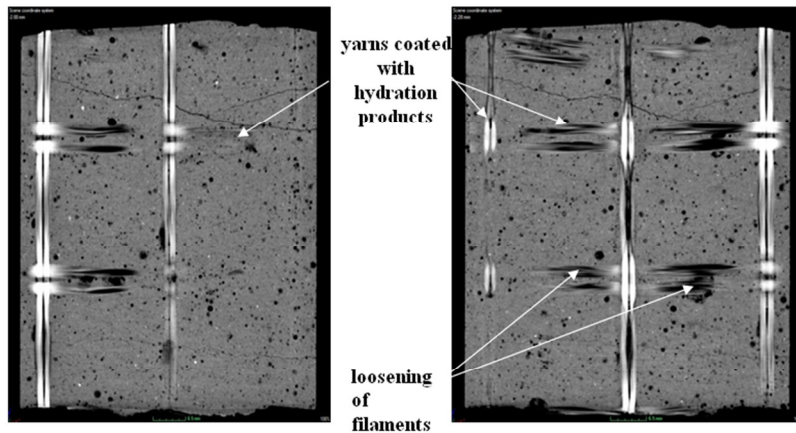
(b)   1st layer of textile   (c) 2nd layer of textile
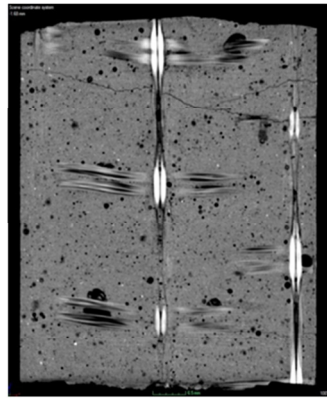
(d) 3rd layer of textile   (e) 4th layer of textile
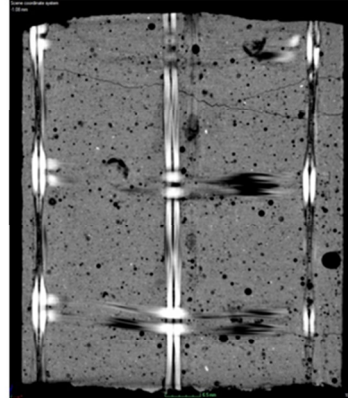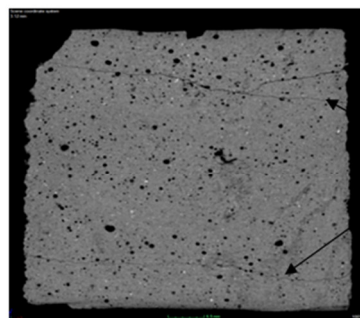
(f) External surface (backside)

Figure 4.34 In-plane view (length × width) of slices of *FABcrete*
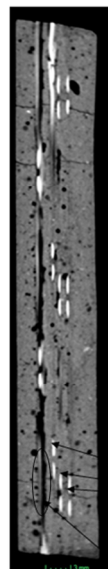
Figure 4.35 View of *FABcrete* slice across thickness (in the plane of length × thickness)

4.5.6 Effect of mechanical stretching in *FABcrete*

The specimens 3MT_3a and 3ST_3a were used to compare the stretching effect in *FABcrete*. The X-ray CT images of these specimens are shown in Figure 4.36. This study will help correlate the mechanical performance of *FABcrete* with stretched and unstretched textiles from a microstructural view. The major cracks in the 3MT and 3ST specimens are shown in Figures 4.36(a) and 4.36(d), it is noticed that the crack width of the manually stretched specimen is slightly more compared to that of mechanically stretched specimen. For the 3MT specimen, more loosening of filaments is seen in the longitudinal yarns (see Figure 4.36(b)), whereas the filaments in the longitudinal yarns are intact in the 3ST specimens (Figure 4.36(e)). It can be concluded that the frictional bond loss is more between the filaments in the yarns of manually stretched specimens. However, the frictional bond loss is not seen in the longitudinal yarns of textiles in mechanically stretched specimen. Further, there is more debonding of textile layer at various locations for the manually stretched specimen (Figure 4.36(c)), whereas debonding is not seen for the mechanically stretched specimen (Figure 4.36(f)) in longitudinal yarns from the matrix. This indicates that the junctions in mechanically stretched specimens are more efficient in the load transfer, and that local failures in longitudinal yarns are not predominant. The matrix cracks pass through the debonded region for 3MT specimen, which would have led into increase in the crack width. In addition, the presence of more voids that are larger in size can also be seen in manually stretched specimens. In the 3 layer mechanically stretched specimen, the cause of final failure is due to matrix cracking and for the manually stretched specimen, there is debonding of the textile layer from the matrix, delamination of the inner filament from the matrix and pullout of the inner filaments from the external filaments of the yarns, matrix cracking and loosening of filaments in yarns. From the tomography analysis, it is more evident that the potential of yarns in the textile layers is underutilized with manually stretching, which is the cause for the lower efficiency seen in the uniaxial tensile characterization studies.

(a)
3MT (Final crack width is more compared to 3ST)

(b)
3MT (Debonding of matrix from textile, loosening of filaments in longitudinal yarns)

(c)
3MT (Debonding of textile from matrix)

(d)
3ST (Final crack width is less compared to 3MT)

(e)
3ST (No debonding of matrix from textile, No loosening of filaments in longitudinal yarns)

(f)
3ST (Cracking is the cause for final failure)
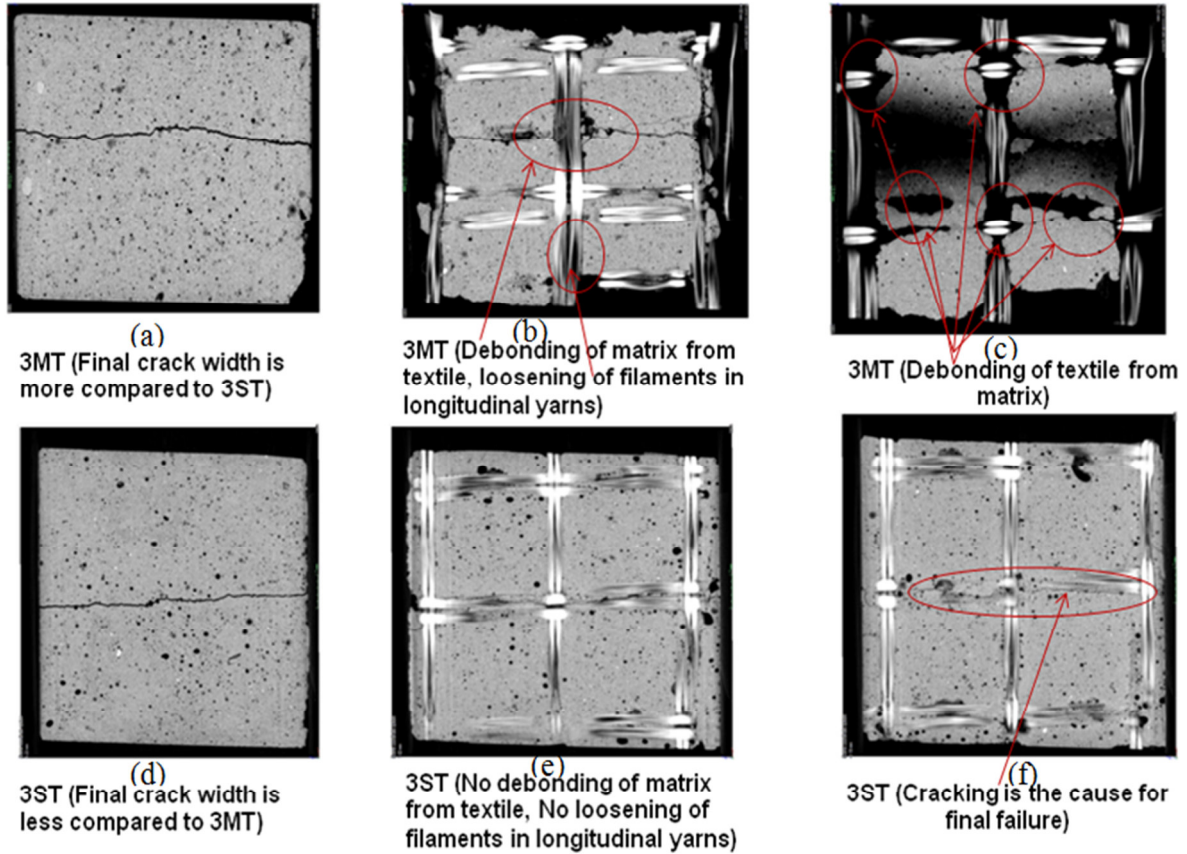
Figure 4.36 Comparison of X-ray CT images of *FABcrete* with manually and mechanically stretched textiles

4.5.7 Influence of number of layers in *FABcrete*

Specimens with 3, 4 and 6 layers of textile (3ST_3a, 4ST_4a and 6ST_6a) were used to understand the influence of number of layers in *FABcrete*. The X-ray CT images used for the analysis are shown in Figure 4.37. The 3D image of textile is shown and the matrix image is omitted to allow an unobstructed view of the stretched yarns in various textile layers (Figures 4.37(a) to 4.37(c)). The 3D images of textiles reveal that the stretching of the yarns is evident for all longitudinal yarns, in all layers of textiles. This indicates the effectiveness of the mechanical stretching mechanism developed for casting uniaxial tensile test specimens.
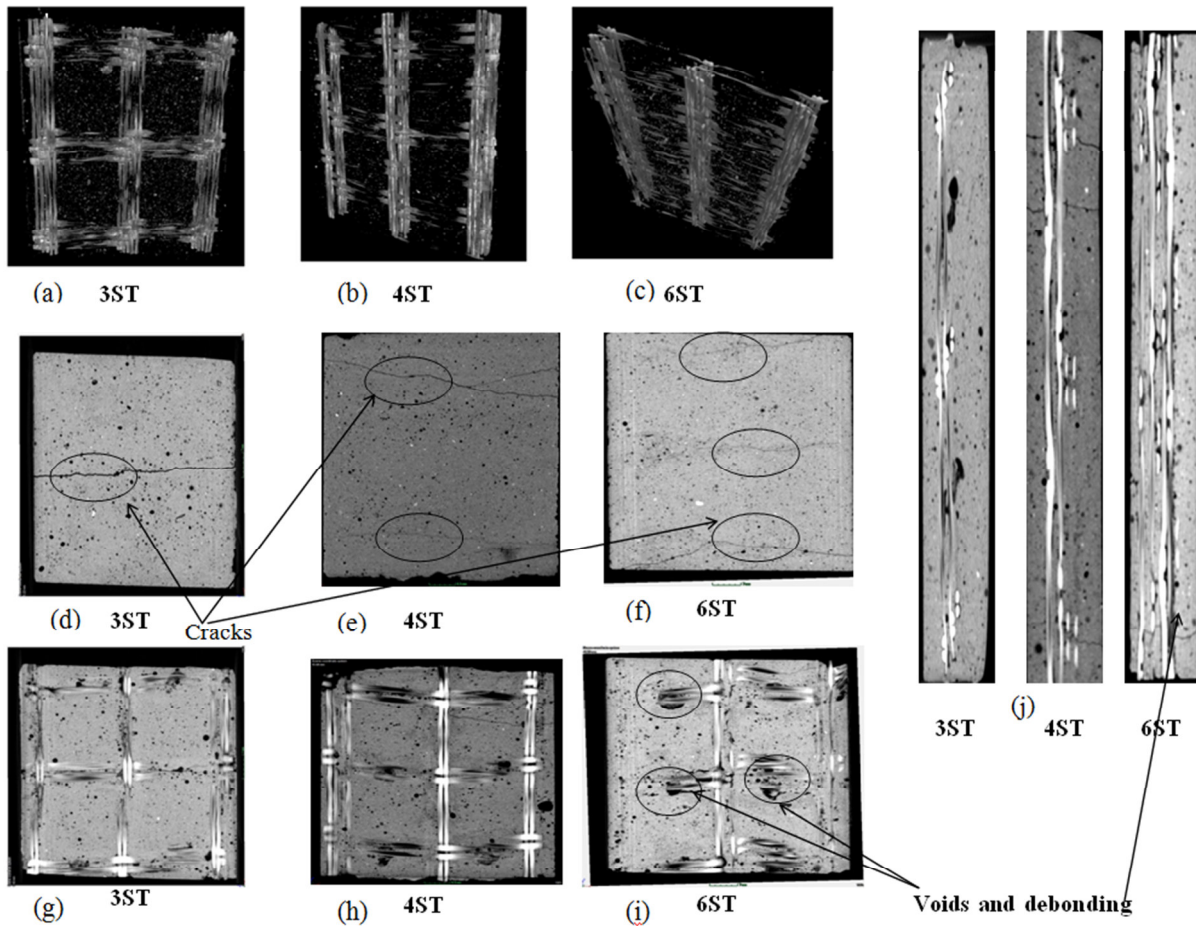
Figure 4.37 Comparison of X-ray CT images of 3,4 and 6 layer textile reinforced mechanically stretched *FABcrete* specimens

In Figures 4.37(d), (e) and (f), the tomography images show that the crack width reduces as the number of layers increases and the number of cracks per meter length also increases. This is in line with the observation reported in Table 4.3 while discussing the uniaxial tensile characterization. Further, a number of voids is seen in 6 layer specimen (Figure 4.37(i)) compared to 4 and 3 layered specimens (Figures 4.37(g) and (h)). The debonding of textile layer from matrix is more as the number of layers increases to 6. Examining the specimens through thickness (see Figure 4.37(j)) also indicates that as the number of layers increases (for 6ST), debonding is seen, compared to 3ST and 4ST. This is the reason for having lower efficiency (0.66) for the 6-layer reinforced specimens compared to the 4layer (efficiency of 0.80) specimens as obtained from the uniaxial tests.

4.5.8 Image analysis for quantification of defects in *FABcrete*

For the quantification of defects such as voids, pores and delaminations in *FABcrete*, image analysis was carried out using the ImageJ software. To carry out the image analysis, X-ray CT scans of various specimens reported earlier was considered. The images were converted into binary since these images provide the clear indication of defects such as voids and delaminations. The images considered for the analysis are eight-bit (there are 8 bits in the binary representation of the gray level) with 256 possible gray levels, ranging from 0 to 255. In this study 0 and 255 represent black and white, respectively. The convention used in this study is that a gray level of zero represents black and 255 represents white (white color were considered as the defects). The binary images for various specimens obtained are shown in Figure 4.38 to 4.43. In the binary images, the properly bonded area in *FABcrete* is represented by black color. The area of defects represented in white color is calculated in pixels with the aid of the ImageJ software. Since the area of defects includes the measurement of individual voids, pores and delaminations and summing up of all them individually and dividing the sum by the total area of the image gives the defects in *FABcrete*. The percentage defects obtained for various specimens at the location of various textile layers is given in Table 4.10. It is noticed that the specimens tested under uniaxial tensile load with manually stretched textiles (3MT) have more defects compared to all the other specimens. Next, the defects are more in the case of untested specimen with manually stretched textile. In the case of tested specimens with mechanically stretched textiles (3ST, 4ST and 6ST) , the total defects are almost same. However, the untested specimen (3MU) with mechanically stretched textile has fewer defects compared to the tested specimen. It leads to the conclusion that the delamination of textile from matrix would have caused the defects in the tested *FABcrete* specimen.

Table 4.10 Percentage of defects obtained from image analysis

Specimen	% Defects
3MU	0.48
3MT	1.19
3SU	0.34
3ST	0.36
4ST	0.39
6ST	0.40

(layer-1)   (layer-2)   (layer-3)

(layer-4)   (layer-5)   (layer-6)
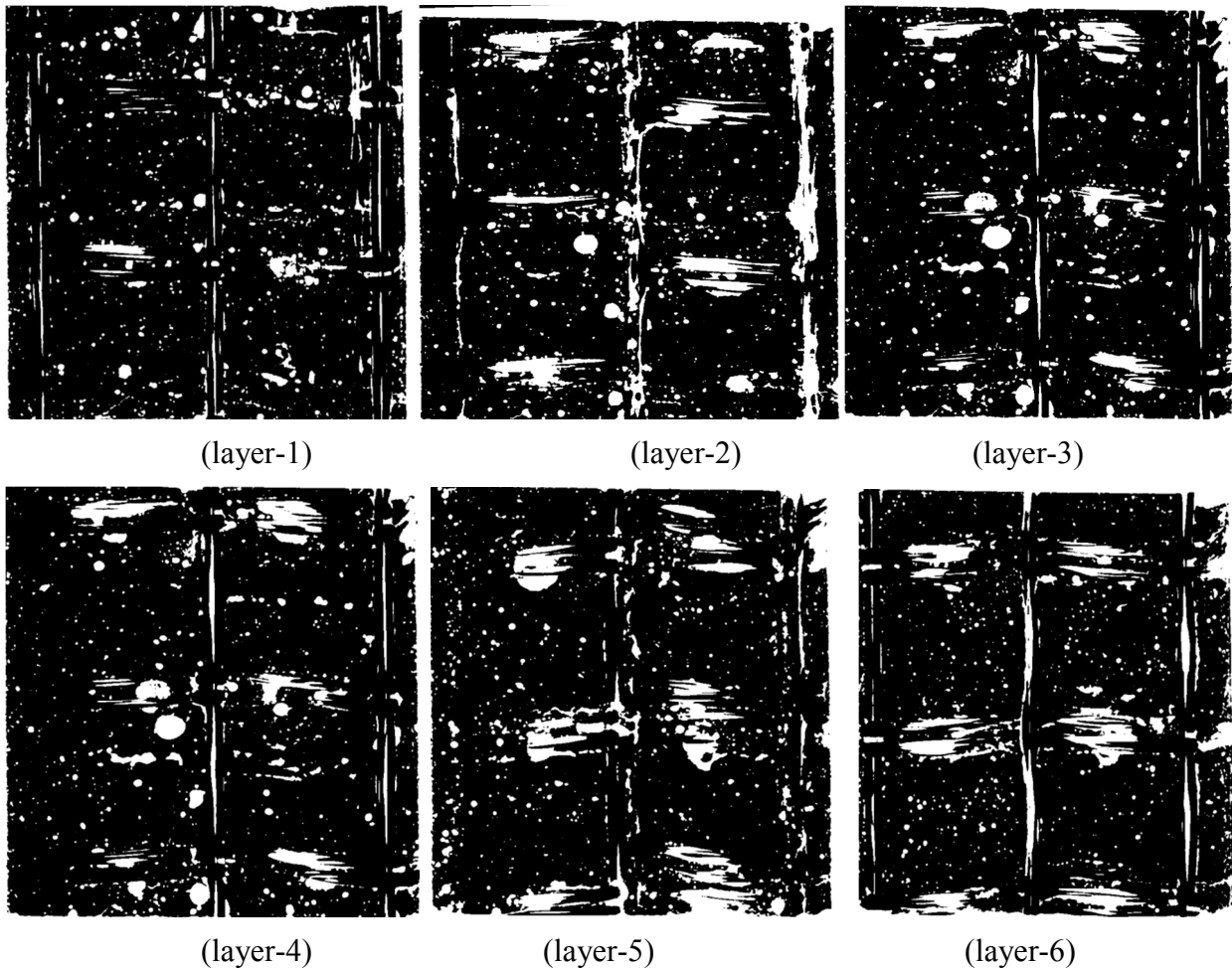
Figure 4.38 Defects (white colour) obtained at the location of different layers in specimen 6ST
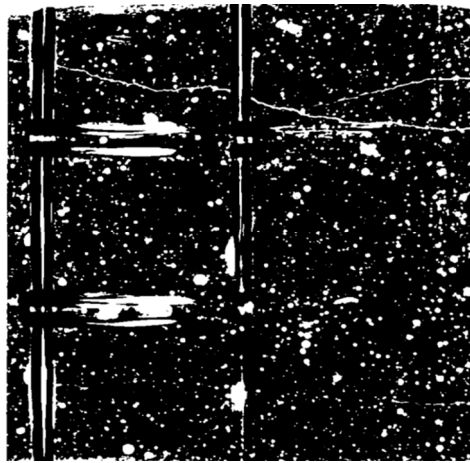
(layer-1)
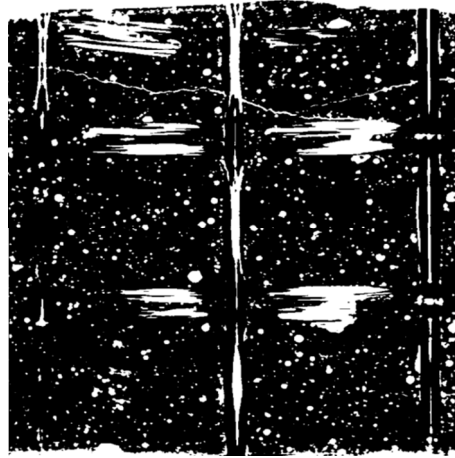
(layer-2)
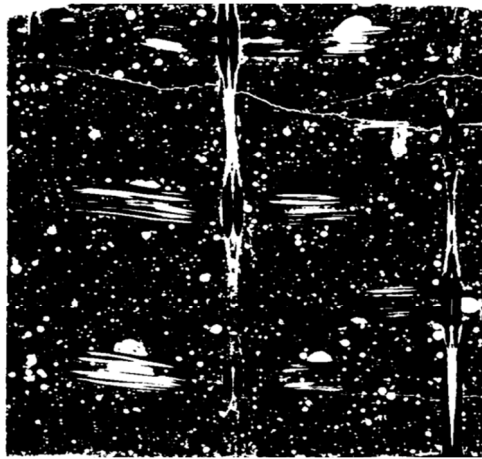
(layer-3)
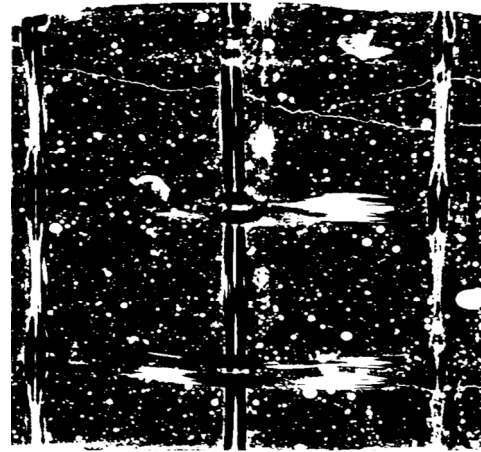
(layer-4)

Figure 4.39 Defects (white colour)obtained at the location of different layers in specimen 4ST
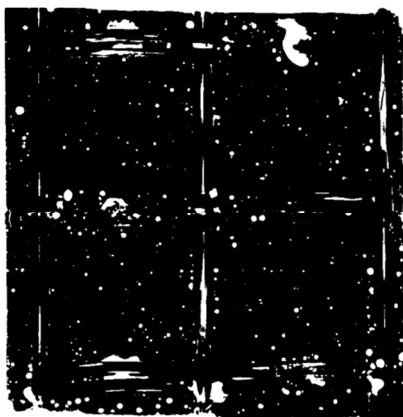
(layer-1)
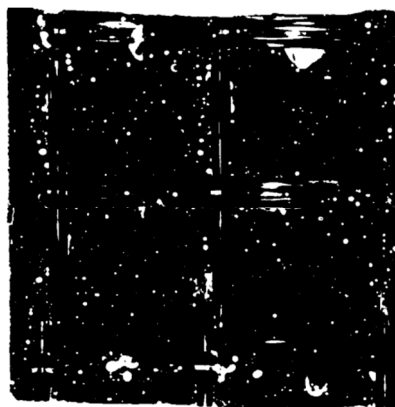
(layer-2)
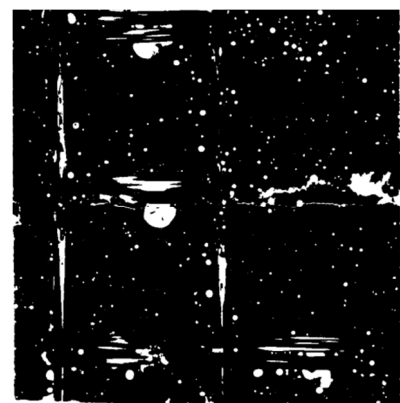
(layer-3)

Figure 4.40 Defects (white colour) obtained at the location of different layers in specimen 3ST

| (layer-1) | (layer-2) | (layer-3) |
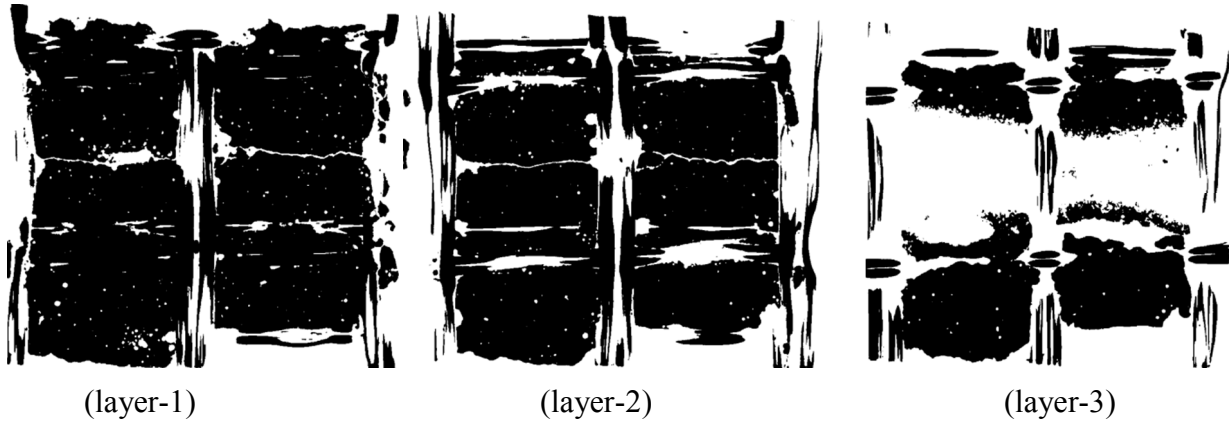
Figure 4.41 Defects (white colour) obtained at the location of different layers in specimen 3MT

| (layer-1) | (layer-2) | (layer-3) |
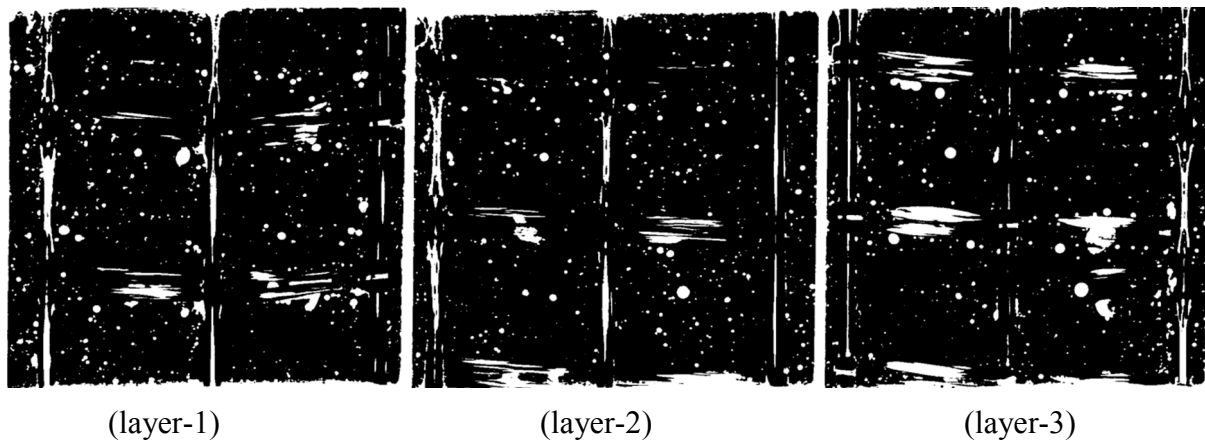
Figure 4.42 Defects (white colour) obtained at the location of different layers in specimen 3SU

| (layer-1) | (layer-2) | (layer-3) |
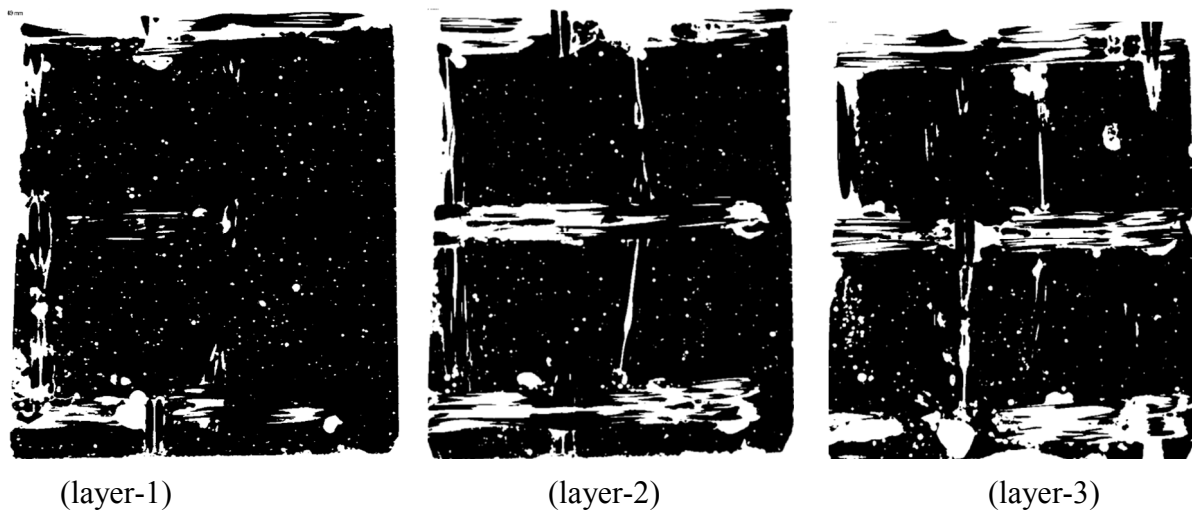
Figure 4.43 Defects (white colour) obtained at the location of different layers in specimen 3MU

4.6 SUMMARY

In this chapter, the methodology developed for characterizing the uniaxial tensile behaviour for *FABcrete* specimens is discussed in detail. From the tensile characterization, it is concluded that the type of textile and volume fraction have considerable influence on the stress versus strain behaviour of *FABcrete*. Further, it can be concluded that using SRG-45 as reinforcement in *FABcrete* leads to reduced crack width and spacing. It also helps prevent abrupt failure when the textile elongates without causing further cracking to the binding matrix. From the behaviour of *FABcrete* with the AR1 textile, it can be concluded that the use of AR1 contributes more towards achieving lower crack width and more straining ability. If combinations of glass textiles are used, it opens up a possibility for optimization of mechanical characteristics in *FABcrete* to achieve desired mechanical properties and parameters. The idealized bilinear stress versus strain behaviour of *FABcrete* reported in the characterization studies will serve in design and can be used for the development of mathematical models for textile reinforced concrete. Further, the efficiency factor determined in this study will provide input for the design of strengthening of concrete members with *FABcrete*. The damage examined using X-ray CT revealed various failures, such as cracking of matrix, delamination of matrix from textile and occurrence of pullout of internal filaments inside *FABcrete*. The enhanced performance shown by *FABcrete* with mechanically stretching of the textiles is also revealed qualitatively by X-ray CT images.

CHAPTER 5

FLEXURAL STRENGTHENING OF RC BEAMS WITH *FABcrete*

5.1. INTRODUCTION

The applicability of *FABcrete* for flexural strengthening of reinforced concrete beams has been investigated with the aim of increasing the load-carrying capacity, together with increasing the stiffness and ductility. While examining existing strengthening systems, it is noticed that custom anchoring methods are needed to attach the strengthening layer to the existing concrete beam. In the case of *FABcrete* there is better integrity of the bond in the strengthened system without the need to use special anchoring techniques. Further, considering the numerous structural components that need retrofitting, it is beneficial to have a mathematical model to predict the response behaviour of strengthened systems. Hence, two modelling methods using finite element analysis by integration of various constitutive models and by developing a closed form solution were attempted. The analytical model is proposed using the material properties from characterization studies for predicting the response behaviour of RC beams strengthened with *FABcrete*.

At the outset, the applicability of *FABcrete* with manually stretched textiles for strengthening of plain concrete beams is investigated. Next, a mechanical stretching mechanism is used to stretch the textiles while casting *FABcrete* for strengthening of RC beam. The details and results of the experimental investigations are presented in Section 5.2. Further, the results are compared with the flexural capacity obtained using the ACI 549 (2013) guidelines in Section 5.3. In addition, mathematical models are developed and reported in Section 5.4. A simplified design procedure is also proposed in Section 5.5.

5.2 EXPERIMENTAL INVESTIGATIONS

Tests were carried out to assess the feasibility, applicability and performance of *FABcrete* for the flexural strengthening of plain and reinforced concrete beams. Casting of *FABcrete* by placing textiles in a manually stretched manner was attempted for flexural strengthening of plain

concrete beams. This was done to find the applicability and practical feasibility of *FABcrete* to achieve significant enhancement in structural performance by accommodating more number of textile layers. Considering the results reported in Chapter 4, it was concluded that stretching of the textiles will lead to better efficiency in composite performance. Hence, a mechanical stretching was used for textiles while casting the *FABcrete* strengthening layer for the RC beams. Two types of RC beams, namely uncracked (virgin) RC beams and pre-cracked RC beams, were strengthened with *FABcrete*. The strengthening of the uncracked beam was done to evaluate *FABcrete* as a retrofitting material whereas that of the cracked beam was done to investigate its ability for structural capacity restoration.

5.2.1 Materials used

All the beams were cast using concrete having mix proportions of cement: fine aggregate: coarse aggregate as 1:2.12:2.23, with a water-cement ratio of 0.45. Concrete cubes of 100×100×100mm and cylinders of 100×200mm were cast to find the compressive and split tensile strengths. The specimens were cured under water for 28 days and tested on the 28th day; the results obtained are given in Table 5.1.

Table. 5.1 Characteristic properties of concrete

Characteristic parameters	
Cube compressive strength (MPa)	50.86
Cylinder compressive strength (MPa)	39.43
Split tensile strength (MPa)	3.28

For casting the *FABcrete* strengthening layer, the cementitious binder used is the *FABmix* discussed in Section 3.2 along with the textile SRG-45, the properties of which have been reported in Section 3.3.

5.2.2 Details of the test specimens for strengthening of plain concrete beams

Eight plain concrete beams having a size of 100mm (width) × 100mm (depth) × 500mm (length) were cast. After water curing for 28days, the beams were strengthened using *FABcrete* by cast-in-place wet lay-up method. Three types of specimens with 4, 6 and 9 layers of SRG-45 glass textiles were used for strengthening of concrete beams. The layers of textiles were manually stretched while casting *FABcrete*.

For casting of the *FABcrete* layer, the cementitious binding matrix, *FABmix* was applied at the bottom face of the beam in approximately 2mm thick layer with a metal trowel. After application of the first matrix layer on the concrete surface, the layers of SRG-45 textiles were placed by manually stretching, and pressed slightly into the matrix. After placing required number of layers, the final matrix layer was then applied and leveled. Different specimens were strengthened by varying the number of layers of the textiles. Even though it was decided to cast a 10mm thick *FABcrete* strengthening layer, it was difficult to control the thickness of the strengthening layer due to the practical difficulty of manually stretching of more number of layers. As a result, only the 4 layer reinforced *FABcrete* had 10mm thickness whereas that of 6 and 9 layers reinforced *FABcrete* had thickness of 12 and 14mm, respectively. The Figure 5.1 shows the application method used for *FABcrete* to strengthen one of the concrete beam. After strengthening, the beams were cured in water for 28 days before testing.
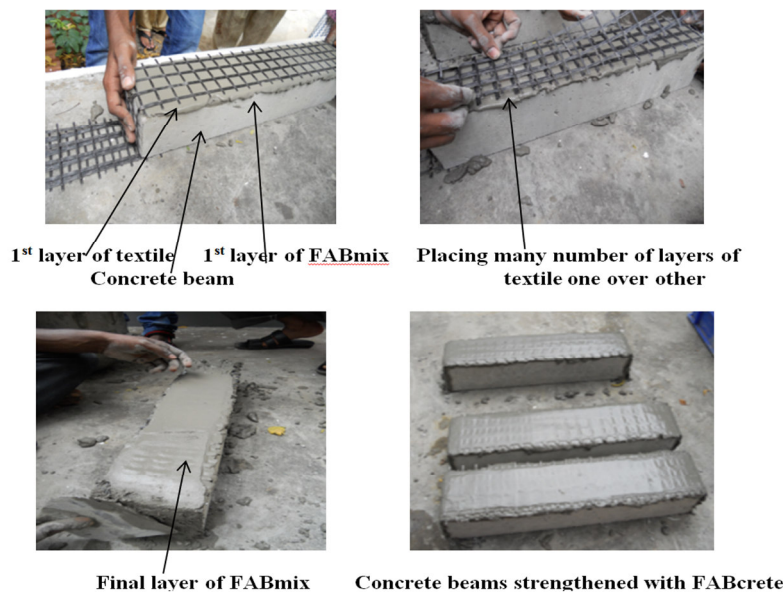
Figure 5.1 Steps followed for *FABcrete* strengthening of plain concrete beam

5.2.2.1 Test setup

Three point bending tests were performed on the strengthened and un-strengthened plain concrete beams using a 500kN MTS servo hydraulic actuator. The effective span of the beams were kept as 400 mm and the simply-supported boundary condition was provided by placing a roller support at one end and a hinged support at the other end as shown in Figure 5.2. The tests were carried out under a displacement rate of 0.5mm/min. A typical view of the flexural test setup is shown in Figure 5.2. An LVDT was placed at the centre of the beam to measure the midspan deflection and monitored through a HBM MGC Plus datalogger.
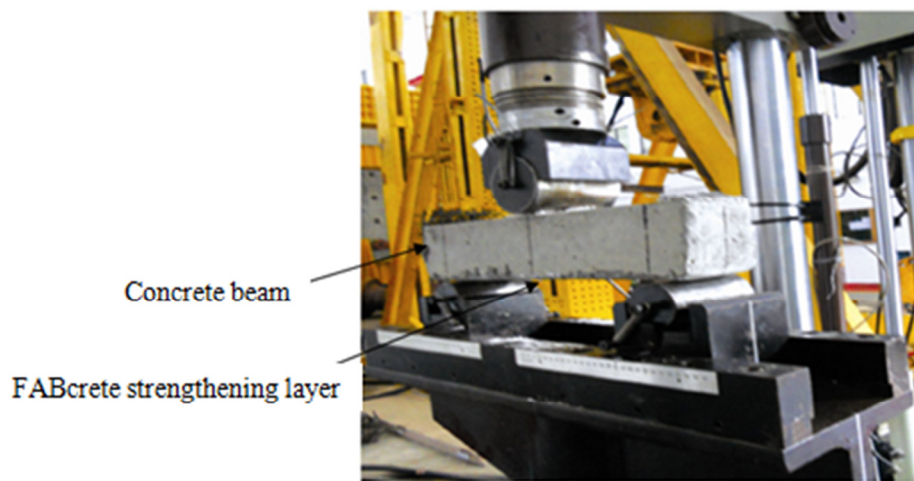
Figure 5.2 Setup for tests on *FABcrete* strengthened concrete beams

5.2.2.2 Results and Discussion

The typical load versus displacement curves of the *FABcrete* strengthened concrete beams are presented in Figure 5.3. It can be observed that the plain concrete control beams under flexural load is quite brittle. When the beams were strengthened by *FABcrete,* the flexural load carrying capacity is enhanced along with significant increase in the energy absorption (area below the load versus displacement curve). In the case of *FABcrete* strengthened beams with 9 layers of textile, it is found that the flexural load is increased approximately by 1.7 times over un-strengthened beam.
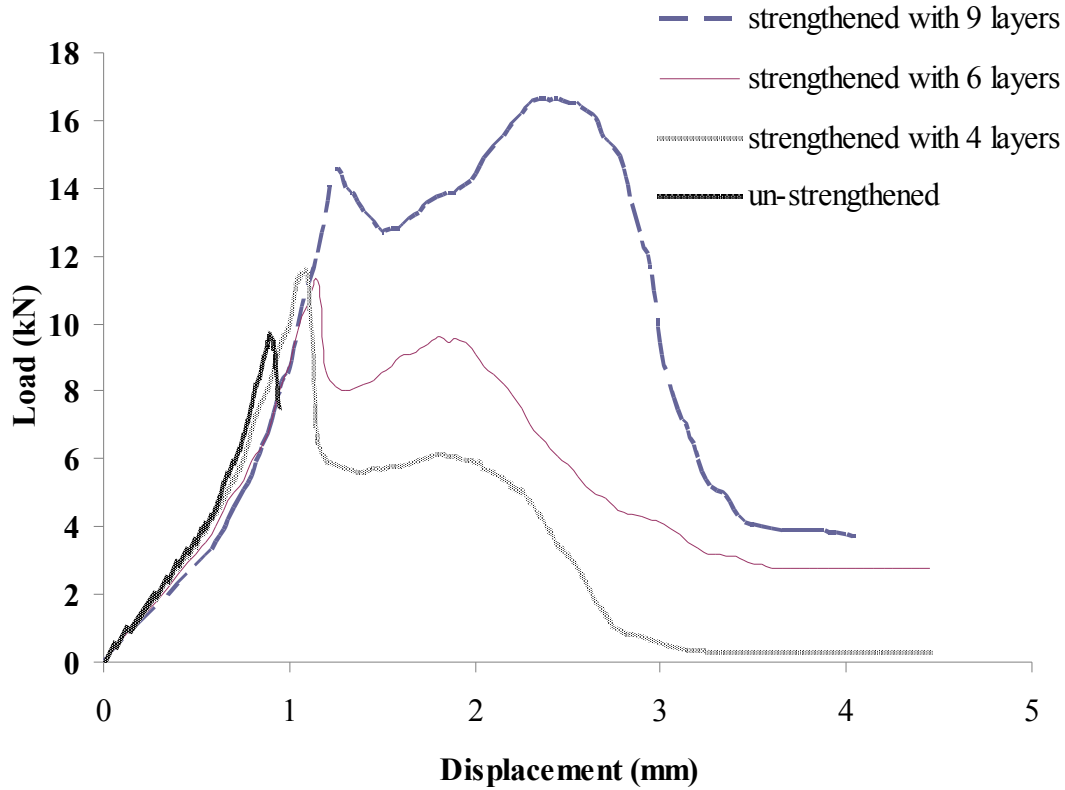
Figure 5.3 Typical load versus displacement for concrete beams strengthened with *FABcrete*

In the case of strengthened beams, the cracks formed in the main beam had smaller crack width compared to that in the unstrengthened beams. Multiple cracking was also observed in the *FABcrete* layer. After reaching the ultimate load, there is a drop in load carrying capacity, which is mainly due to the matrix delamination from textile. For 6 and 9 layers, there is again an increase in the load carrying capacity. Since all the layers of textiles were provided as a single layer, it is also possible that once one layer could have ruptured and the force is transmitted to the remaining layers. This mechanism would have led to the increase of the energy absorption of the strengthened beams.

Based on the investigations on strengthening of concrete beams with *FABcrete* with manually stretched textiles, it was concluded that, there is practical difficulty to accommodate more number of layers to achieve a particular thickness. Further, the increase in load carrying capacity is not that significant as the number of layers increases, leading to underutilization of the

potential of textiles. Nevertheless, no debonding of *FABcrete* layer from the concrete surface was seen in any of the strengthened beams indicating that no additional anchoring methods are needed for *FABcrete* strengthening.

5.2.3 Details of test specimens for strengthening of RC beams

Six identical RC beams of 100mm (width) × 150mm (depth) × 1500mm length were cast; beams SGB1, SGB2 and SGB3 were cast from one batch, and beams SGC1, SGC2 and SGC3 were cast from another batch. The reinforcement provided in each beam consists of two 10mm bars at the bottom (i.e., on the tension side) and two 10mm bars at the top (i.e., on the compression side), along with shear reinforcement of 6mm bars at 100mm c/c. The clear cover provided was 20mm. The detailing and test configuration are depicted in Figure 5.4.
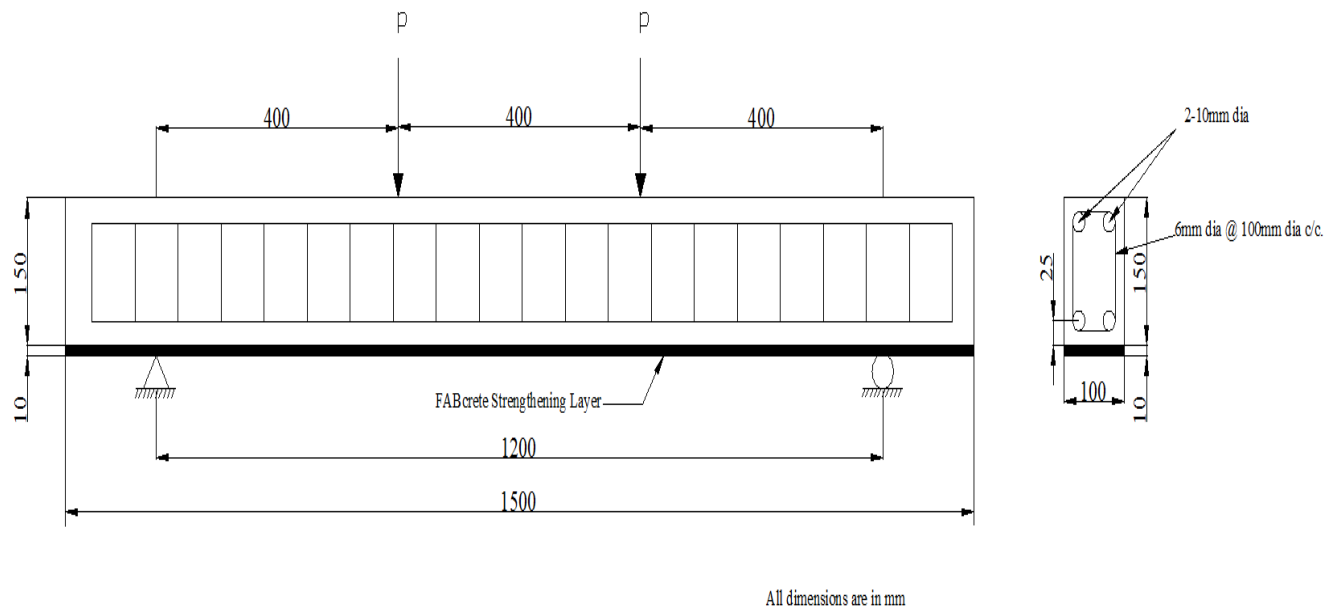
Figure 5.4 Test specimen

Following 28 days of water curing, the beams were air cured for 15 more days. Before testing, a thin coating of Plaster of Paris (PoP) was applied on the beams to facilitate visual tracking of cracking during testing.

5.2.3.1 Test setup

The flexural loading was applied with a 250kN MTS servo hydraulic actuator. The effective span of beams were kept as 1.2m, and the simply-supported boundary condition was provided by placing a roller support at one end and a hinged support at the other end as shown in Figure 5.4. The beams were subjected to four point bending, and the tests were carried out under a constant displacement rate of 0.5mm/min. The applied load is transferred from the actuator through an I-section to the two loading points at distances of 400mm from each support through the steel rods placed at those points. The test setup is shown in Figure 5.5. To measure the midspan deflection an LVDT was placed and monitored through a HBM MGC Plus datalogger.
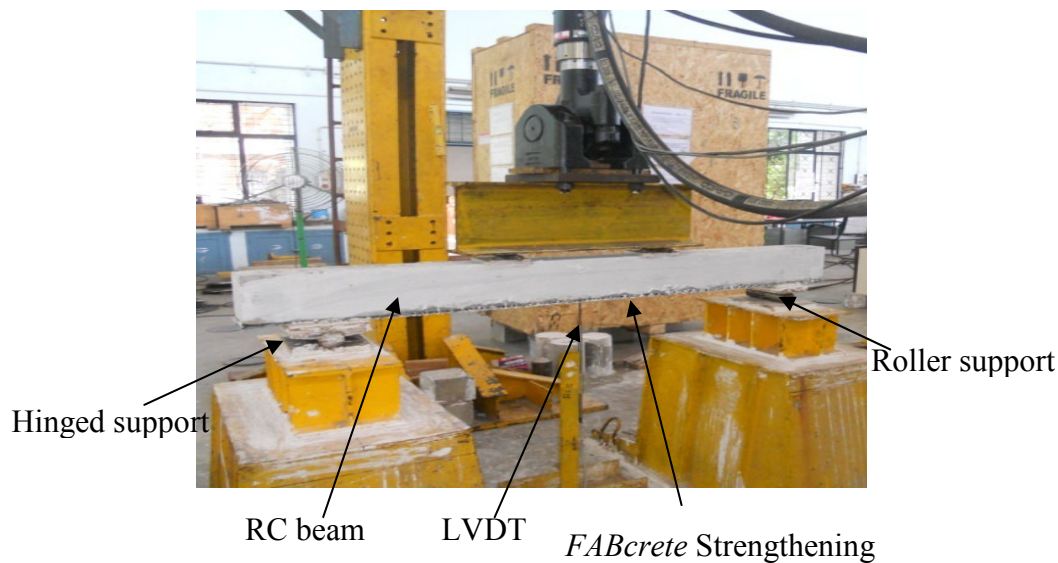
Figure 5.5 Test setup

Strain gauges were also mounted, in certain specimens, at the compression and tension zones, to monitor the strain evolution. In addition, an Imetrum non-contact video gauge was used in the tests of the strengthened beams; see configuration in Figure 5.6 for selecting locations for strain measurement. This system consists of a high resolution digital camera to capture and record the movements at the required measurement points, which are identified in the computer as pattern recognition blocks. The preparation time needed to apply the required speckle pattern is only a few minutes compared to more than an hour taken to prepare and apply strain gauges, and the measurements can be made at various locations with minimal effort. The strains and

displacements are obtained through digital image correlation. Further details on the non-contact video gauge are given in Appendix-C.

Selection of locations for strain measurements

Figure 5.6 Setup for measurements using non-contact video gauge

5.2.3.2 Tests on Uncracked RC Beams

Two uncracked beams, SGB2 and SGC1, were considered as the control (reference) beams. Their load versus displacement behaviour is shown in Figure 5.7. The first visible crack was observed for SGB2 and SGC1 at 9.0kN and 11.5kN, respectively. The typical crack pattern is shown in Figure 5.8, and a closer view of the main flexural crack (at the centre of the beam) is shown in Figure 5.9. The yielding of the reinforcement in both the beams, as indicated by the major change in slope, started at a load of around 44kN at a displacement of around 6mm. The maximum loads obtained in the beams SGB2 and SGC1 were 46.8kN and 46.2kN, respectively. The tests were terminated when significant concrete crushing was observed, at a displacement of about 15mm.
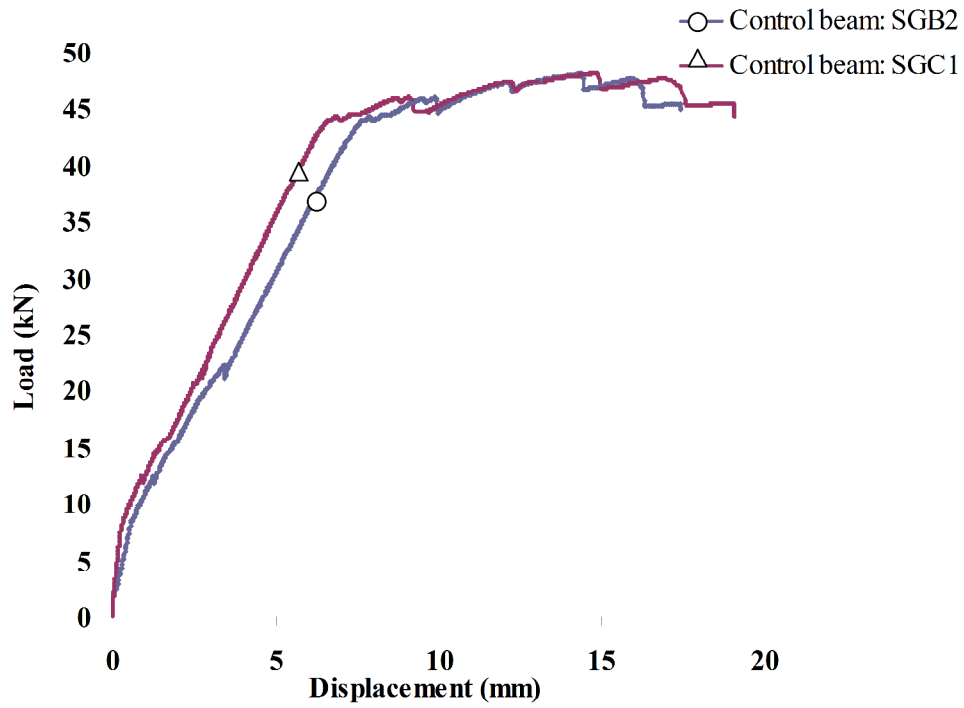
Figure 5.7 Load versus displacement of control RC beams
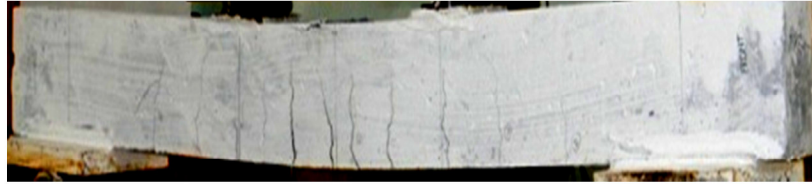
Figure 5.8 Typical crack pattern in one of the control beams

centre crack

zoomed-in view
(bottom crack width of 2.4mm at failure)
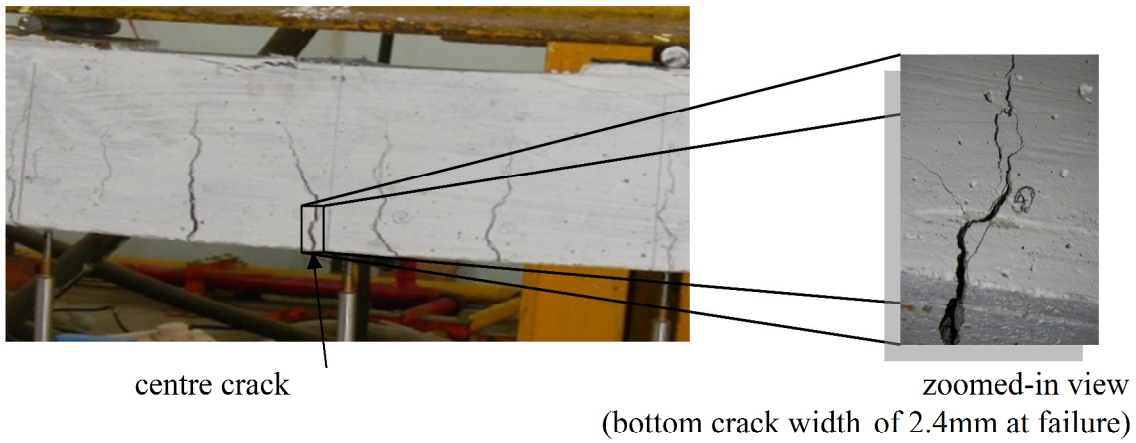
Figure 5.9 Closer views of major flexure crack in one of the control beams

5.2.3.3 Pre-cracking of RC beams

To understand the efficiency of *FABcrete* for retrofitting of cracked beams, two beams, SGC3 and SGB3, were loaded up to 30% of the maximum load-carrying capacity, as obtained in the tests of the control beams. The beams were loaded until 16kN, at which stage there were 6 visible cracks, as can be seen in Figure 5.10. The corresponding load versus displacement diagrams are given in Figure 5.11.

cracks at load of 16kN
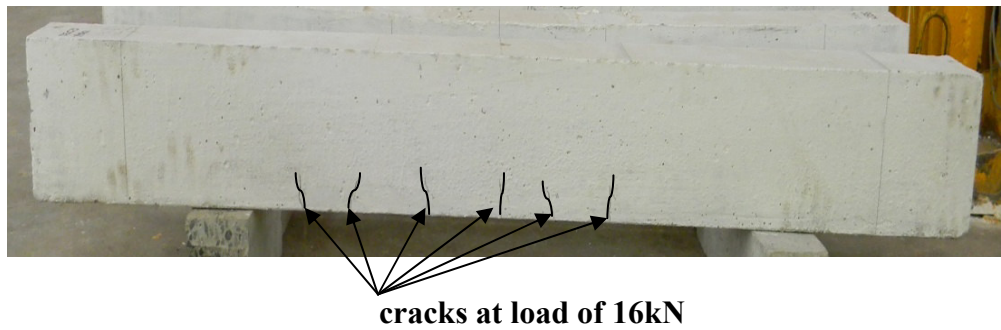
Figure 5.10 Cracking in one of the RC beams loaded to 30% of maximum load
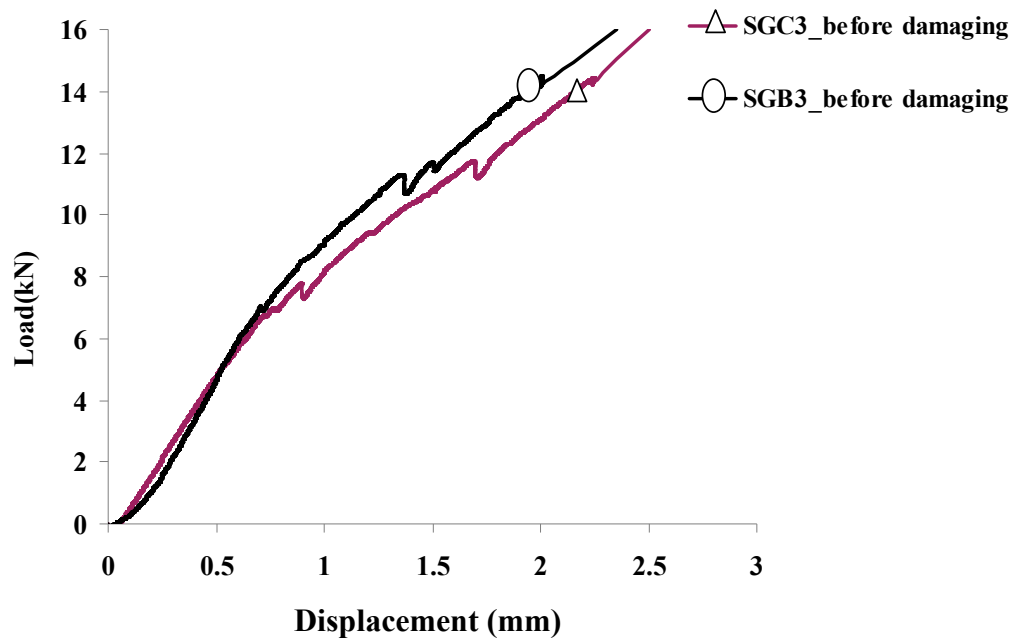
Figure 5.11 Load versus displacement of RC beams loaded to 30% of maximum load

5.2.3.4 Strengthening of RC beams with *FABcrete*

Two types of RC beams, uncracked (SGB1, SGC2) and cracked (SGC3, SGB3), were strengthened with *FABcrete* by cast-in situ wet layup process, after preparing the surface by grinding to remove unevenness.

In order to stretch the glass textiles in the strengthening layer, a mechanism scaled-up from that mentioned in Chapter 4 was used. The setup consists of steel frames, which are attached at both ends of the RC beam, as seen in Figure 5.12. The frame is fixed to one end of the beam, as shown in Figure 5.12(a), and the textiles are pulled through the clearance in the steel frame at the other end and the two connection bolts between the steel channels, seen in Figure 5.8(b), are tightened to stretch the textile. The tightening of the bolts was done until the textile layers appeared straight by visual examination.

To cast the strengthening layer of *FABcrete* on the RC beams, the following procedure was followed, as shown in Figure 5.13. Firstly, ten layers of glass textile SRG-45 were kept in position for stretching. Then, a layer of *FABmix* of about 2mm thickness was applied to the surface of RC beam. Following this, all the layers of textile were placed one over the other in a staggered manner and stretched. Subsequently, an additional layer of *FABmix* was applied and leveled until a 10mm thick *FABcrete* layer was achieved. The strengthened beams were immersed under water for curing up to 28 days.

Steel frame

(a) Fixed end

Steel frame   Bolts used for stretching
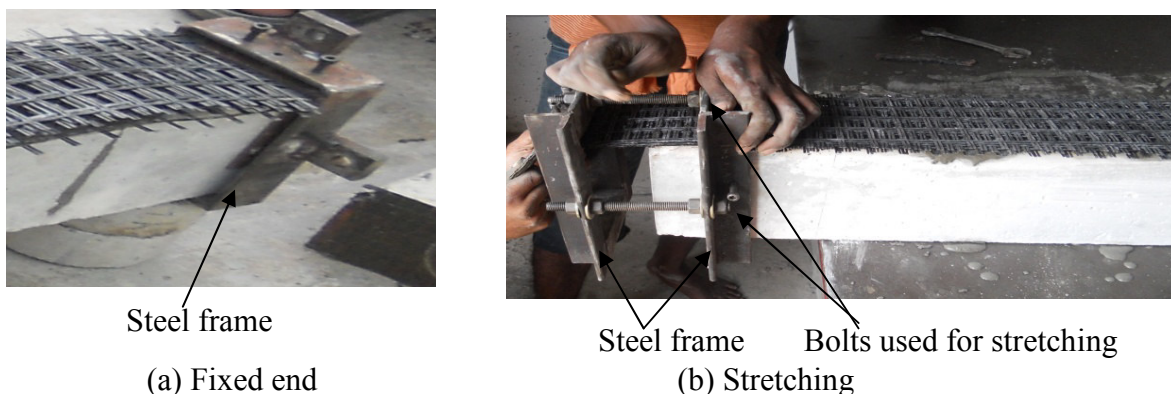
(b) Stretching

Figure 5.12 Details of stretching mechanism for textiles

Applying first layer of *FABmix*

Stretching of textiles

Applying final layer of *FABmix*

FABcrete strengthened beams

Figure 5.13 Steps involved in strengthening of RC beam with *FABcrete*

The details of the textile stretching mechanism and the demonstration of an on-site application are given in chapter 6.

5.2.3.5 RESULTS AND DISCUSSION

The results obtained from experimental investigations on uncracked and cracked RC beams strengthened with *FABcrete* were examined with respect to load-carrying capacity, ductility, crack pattern and failure pattern. In addition, the strains obtained from the non-contact video gauge were used to understand the variations across the depth of the beam and along the length of the *FABcrete* strengthening layer.

5.2.3.5.1 Load versus displacement response

The load versus displacement curves of strengthened uncracked and cracked beams are seen in Figures 5.14 and 5.15, respectively, along with those of the control (unstrengthened) beams. It is seen that the response features six distinct stages. The first stage is until initiation of cracking either in *FABcrete* layer or in the main beam. At this stage, the initial load versus displacement response is stiffer compared to corresponding control beams, and this stage ends with the initiation of first crack in the strengthening layer. As expected, the first crack load in the strengthened uncracked beam is higher than the corresponding control beam (see Fig. 5.14). The first crack is reflected by a change of slope in the curve, after which more cracking occurs in both the strengthening layer and the RC beam till the yielding of the steel, which denotes the end of Stage 2. After yield, no new cracks occur in the RC beam but the strengthening layer has new cracks until the peak load, which is the end of Stage 3. After this stage, one of the cracks in the RC widens and the load starts decreasing (Stage 4). After this, there is no substantial reduction in the load-carrying capacity and textile elongation, along with steel yielding (Stage 5) takes place. Finally, the textile ruptures at the location of the major crack, at the beginning of Stage 6. At this stage, the crack width at the centre of the SGC2 beam was measured using a crack width microscope and found to be 1.5mm in the RC beam. It is observed that the textile rupture occurs only in a few layers (e.g., 3 layers), and the presence of more number of layers (in this case, 10 layers) helps sustain the residual load capacity, along with deformability. After the textile ruptures, concrete crushing occurs later on. The tests were terminated when the displacement was 30mm for the uncracked and strengthened beams, and at 50mm for cracked and strengthened beams.
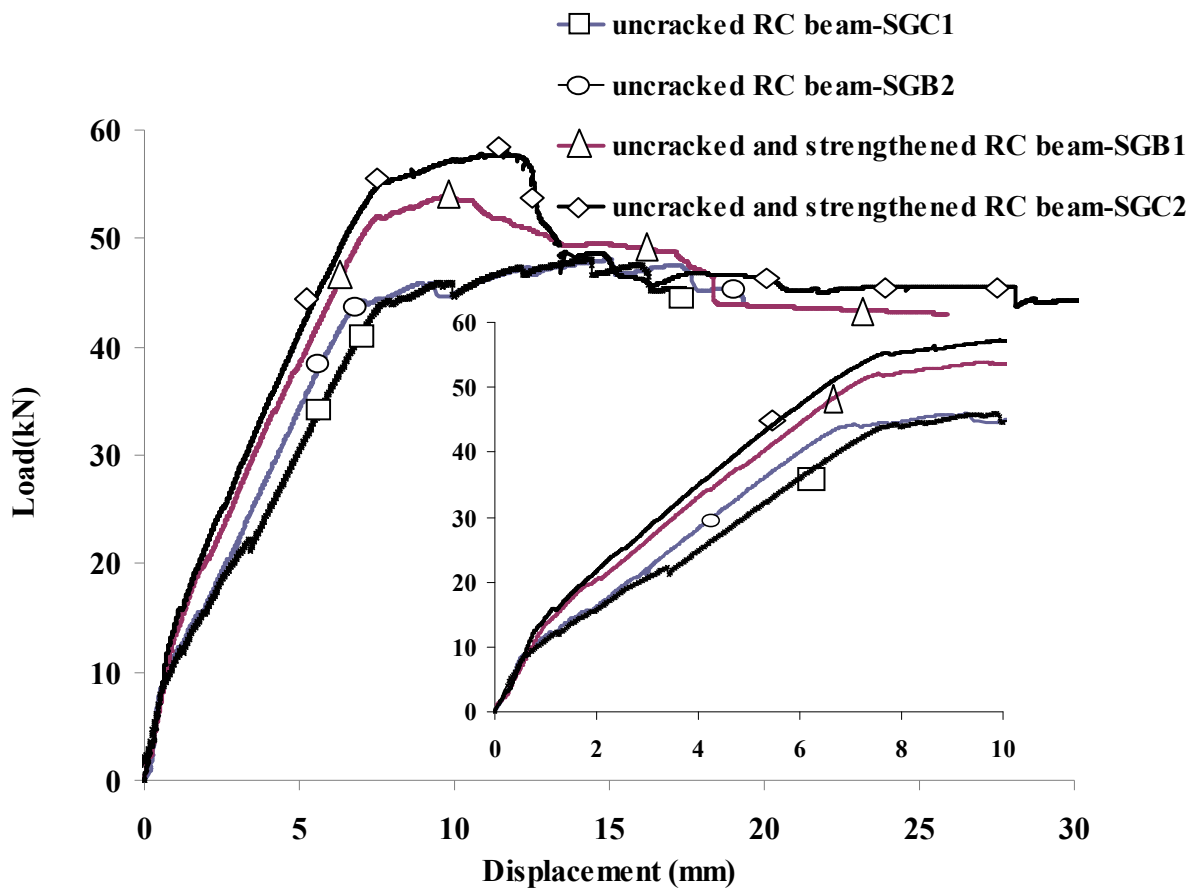
Figure 5.14 Load versus displacement curves of the control and strengthened RC beam (inset shows the plot until a displacement of 10mm)
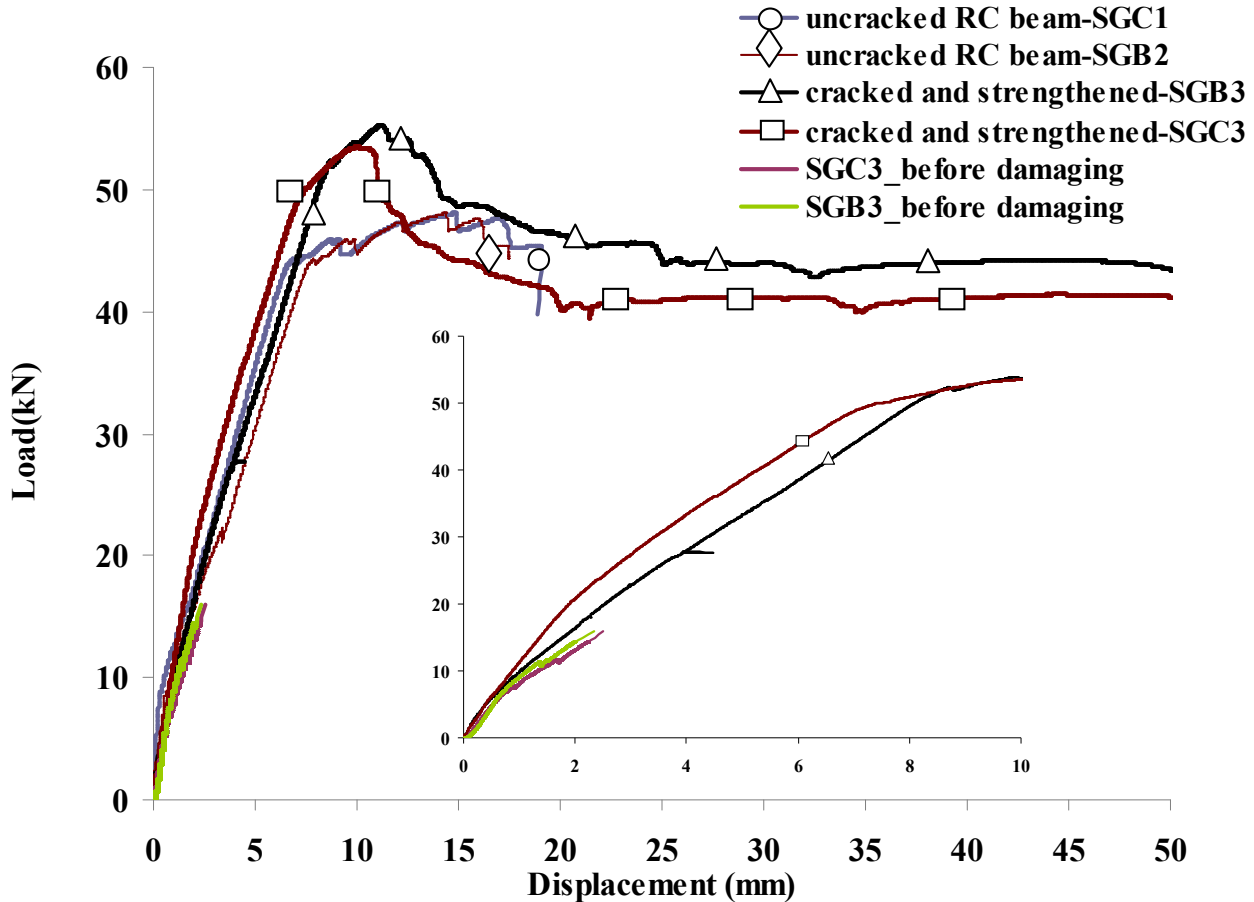
Figure 5.15 Load versus displacement curves of the cracked and strengthened RC beam (inset shows the plot until a displacement of 10mm)

A summary of the experimental results in terms of cracking load, yield load, peak load and corresponding deflection for control and strengthened beams is presented in Table 5.2. While comparing the response of strengthened uncracked beams (SGB1, SGC2) with that of the control beams (SGB2, SGC1), it is observed that the first cracking load in the former beams is more than twice that of the latter due to the higher moment of inertia of the strengthened beam and good bond of the *FABcrete* with the RC beam. There is an increase of 20% in the load for the strengthened beam at yield, though the corresponding deflections are similar compared to the control beams. Moreover, there is also a 20% increase in maximum (peak) load-carrying capacity for the strengthened beams compared to the control beams, and a 30% reduction in the corresponding deflections.

Table 5.2 Experimental results of strengthened and un-strengthened RC beams

Beam	First crack in strengthening layer		First crack in RC beam		Yield load (kN)	Displacement at yield load (mm)	Peak load (kN)	Displacement at peak load (mm)
	Load (kN)	Displacement (mm)	Load (kN)	Displacement (mm)				
SGC1	-	-	9.0	0.7	44.3	7.8	46.2	14.8
SGB2	-	-	11.5	0.8	44.3	7.4	46.8	15.0
SGB1	15.9	1.2	23.4	2.2	51.5	7.3	53.6	9.6
SGC2	15.5	1.2	20.9	2.1	55.1	7.8	57.7	11.3
SGC3	11.9	1.0	-	-	51.0	7.5	53.4	10.3
SGB3	11.4	1.3	-	-	51.8	8.5	55.1	11.3

In the case of the cracked beams that were strengthened (SGB3, SGC3), it is seen that the yield and peak loads are higher than the control beams (SGC1, SGB2). It is also observed (see Fig. 5.15) that the post-peak response is ductile and there is good residual load-carrying capacity. While comparing with the control beams, there is an increase of 16% in the yield load, in the strengthened beams and a 17% increase in the maximum load. After the peak, there is a 22% decrease in the load-carrying capacity, without any subsequent load reduction over a large deflection range of 25 to 50mm.

Based on the overall observations, a generalization of possible phenomena occurring in the *FABcrete* strengthened beam is proposed in Figure 5.16.
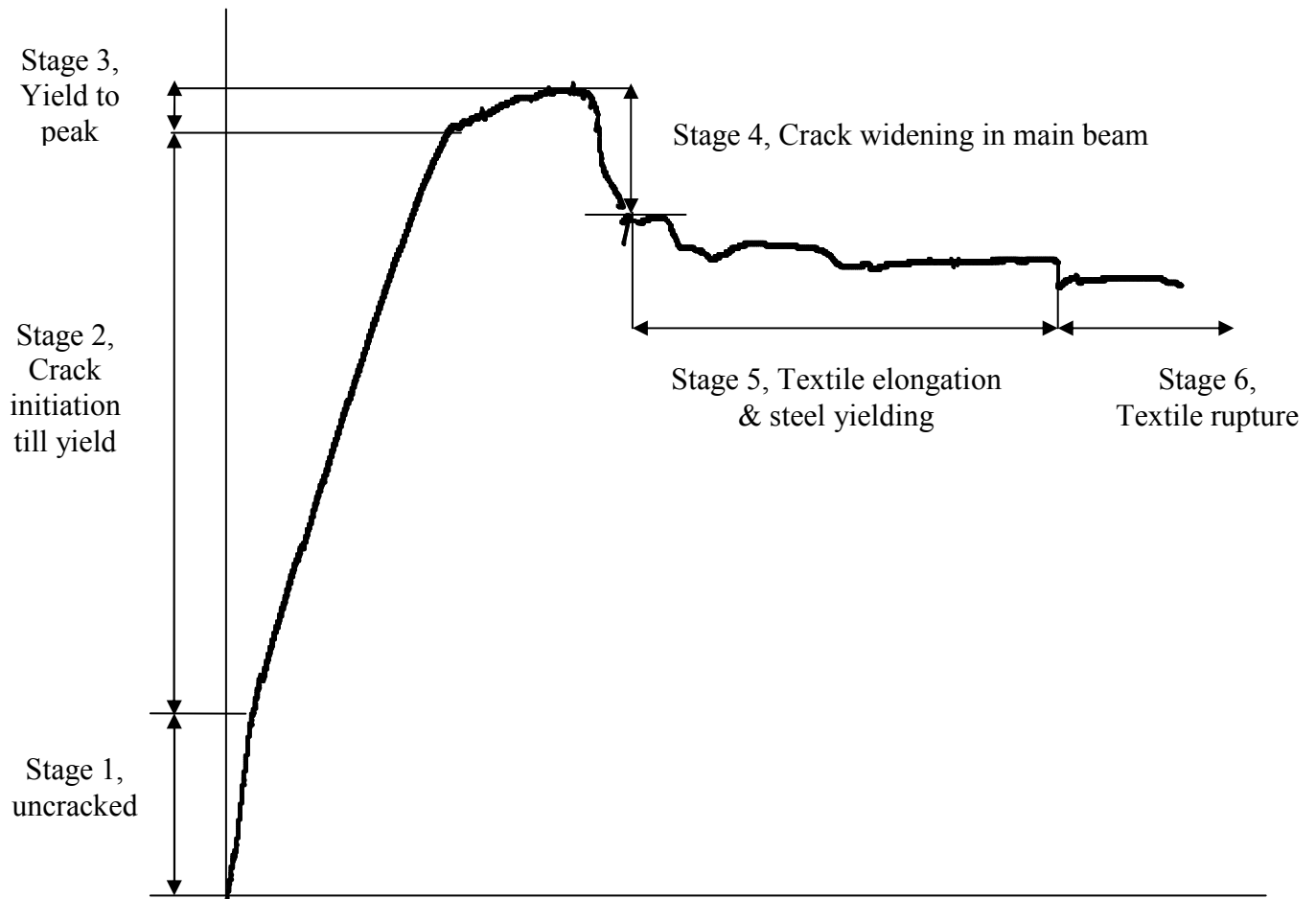
Figure 5.16 Generalized behaviour of a *FABcrete* strengthened RC beam

5.2.3.5.2 Cracking and failure pattern

All the strengthened beams showed multiple cracking and the final failure was by rupture of the textile. There was no debonding of the *FABcrete* layer in any case. The crack patterns in the strengthened beams (SGB1 and SGB3) can be seen in Figure 5.17. It can be noted that all the cracks formed in the strengthening layer are hairline, except for one crack that widens until the rupture of the textile.
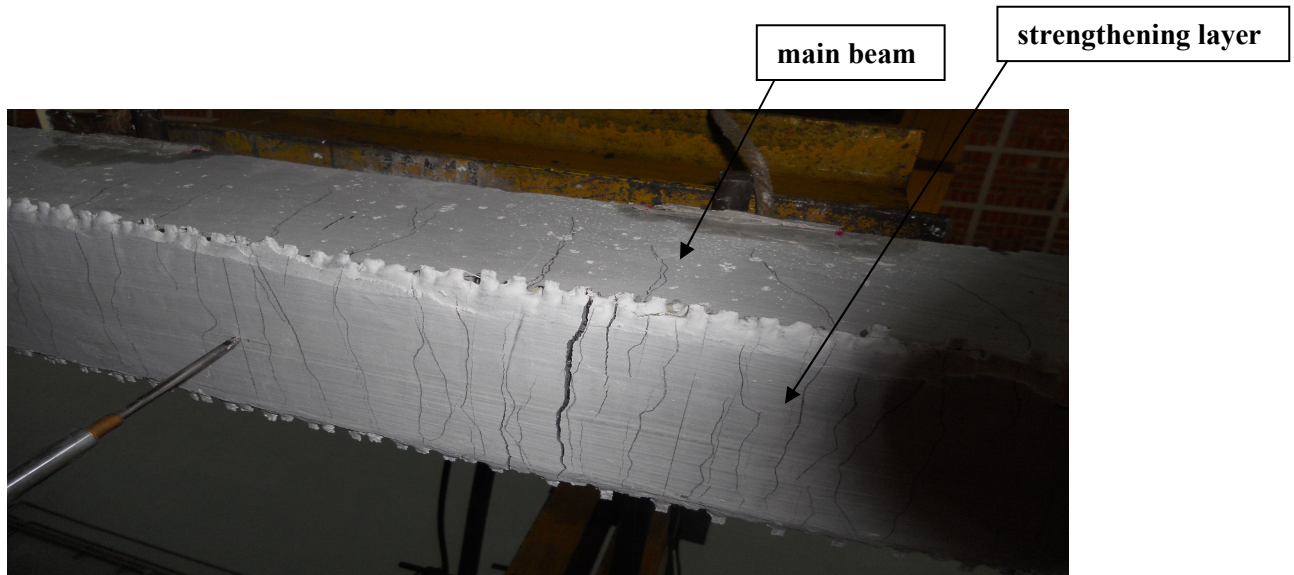
(a) uncracked and strengthened beam (SGB1) at displacement 30mm
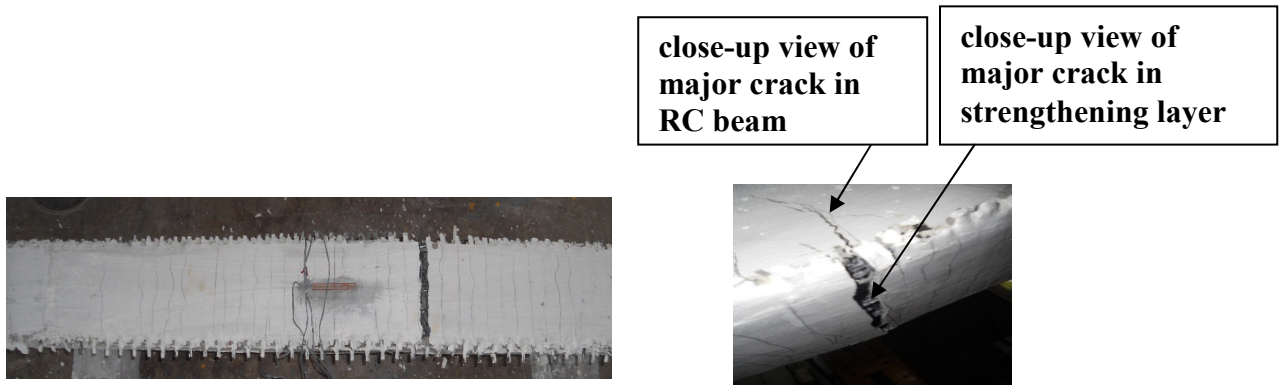
(b) cracked and strengthened beam (SGB3) at displacement 50mm

Figure 5.17 Crack and failure patterns of the strengthened beams

The observed sequence and location of crack formation in typical control and strengthened beams are shown in Figure 5.18. It is noticed that, as expected, more cracks are formed in the constant bending moment zone (at 400 to 800 mm distance from hinged support). For the strengthened beam SGB1, there were totally 9 visible cracks in the RC beam and 23 in the *FABcrete* layer whereas the RC control beam had 11 cracks. In the strengthened beam, most cracks occur in the RC beam between the loads of 20 and 30kN. Moreover, the cracks in the strengthening layer are distributed along the length of the beam and initiate over the entire load range, between 15kN to 53kN. The average crack spacing is obtained as the length over which

128

the cracks occurred divided by the number of cracks minus one; consequently, the average crack spacing in the RC beam was about 110mm and in strengthening layer it is about 50mm.
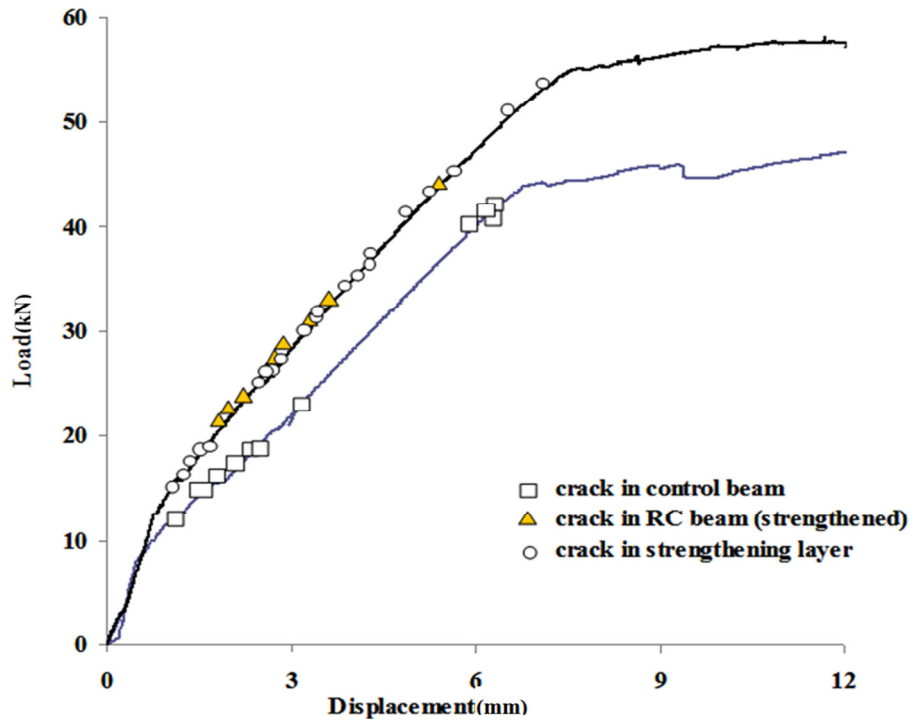
(a) Cracks observed and corresponding load and displacement
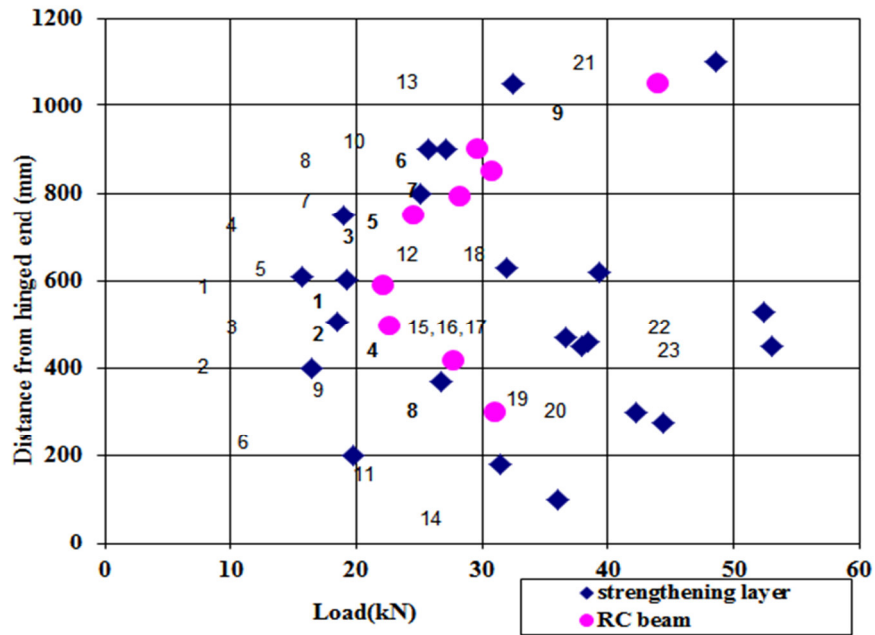
(b) Cracking locations and loads
Figure 5.18 Crack details

5.2.3.5.3 Strain measurements

Strains were measured in the strengthened beam (SGC2) using 60mm strain gauges on the compression and tension sides of the strengthened beam. Figure 5.19 shows the locations of the strain gauges and the video gauge pattern recognition blocks (shown with dotted lines). A comparison was done for the compressive strains at the midspan on the front face, and the tensile strains in the strengthening layer using both the instrumentation techniques.
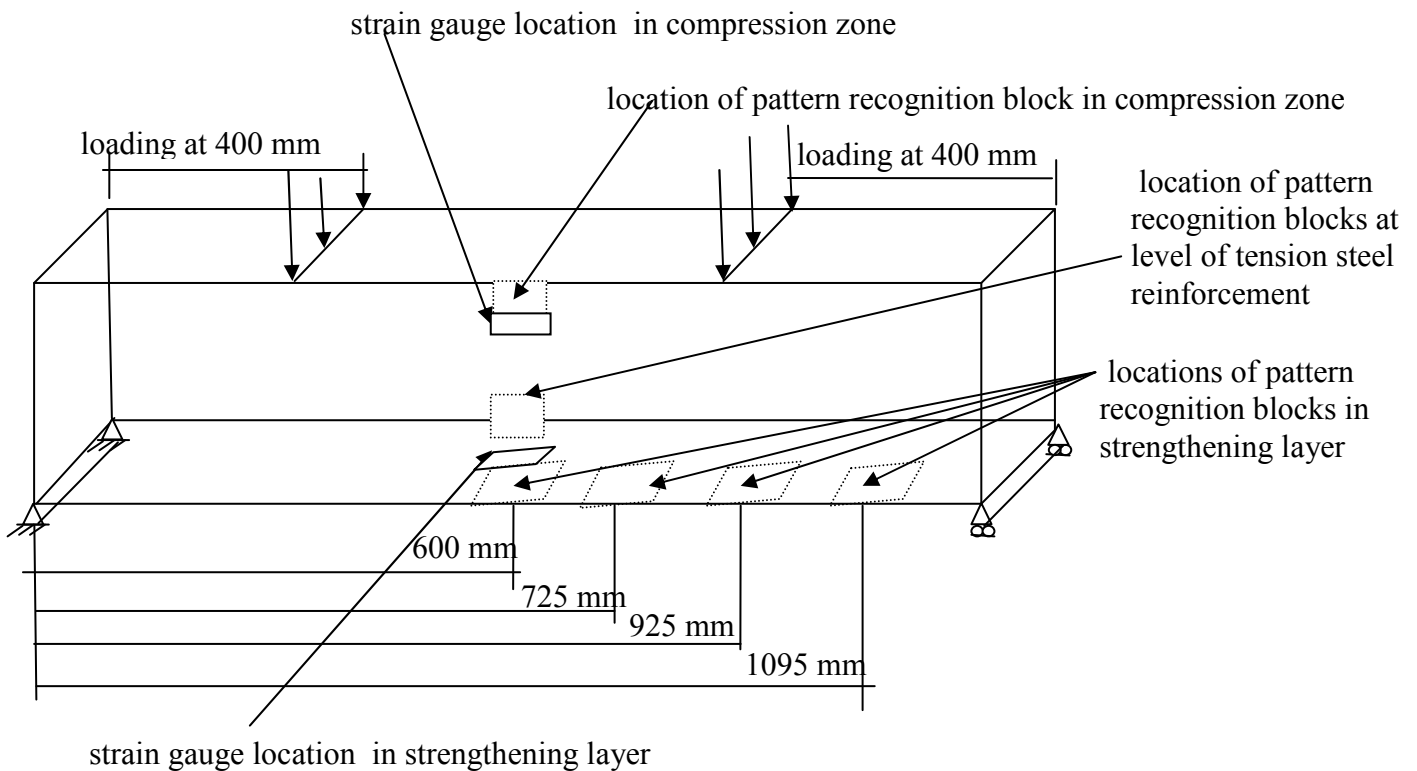
Figure 5.19 Location for strain measurements using strain gauges and video gauge

The strains obtained at various load levels are shown in Figure 5.20. While examining the compressive strains (Figure 5.20a), it is noted that the strain values obtained using both the techniques are practically the same until a load of about 47kN, when the strain gauge malfunctioned probably due to cracking. In the tensile zone (Figure 5.20b), it is observed that the strain gauge malfunctioned at the load of about 20 kN. However, the non-contact video gauge could monitor the strains till the end of test. Hence, in the present study, only the strains obtained from the video gauge are used in further analysis.
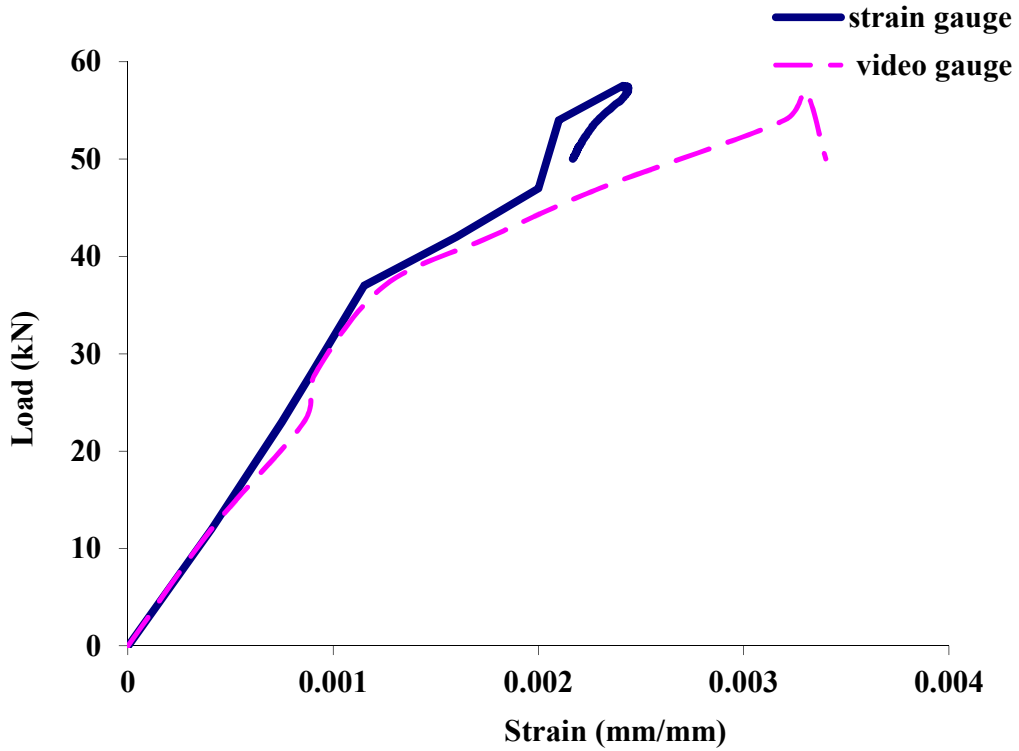
(a) compressive strain
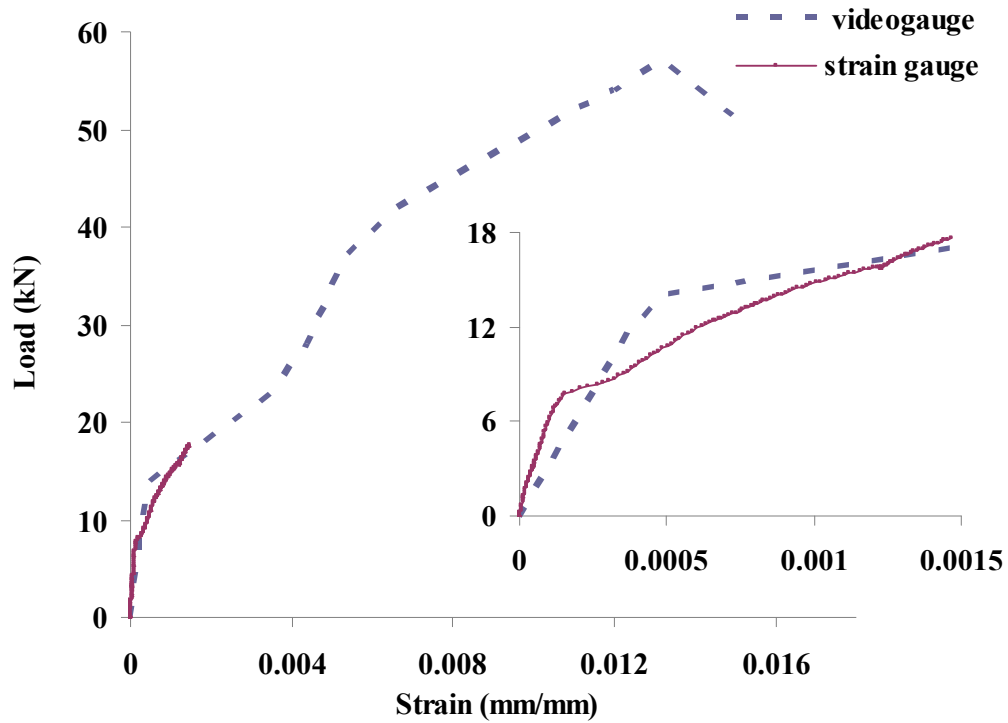
(b) tensile strain in strengthening layer (inset shows the plot until a strain of 0.0015)

Figure 5.20 Comparison of strains from strain gauges and video gauge at midspan

131

The strains obtained using the video gauge were used in Figure 5.21 to plot the variations at different load levels, along the depth of the strengthened beam, at mid span, with data points corresponding to 5mm depth (on the front face, in the compression zone), at the level of the bottom tensile steel in the main beam (at a depth of 130mm), and on the bottom face of the strengthening layer. Note that positive values represent tensile strains and negative values represent the concrete compressive strains.

While examining the strain distribution in the tensile zone, it is noticed that until the peak load (57kN), the strain at the level of steel and *FABcrete* increases, as expected. The increase in strain at the level of steel, with load, is more after the steel starts yielding (i.e., loads greater than 54kN). Since there is a continuous increase of strain in the *FABcrete* throughout the experiment, it clearly indicates the integrity of the bond with the RC beam and absence of debonding of strengthening layer.
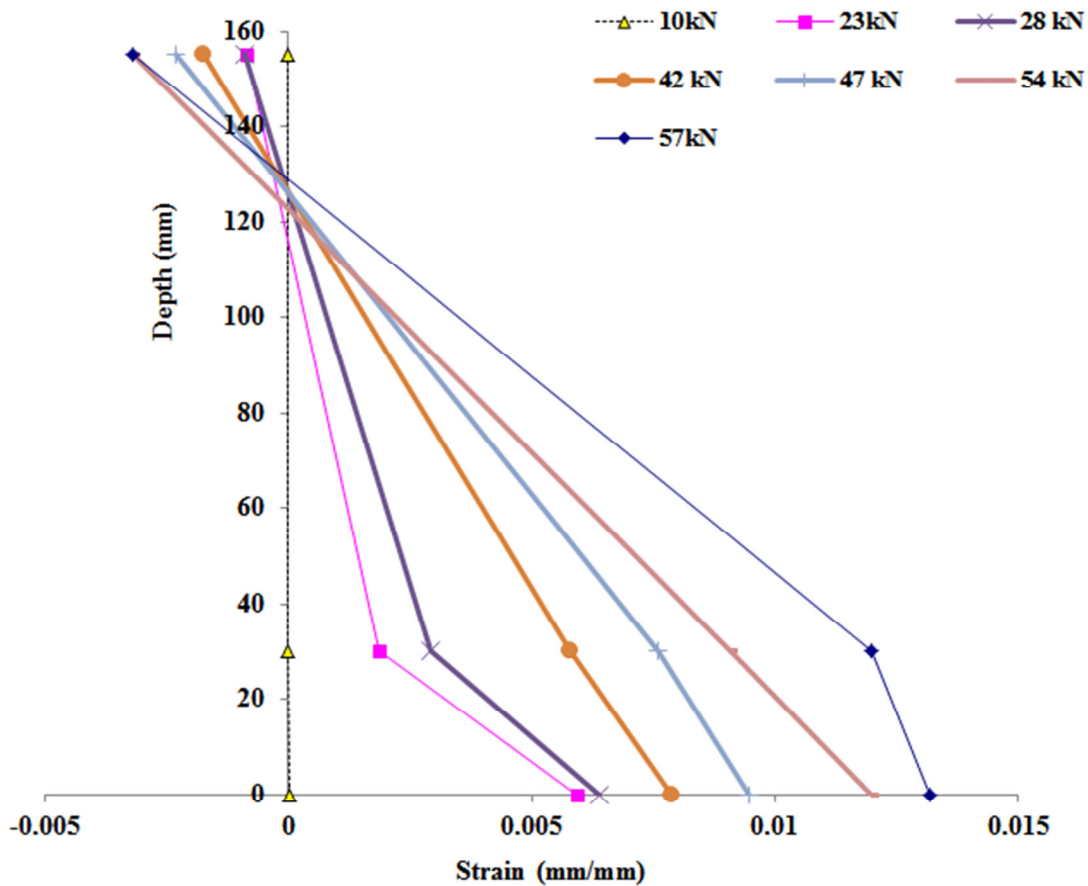
Figure 5.21 Strain variation across depth of the strengthened beam

To measure the tensile strain in the strengthening layer, multiple pattern recognition blocks were selected at 600mm, 725mm and 925mm and 1095mm from the hinged support (refer Figure 5.16). The strain obtained at these locations are plotted in Figure 5.22. It is observed that when the load is around 14kN, the strain distribution is uniform along the length. As more number of cracks are formed in the strengthening layer, the strain at 725mm is higher than in the other locations. It was also noted that many cracks (i.e., cracks 1 to 6 forming between 200mm to 800mm; refer Figure 5.18b,) occur in the strengthening layer before the first crack appears in the RC beam (i.e., between the loads of 15kN to 23kN). The first crack in the RC beam appeared at midspan, with further cracking until a load of 33kN (cracks in RC beam denoted as circles 1 to 8; refer to Figure 5.18b). Simultaneously, there were further cracks in the strengthening layer (cracks 7 to 13). From this stage onwards, the strain exhibited at 725mm is more compared to all other locations. Beyond 33kN, all cracks (14 to 23) were formed in the strengthening layer, except the 9th crack in RC beam, that is formed at 1025mm. At the peak load, the maximum strain of 0.018mm/mm is seen at 725mm. It was observed that crack widening in the strengthening layer and final rupture of the textile was near this location.
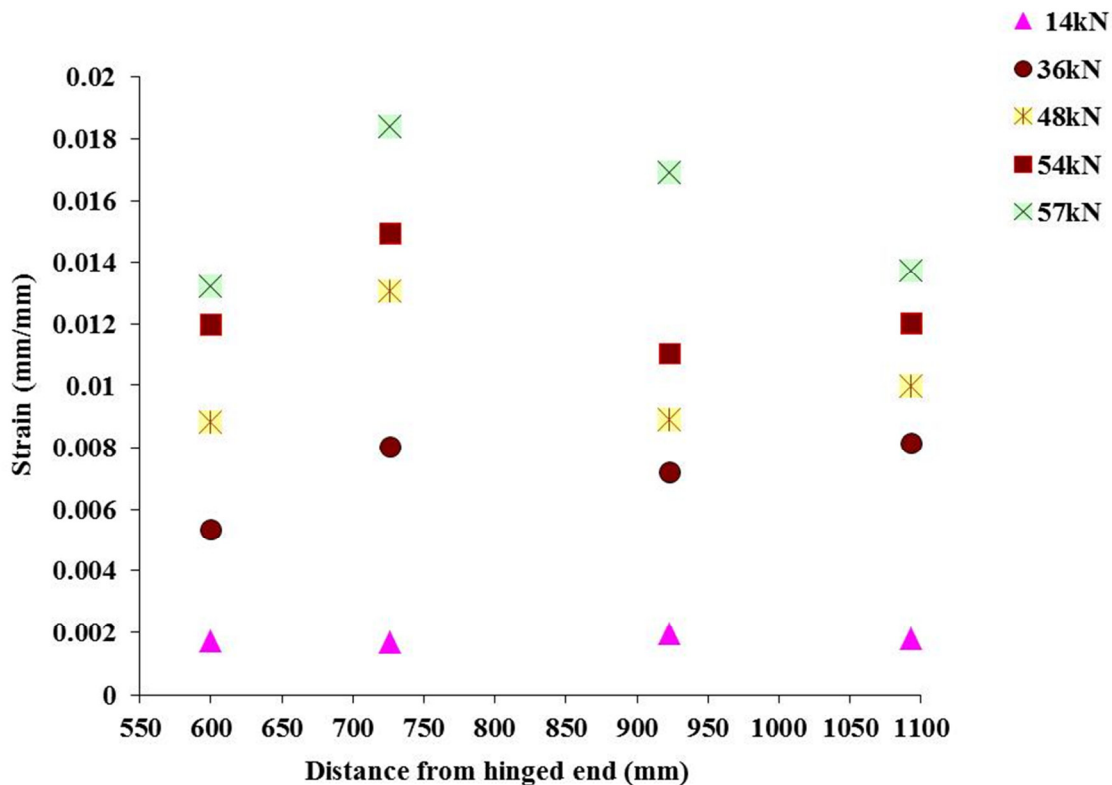
Figure 5.22 Strain along length of strengthening layer

5.2.3.5.4 Crack width from strain measurement

The strain obtained using video gauge was further used to calculate crack widths in the strengthening layer and in the RC beam. The crack width is calculated as the product of length of the pattern recognition block (30mm) and the strain at that location. The crack widths obtained at various locations in the strengthening layer between 500mm and 1100mm are shown in Figure 5.23. In addition, the crack width in the RC beam at mid span is also shown. It is observed that the cracks in the strengthening layer are of almost the same width till the first crack appears in RC beam (around 25kN) and thereafter there is strain localization leading to more differences in crack width between various locations in the strengthening layer. It is further noted that the increase in crack width in the RC beam is higher after yielding of the steel (for load greater than 54kN).
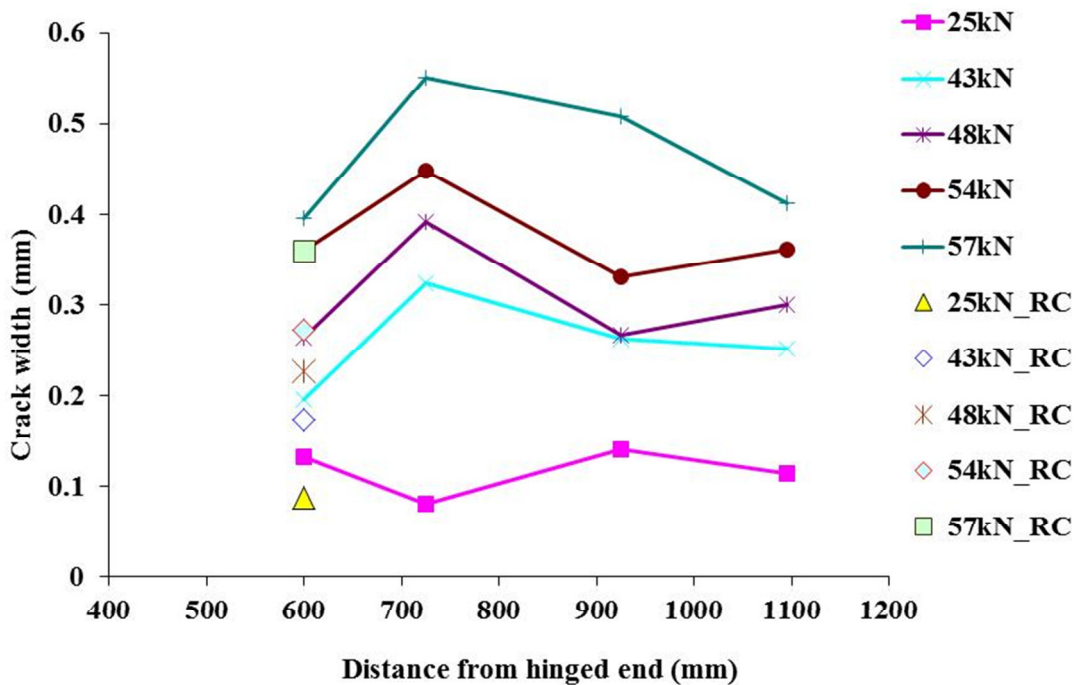
Figure 5.23 Crack widths in the RC beam and strengthening layer

5.2.3.5.5 Bending stiffness

The strains obtained using the video gauge was further used to evaluate the bending stiffness (EI) of the strengthened beam. After cracking and yielding of steel, the moment of inertia at midspan and stiffness change are as seen in Figure 5.24, following the Eqns. 5.1 and 5.2:

134

$$EI = \frac{M}{\emptyset} \quad \text{with} \quad M = \frac{Pa}{2} \quad\quad\quad (5.1)$$

$$\emptyset = \frac{(\varepsilon_c + \varepsilon_t)}{h} \quad\quad\quad (5.2)$$

where, M = bending moment (kN-mm), P= applied load (kN), a = distance between the first loading point and support, $\emptyset$ = curvature (mm^{-1}), ε_c = concrete compression strain at top of beam, ε_t = tensile strain at the bottom of *FABcrete*, and h= cross section height of strengthened beam.

From Figure 5.24, it is observed that there is a rapid decrease of bending stiffness in the initial stages due to crack formation over a small increase in load (till the 1st crack appearance in the RC beam). However, after that the decrease in bending stiffness is not that rapid indicating the continuous integrity of the strengthening system with base concrete over the entire loading range.
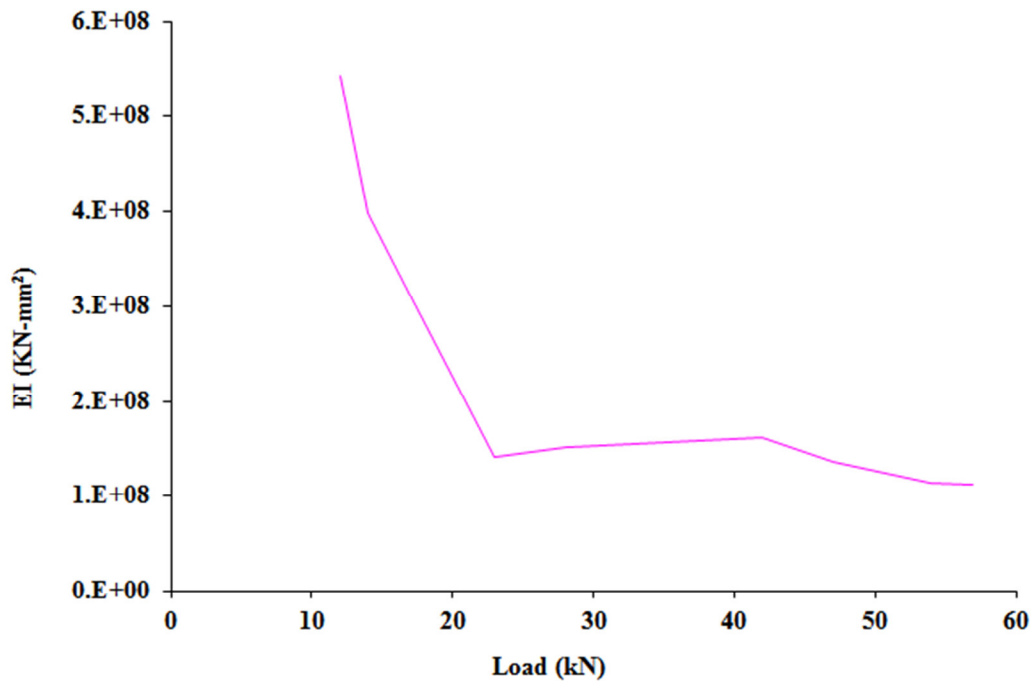
Figure 5.24 Load versus bending stiffness

5.2.3.5.6 Ductility and Work done

The multiple cracking with smaller crack widths in the strengthening layer leads to higher work done, deformations and ductility (i.e., the ability to deform without much reduction in load) for

the *FABcrete* strengthened RC beams. The work done for the strengthened beam calculated as the area under the load versus displacement curve till cracking, yielding and ultimate stages, is given in Figure 5.25. It is noted that there is a 38% increase in work done till cracking for the strengthened beam compared to the control beam. Further, for the work done till yield load there is an increase of 21% and 23%, respectively, for the uncracked and strengthened beam, and the cracked and strengthened beam compared to the control beam. Until a deflection of 30mm in the strengthened beams, the work done in the uncracked and strengthened beam is 2.6 times that of the control beam and 2.3 times in the cracked and strengthened beam.

Work done (kN-mm)

At Displacement of 30 mm — 1269; 1155; 347

At Peak load — 302; 294; 347

At Yielding load — 201; 206; 167

At first Cracking load — 9; 7; 7

Legend:
☐ uncracked and strengthened
■ cracked and strengthened
☐ control beam
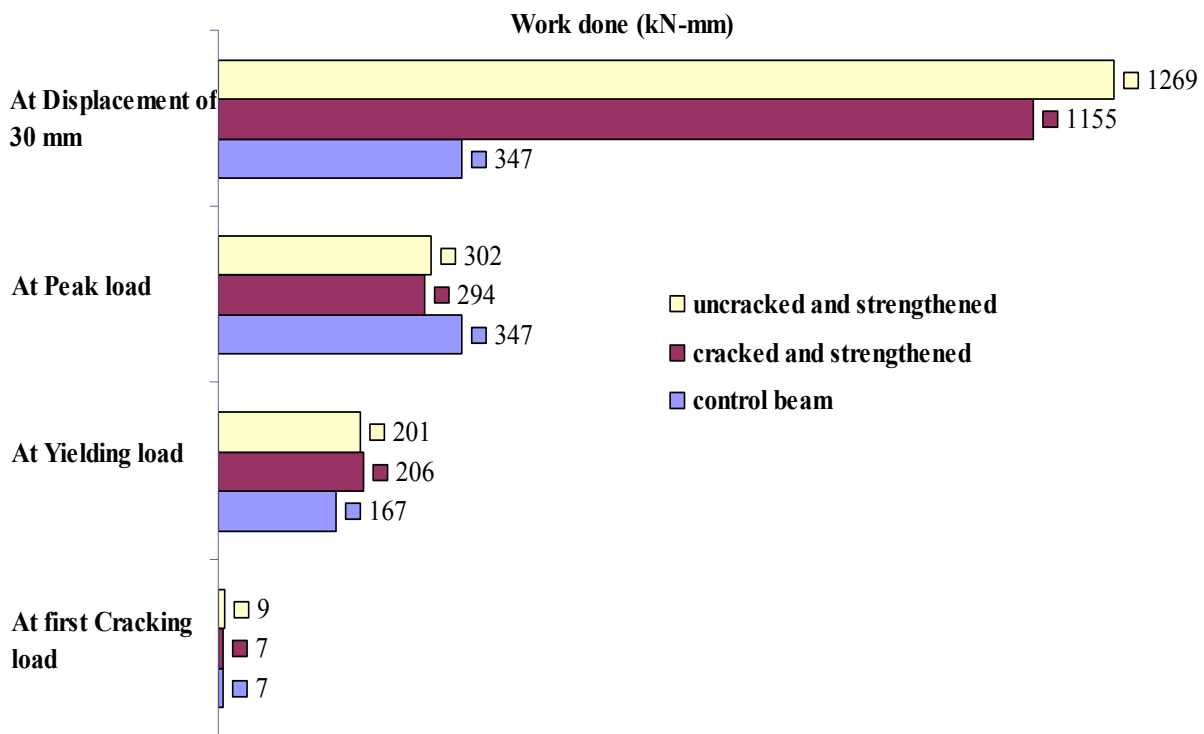
Figure 5.25 Work done up to various stages in the strengthened and un-strengthened beams

In order to quantify the ductility of *FABcrete* strengthened beams based on energy principles, ductility index was calculated as the ratio between the areas under the load versus displacement curve till a deflection of 30mm and till yielding (refer to Table 5.3). It is observed that the ductility index of uncracked and strengthened beam is about 3 times that of the control beams, whereas for the cracked beam the ductility index is 2.7 times that of control beam. In both the

cases, it can be concluded that the strengthened beam is capable of dissipating more energy during failure.

Table 5.3 Ductility index

Beam	Area under load vs. displacement curve till yield load (kN-mm)	Area under load vs. displacement curve till 30mm displacement (kN-mm)	Ductility index
Control beam	167	347	2.07
Uncracked & strengthened beam	201	1269	6.31
Cracked & strengthened beam	206	1155	5.60

5.3 COMPARISON OF TEST RESULTS WITH THE ACI APPROACH FOR ANALYSIS AND DESIGN

The RC beam strengthened with *FABcrete* was analysed to compute the flexural capacity using the method given in ACI 318 (2011), and ACI 549 (2013). In addition, the design check was done using the recommendations of ACI to verify the feasibility of following these methods for *FABcrete* strengthening.

5.3.1 Analysis

Based on the approach of ACI, the load and displacement at cracking, yielding and ultimate points were determined. The beam is considered to be cracked when the tensile stress in concrete reaches to the modulus of rupture. The reinforcement of the beam is considered as yielded when the strain reaches the yielding strain. The ultimate point is when the strain in *FABcrete* reaches the failure strain of textile.

The various input details used for the analysis are cross section height (h), cross-section width (b), clear span (L), effective depth upto steel reinforcement (d), uncracked moment of inertia (I_g), characteristic compressive strength of concrete (f_c'), maximum compressive strain in concrete

(ε_{cmax}), cross-sectional area of steel reinforcement (A_s), steel tensile yield strength (f_y), modulus of elasticity of concrete (E_c), modulus of elasticity of steel (E_s), yield strain (ε_{sy}), modular ratio ($n=E_s/E_c$), area of textile per unit width (A_f), ultimate tensile strain (ε_{fe}), tensile modulus of elasticity of cracked TRC (E_f), ultimate tensile strength (f_{fe}), and the number of layers of textile (N_{lay}).

To carry out the analysis, the following assumptions are made: plane sections remain plane after loading; the bond between *FABcrete* and concrete substrate as well as that of the textile to the matrix is perfect; the maximum allowable compressive strain in the concrete is 0.003 mm/mm; and *FABcrete* is assumed to have a bilinear-elastic behaviour up to failure. Also, the contribution of *FABcrete* before cracking is neglected. The stress versus strain distribution at the ultimate stage is represented in Figure 5.26.
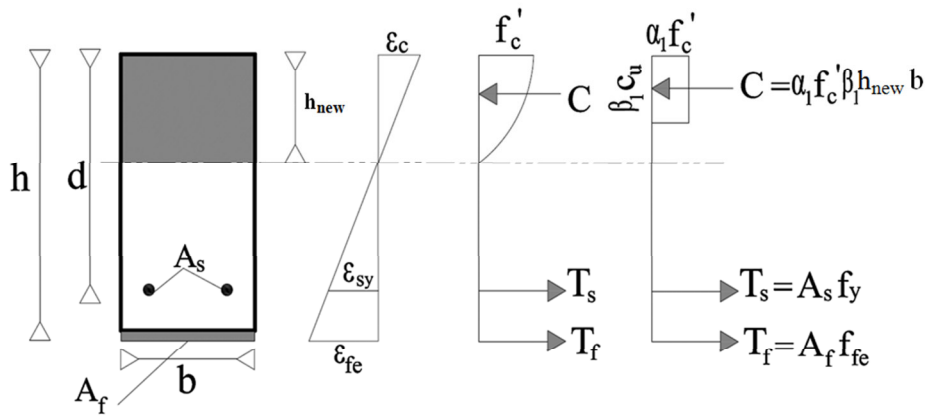
Figure 5.26 Stress-strain distributions at the ultimate stage

To calculate the yield load, the stresses in both concrete and reinforcement are calculated based on the strain level reached in each material using the appropriate constitutive laws. In concrete, a linear elastic relationship is used upto a stress of $0.45f_c'/E_c$; and the equivalent stress block as shown in Figure 5.26 is used beyond the linear elastic point up to ultimate state. The concrete stress block factors, β_1 and α_1, are expressed as functions of the neutral axis depth (h_{new})and computed in accordance with the Eqns. (5.3) and (5.4) and the solution is the result of an iteration process at each strain level (ε_{con}) for a particular level of neutral axis.

$$\beta_1 = \frac{4\varepsilon_{cmax}-\varepsilon_{con}}{6\varepsilon_{cmax}-2\varepsilon_{con}} \qquad (5.3)$$

138

$$\alpha_1 = \left[3\varepsilon_{cmax}\,\varepsilon_{con} - \left(\frac{\varepsilon_{con}{}^2}{3\beta_1\varepsilon_{cmax}{}^2}\right)\right] \tag{5.4}$$

The internal force equilibrium is checked at each iteration process according to Eqn. (5.5).

$$T_s + T_f = C \tag{5.5}$$

where
$$T_s = A_s \cdot f_y \tag{5.6}$$

$$T_f = N_{lay}\,A_f b E_f \varepsilon_{fib} \tag{5.7}$$

$$C = \alpha_1 f_c' \beta_1 h_{new} b \tag{5.8}$$

Using strain compatibility, the effective tensile strain level in *FABcrete* (ε_{fib}), steel tensile yield strain (ε_{sy}), and the compressive strain in concrete (ε_{con}) are related according to the Eqn. (5.9).

$$\frac{\varepsilon_{fib}}{h - h_{new}} = \frac{\varepsilon_{sy}}{d - h_{new}} = \frac{\varepsilon_{con}}{h_{new}} \tag{5.9}$$

Once equilibrium is satisfied, contribution of steel reinforcement and *FABcrete* is calculated according to Eqns. (5.10) and (5.11).

$$M_s = A_s f_y \left(d - \frac{\beta_1 h_{new}}{2}\right) \tag{5.10}$$

$$M_f = N_{lay} A_f b E_f\,\varepsilon_{fib}\left(h - \frac{\beta_1 h_{new}}{2}\right) \tag{5.11}$$

Design flexural strength is calculated in accordance with the following equation.

$$M_n = (M_s + M_f) \tag{5.12}$$

At the ultimate load, it is assumed that the *FABcrete* reaches its maximum tensile strain. This is verified by checking that the compressive strain in concrete does not exceed ε_{cmax}. The effective tensile strain level in *FABcrete* at failure, ε_{fib}, is limited to the ultimate tensile strain, ε_{fe}. The value for glass textile defined in Eqn. 5.13 is that suggested by ACI 549 (2013):

$$\varepsilon_{fib} = \varepsilon_{fe} \le 0.012 \tag{5.13}$$

The effective tensile stress level (f_{fe}) in *FABcrete* at failure is calculated in accordance with Eqn. (5.14).

$$f_{fe} = E_f \varepsilon_{fe} \tag{5.14}$$

Subsequently, the moment at the level of *FABcrete* at ultimate state is calculated using Eqn. (5.15).

$$M_f = N_{lay} A_f b f_{fe} \left(h - \frac{\beta_1 h_{new}}{2} \right) \tag{5.15}$$

In addition, the strength reduction factor, $\emptyset_m$, is also applied to the total moment that follows the philosophy of ACI 318 (2011). The strength reduction factor according to ACI 549(2013) is calculated by the following equation:

$$\begin{aligned}
\emptyset_m &= 0.9 & \text{for } \varepsilon_{nt} &\geq 0.005 \\
&= 0.65 + \frac{0.25(\varepsilon_{nt} - \varepsilon_{sy})}{0.0005 - \varepsilon_{sy}} & \varepsilon_{sy} < \varepsilon_{nt} &< 0.005 \\
&= 0.65 & \varepsilon_{nt} &< \varepsilon_{sy}
\end{aligned} \tag{5.16}$$

where ε_{nt} is the net tensile strain in extreme tension steel reinforcement; ε_{sy} is the steel yield strain. The total moment is calculated using Eqn.(5.17).

$$M_u = \emptyset_m(M_s + M_f) \tag{5.17}$$

The midspan deflection (Δ), of a flexural member with simple supports under four point bending is calculated using the following equation:.

$$\Delta = \frac{23ML^2}{216\ E_c I} \tag{5.18}$$

where M is the applied moment, L= clear span, I=corresponding moment of inertia, the term M/EI is the curvature of the cross section at mid span and computed according to:

$$\emptyset = \frac{\varepsilon_{fib}}{d - h_{new}} \tag{5.19}$$

The method was implemented in a computer program following the flowchart given in Appendix-D. The various geometrical and material related inputs used for the calculations are given in Table 5.4.

Table 5.4 Inputs used for ACI analysis

Paramater	Uncracked & Strengthened (ACI 549)
h (mm)	160
b (mm)	100
d (mm)	125
f_c' (MPa)	39.4
ε_{cmax}	0.003
A_s (mm^2)	157
f_y (MPa)	415
E_c (MPa)	29500
E_s (MPa)	2×10^5
A_f (mm^2/m)	33.58
ε_{fe}	0.012
E_f (GPa)	72
f_{fe} (MPa); ($f_{fe} = E_f \varepsilon_{fe}$)	864
N	10
Reduction factor for moment ($\emptyset_m$)	0.9

A relative comparison between the load and deflection for experimentally obtained values and that for ACI methodology is given in Table 5.5. At cracking and yielding, the load values from ACI predictions are conservative. However, the ultimate load predicted by ACI formulation is higher than that is observed in the experiment. Moreover, the expression prescribed by ACI to compute the limiting strain is only based on a general recognized trend. In addition, in the case of deflection prediction, it is seen that the values at cracking point and yield point are lower compared to experimental values, whereas that at ultimate point there is an over prediction compared to experimentally observed value. Based on the investigation, it can be concluded that there is a need to develop analytical models towards the prediction of response behaviour of *FABcrete*/TRC strengthened systems.

Table 5.5 Comparison between ACI prediction and experimental load values

Parameter	Uncracked & Strengthened	
	Experiment	ACI 549 (2013)
Cracking load (kN)	22.11	10.26
Yield load (kN)	53.31	40.41
Ultimate (Peak) load (kN)	55.66	62.85
Deflection at cracking load (mm)	1.19	0.20
Deflection at yield load (mm)	7.54	3.23
Deflection at ultimate (Peak) load (mm)	10.78	15.14

5.3.2 Design Check

Even though there is enough research evidence highlighting the capability of textile reinforced strengthening to increase the load bearing capacity of RC members, their design related aspects have not been addressed adequately. The design provisions have been established by ACI 549 (2013) for TRC/FRCM strengthening of reinforced concrete members, according to which the tensile stress in the steel reinforcement under service load should be limited to 80% of the steel yield strength. Further, the design provision limits the maximum force provided by the TRC (M_f) 50% of the capacity of unstrengthened beam, as given in Eqn. (5.20).

$$M_f \leq 50\% \ M_{unstrengthened} \tag{5.20}$$

In addition, the strength reduction factor, $\emptyset_m$, according to Eqn. (5.17) is also applied to arrive at the design moment. Following the above mentioned method, the design load was calculated for uncracked and strengthened beam that was tested for four point bending by using a reduction factor of 0.9. Further details used for the design approach are reported in Table 5.6. Based on the calculations, the design load for the *FABcrete* strengthened RC beam is obtained as 58.73 kN, whereas that observed in experiment is around 53 to 57kN.

Table 5.6 Calculation of design load using ACI approach

Parameter	Based on ACI approach
M_f (kN-mm)	4.27
50 % of $M_{unstrengthened}$	7.61
$Mn=1.5\ M_{unstrengthened}$	22.83
$\varnothing_m$	0.9
Mn, Designed= $\varnothing_m\,M_n$	20.55
Pn, Design load (kN)	58.73

Further, it can also be noted that it is necessary to assess possible failure modes and subsequent strains and stresses in each material while determining the nominal strength of a strengthened member. Recently, the design load for RC beam strengthened with polypara-phenylene benzobisoxazole (PBO)-FRCM was calculated by Babaeidarabad et al. (2014) using the methodology reported in ACI 549 (2013) and ACI 318 (2011). It was concluded that the design values become more conservative after applying the appropriate strength reduction factor and 50% limit on the strength increase. However, in the present study the design load is not conservative even after applying the reduction factor.

5.4 MATHEMATICAL MODELLING OF RC BEAMS STRENGTHENED WITH *FABcrete*

From the structural performance of *FABcrete*/TRC strengthened systems, it can be noticed that the strengthening effect mainly depends on the characteristics of textile material and the composite behaviour. Towards this aim, a methodology is developed by integrating various material models and by performing finite element analysis for *FABcrete* strengthened RC beams. Since, only a limited study was conducted, the work is reported as an Appendix- E in this thesis. More importantly, an analytical model is developed to address the requirement for accurate predictions of various salient points of load versus displacement behaviour of *FABcrete* strengthened beams using the material properties from characterization studies, which can be easily implemented and used in design.

5.4.1 DEVELOPMENT OF AN ANALYTICAL MODEL

The analysis and design guidelines for non-conventional concrete composites needs to be simple, consistent and unified for their easy implementation in field applications. As of today, the strengthening of beams with TRC is lacking in having a unified non-iterative and simple analysis methodology that will be directly useful for design practices. One way to accomplish this is by using generic material models to describe the material behaviors and derive closed form solutions for generating load versus displacement behaviour. Even, the closed form solutions can further be simplified to obtain design equations to estimate flexural capacity of a structural member. To develop such solutions, material characterization and the definitions of material parameters are very important.

In the present work, an analytical model is proposed to predict the load versus displacement behavior of RC beams strengthened with *FABcrete*. Two material and 10 non-dimensional parameters are used for this purpose.

5.4.1.1 Methodology

To predict response of RC beams strengthened with *FABcrete,* the material parameters are described by using Young's modulus and first cracking strain of *FABcrete* in addition to 10 non-dimensional parameters that define strain hardening of *FABcrete*, tensile strength of steel, compressive strength of concrete and ultimate strain levels. Curvature at particular section is calculated by using the extreme strain values in compression and tension zone. Further, closed-form solutions for moment-curvature response have been derived and the mid span deflection of strengthened beam under four-point bending tests is calculated using the values of curvature. According to the experimental results of RC beam strengthened with *FABcrete,* the response has 6 distinct stages in the load versus displacement behavior (Figure 5.13). The possible behavior of concrete, steel and *FABcrete* in these stages are given in Figure 5.27.
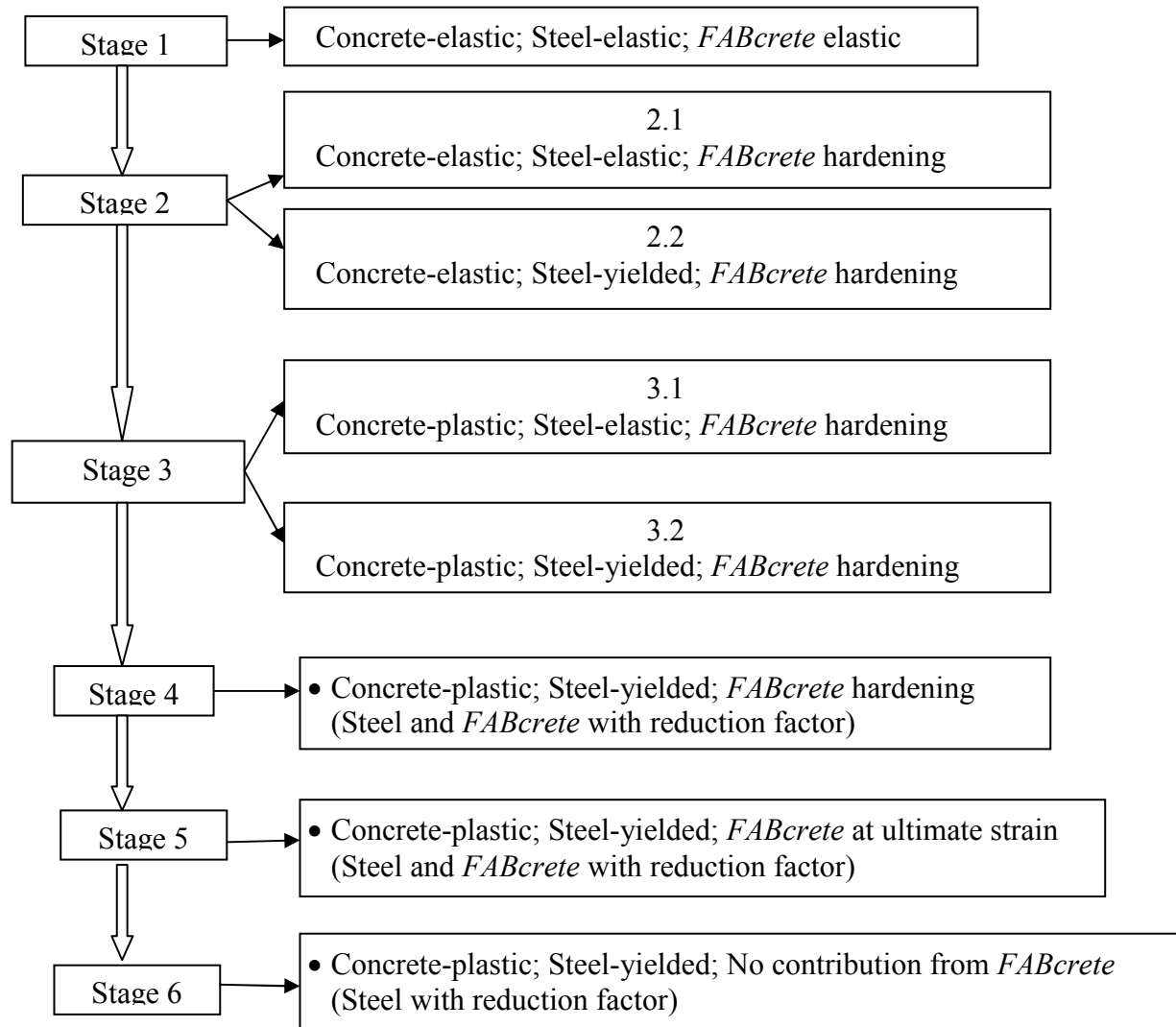
Figure 5.27 Different states of materials in various stages for the *FABcrete* strengthened beam

Three distinct material models are considered for concrete, *FABcrete* and steel for modelling the flexural response of strengthened beam as shown in Figures 5.28(a-c). For the idealization, the material parameters are described as combination of ten normalized parameters and two intrinsic material parameters such as tensile modulus (E) and the cracking tensile strain (ε_{cr}) of *FABcrete*.

(a) Concrete compression model

(b) *FABcrete* tension model

(c) Steel tension model

(d) Beam cross section
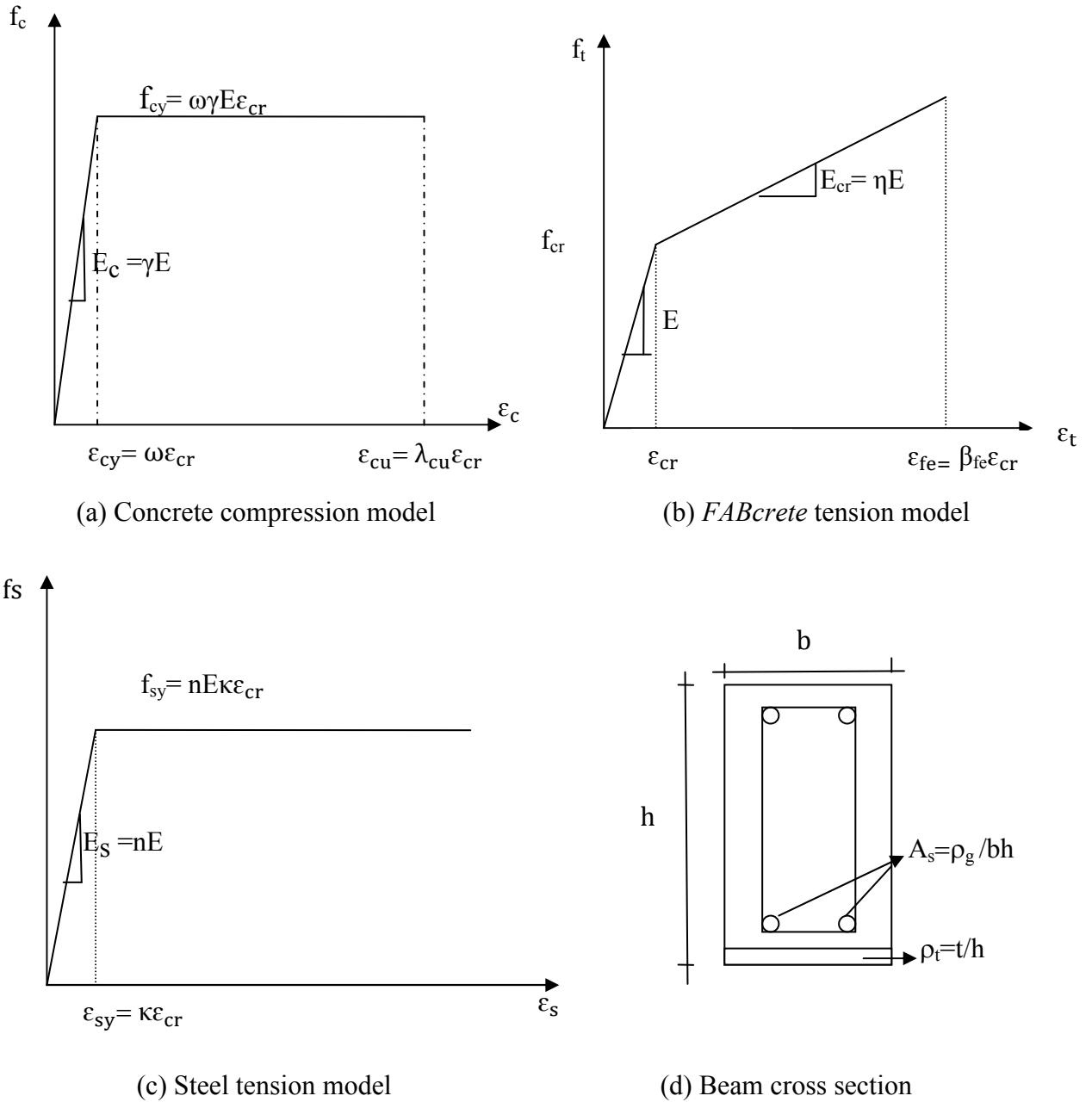
Figure 5.28. Material models for RC beam strengthened with *FABcrete*

Figure 5.28(a) shows the elastic-perfectly plastic model for concrete compression response. The compressive modulus of concrete defined as $E_c = \gamma E$, which is different from the tensile modulus of *FABcrete* by a factor of γ. The elastic-plastic model is defined by compressive yield strain $\varepsilon_{cy} = \omega\varepsilon_{cr}$, and hence compressive yield stress $f_{cy} = \omega\gamma\varepsilon_{cr}E$, which is terminated at the ultimate

compressive strain ε_{cu}. The ratio of strain to cracking strain is denoted by λ. For the compressive behavior of concrete, the constitutive relation considered is as given in Eqn. (5.21).

$$
\begin{aligned}
f_c(\varepsilon_c) &= E_c\,\varepsilon_c & 0 \le \varepsilon_c \le \varepsilon_{cy} \\
&= E_c\,\varepsilon_{cy} & \varepsilon_{cy} < \varepsilon \le \varepsilon_{cu} \\
&= 0 & \varepsilon > \varepsilon_{cu}
\end{aligned}
\tag{5.21}
$$

An idealized tension model for *FABcrete* is shown in Figure 5.28(b). In the elastic range, the tensile stress increases linearly with a Young's modulus (E) up to the cracking tensile strength σ_{cr} corresponding to the cracking strain, ε_{cr}. After first crack formation, there is a strain hardening state and the tensile strength during this state depends on the cracked elastic modulus (E_{cr}) of *FABcrete*. The hardening state is terminated at the ultimate tensile strain $\varepsilon_{fe} = \beta_{fe}\varepsilon_{cr}$. The ratio of modulus of *FABcrete* in cracked state to that in uncracked state is represented by a parameter η. The cross sectional area of *FABcrete* is the product of width of beam (b) and thickness of *FABcrete* layer (t). For the tensile behavior of *FABcrete*, the constitutive relation considered is as given in Eqn.(5.22).

$$
\begin{aligned}
f_t(\varepsilon_t) &= E\,\varepsilon_t & 0 \le \varepsilon_t \le \varepsilon_{cr} \\
&= E\,\varepsilon_{cr} + E_{cr}(\varepsilon_t - \varepsilon_{cr}) & \varepsilon_{cr} < \varepsilon_t \le \varepsilon_{fe} \\
&= 0 & \varepsilon_t > \varepsilon_{fe}
\end{aligned}
\tag{5.22}
$$

Figure 5.28(c) presents the elastic-plastic steel model, which is similar to the compression model except that the yield strain ($\varepsilon_{sy} = \kappa\varepsilon_{cr}$) and yield stress ($f_{sy} = \kappa n\varepsilon_{cr}E$) are defined by different normalized parameters: κ and n. In addition, the geometrical parameters are defined as a combination of normalized parameters and beam dimensions; width b and full depth h. Figure 5.28(d) shows a beam cross section that contains an area of steel $A_s = \rho_g bh$ at the reinforced depth $d = \alpha h$. The reinforcement ratio ρ_g is defined per gross sectional area (bh) of strengthened beam. For the tensile behavior of steel reinforcement, the constitutive relation considered is as given in Eqn.(5.23).

The steel behavior is expressed as :

$$
\begin{aligned}
f_s(\varepsilon_s) &= E_s\,\varepsilon_s & 0 \le \varepsilon_s \le \varepsilon_{sy} \\
&= E_s\,\varepsilon_{sy} & \varepsilon_s \ge \varepsilon_{sy}
\end{aligned}
\tag{5.23}
$$

147

The material model parameters defined in Eqns. (5.21) to (5.23) are replaced by two intrinsic parameters (E) and (ε_{cr}) and ten normalized parameters used are λ, η, ω, γ, n, ρ_g, κ, ρ_t, β; which are defined as :

$$\lambda = \frac{\varepsilon_c}{\varepsilon_{cr}}; \quad \eta = \frac{E_{cr}}{E}; \quad \omega = \frac{\varepsilon_{cy}}{\varepsilon_{cr}}; \quad \gamma = \frac{E_c}{E}; \quad n = \frac{E_s}{E_c}; \quad \rho_g = \frac{A_s}{bh}; \quad \kappa = \frac{\varepsilon_{sy}}{\varepsilon_{cr}}; \quad \rho_t = \frac{t}{h}; \quad \beta = \frac{\varepsilon_t}{\varepsilon_{cr}}; \quad \alpha = \frac{d}{h} \quad (5.24)$$

To derive the closed form solutions for moment–curvature response in non-dimensional forms, the strains, modulus, strengths and reinforcing depth defined in Figures 5.24 (a-d) are normalized with respect to cracking tensile strain ε_{cr}, tensile modulus E, cracking tensile strength $f_{cr} = \varepsilon_{cr} E$ and full depth of beam, respectively. The normalized stresses derived in terms of non-dimensional parameters are as follows.

The concrete behavior is expressed as :

$$\frac{f_c(\varepsilon_c)}{E\varepsilon_{cr}} = \gamma \lambda \qquad\qquad 0 < \lambda \leq \omega$$

$$= \gamma \omega \qquad\qquad \omega < \lambda \leq \lambda_{cu} \qquad (5.25)$$

$$= 0 \qquad\qquad \lambda > \lambda_{cu}$$

The *FABcrete* behavior is represented as:

$$\frac{f_t(\varepsilon_t)}{E\varepsilon_{cr}} = \beta \qquad\qquad 0 < \beta < 1$$

$$= 1 \qquad\qquad \beta = 1 \qquad (5.26)$$

$$= 1 + \eta(\beta-1) \qquad\qquad 1 < \beta \leq \beta_{fe}$$

$$= 0 \qquad\qquad \beta > \beta_{fe}$$

The steel behavior is given by

$$\frac{f_s(\varepsilon_s)}{E\varepsilon_{cr}} = n\chi \qquad\qquad 0 < \chi < \kappa \quad \text{where } \chi = \frac{\varepsilon_s}{\varepsilon_{cr}};$$

$$= n\kappa \qquad\qquad \chi \geq \kappa \qquad (5.27)$$

In order to perform analysis for cracked and *FABcrete* strengthened beams, the constitutive relation of concrete in Eqn. (5.21) compression is modified by introducing a reduction factor. This is according to the observations on the compressive strength reduction for the cracked concrete by Vecchio and Collins (1993). The amount of reduction is calculated based on the tensile strain experienced by concrete at the crack. Figure 5.29 is used to arrive at the reduction factor in the present study.
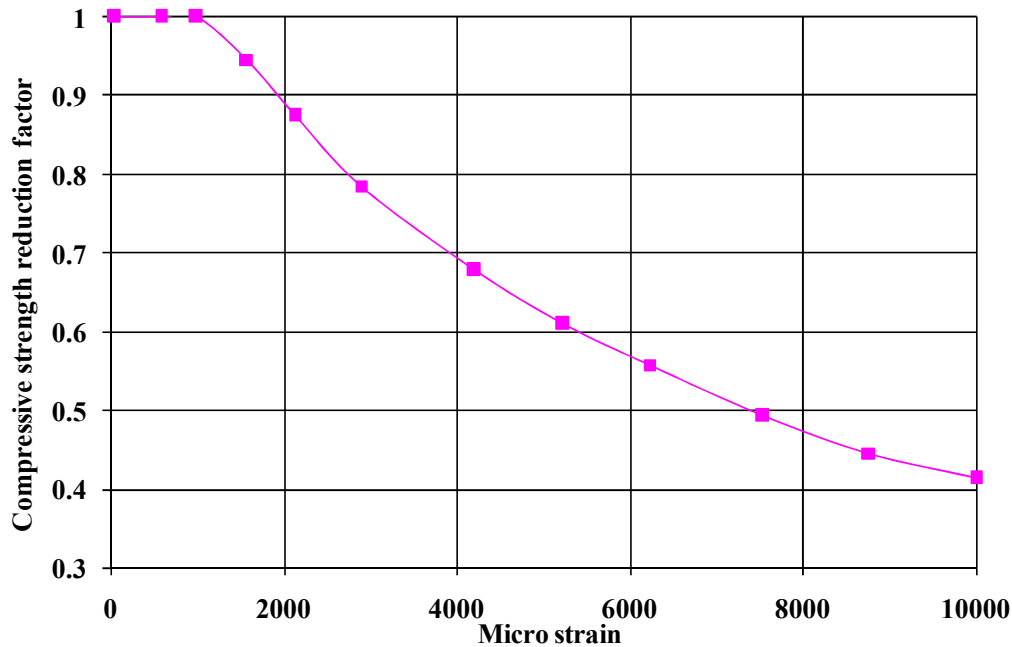
Figure 5.29 Compressive strength reduction factor based on tensile strain in concrete (Vecchio & Collins, 1993)

5.4.1.2 Derivation of the moment-curvature response

To derive a moment-curvature relationship for a *FABcrete* strengthened beam of rectangular cross section with width 'b' and depth 'h' upto bottom of strengthening layer, having steel reinforcement at depth 'd'; classical beam theory that ignores the shear deformation is used. In addition, a linear distribution of the strain is assumed along the depth. With these assumptions and by using material models described in Figures 5.28 (a - c), the stress and strain diagrams along the depth is shown in Figure 5.30. According to Figure 5.30, further calculations made are as follows for the model development. The heights of compression and tension zones are normalized with respect to the beam depth h, magnitudes of stresses at the vertices are normalized with respect to the cracking tensile strength $E\varepsilon_{cr}$ and their normalized forms are

149

presented in Tables 5.7 and 5.8, respectively. The internal force in each compression and tension zone is obtained from the area of stress diagram, and the normalized form with respect to the cracking force (bhEε_{cr}) is presented in Table 5.9. Similarly, the moment-arm measured from the neutral axis to the center of each force component is also presented as a normalized form in Table 5.10. Table 5.11 shows the steps in the determination of net section force, moment, and curvature at each stage. The net force is obtained as the difference of the tension and compression forces, equated to zero for internal equilibrium, and solved for the neutral axis depth ratio k. The internal moment is then obtained using the force components and their location with respect to the neutral axis. The curvature is determined as the ratio of the compressive strain at top to the depth of neutral axis.

(a) stages-1&2: strain diagram   stress diagram

(b) stage-3,4,5& 6: strain diagram   stress diagram
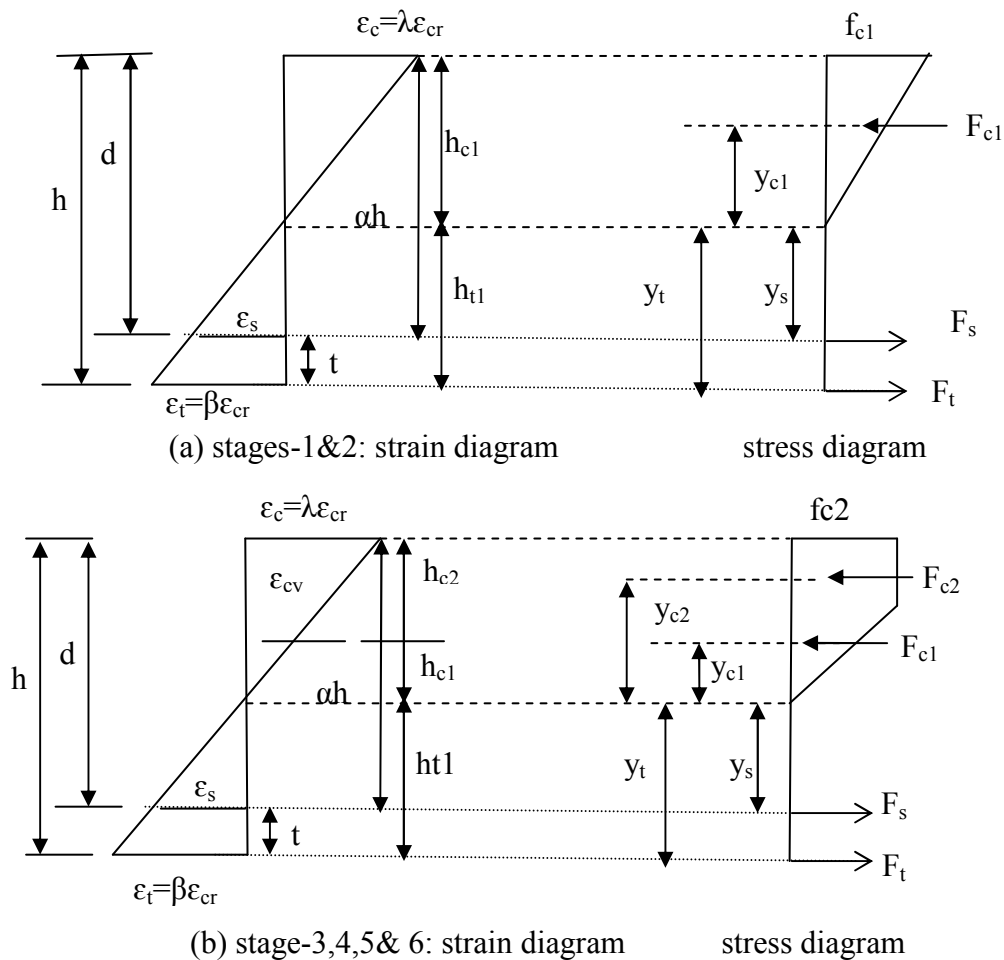
Figure 5.30 Strain and stress diagram at six stages of applied tensile strain at bottom of *FABcrete*

(a) stage 1 (b) stages 2, 3,4,5 & 6

A normalized tensile strain (β) at the bottom of *FABcrete* is used as an independent variable to incrementally impose flexural deformation in all stages of material behaviour. In the first stage, when the tensile strain at the bottom fiber in strengthening layer of *FABcrete* reaches the cracking tensile strain, is considered as the end of elastic response in region 1. During this stage the compressive strain is obtained by determining the value of λ, corresponding to particular value of β. In Stage 2, after *FABcrete* cracks, compressive zone continues in the elastic range but the *FABcrete* in tensile strain enters the hardening region. The stage 3 corresponds to the compressive strain is in plastic range and the tensile strain is in hardening range. Referring to Table 5.9, for Stage 2 and 3 there are two possible scenarios for steel reinforcement. The tensile steel can either be elastic or yielding. These cases depend on the material properties used in cross section. When steel is elastic in Stages 1, 2.1 and 3.1, the expressions for net force are in the quadratic forms and result in two possible solutions for the neutral axis parameter 'K'. With a large scale of numerical tests covering a practical range of material parameters, only one solution for 'K' yields the valid value in the range $0 < K < 1$. On the other hand, when steel is yielding in Stage 2.2 or 3.2 (Table 5.9), it results in only one solution for 'K'. In stage 4, a reduction factor of 0.9 is introduced for the *FABcrete* and steel behaviour. In Stage-5, *FABcrete* reaches the ultimate strain, and at the end of this stage, textile rupture takes place (Stage 6) and thereafter contribution is only from steel.

Table 5.7 Normalized heights of compression and tension zones with respect to depth h

Normalized height	Stage 1	Stage 2	Stage 3	Stage 4	Stage 5	Stage 6
$\dfrac{hc1}{h}$	K	K	$\dfrac{K\omega}{\lambda}$	$\dfrac{K\omega}{\lambda}$	$\dfrac{K\omega}{\lambda}$	$\dfrac{K\omega}{\lambda}$
$\dfrac{hc2}{h}$	-	-	$\dfrac{K(\lambda - \omega)}{\lambda}$	$\dfrac{K(\lambda - \omega)}{\lambda}$	$\dfrac{K(\lambda - \omega)}{\lambda}$	$\dfrac{K(\lambda - \omega)}{\lambda}$
$\dfrac{ht1}{h}$	(1-K)	(1-K)	(1-K)	(1-K)	(1-K)	(1-K)

Table 5.8 Stresses at the vertices normalized with respect to the cracking tensile strength $E\varepsilon_{cr}$

Normalized stresses	Stage 1	Stage 2		Stage 3		Stage 4	Stage 5	Stage 6
		2.1	2.2	3.1	3.2			
$\dfrac{fc1}{E\varepsilon_{cr}}$	γλ	γλ	γλ	γω	γω	γω		
$\dfrac{fc2}{E\varepsilon_{cr}}$	-	-	-	γω	γω	γω		
$\dfrac{ft1}{E\varepsilon_{cr}}$	$\dfrac{\lambda(1-K)}{K}$	1+η (β -1)	1+η (β -1)	1+ η(β -1)	1+η(β -1)	[1+η(β -1)]		
$\dfrac{fs}{E\varepsilon_{cr}}$	$\dfrac{n\lambda(\alpha-K)}{K}$	$\dfrac{n\lambda(\alpha-K)}{K}$	nκ	$\dfrac{n\lambda(\alpha-K)}{K}$	nκ	nκ		

Table 5.9 Force components normalized with respect to cracking tensile force $bhE\varepsilon_{cr}$

Normalized force component	Stage 1	Stage 2		Stage 3		Stages 4,5 & 6
		2.1	2.2	3.1	3.2	
$\dfrac{Fc1}{bhE\varepsilon_{cr}}$	$\dfrac{\gamma\lambda K}{2}$	$\dfrac{\gamma\lambda K}{2}$	$\dfrac{\gamma\lambda K}{2}$	$\dfrac{K\gamma\omega^2}{2\lambda}$	$\dfrac{K\gamma\omega^2}{2\lambda}$	$\dfrac{K\gamma\omega^2}{2\lambda}$
$\dfrac{Fc2}{bhE\varepsilon_{cr}}$	-	-	-	$\dfrac{\gamma\omega K(\lambda-\omega)}{\lambda}$	$\dfrac{\gamma\omega K(\lambda-\omega)}{\lambda}$	$\dfrac{\gamma\omega K(\lambda-\omega)}{\lambda}$
$\dfrac{Ft}{bhE\varepsilon_{cr}}$	$\dfrac{\rho_t\lambda(1-K)}{K}$	$\rho_t[1+\eta(\beta-1)]$	$\rho_t[1+\eta(\beta-1)]$	$\rho_t[1+\eta(\beta-1)]$	$\rho_t[1+\eta(\beta-1)]$	$\varphi_m\,\rho_t[1+\eta(\beta-1)]$
$\dfrac{Fs}{bhE\varepsilon_{cr}}$	$\dfrac{\rho_g n\lambda(\alpha-K)}{K}$	$\dfrac{\rho_g n\lambda(\alpha-K)}{K}$	$\rho_g n\kappa$	$\dfrac{\rho_g n\lambda(\alpha-K)}{K}$	$\rho_g n\kappa$	$\varphi_m\,\rho_g n\kappa$

Table 5.10 Normalized lines of action of stress component with respect to height h

Normalized line of action of stress	Stage 1	Stage 2	Stage 3	Stage 4	Stage 5	Stage 6
$\dfrac{yc1}{h}$	$\dfrac{2K}{3}$	$\dfrac{2K}{3}$	$\dfrac{2K\omega}{3\lambda}$	$\dfrac{2K\omega}{3\lambda}$	$\dfrac{2K\omega}{3\lambda}$	$\dfrac{2K\omega}{3\lambda}$
$\dfrac{yc2}{h}$	-	-	$\dfrac{K(\lambda + \omega)}{2\lambda}$	$\dfrac{K(\lambda + \omega)}{2\lambda}$	$\dfrac{K(\lambda + \omega)}{2\lambda}$	$\dfrac{K(\lambda + \omega)}{2\lambda}$
$\dfrac{ys}{h}$	$(\alpha - K)$	$(\alpha - K)$	$(\alpha - K)$	$(\alpha - K)$	$(\alpha - K)$	$(\alpha - K)$
$\dfrac{yt}{h}$	$(1-K)$	$(1-K)$	$(1-K)$	$(1-K)$	$(1-K)$	$(1-K)$

Table 5.11 Steps in determination of net section force, moment, and curvature at each stage

Stage	Force Equillibrium	Moment	Curvature
1	$\sum F1 = -Fc1 + Fs + Ft$	$M1 = Fc1yc1 + Fsys + Ftyt$	$\varphi_1 = \dfrac{\varepsilon_{top}}{Kh}$
2	$\sum F2 = -Fc1 + Fs + Ft$	$M2 = Fc1yc1 + Fsys + Ftyt$	$\varphi_2 = \dfrac{\varepsilon_{top}}{Kh}$
3	$\sum F3 = -Fc1 - Fc2 + Fs + Ft$	$M3 = Fc1yc1 + Fc2yc2 + Fsys + Ftyt$	$\varphi_3 = \dfrac{\varepsilon_{top}}{Kh}$
4	$\sum F4 = -Fc1 - Fc2 + Fs + Ft$	$M4 = Fc1yc1 + Fc2yc2 + Fsys + Ftyt$	$\varphi_4 = \dfrac{\varepsilon_{top}}{Kh}$
5	$\sum F5 = -Fc1 - Fc2 + Fs + Ft$	$M5 = Fc1yc1 + Fc2yc2 + Fsys + Ftyt$	$\varphi_5 = \dfrac{\varepsilon_{top}}{Kh}$
6	$\sum F6 = -Fc1 - Fc2 + Fs + Ft$	$M6 = Fc1yc1 + Fc2yc2 + Fsys + Ftyt$	$\varphi_6 = \dfrac{\varepsilon_{top}}{Kh}$

Using the equilibrium of force expressions for neutral axis is derived in terms of β as given below. The value of β is related to λ by the expression,

$$\beta = \lambda \frac{(1-K)}{K} \qquad (5.28a)$$

$$\beta = \frac{\kappa(1-K)}{(\alpha - K)} \qquad (5.28b)$$

In stage 1, the neutral axis parameter is calculated using the expression given in Eqn.(5.29).

$$K_1 = \frac{(2\rho_t + 2n\rho_g) \pm \sqrt{(-2\rho_t - 2n\rho_g)^2 + 8\gamma(\rho_t + n\alpha\rho_g)}}{-2\gamma}$$

(5.29)

In stage 2.1, the neutral axis parameter is calculated using Eqn.(5.30).

$$K_{21} = \frac{-(2\rho_t + 2\rho_t\,\eta\beta - 2\rho_t\,\eta + 2n\beta\rho_g) \pm \sqrt{(2\rho_t + 2\rho_t\,\eta\beta - 2\rho_t\,\eta + 2n\beta\rho_g)^2 - 8\gamma^\beta(-\rho_t + \eta\rho_t - n\alpha\beta\rho_g)}}{2\gamma\beta}$$

(5.30)

For stage 2.2, the neutral axis parameter is as given in Eqn.(5.31).

$$K_{22} = \frac{-(2\eta\rho_t + 2n\kappa\rho_g + 2\rho_t + 2\rho_t\,\eta\kappa) \pm \sqrt{(-2\eta\rho_t + 2n\kappa\rho_g + 2\rho_t + 2\rho_t\,\eta\kappa)^2 - 8\gamma\kappa(\eta\alpha\rho_t - \alpha\,n\kappa\rho_g - \alpha\rho_t - \kappa\eta\rho_t)}}{2\gamma\kappa}$$

(5.31)

In stage 3.1, the neutral axis parameter can be calculated from Eqn.(5.32) as:

$$K_{31} = \frac{-(-2\gamma\omega^2 - 2\gamma\omega\beta - 2\beta\rho_t - 2\beta^2\rho_t\eta + 2\beta\eta\rho_t - 2n\beta^2\rho_g) \pm \sqrt{(-2\gamma\omega^2 - 2\gamma\omega\beta - 2\beta\rho_t - 2\beta^2\rho_t\eta + 2\beta\eta\rho_t - 2n\beta^2\rho_g)^2 - 4(\gamma\omega^2 + 2\gamma\omega\beta)(\gamma\omega^2 + 2\beta\rho_t - 2\beta\eta\rho_t + 2n\beta^2\alpha\rho_g)}}{2(\gamma\omega^2 + 2\gamma\omega\beta)}$$

(5.32)

For stages 3.2, 4, 5 and 6, the neutral axis parameter is calculated using Eqn.(5.33).

$$K_{32} = \frac{-(-\gamma\omega^2\alpha - \gamma\omega^2 - 2\gamma\omega\beta\alpha + 2\beta\rho_t\alpha + 2\beta n\kappa\rho_t - 2\beta\eta\rho_t\alpha + 2\beta n\kappa\rho_g\alpha) \pm \sqrt{(-\gamma\omega^2\alpha - \gamma\omega^2 - 2\gamma\omega\beta\alpha + 2\beta\rho_t\alpha + 2\beta n\kappa\rho_t - 2\beta\eta\rho_t\alpha + 2\beta n\kappa\rho_g\alpha)^2 - 4(\gamma\omega^2\alpha)(\gamma\omega^2 - 2\beta\rho_t + 2\gamma\omega\beta - 2\beta\kappa\eta\rho_t - 2\beta\eta\rho_t - 2n\beta\kappa\rho_g)}}{2(\gamma\omega^2 - 2\beta\rho_t + 2\gamma\omega\beta - 2\beta\kappa\eta\rho_t - 2\beta\eta\rho_t - 2n\beta\kappa\rho_g)}$$

(5.33)

Once, the neutral axis parameter 'K' and the applicable case are determined; the expressions from Eqns.(5.29) to (5.33) are used appropriately to arrive at the moment-curvature relation.

154

5.4.1.3 Algorithm to Predict Load-Deflection Responses

Load-deflection response of four point bending test of strengthened beam can be simulated using moment-curvature diagram for a given set of material parameters and beam dimensions using the closed form solutions presented in the previous section. The applied load vector P for simulation of beam test can be obtained from the discrete points along the moment curvature diagram as P = 2M/X where X is the distance from the support to the first point load. The displacement is calculated by knowing the neutral axis location and by using Eqn. (5.34). The midspan deflection (Δ), of a flexural member with simple supports under four point bending at cracking is calculated using the following equation:

$$\Delta = \frac{23ML^2}{216\ E_cI}$$

(5.34)

where M is the applied moment, L=beam span, I=corresponding moment of inertia, the term M/EI is the curvature of the cross section at mid span.

After cracking, the central deflection is calculated as by applying the moment-area method to the moment-curvature diagrams. The midspan deflection of four-point bending tests is derived explicitly, and is given in Eqn. (5.35). Similar expressions are also used in the literature by Sornakom and Mobasher (2007).

$$\Delta_i = \frac{L^2}{216\ M_i^2}\{(23M_i^2 - 4M_iM_{cr} - 4M_{cr}^2)\varphi_i + (4M_i^2 + 4M_iM_{cr})\varphi_{cr}\}$$

(5.35)

where Mi=moment at any stage after cracking, φ_i= curvature at any stage after cracking, φ_{cr} = curvature at cracking, Mcr = cracking moment.

5.4.2 Validation of the Model

The experimental results of strengthened RC beam with *FABcrete* reported in Section 5.2 were used in the model verification. The material model used for steel reinforcement based on Eqn.(5.23) is shown in Figure 5.31 and that of concrete based on Eqn.(5.21) is shown in Figure 5.32. The stress-strain behaviour of cracked concrete was arrived by applying a reduction factor of 0.9 based on Figure 5.29, corresponding to a cracking strain of 2000microns. The stress-strain behaviour of cracked concrete in compression is also shown in Figure 5.32.
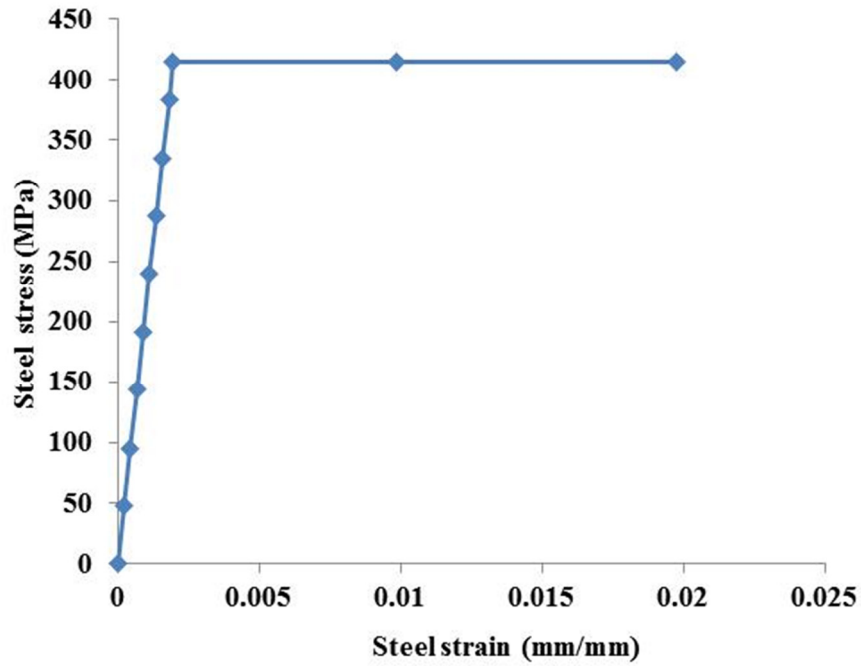
Figure 5.31 Steel reinforcement model
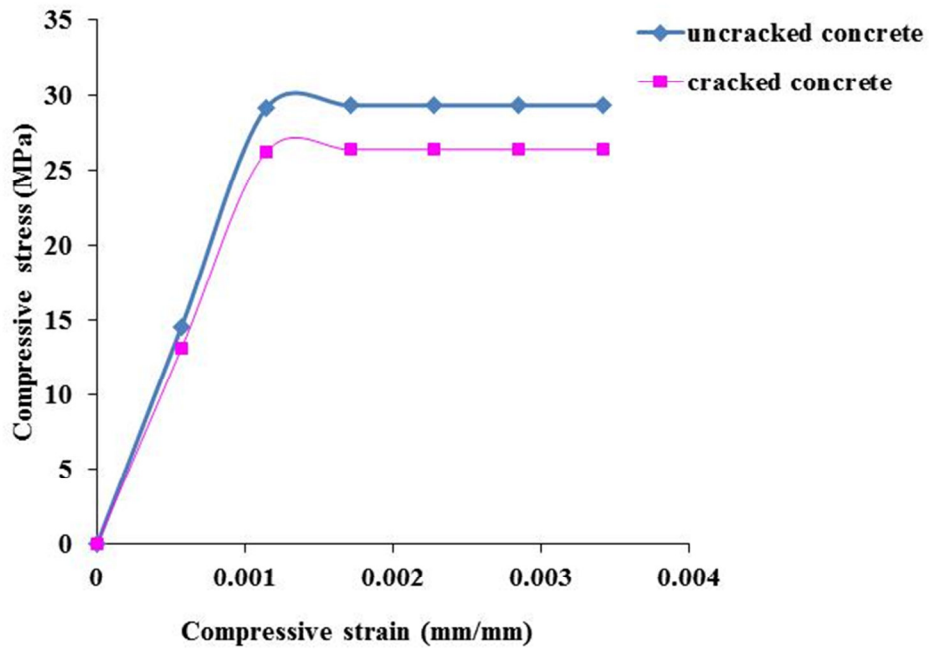
Figure 5.32 Concrete model

Based on the uniaxial tensile characterization studies reported in Chapter 4, a generalized expression was arrived for determining the uncracked elastic modulus of *FABcrete* for various volume fractions of textile (see Figure 5.33). It is noted that the relation between uncracked elastic modulus of *FABcrete* and volume fraction follows a second order polynomial trend line with least square value of 0.96. If V_f is the volume fraction in %, then the elastic modulus of *FABcrete* is calculated using the equation given below.

$$E = -1585.7\ V_f^2 + 8594.2\ V_f + 17203 \tag{5.36}$$

By making use of the above equation, the value of modulus of *FABcrete* (E) is obtained as 28.39 GPa. Further, first cracking tensile strain ε_{cr} is calculated by dividing the uniaxial tensile strength of *FABmix* (2.5MPa) with elastic modulus of *FABmix*, based on the results of characterization studies reported in Chapter 3 for *FABmix*.
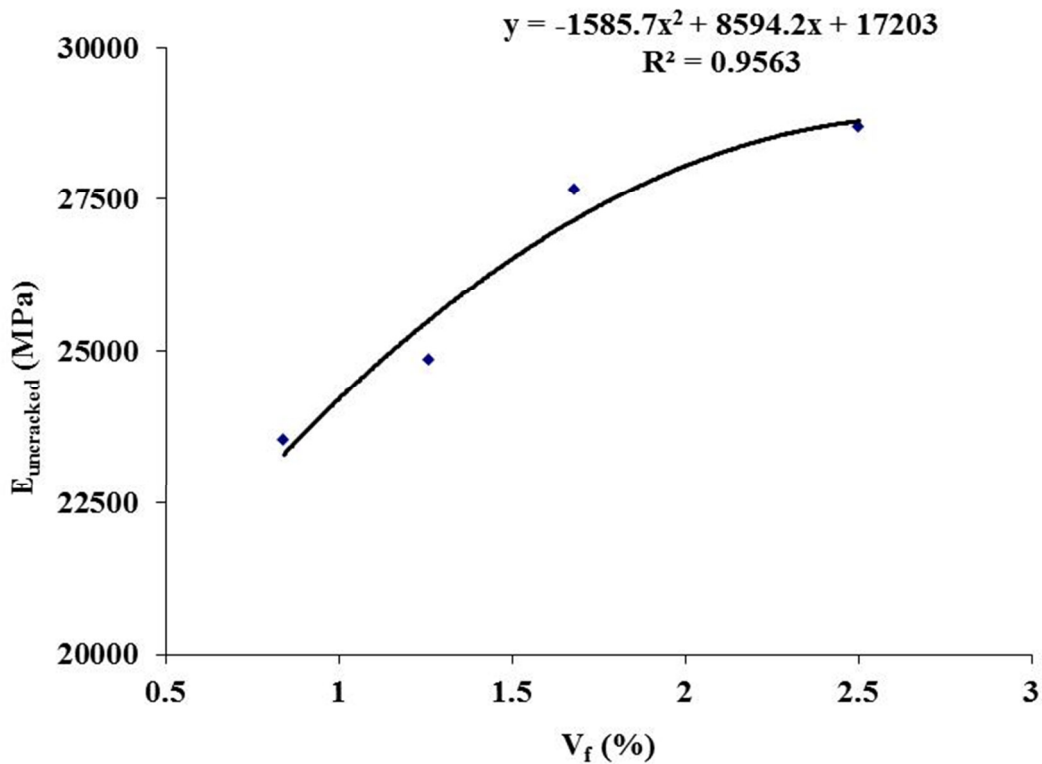
Figure 5.33 Modulus of *FABcrete* w.r.t. volume fraction

The other normalized parameters for tension and compression models of concrete, *FABcrete* and steel considered for the analytical model were $\lambda_{cu} = 17.5$; $\omega = 10.8$; $\gamma = 0.87$; $n = 7.2$;

$\rho_g = 0.009813$; $\kappa = 17.33$; $\rho_t = 0.0625$; $\alpha = 0.78$. The values were arrived based on the input parameters reported in Eqn. (5.24). In addition, generalized expressions were arrived for calculating the normalized stiffness and strain parameter based on the tensile characterization results reported in Chapter 4 for various volume fraction of textile in *FABcrete*. The relation between volume fraction and normalized strain parameter, β, is shown in Figure 5.34. It is noticed that the relation between β and volume fraction follows a second order polynomial trend with least square value of 0.97. If V_f is the volume fraction in %, then the normalized strain parameter β for *FABcrete* is calculated using the equation

$$\beta = 0.3225 \, V_f^2 + 8.9985 \, V_f + 2.6708 \tag{5.37}$$

Further, the relation between normalized stiffness parameter and volume fraction is shown in Figure 5.35. It is noticed that their relation follows a second order polynomial trend with least square value of 1. If V_f is the volume fraction in %, then the normalized stiffness parameter η for *FABcrete* is calculated using the equation

$$\eta = 0.0294 \, V_f^2 - 0.0622 \, V_f + 0.0416 \tag{5.38}$$
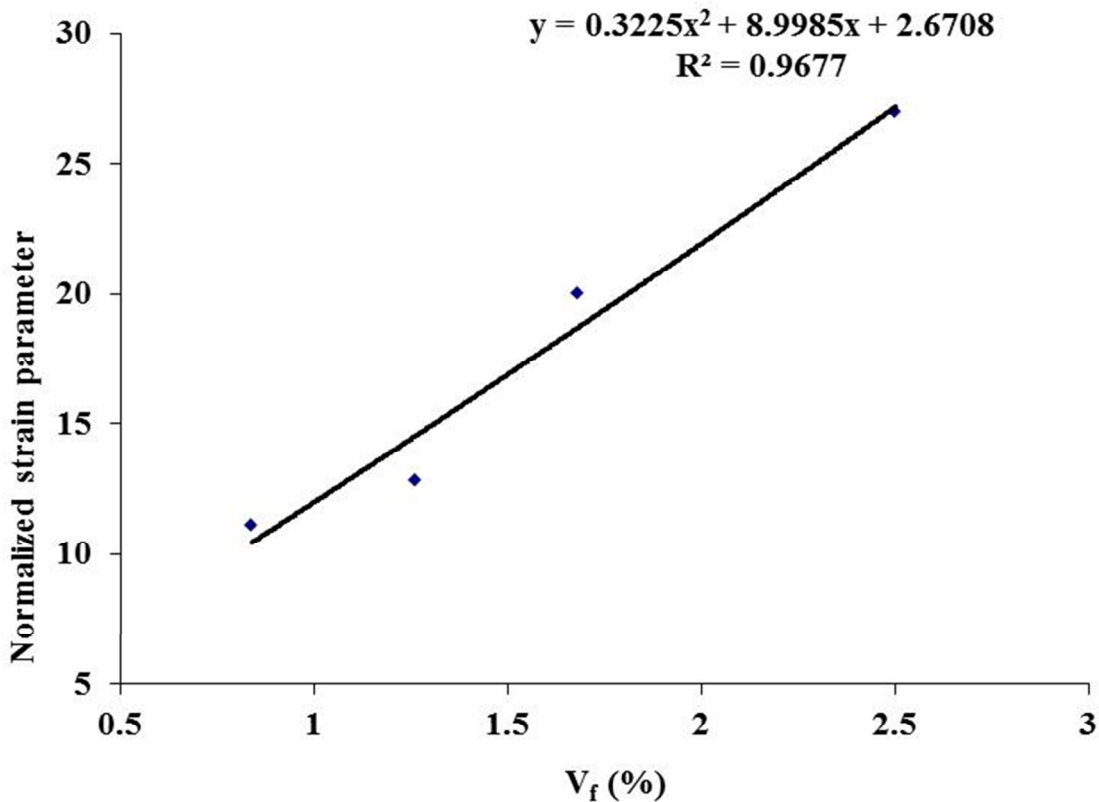
Figure 5.34 Normalized strain for *FABcrete* w.r.t. volume fraction
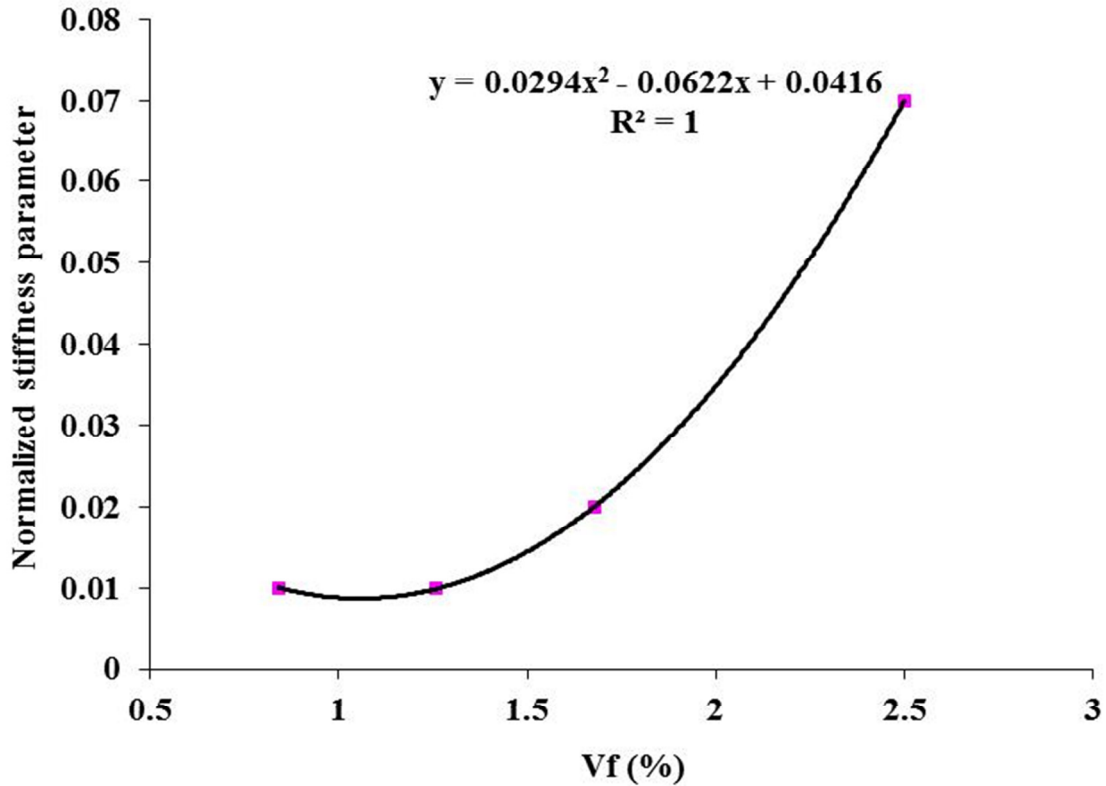
Figure 5.35 Normalized stiffness for *FABcrete* w.r.t. volume fraction

To understand the influence of β and η values on the stress-strain behaviour of *FABcrete* for the extrapolated values, a parametric investigation was carried out for its different combinations upto a strain of 0.006. The normalized stiffness parameter η is varied as 0.07 and 0.1 and normalized strain parameter β value varied as 30,35 and 40. Figure 5.36 shows the effect of β and η on the tensile behaviour of *FABcrete*. It is noted that for β=30, as η increases from 0.07 to 0.1, there is around 24% increase in ultimate stress, whereas the increase is 34% for β=35 and 40. Further, it is noted that for η=0.07, as β increases from 30 to 40, there is 21% increase in ultimate stress and for η=0.1, the increase is 24%. Since the increases in ultimate stress is almost same beyond β=30, the parameter η governs the composite performance.
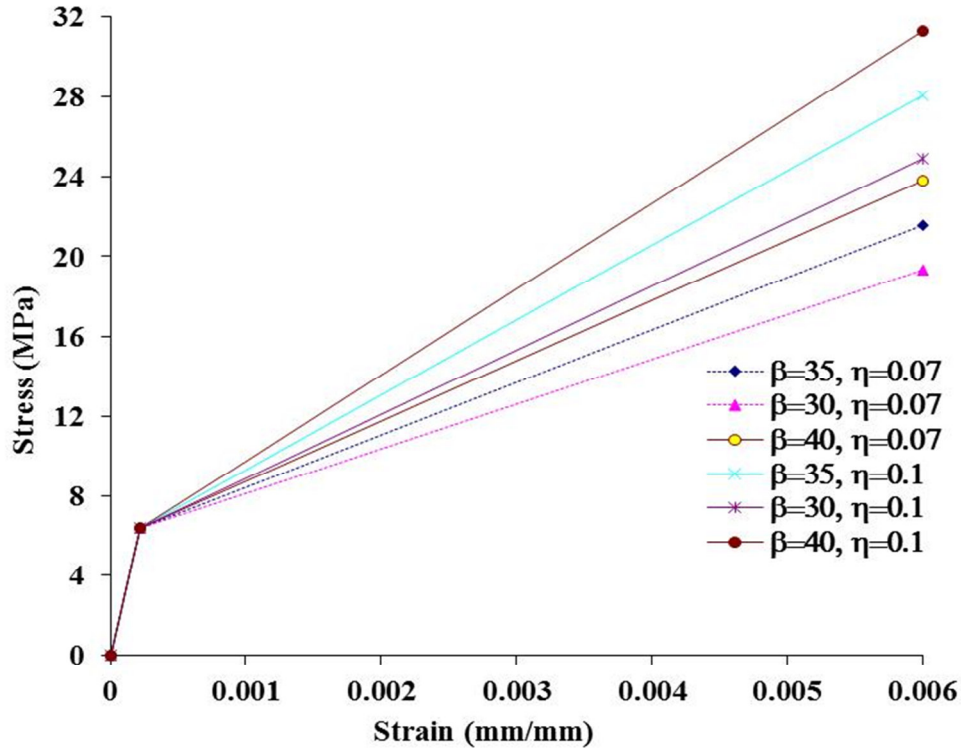
Figure 5.36 *FABcrete* model

5.4.2.1 Un-cracked and strengthened beam

The load versus displacement predicted for *FABcrete* strengthened beam using the models explained above is shown in Figure 5.37. The non-dimensionalized strain (β) and hardening coefficients (η) for 10 layers of SRG-45 in *FABcrete* for a 3.25% volume fraction were arrived by extrapolating the results of characterization studies reported in Chapter 4 based on the Figures 5.34 and 5.35. Accordingly the values are β and η are obtained as 33 and 0.15 respectively. Since the contribution of FABcrete towards enhancement in load is more predominant after yield load, the η is varied as 0.07 and 0.1 and β value varied as 30,35 and 40 to predict the load versus displacement behaviour analytically. The related results are shown in Figures 5.37 (a) and 5.37(b). It is observed that the yield and ultimate load values are under predicted when 'β' is 30 and 35 whereas for 'β' =40, the ultimate load is almost same as that observed in the experiment. Further, the values are also compared along with the ACI predictions shown in Figures 5.37(a) and 5.37(b) and it can be concluded that ACI overestimates the ultimate load, whereas the present model prediction is close to experimental values.

(a) [β = 30, 35, 40 & η = 0.07]
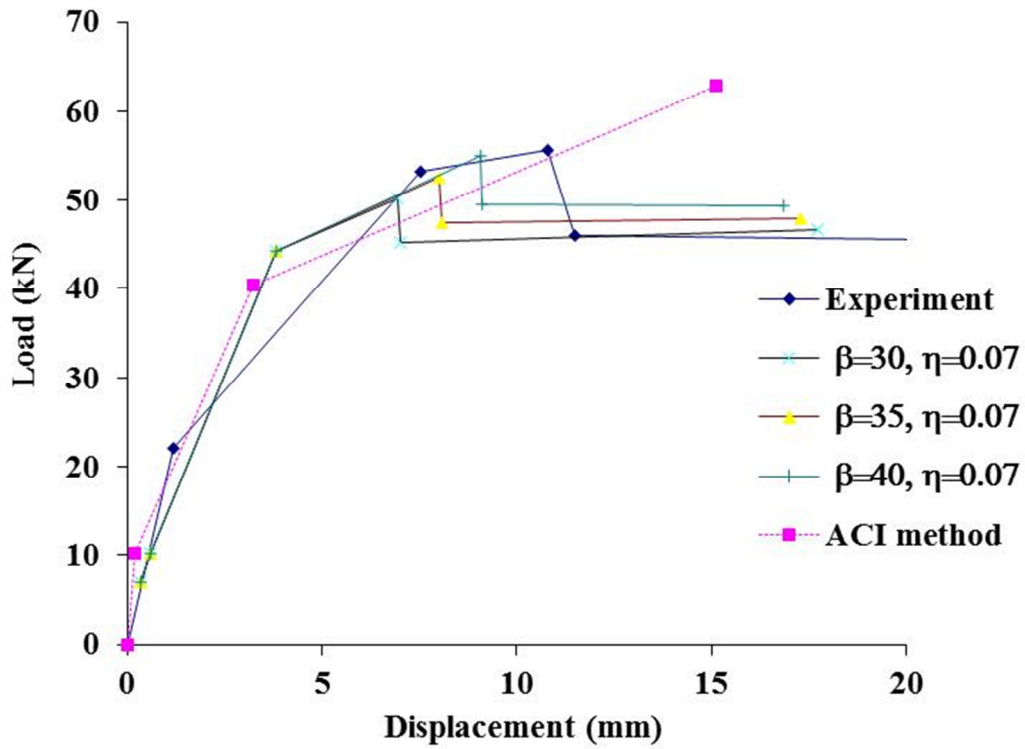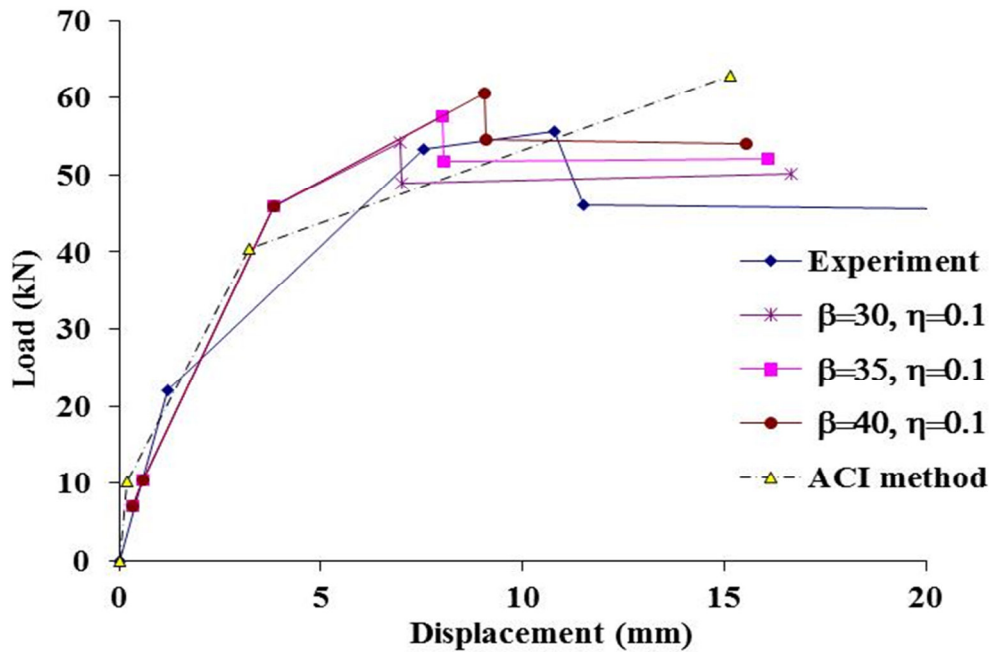
(b) [β = 30, 35, 40 & η = 0.1]

Figure 5.37 Comparison of load versus displacement behaviour of un-cracked and strengthened beam

161

5.4.2.2 Cracked and strengthened beam

The behaviour of cracked concrete is considered in the modelling to represent the damaged concrete in RC beam. Analysis is carried out by using β =30,35 and 40 and η=0.07 and 0.1. The load vs. displacement predicted for cracked RC beam strengthened with *FABcrete* is shown in Figure 5.38.It is noticed that in this case also β =40, and η=0.07 predicts the ultimate load close to experimental value.

(a) [β = 30, 35, 40 & η = 0.07]
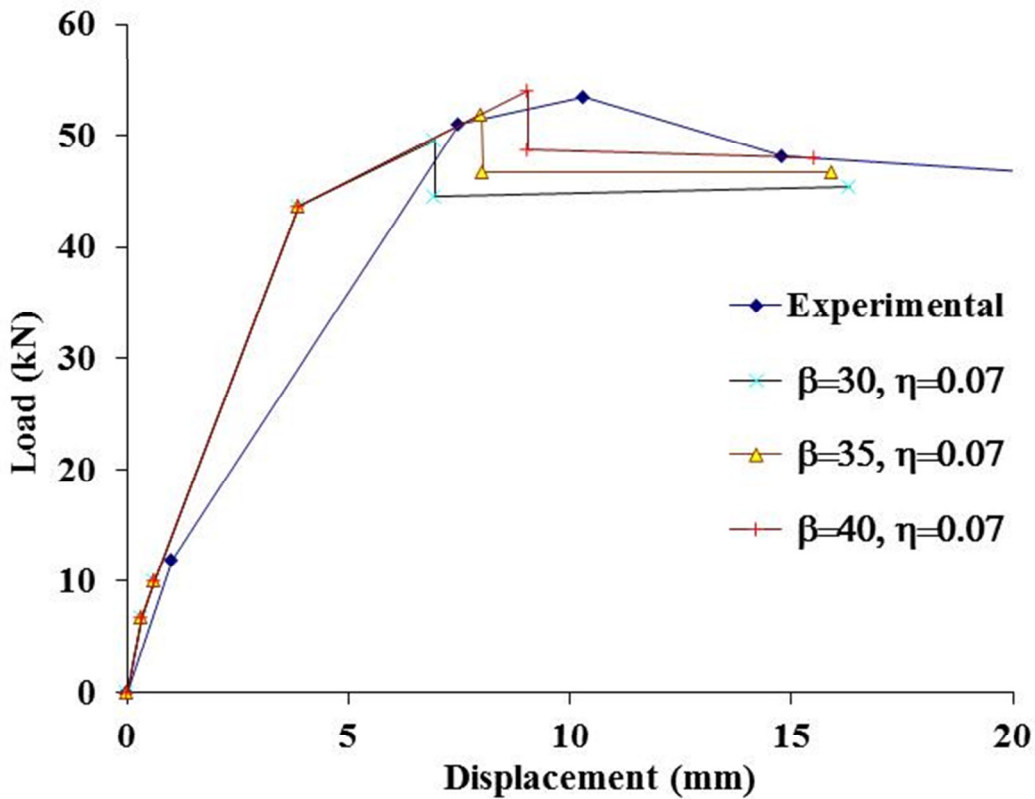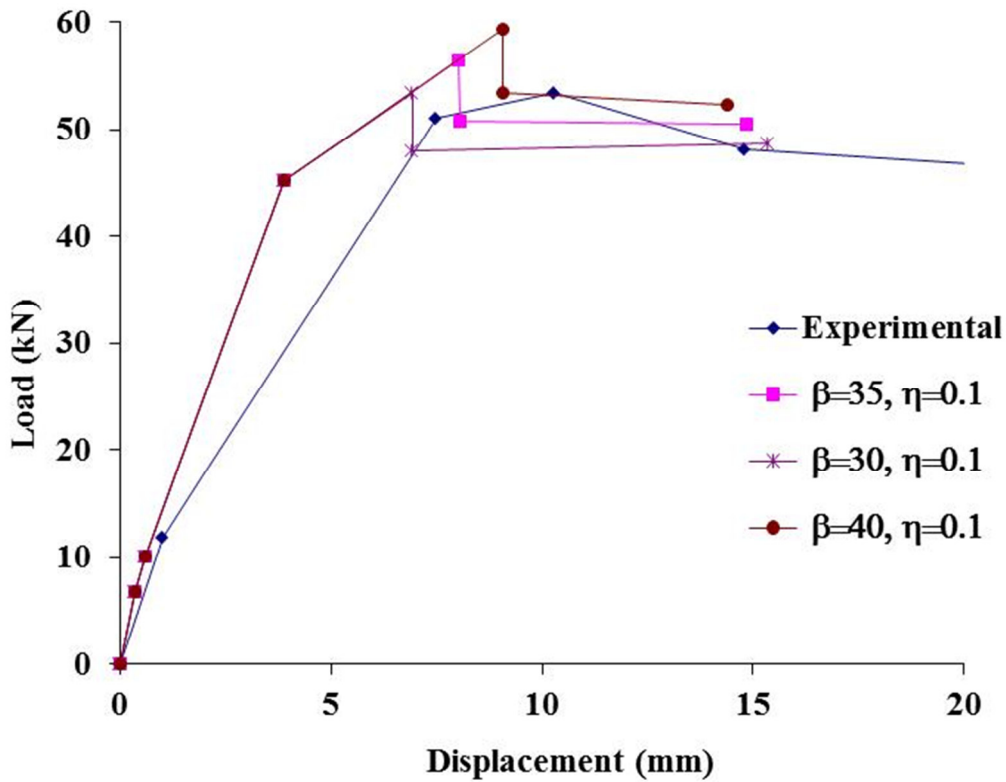
(b) [β = 30, 35, 40 & η = 0.1]

Figure 5.38 Comparison of load versus displacement behaviour for cracked and strengthened beam

5.4.2.3 Parametric studies

To understand the influence of the thickness of the strengthening layer with the same number of layers for strengthening of RC beam, a parametric investigation was carried out for two different thickness of *FABcrete* layer 8mm and 15mm. The values of β =35, and η=0.07 are considered for the analysis. The load vs. displacement curve obtained for this is shown in Figure 5.39. It is noted that as the thickness of strengthening layer increases (say 15mm), the overall load vs. displacement shows a higher slope and enhanced loads at cracking, yield and ultimate points, which is also in line with the moment of inertia concept.
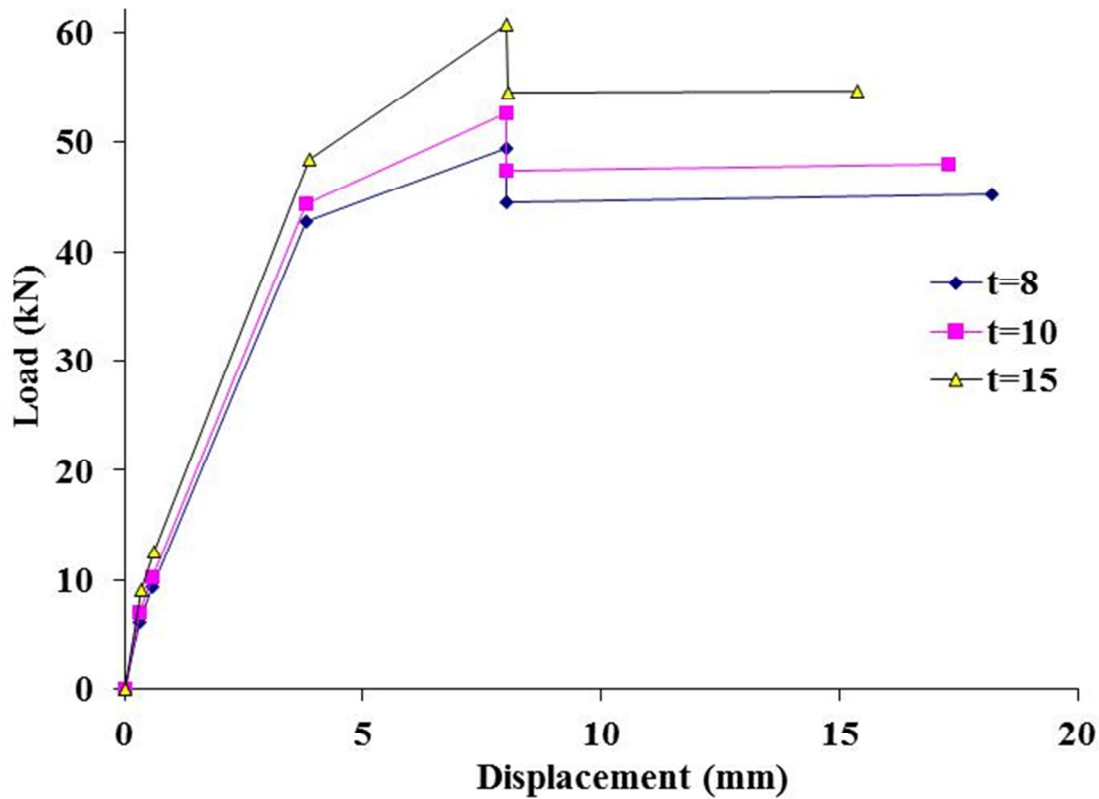
Figure 5.39 Effect of thickness of strengthening layer ($\beta = 35$, $\eta = 0.07$)

5.5 GUIDELINES FOR SIMPLIFIED DESIGN METHODOLOGY

The ACI 549 (2013) procedure is the only option available as of today for the analysis and design of TRC elements for structural strengthening. However, the procedure is iterative in nature and found to be non-conservative in the present study. Hence, a design methodology for *FABcrete* strengthening is developed based on the analytical formulations reported in Chapter 5.The methodology will directly yield the thickness of the *FABcrete* layer and also the number of layers of textile to be used in *FABcrete*. Mainly two equations are used: one for calculating the neutral axis depth at ultimate state and another one for calculating the ultimate moment of strengthened beam. These formulations are independent of the initial concrete strain at the beam's soffit at the time of strengthening. Further, the proposed procedure is very simple and quick to implement for practicing engineers. The various design steps involved are summarized in the following steps.

164

1. Determine the existing moment carrying capacity of un-strengthened RC beam (M_{unstr}).

2. Decide the amount of structural capacity enhancement after strengthening (10 to maximum 50%) and calculate the required moment after strengthening (M_{str}).

3. Assume a thickness for *FABcrete* strengthening layer (considering the practical feasibility it can vary between 10mm to 25mm).

4. Input parameters used in the analytical model such as fc', As, f_y, b, L, E, λ, η; ω, γ, n; ρ_g, κ, ρ_t, β, α.

5. Calculate the neutral axis depth using the parameter K_{32} at ultimate load using Eqn. (5.33).

6. Calculate the ultimate moment M_{32} using following Eqn.

   $M_{32} = F_{c1}Y_{c1} + F_{c2}Y_{c2} + F_sY_s + F_tY_t$

7. The force in textile, $T_f = bhE\varepsilon_{cr}\rho_t[1+\eta(\beta-1)]$

8. Ultimate stress in textile f_{fe} (this will take care of the type of textile used, and should be obtained from characterization studies).

9. Total area of textile, $A_f = T_f/f_{fe}$

10. Number of layers of textiles to be used $N_{lay} = \{A_f / $ area of one layer of textile in $mm^2/mm\}$

11. If ($M_{32} \leq M_{str}$) try another thickness and repeat steps 5 to 11.

5.6 SUMMARY

This chapter presents the experimental investigations carried out to find the applicability, feasibility and performance of *FABcrete* for flexural strengthening of plain concrete and RC beams. Both uncracked and cracked RC beams were strengthened with *FABcrete*. The results obtained were evaluated with respect to enhancement in load carrying capacity, ductility, work done, crack pattern and failure pattern. Both type of beams showed enhancement in load carrying capacity and ductility. Further, it is observed that both the beams had a residual load carrying capacity near to ultimate load of unstrengthened beam and both of them showed a displacement to the extent of maximum straining ability of glass textile. With respect to crack pattern, the *FABcrete* strengthening layer showed multiple cracking behaviour. The number of cracks and width of cracks were decreased in the main beam when it was strengthened with *FABcrete*. The

final failure pattern of strengthened beams was by rupture of glass textile in *FABcrete*. Also, an added advantage of *FABcrete* was brought out from the experiment by noticing the fact that no additional anchorage or adhesives were required for strengthening of RC beams with *FABcrete*. Further, an analytical model based on ACI recommendations were assessed to find the adequacy of existing design and analytical method for *FABcrete* strengthening.

Two mathematical models are presented in this chapter to predict the response behaviour of RC beams strengthened with *FABcrete*. The methodology developed is generalized and can be used to simulate the behaviour of TRC strengthened beams. It is concluded that, due to numerical difficulties encountered during the finite element analysis, many constituent material ingredients interactions could not be accommodated in the model. Further, a simplified analytical model was proposed by using the material properties from mechanical characterization. It is found that the predictions from the developed model are in good agreement with experimental behavior and the formulation can be used for the design of TRC strengthened beams. Based on the analytical model, a simplified design methodology for designing the strengthening of RC beams with *FABcrete* is also proposed.

CHAPTER 6

DEVELOPMENT AND ON-SITE ILLUSTRATION OF TRC-BASED STRENGTHENING OF BEAMS AND WALLS

6.1 INTRODUCTION

Even though the applicability of TRC as a structural strengthening material is well proven in literature, it is lacking methodologies for its cast-in-place practical application. Present Chapter reports development and illustration of an on-site approach for TRC-based structural strengthening of reinforced concrete beams. The applicability of same apparatus has also been demonstrated for application of TRC on brick masonry wall. The binder used in TRC for on-site illustration is *FABmix* and the textile used is SRG-45, the characteristics of which are reported in Chapter 3. A tautening apparatus has been developed for providing mechanical stretching to textiles, while casting the TRC layer. This is based on the advantages, which are realized during the tensile characterization of *FABcrete* with manually and mechanically stretched textiles reported in Chapter 4. Moreover, the proposed methodology is a scale-up of the method of casting TRC layer reported in Chapter 4 and 5 that can be used for on-site applications while performing structural strengthening.

6.2 DEVELOPMENT OF APPARATUS FOR TRC-BASED STRENGTHENING

In order to scale up the methodology of strengthening of RC beam with *TRC* from laboratory level to practical on-site applications, a mechanism has been designed. The main purpose of the tautening apparatus (Figure 6.1) is to provide stretching to the number of layers of textile that needs to be used in strengthening layer. Tautening apparatus consists of a non-stretching unit and a stretching unit. Non-stretching unit shown in Figure 6.1(a) consists of U-frame, with a width equivalent to that of beam to be strengthened. The bolts are provided in the U-frame by which it can be bolted to the surface of the beam to be strengthened. The U-frames is also intended to provide a clearance for the placement of required number of textile layers at bottom of the beam

that need to be stretched. The stretching unit of tautening apparatus shown in Figure 6.1(b) consists of three rollers of which two are fixed and the third is movable and are attached to guides through a chain mechanism and springs; fixing frame with bolts; handle unit; and a locking knob. The gap between the movable roller and fixed roller can be adjusted depending on the number of layers to be stretched. By rotating the handle of the movable roller, the required stretching can be ensured for the layers. After providing the required stretch, the position of moving roller can be locked by using the locking knob shown in Figure 6.1(c).
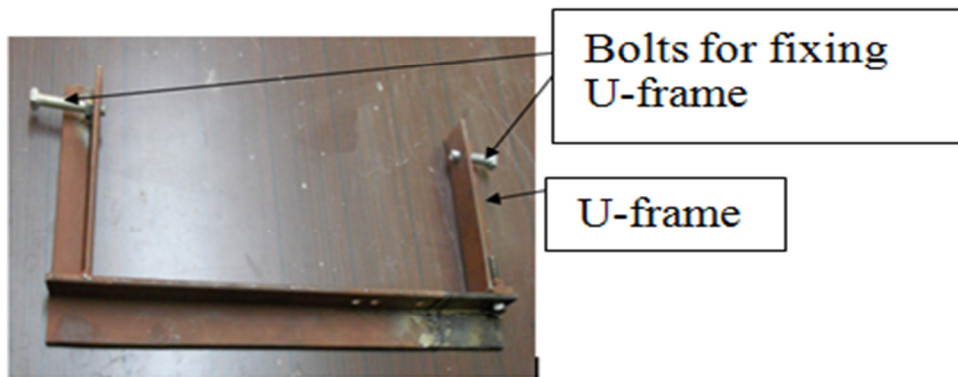
(a) Fixture for non-stretching unit
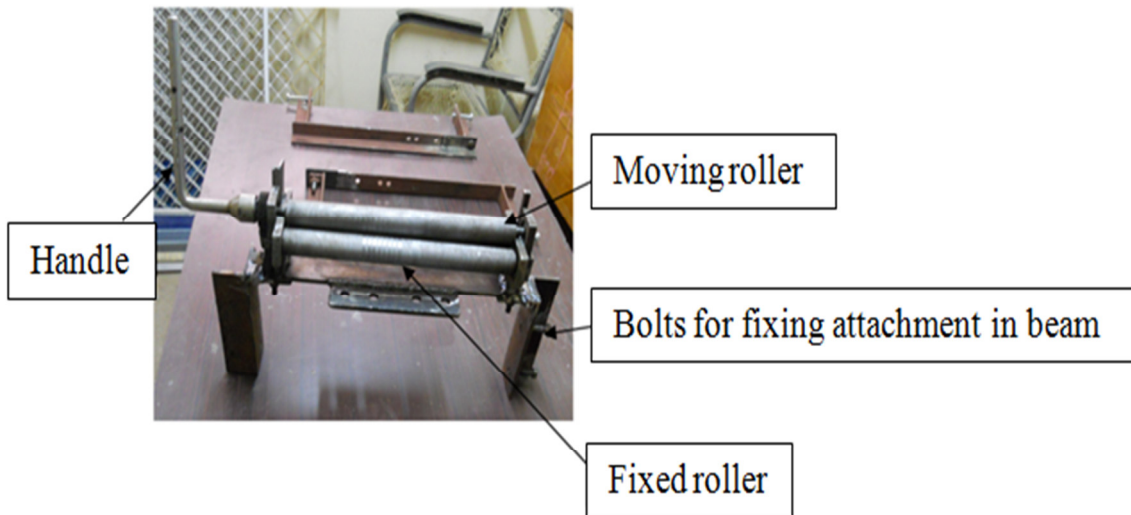
(b) Stretching unit
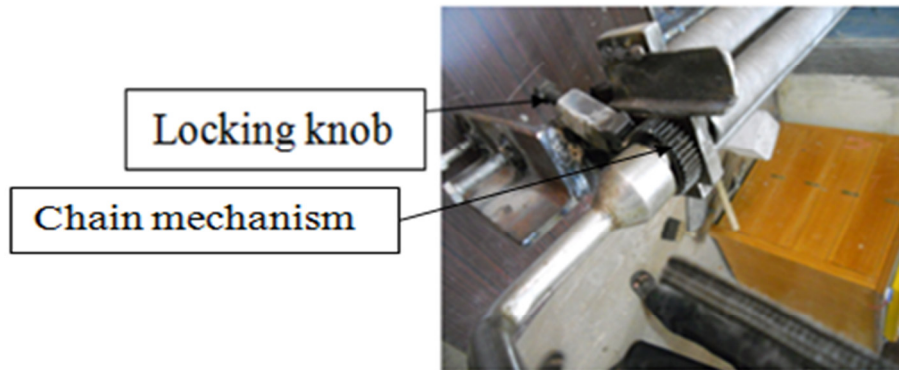
(c) Details of stretching unit

Figure 6.1 Components of tautening apparatus for on-site applications of beams

The tautening apparatus used for beam strengthening is slightly modified for the TRC-based strengthening applications on brick masonry walls, and is shown in Figure 6.2. In this case also, the apparatus consist of both non-stretching unit and stretching unit. The non-stretching unit shown in Figure 6.2(a) consists of an angle section with wall mounting screws, and a movable plate through which the gap for placing number of layers of textiles can be adjusted. Three tightening knobs are used to fix the textile layers for a width of 1m. The stretching unit of tautening apparatus shown in Figure 6.2(b) consist of a wall mounting plate with bolts, adjustable roller, fixed roller, stretching knob and a chain mechanism. The gap between moving and adjustable roller can be adjusted to accommodate the required number of layers of textiles using the bolts attached to the units at the extreme ends. After placing the required number of layers of textiles, the stretching knob can be rotated till the required amount of stretch is ensured. The stretching knob is connected to adjustable roller by a chain mechanism, which is shown in Figure 6.2(c). After stretching of the textiles, the position is locked using the bolts attached to the roller part.
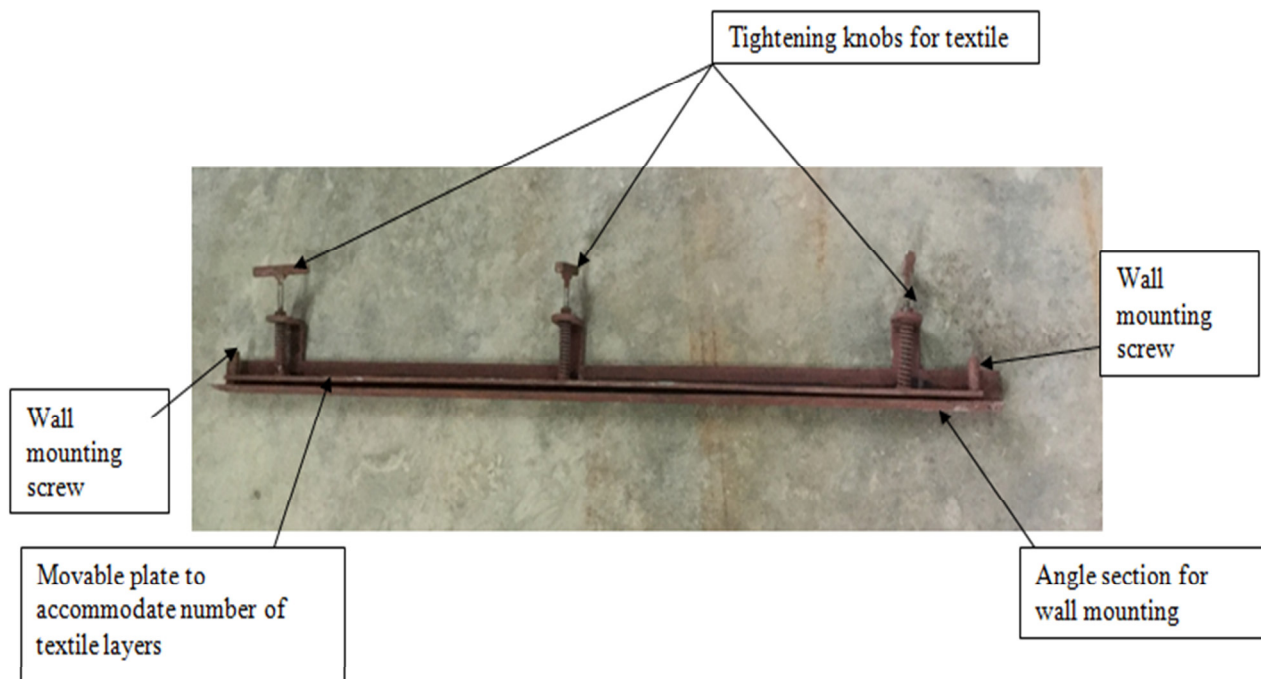
(a) Fixture for non-stretching unit
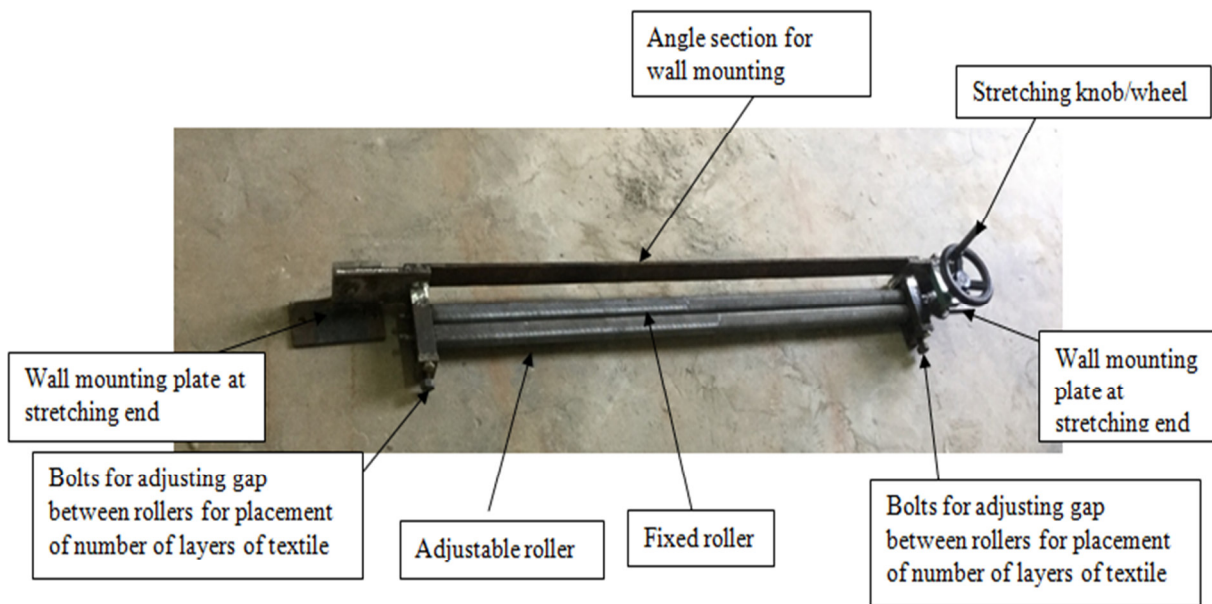
(b) Stretching end of stretching unit
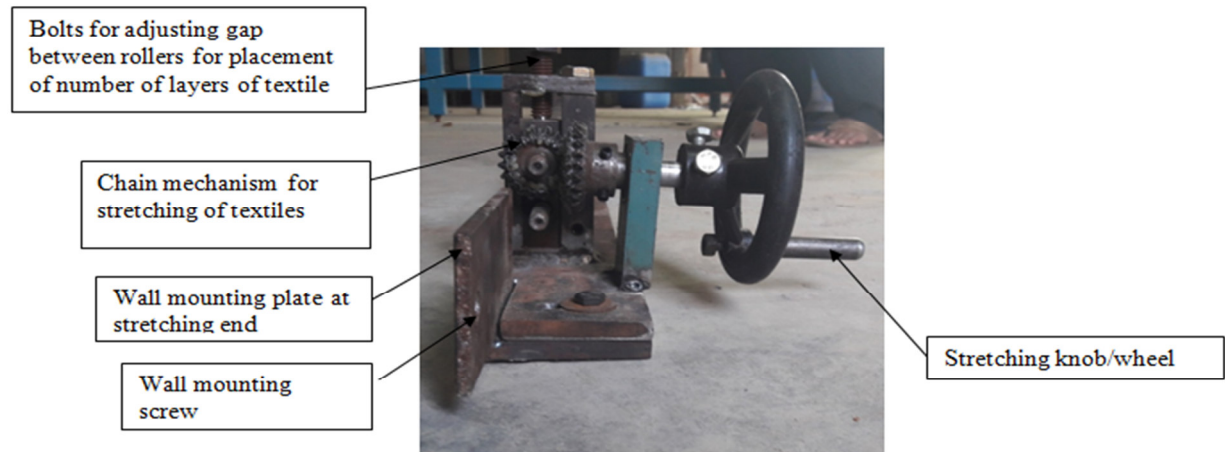
(c) Side view of stretching unit

Figure 6.2 Components of textile stretching mechanism for on-site applications of walls

6.3 ON-SITE ILLUSTRATION FOR APPLICATION OF TRC ON RC BEAMS

An on-site illustration for the application of TRC has been demonstrated for repairing of an existing beam in the Mechanical Science Block at IIT Madras. The beam was of width 350mm and the TRC layer was applied for a span of 2m. Three number of SRG-45 textile layers were used in the illustration. The various steps associated with TRC application is shown in Figure 6.3. First, the plastering on the existing beam was removed. Then U-frame was clamped to the beam by providing clearance to the placement of textiles(Figure 6.3a) at the non-stretching end. Subsequently, the stretching unit was also clamped to the beam (Figure 6.3b). The layers of textiles were arranged that pass through the clearance between U-frames and also through the gap in between the rollers in the stretching unit (Figure 6.3c). The moving roller was adjusted for this purpose using the springs attached in the mechanism. After placing the textiles in position, the 1st layer of *FABmix* was applied (Figure 6.3d), subsequent layers were stretched by rotating the handle in the stretching mechanism (Figure 6.3e) and locked after all the yarns in the textiles appeared straight (Figure 6.3f). Following this, the final layer of FABmix was applied (Figure 6.3g). After 1hr, the stretching unit was removed from the beam and the U-frames were removed on the next day. The status of beam after application of TRC is shown in Figure 6.3h.

(a) Fixing the non-stretching unit in beam

(b) Fixing stretching unit in beam

(c) Placing number of textile layers in position

(d) Application of 1st layer of FABmix

(e) Stretching the textiles by rotating the knob

(f) Textiles in stretched position

(g) Application of final layer of FABmix

(h) Beam after application of TRC

Figure 6.3 Demonstration of TRC application on RC beam

6.4 ON-SITE ILLUSTRATION FOR APPLICATION OF TRC ON MASONRY WALLS

An on-site illustration for the application of TRC has been demonstrated on an existing brick masonry partition wall at the textile reinforced concrete prototyping room at CSIR-SERC. The portion of masonry wall considered for TRC application is having 1m width and 2m height. Three numbers of layers of SRG-45 textiles were used for casting TRC layer. The various steps associated with the application of TRC layer on brick masonry wall is shown in Figure 6.4. First, the plastering of the existing wall was removed. Next, the non-stretching and stretching units of tautening apparatus was fixed in the walls by drilling holes and fixing the wall mounting screws. Subsequently, the number of layers of textiles to be used in TRC was kept ready in the stretching unit (Figure 6.4a). The gap between fixed roller and adjustable roller was adjusted by adjusting the screws attached to the chain mechanism, which is connected to the movement of the roller. After textiles are kept ready, the wall was made wet by applying water before application of FABmix (Figure 6.4b). Subsequently, the first layer of FABmix of 3mm thickness was applied on the masonry wall by trowel and levelled (Figure 6.4c). After application of first layer of FABmix, the textiles were fixed at the non-stretching end of tautening apparatus by clamping screws attached to the unit (Figure 6.4d). Three clamp screws are provided in the apparatus for placement of 1m width of textiles. The movement of clamping screw also helps to adjust the movement of movable plate of non-stretching unit to

accommodate the required number of layers of textiles. After fixing the textile at non-stretching end, the stretching knob in the stretching unit was rotated till all layers appeared straight and locked by tightening the bolts attached to the roller (Figure 6.4e, 6.4f). Following this, the final layer of FABmix was applied (Figure 6.4g, 6.4h). The levelling of final layer of FABmix was done till the TRC surface appeared uniform and smooth (Figure 6.4i). The final state of brick masonry wall after application of TRC layer is shown in Figure 6.4j. In this case, it was able to achieve the same plastering thickness, which the masonry wall had even after application of TRC layer. The tautening apparatus was removed after the final set of TRC. Water curing for the TRC layer was done from next day onwards for the required period.

(a) Tautening apparatus fixed in the wall   **(b) wetting of masonry wall**

(c) Application of first layer of FABmix

(d) Fixing of number of layers of textiles at non-stretching end

(e) Stretching of textiles by rotating knob

(f) Textiles in stretched position

(g) Application of final layer of FABmix   **(h) After application of final layer of FABmix**

(i) Levelling of final layer of FABmix

(j) Masonry wall after application of TRC

Figure 6.4 Demonstration of TRC application on masonry wall

6.5 ADVANTAGES OF THE PROPOSED METHOD

While performing cast-in-place TRC-based applications on beams and walls, the method of providing mechanical stretching to the textiles using the proposed apparatus will lead towards better composite performance. By using the tautening apparatus, the practical difficulty of placing more number of layers of textile is avoided. Moreover, higher number of layers can be accommodated in a particular thickness of TRC layer using the proposed apparatus, which enhances the efficiency of textiles in the strengthened system. In addition, placing textiles in a stretched way helps to have better control on the uniformity of overall thickness of TRC. Manual effort required to handle the textile layers while performing retrofitting for larger areas can be avoided with the use of proposed method and apparatus. Better bonding between textile layers and the binder

system is ensured by mechanically stretching the textiles & maintains uniformity in the final thickness of TRC layer.

6.6 SUMMARY

A technology consisting of a method and apparatus is developed for cast-in-place application of TRC-based systems on concrete beams and masonry walls (Indian Patent application: 2339DEL2015). Using this technology, it is possible to have technical advantage of having enhanced structural performance due to mechanical stretching provided to the textiles in textile reinforced concrete, leading to proper utilization of efficiency of textiles. In addition, the control over thickness, placement of more number of layers of textiles in a particular thickness, more uniformity, better bonding of textiles in binder system, avoidance of anchoring methods and special adhesives etc are also achieved.

CHAPTER 7

CONCLUDING REMARKS AND SUGGESTIONS FOR FURTHER RESEARCH

7.1 GENERAL CONCLUSIONS

The thesis deals with material development of one type of TRC called *FABcrete*; mechanical characterization of ingredients of *FABcrete* and composite as a whole; investigations on *FABcrete* as a flexural strengthening material and development of a methodology for its on-site application; and development of mathematical models for numerical and analytical simulation. Main conclusions arrived from the work presented in this thesis is summarized in this Chapter. In general, the objectives specified in Chapter 1 have been satisfied.

A fine grained binder *FABmix* was developed for *FABcrete* and its mechanical characteristics were found to be suitable for the end application of flexural strengthening of RC beams. Uniaxial tensile test were carried out on two types of glass textiles to find their suitability as reinforcement in *FABcrete*. It was concluded that the production method used for textiles has significant effect on the response behaviour and there is a delay in the activation of filaments in textile due to waviness, which needs to be overcome during *FABcrete* specimen preparation.

A generalized uniaxial tensile test methodology was developed for characterization of *FABcrete* and stress-strain behaviour was studied with respect to the volume fraction and type of glass fibre textile. A methodology that provides mechanical stretching to textiles in *FABcrete* during specimen preparation was found to enhance the load carrying ability in *FABcrete*. Parameters that can be used for development of design guidelines were arrived from the tensile characterization of FABcrete. The various failure phenomena occurring in *FABcrete* were captured using a non destructive imaging technique and could correlate with the mechanical behaviour.

Further, the experimental investigations carried out on cracked and un-cracked RC beams strengthened with *FABcrete* confirmed the suitability, applicability and performance of *FABcrete* towards flexural strengthening. An on-site approach developed for application of *FABcrete* on RC beams revealed it's practical feasibility. Mathematical models were also

developed that are capable of predicting the response of RC beams strengthened with *FABcrete*. Finally, the design guidelines were also proposed for implementation of *FABcrete* for flexural strengthening.

7.2 SPECIFIC CONCLUSIONS

Material Development

- **Binder:** A cementitious binder (*FABmix*) with cube compressive strength of 44.5±4.2 MPa, split tensile strength of 4.5±0.8MPa, uniaxial tensile strength of 2.5MPa, bond strength of 2.35±8.7%MPa, chloride permeability of 1250 ±6.7% Coulombs and workability retention of 80% flow for one hour was developed. This binder was found to perform satisfactorily in *FABcrete* for the end application of flexural strengthening.

- **Textile as reinforcement:** Two types of glass textiles with brand name SRG-45 and AR1 with different mesh openings and weight per unit area was investigated to find the applicability as reinforcement in *FABcrete*. In the case of SRG-45, there are two possible yarn arrangements in the warp direction: one in which there are two yarns per line in warp direction and another in which there is only one yarn per line. From the investigations on the variability in load versus strain behaviour, it was noted that for SRG-45 with two yarns per line, there was more uniform distribution of load, whereas in the textile with one yarn per line, the stress redistribution was more local. The textile with one yarn per line was capable of elongating more due to the loosening of more filaments in a yarn; however, the weft yarns hold the filaments of warp yarn at the warp-weft junctions for the textile with two yarns per line more effectively. Further, the initial nonlinearity observed was more in the case of one yarn per line, which delays the activation of the textile in the TRC further leading to practical difficulties while placing more number of layers in applications. Also, the total contact area between the binder of *FABcrete* and the outer filaments of the yarns in the case of the textile with two yarns per line will be more than in the case of the textile with one yarn per line, leading to better bond performance. Consequently, it was concluded that the use the SRG-45 with two yarns per line will be more appropriate as reinforcement in *FABcrete*. While comparing SRG-45 and AR1, it was be concluded that as the weight per unit area of glass textile decreases, ultimate load carrying capacity per meter width decreases and elongation

increases. Further, as the number of yarns in loading direction increases, there was a linear increase in the load carrying of the textile. Moreover, the tensile characterization of both types of glass textiles revealed that the initial region of load vs strain posses a point of inflexion and a force is required to straighten all the yarns in textile for enhanced composite action in *FABcrete*.

- **Bond of textile with binder:** From the microscopical investigations on bond behaviour between glass textile and *FABmix* in *FABcrete* specimens, it can be concluded that the delaminating cracks form between textile and matrix when specimen and filaments in the yarns show a loosening effect when subjected to tensile load. Also, the penetration of *FABmix* into the filaments of textile was visible in the microscopic examination, reaffirming the effectiveness of binder composition in *FABcrete*.

- **Integrity of *FABcrete* with substrate:** When *FABcrete* is used as a strengthening material in cast-in-place application, the cementitious binder itself has to act as an adhesive to existing concrete. To confirm this, the bond strength of *FABmix* was determined by conducting pull-off tests and the bond strength of around 2.4MPa was obtained. Further, to check the integrity of *FABcrete* with substrate concrete and to examine the final failure pattern, study on concrete specimens jacketed with *FABcrete* was carried out. There was no debonding of *FABcrete* from the concrete surface throughout the test and the failure of all specimens were in a controlled manner.

Uniaxial Tensile Characterization of *FABcrete*

- **Test Configuration**: Based on the experience gathered from the present investigation, a tensile test configuration for TRC specimens is arrived. The conclusions are as follows. A servo hydraulic machine can be used for the investigations related to uniaxial tensile characterization of TRC for static loads. Rectangular geometrical configuration can be considered for specimen preparation with a specimen size of 500 mm length, 60mm width and 8mm thickness. The textile has to be mechanically stretched while preparing the specimens to get an improved tensile performance. The load transfer from the machine to the specimen has to be by adhesive tension. Carbodur plates can be glued to the TRC specimen in the gripping portion. For this tapered Carbodur plates upto a length of 125mm with

straight cut upto 75mm and a taper for a length of 50mm has to be considered for a gradual load transition. The experimental investigations can be carried out under displacement controlled loading at a rate of 0.5mm/min. A gauge length covering free length of the specimen can be considered to take the deflection/strain characteristics of the specimen. Two LVDTs needs to be placed at the centre line of the specimen at front and back sides to record the deformation occurring in the measuring length. A video microscope can be focused in the measuring area to capture the crack width.

- **Tensile behaviour of *FABcrete*:** From the uniaxial tensile characterization of *FABcrete*, it can be concluded that if volume fraction of the textile in the specimen is above critical volume fraction, the specimen undergoes three stages of stress-strain behaviour, namely, uncracked state, multiple crack formation state and steady state. The volume fraction and mesh size has considerable influence on the stress-strain behaviour of *FABcrete*. As the volume fraction increases, the ultimate stress and ultimate strain increases. If combination of glass textile with more and less weight per unit area are used, it opens up possibility of optimization of material ingredients in *FABcrete* components. The cracking pattern in *FABcrete* is of multiple cracking nature with hairline crack width. With high volume fraction, it was possible to have a closing behaviour for all the cracks upon the release of the load. As volume fraction increases the crack width and average crack spacing reduces. While using more number of layers, it is preferable to calculate the efficiency of textiles as the ratio of load in kN/m to tensile strength of textile in kN/m. Efficiency factor arrived based on characterization studies need to be incorporated in the design of *FABcrete* components.

- **Effect of mechanical stretching**: While comparing the *FABcrete* specimens with manually and mechanically stretched textiles, it is concluded that the mechanically stretched textile in *FABcrete* leads to enhanced tensile performance. Such mechanism will open up possibilities of various optimized configurations and combinations of textiles to be used in *FABcrete* rather than enhancing the mechanical properties of textiles, which leads to increase in cost and production difficulties.

- **Damage assessment using X-ray computed tomography:** The various failure mechanisms such as matrix cracking, delamination of matrix from textile and pullout of internal filaments from external filaments was identified internally by using X-ray computed tomography. The

efficiency of mechanical stretching of textiles was also reveled micro structurally using this method. The quantitative image analysis was also carried out to determine the defects present in tested and untested specimens of *FABcrete*.

Flexural strengthening of RC beams with *FABcrete*

- *FABcrete* **as a retrofit material:** Experimental investigations on *FABcrete* strengthened un-cracked RC beams were carried out to find the capability of *FABcrete* as a retrofit material. While comparing with the enhancement in load carrying capacity of un-strengthened RC beam, it is observed that there is an increase of 20% for uncracked and strengthened RC beam. It is observed that *FABcrete* strengthened beams have a residual load carrying capacity near to that of ultimate load of un-strengthened beam capability to elongate upto the extent of maximum elongation of glass textile. The energy absorption for un-cracked and strengthened beams at 30mm deflection is 266.3% higher compared to the maximum energy absorption capacityof un-strengthened beams. With respect to crack pattern, the *FABcrete* strengthening layer showed multiple cracking behaviour. The number of cracks and width of cracks was decreased in the main beam when it was strengthened with *FABcrete*. It was also noted that no additional anchorage or adhesives were required for strengthening of RC beams with *FABcrete* and the final failure pattern of strengthened beams was by rupture of glass textiles in *FABcrete*.

- *FABcrete* **as a restoration material:** Experimental investigations on FABcrete strengthened RC beams to find the capability of *FABcrete* as a restoration material. While comparing with the enhancement in load carrying capacity of un-strengthened RC beam, it is observed that there is an increase of 16.5% for cracked and strengthened RC beams. It is observed that *FABcrete* strengthened beams have a residual load carrying capacity near to that of ultimate load of un-strengthened beam capability to elongate upto the extent of maximum elongation of glass textile. The energy absorption for un-cracked and strengthened beams at 30mm deflection was 233.42% higher compared to the maximum energy absorption capacity of un-strengthened beams.

- **Use of non-contact video gauge:** The instrumentation technique using non-contact video gauge was used to measure the strain in the strengthened beam. The accuracy of results were

very much comparable with that of strain gauges. Moreover, considering the multiple cracking nature of *FABcrete*, it is concluded that non-contact video gauge strain measurements are better option and the information gathered will be helpful while formulating the design guidelines for *FABcrete* strengthening at a larger context.

- **Adequacy of existing ACI recommendations for *FABcrete*:** The existing recommendations for strengthening of concrete structures using textile reinforced concrete by ACI 549 (2013) was used to analyze the *FABcrete* strengthened RC beams and observed an over prediction for the ultimate behaviour.

Practical application of TRC for strengthening of beams and walls

- **Demonstration of practical application:** A technology consisting of method and apparatus for flexural strengthening of RC beams with TRC was developed. The apparatus was named as "Tautening Apparatus" and this development is first of its kind. This technology was demonstrated on-site on an existing RC beam. Further, the applicability of same apparatus was also demonstrated for application of TRC on brick masonry wall.

Mathematical modelling of RC beams strengthened with *FABcrete*

- **Numerical modelling:** Numerical Investigations of *FABcrete* strengthened RC beams were carried out and a generalized methodology is proposed for the finite element analysis and numerical simulation of TRC strengthened beams. Apart from the integration of the existing models for concrete and steel, a tension stiffening model was developed to use as a user defined input for smeared crack model for *FABcrete* in the analysis. It is observed that the numerical model is capable of predicting the load-displacement response upto ultimate state. The response behaviour of the numerical simulation till ultimate state showed good agreement with the corresponding experimental results.

- **Analytical modelling:** A non-iterative analytical model was developed to predict the load-displacement characteristics of *FABcrete* strengthened RC beams. The model makes use of only material parameters of the ingredients from the characterization studies. The model was

validated with the experimental behaviour and found to be in good agreement. The proposed model can be used to arrive at the design configurations for TRC strengthening.

- **Design methodology:** A non-iterative and simple design method was developed to design the *FABcrete* for flexural strengthening of RC beams. In addition to computing the thickness of *FABcrete* layer, the number of layers of textile that needs to be placed for a particular structural capacity enhancement can also be determined using this method.

7.3 SUGGESTIONS FOR FURTHER RESEARCH

The results obtained from the present thesis have paved way for further research towards considering *FABcrete/*TRC as a candidate for various structural applications. The various repair and retrofitting applications for concrete beams/slabs, masonry structures and offshore structures with *FABcrete* can be explored. The possible applications of *FABcrete* as shell structure, Façade elements, sandwich panel, piping component, confinement for beam-column joint, industrial flooring, impact resistant member etc. can be taken up and respective design guidelines can be formulated. When *FABcrete* is used along with various substrate materials (e.g., brick, stone, concrete, etc.), its compatibility needs to be checked on which the system is meant to be installed. In addition, quality assurance needs to be met and guidelines needs to be formulated for installation.

Considering the global availability of large number of textiles of different materials in the market as of today, it is possible to arrive at an optimized material and structural performance with various combinations of textile with various binders. It is also important to qualify various textile to use as reinforcement in TRC; and guideline needs to be formulated for that as well. Even it is also possible to combine fibers with textile to arrive at various hybrid solutions and optimization of matrix and textiles with different architecture can be tailor made and investigated towards various applications (Barhum and Mechtcherine, 2012; Barhum and Mechtcherine, 2013). Even though tailor made composites are advantageous, sometimes this may end up in wide variability in terms of mechanical behaviour, bond performance and expected failure modes. Therefore, a generalized procedure is needed that allows for the whole characterization of TRC composites, which can provide the fundamentals for the advanced engineered developments in the construction sector.

Since TRC applications are new to India, it is essential to formulate characterization methods and design guidelines for TRC to be on par with the developments across the globe and utilize TRC for construction applications. Design guidelines needs to be developed by conducting various parametric studies for retrofitting and standalone applications of TRC. Further, the durability performance of TRC needs to be investigated in detail. Considering the requirements of pre-fabrication industry, technologies need to be developed for the production of various TRC components. Guidelines for the product qualifications are also needed to characterize the TRC systems before they are made available in the market.

Table A.1 Details of Binder, Textile and TRC in Various Applications from Literature

Ref.	Binder	Textile	TRC
Beam Strengthening			
Bruckner et al. (2008)	Compressive strength=27MPa	AR glass & Carbon; Textile weight of carbon= 470g/m^2	
D'Ambrisi, and Focacci (2011)	Cementitious binder : Comp strength=50MPa	Carbon textile thickness =0.047mm; Tensile strength=3051MPa, E=238GPa; failure strain=1.28%	
Larbi et al. (2010)	Fine grained mortar impregnated with epoxy	3 layers of aramid textiles	TRC tensile strength= 18 MPa, Ultimate strain= 0.02 mm/mm
Al-Salloum et al. (2012)	Cementitious mortar Comp=23.9MPa, tensile=2.77MPa modified cementitious Polymer mortar Comp=56.4MPa, tensile=3.4MPa	Basalt textile Tensile strength=623MPa, E=31.94GPa, Nominal thickness per layer=0.064mm	1 layer of basalt textile; Tensile strength=7.7MPa, Ultimate tensile strain=.0299mm/mm, Bond strength=0.39MPa
Larbi et al. (2012)	Mortar of fine particles (maximum diameter of aggregate – less than 0.8 mm, which is a thixotropic repair mortar)	Knitted textile grid: The meshes are rectangular and "open" at 3 × 5 mm (warp × weft). The number of filaments per roving is 1600; the filament diameter is 19 μm and Warp is AR glass and the weft is made of polyester. The roving strength is 1102 MPa; TRC: 3 glass AR fabric	TRC- tensile strength=16MPa, Ultimate strain = 0.013mm/mm
Larrinaga et al. (2010)	4% organic resin Compressive strength=19.8MPa, Flexural strength=7.2MPa	Carbon grid 4×4mm; Tensile strength=3500MPa, failure strain=1.45%, E=240GPa, Nominal thickness=0.056mm Basalt grid 20×20 mm; Tensile strength=900MPa, Failure strain=2.2%, E=55GPa,	

		nominal tk=0.0424mm	
Bruckner et al. (2006)	Fine grained concrete , resin based mortar Compressive strength=82.8MPa; Flexural strength=5-8MPa; Cementitious mortar with maximum aggregate size=1mm; Compressive strength=27.9MPa, Tensile strength=3.6MPa.	AR glass, carbon: 2 layers; AR glass (max 4 layers)+carbon fiber	
Larbi et al. (2010)	Epoxy resin: Tensile strength = 56 ±3 MPa ; Young's modulus= 12,300MPa;Shear modulus= 4500MPa	Glass grid; Number of Layers=5 (3 grids + 2 mat)	Tensile strength= 19.5MPa
Oesch (2015)	Epoxy resin	Polypara-phenylene-benzo-bisthiazole (PBO) fabric	Elastic modulus=270GPa; Tensile strength=5800MPa; Tensile strain=2.15%
Schneider et al. (2006)	Cementitious matrix for carbon and PBO net) Comp strength=28MPa, tensile strength=4MPa, Epoxy resin(carbon sheet) Comp strength=59MPa, E=2515MPa	Carbon fiber net Tensile strength=3500MPa, failure strain=15%, E=240GPa PBO fiber net Tensile strength=5800MPa, Failure strain=2.15%, E=270GPa Carbon sheet Tensile strength=3500MPa, Failure strain=1.5%, E=240GPa	2 layers of PBO-FRCM=28.73% increase in load ; Tensile strength=48MPa.
Ambrisi et al. (2012)	Cement based matrix Tensile strength=2.55MPa, Compressive	Polipara fenilen benzobisoxazole net Tensile strength=5213MPa; E=271GPa;	Axial shear stress=0.6MPa

|	strength=16.1MPa	Failure strain=2.1%, Nominal thickness =0.046mm	
Contamine et al. (2013)		4.36% latex impregnated glass textile: Thickness of fabric used 1.7, 5 and 10mm	Prefabricated trc plates For 1.7mm textile, Tensile strength=8.2MPa, For 5mm textile, Tensile strength=22MPa, E=6470MPa For 10mm textile, Tensile strength=41MPa
Impact Resistant Panel			
Trtik and Bartos (1999)	Cement=8159g, Water=3263g, Silica fume=677g, SP=12ml.	AR glass fabric: Tensile strength=1270MPa-2450MPa, E=78GPa	Tensile strength=20-25MPa; Strain capacity of order 2-5% under static condition
Ortlepp et al. (2009)	Resin	2ply & 3ply multi layer fabric samples woven on 4 harness, four varities of nylon 2-ply & five varities of nylon 3-ply nylon-6 (96 tex, fibers dia 27.2μm) 0.3% volume fraction	Composite tensile strength (warp=115MPa, weft=75MPa); Flexural strength=26-30MPa
Peled and Bentur (2003)	Cement=6473g (42% by vol); silica fume=560gm(5% by vol); SP=10ml(0.1% by vol); w/c=0.37	AR glass fabric, PE fibers, hybrid fabric Straining capacity increases from 0.03mm/mm for glass to above 0.08mm/mm	Tensile strength=20 to 25MPa; straining capacity =2-5%. Aramid-tensile strength=26.2MPa; ultimate strain=0.037mm/mm Hybrid-tensile strength=25.75MPa and ultimate strain 0.063mm/mm
Façade/Cladding			
Insu-Shell-Projekt Life (2009)	Agg size max=2mm	AR glass fabric	Bending strength= 17kN/m
Hegger et al.	Fine grained concrete	AR glass fabric	Bending strength=

(2011)	matrix, max aggregate size=0.6mm		11kN/m
Fydro (2012)	Sand ,cement, special mineral admixures; Comp strength ≥ 40MPa; Bending strength ≥12MPa, E=15-20GPa	3D glass fabric	
Hegger et al. (2010)	Maximum grain size=0.6mm; Comp strength=67MPa, Tensile strength=4.1MPa, E=33100MPa	AR glass Uncoated 489MPa, efficiency=0.288; Coated 619MPa, efficiency=0.682	
Engberts (2006)		AR glass fabric	LOP> 7.5 MPa MOR> 12MPa E=20000MPa Thermal dilation=1.5×10^{-5}
Lieboldt (2006)	Cement based matrix	AR glass(100-500g/m^2=2200tex, 8.33mm mesh-longitudinal and 320tex in transverse direction). 2400tex AR glass: Tensile strength=2000-5000MPa (warp) & 2000-9000MPa (weft)	
Column Confinement			
Orlowsky and Raupach (2006)	Fine grained concrete; max aggregate size 1mm; Comp strength=80MPa	AR glass fabric , Fineness=1200 tex; mesh size 7.2mm; Tensile strength=1232MPa; E=74GPa; Carbon textile: Fineness= 800tex, E=222.98GPa	
Beam-column Strengthening			
Mechtcherine and Lieboldt (2011)	Comp strength=70-80MPa; Flexural strength=9-17MPa	Alkali resistant glass textile	
Slab Strengthening			
Schefflera et al. (2009)	Fine grained concrete matrix:	Biaxial carbon fabrics-800tex: Tensile strength=1032MPa,	

|	Comp strength=30MPa	E=222.98GPa	
Loreto et al. (2014)	Cement + dry polymer <5% Compressive strength (for 1 ply) =28MPa& for 4 fabric ply=40MPa	Dry fiber fabric of polyparaphenylene benzobisoxazole fiber mesh 10x10 and 20x20mm	FRCM coupon 410x51x10mm Ultimate tensile strength=10.58MPa, Ultimate tensile strain=0.00642mm/mm
Stay-in-place Formwork			
Schleser et al. (2006)	Polymer impregnated mix	The randomly in plane oriented fibre textiles used for the shear reinforcement are chopped strand mats with a surface density of 300 g/m2; 4 layers resulting in a thickness of 2 mm and a fibre volume fraction of around 12%.	Interlaminar shear strength 4.4 MPa, Tensile strength 50 MPa, Ultimate strain = 1.2%; Young's modulus (uncracked stage)= 18.0GPa, Young's modulus cracked stage= 4.0GPa.
Shell			
Guldentops et al. (2009)	Compressive strength =22MPa	AR glass textile	TRC Tensile strength=30MPa
Schladitz et al. (2012)		AR glass fiber wrap knitted Tensile strength=2000-5000MPa	
Schatzke et al. (2010)	Matrix Compressive strength=78.6MPa, Bending strength=9.5MPa, Tensile strength=4.7MPa, E=34350MPa	AR glass fabric 1214MPa	
Structured Profile			
Bruckner et al. (2005)	Aggregate <2mm grain size; cement=490kg/m^3, fly ash=175kg/m^3, SF=35kg/m3,w/c=0.57 ; silicious fine=500kg/m^3 Comp strength=15-	Woven fabric, nonwoven fabric, scrim textile, AR glass	

	49MPa, Flexural strength=4.1-13.9MPa, E=22000MPa		
Bridge			
Curbach et al. (2006)	Grain size max=4mm; cement=450kg/m^3; fly ash=100kg/m3; w/c=0.41; silicafume=35kg/m^3; water=213kg/m^3; quartz powder =500kg/m3 Compressive strength=87.1MPa, Flexural strength =10.7MPa	Impregnated AR glass textile Tensile strength=2000MPa	
Hegger et al. (2010)	Cement, Fly ash, metakaolin, w/c=0.41, Density=2256kg/m3 Compressive strength=87.1MPa, Flexural strength=10.7MPa, E=33600MPa	AR textile epoxy impregnated Tensile strength=1035MPa, E=64800MPa	
Masonry Strengthening			
Triantafillou (2010)	Epoxy resin	2 layers of resin-impregnated carbon fabric	

B.1 Response of *FABcrete* specimens with manually stretched textiles
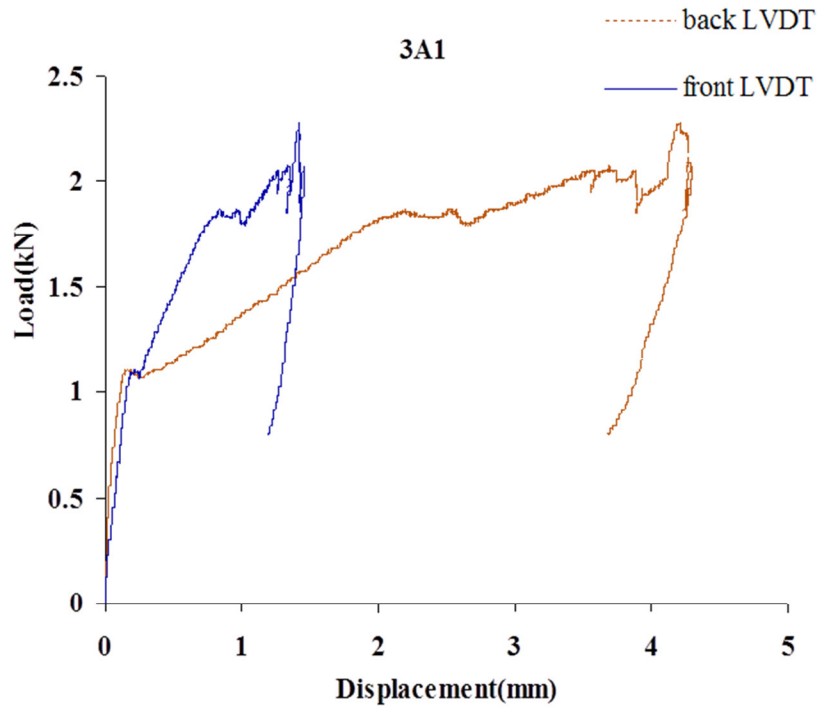
(a) Specimen 3A1
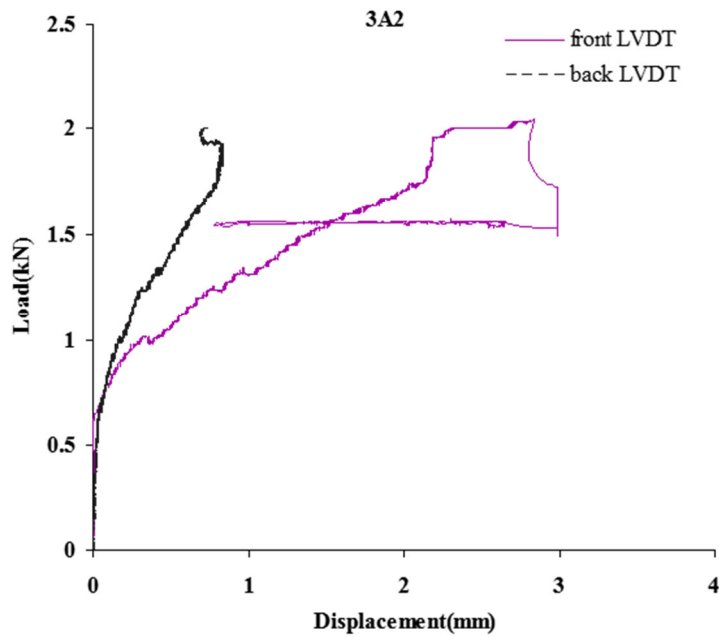
(b) Specimen 3A2

Figure B.1 Load versus LVDT displacement curves for *FABcrete* with 3 layers of manually stretched SRG-45
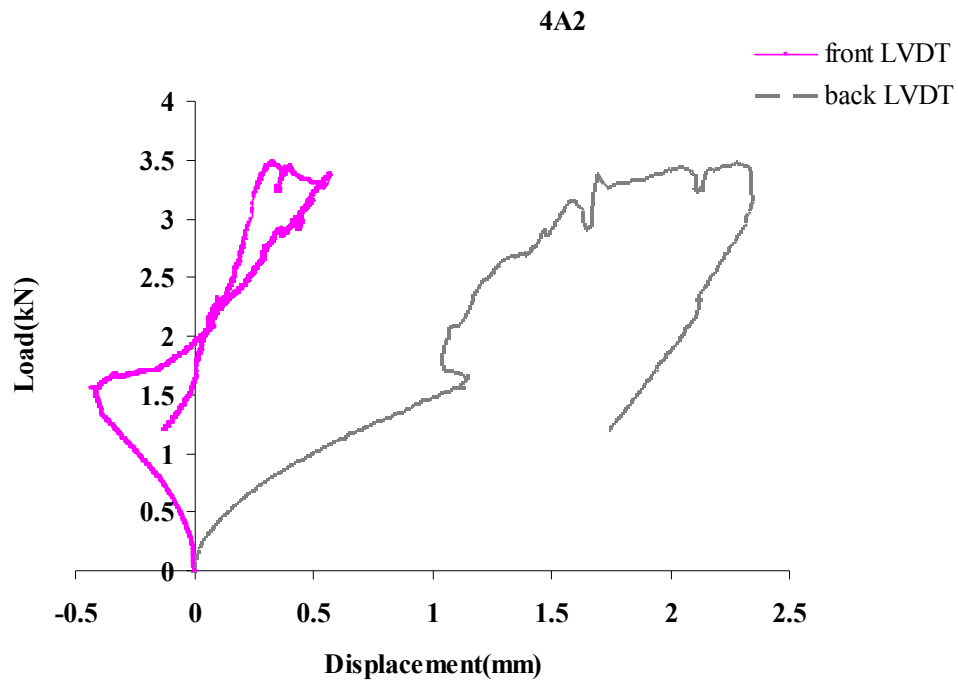
(a) Specimen 4A2
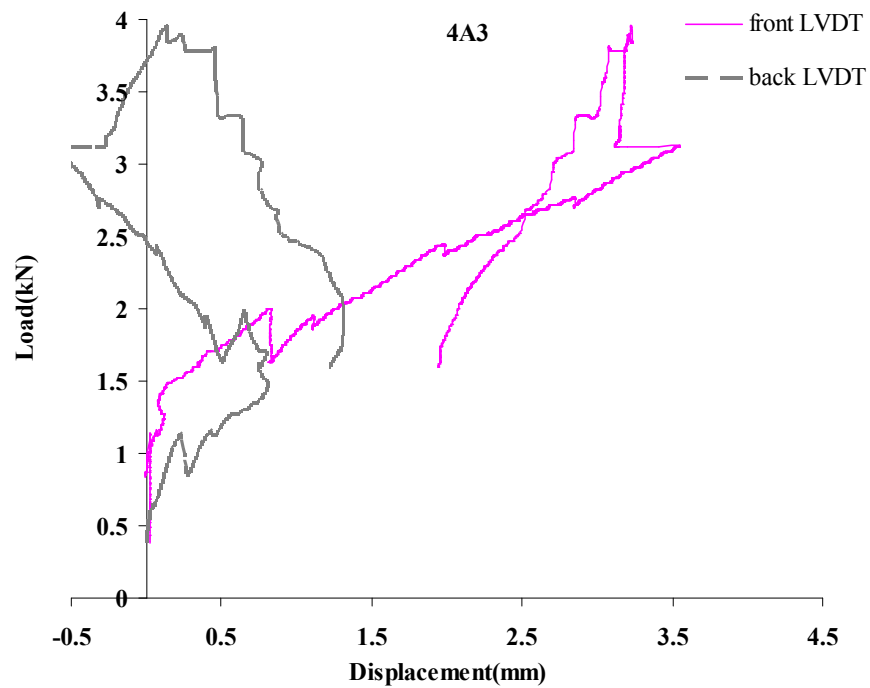
(b) Specimen 4A3

Figure B.2 Load versus LVDT displacement curves for *FABcrete* with 4 layers of manually stretched SRG-45
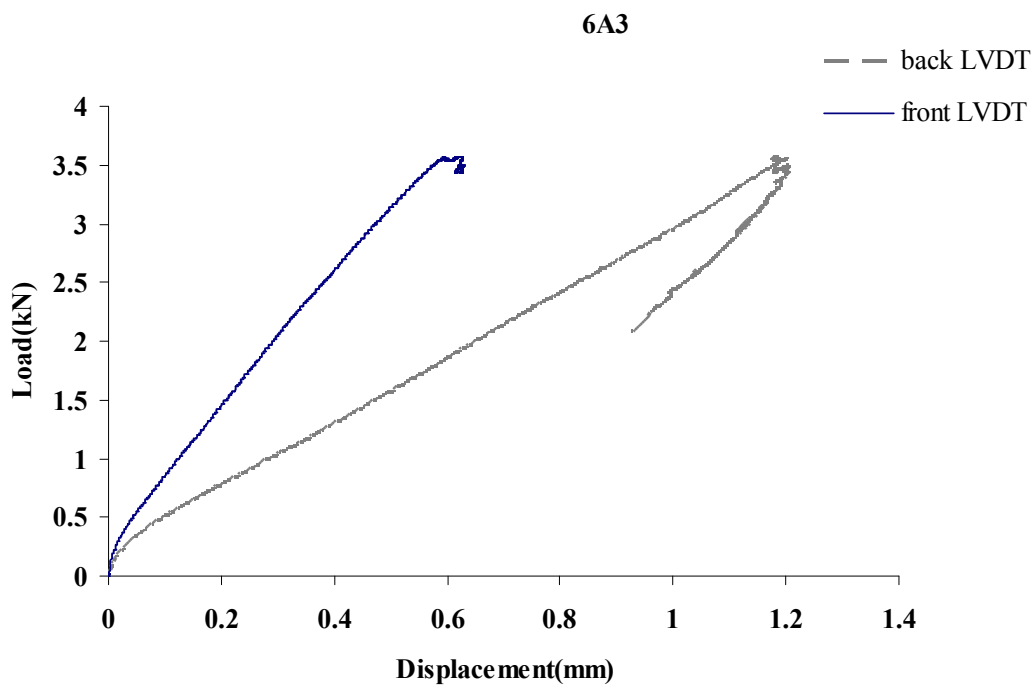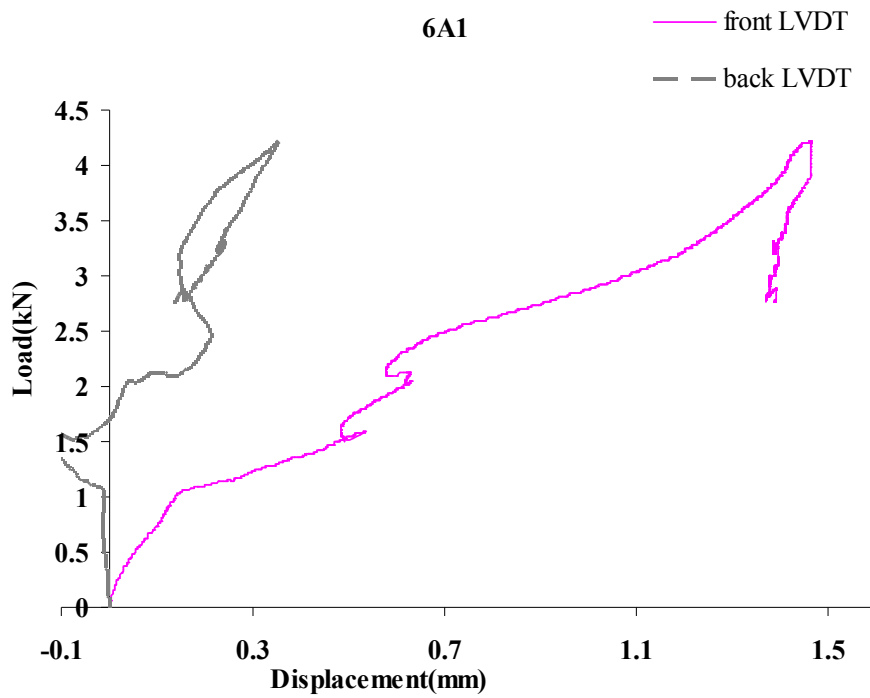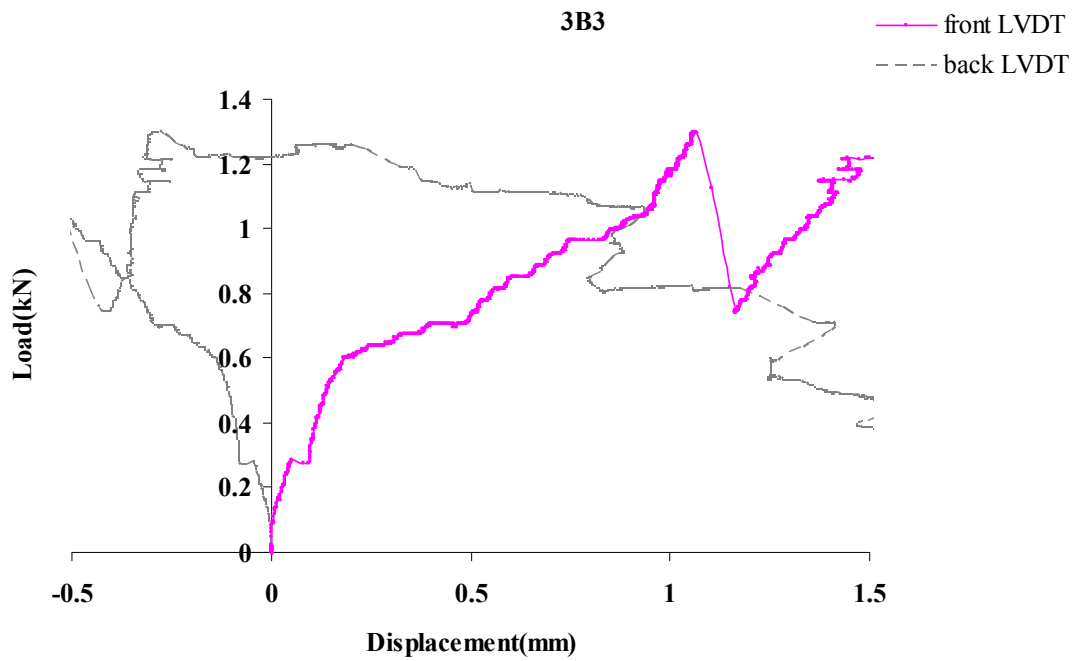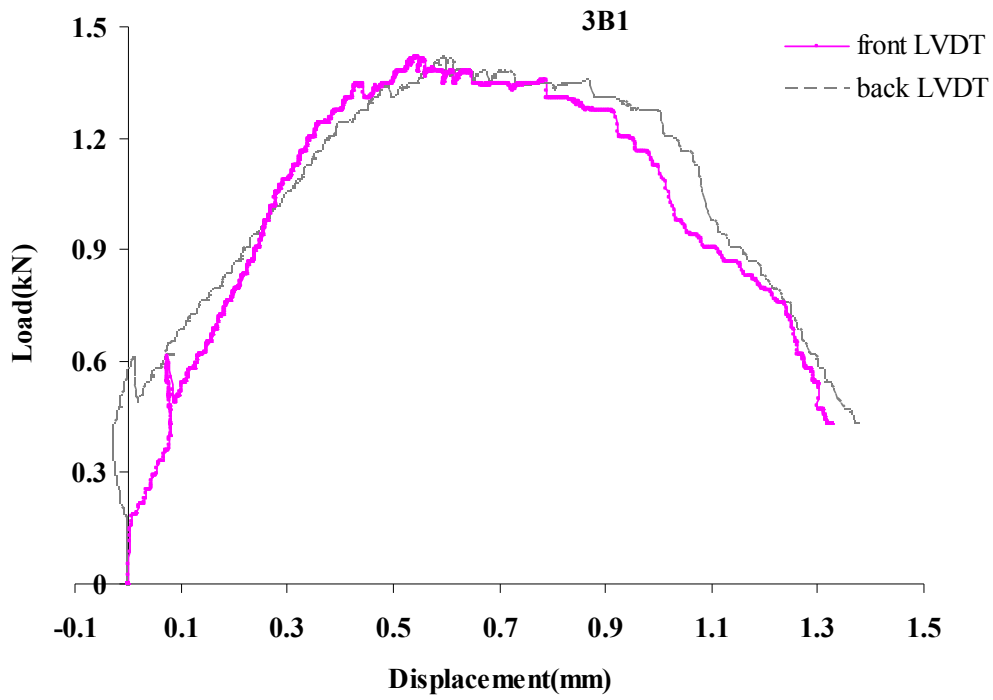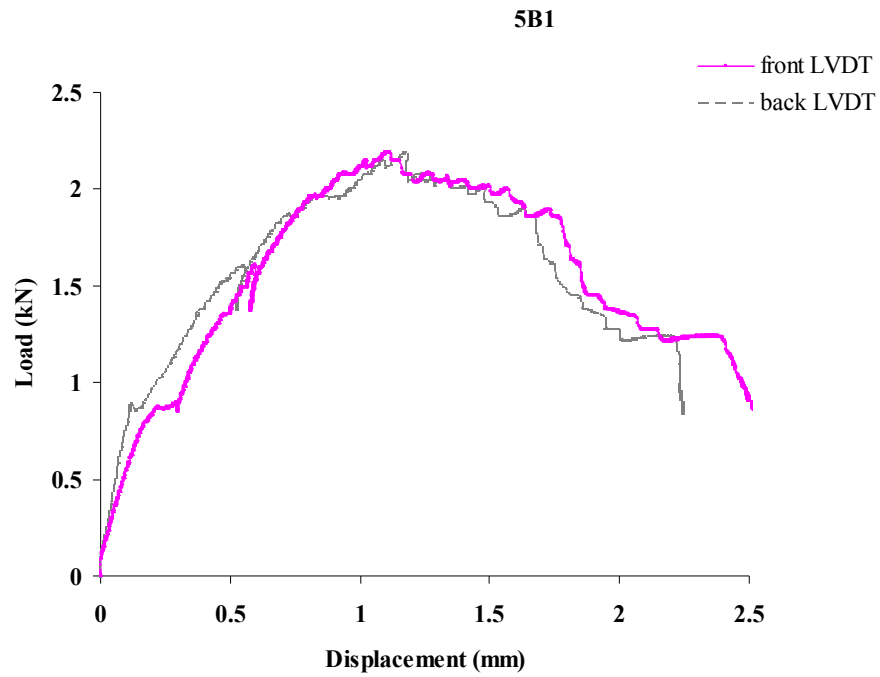
(a) specimen 6A1

(b) Specimen 6A3

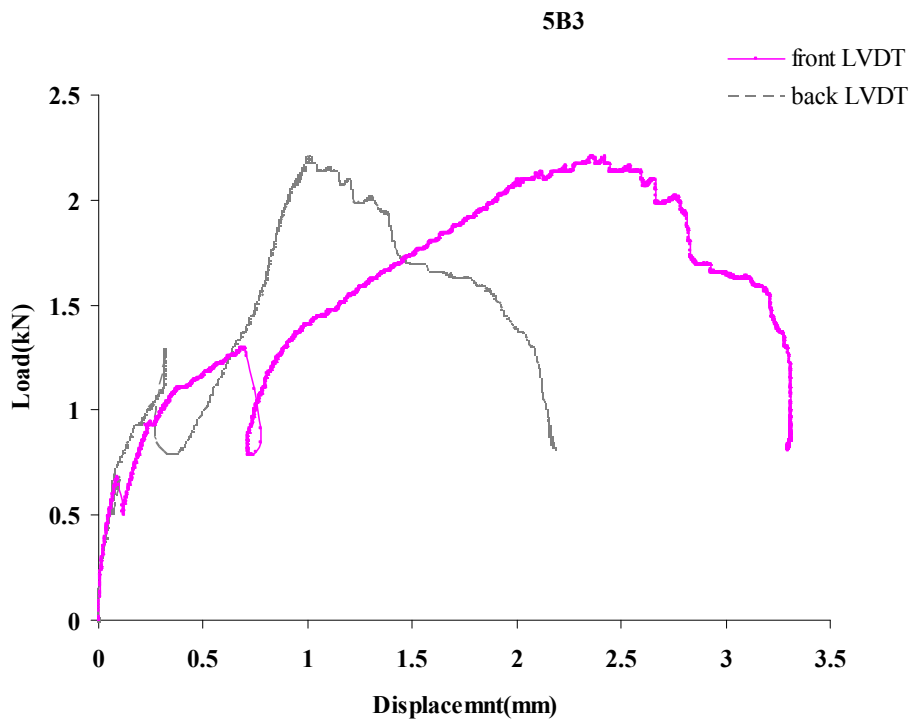Figure B.3 Load versus LVDT displacement curves for *FABcrete* with 6 layers of manually stretched SRG-45

(a) Specimen 3B1

(b) Specimen 3B3

Figure B.4 Load versus LVDT displacement curves for *FABcrete* with 3 layers of manually stretched AR1

5B1

(a) Specimen 5B1

5B3

(b) Specimen 5B3

Figure B.5 Load versus LVDT displacement curves for *FABcrete* with 5 layers of manually stretched AR1
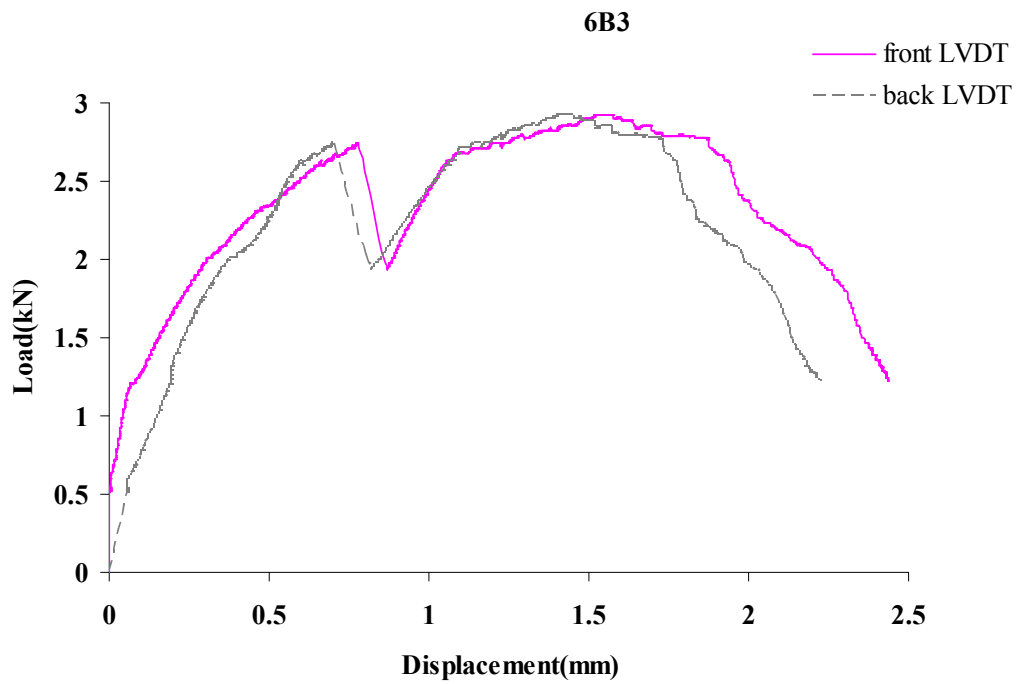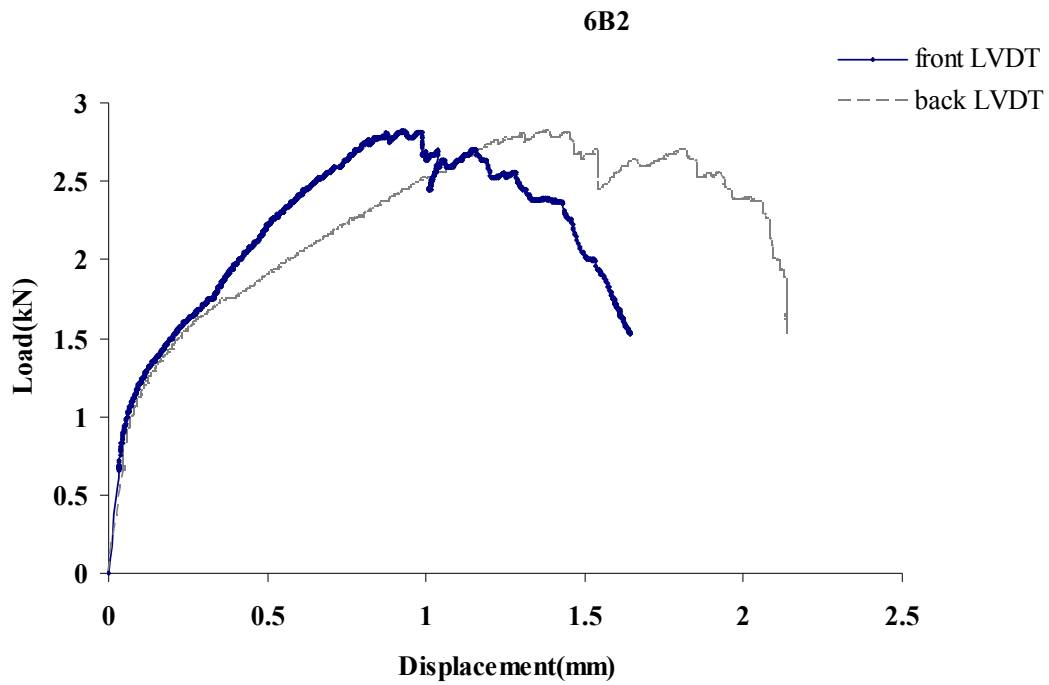
(a) Specimen 6B2

(b) Specimen 6B3

Figure B.6 Load versus LVDT displacement curves for *FABcrete* with 6 layers of manually stretched AR1
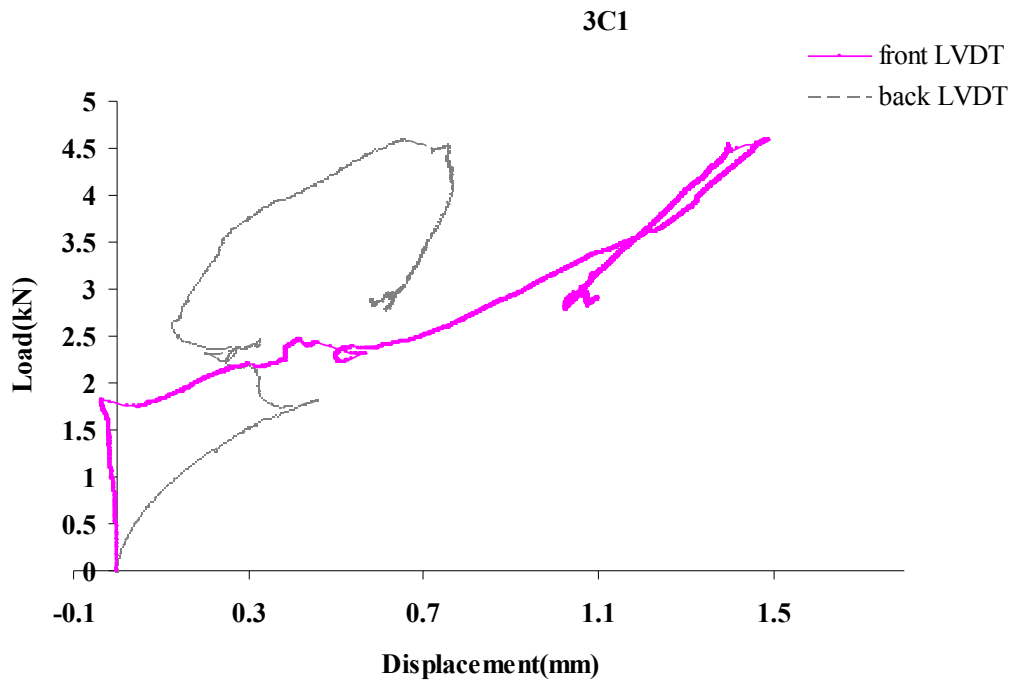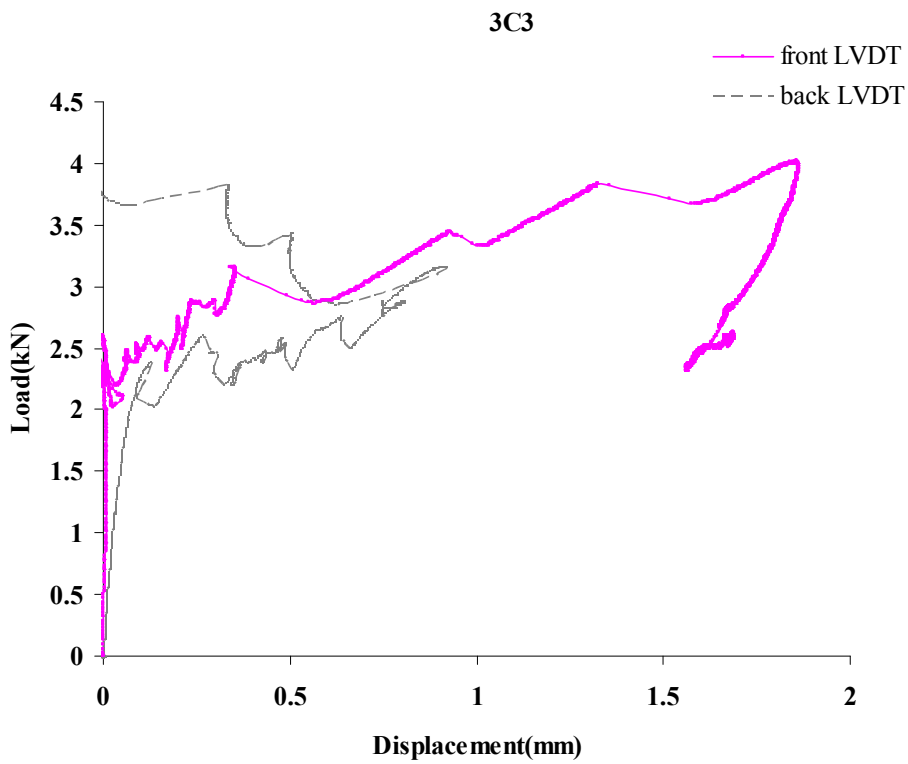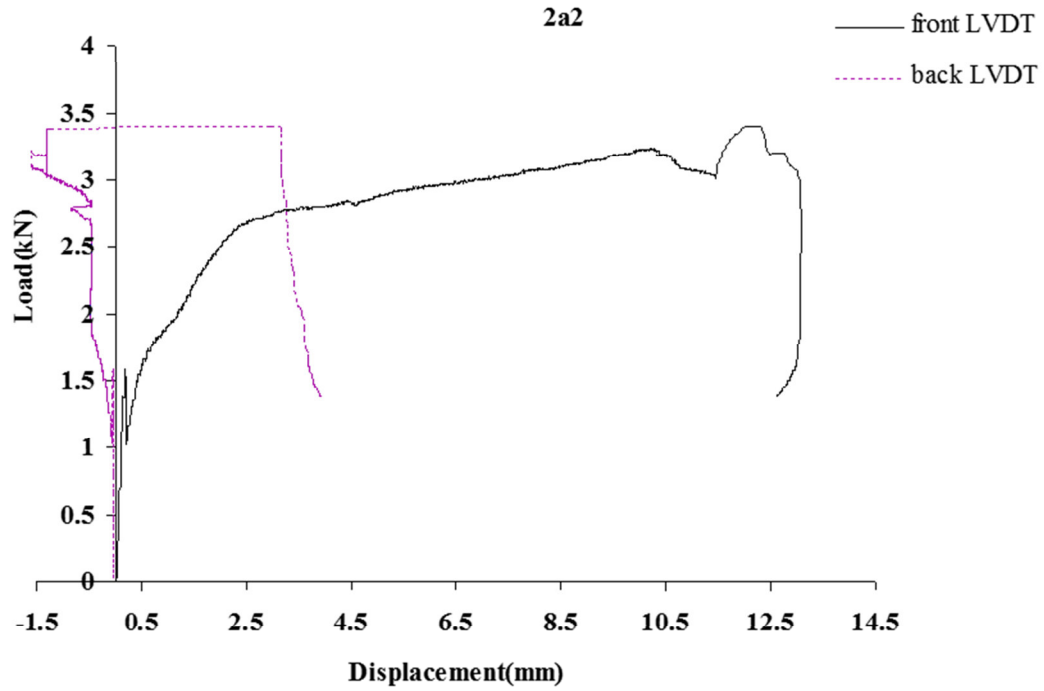
3C1

(a) Specimen 3C1

3C3

(b) Specimen 3C3

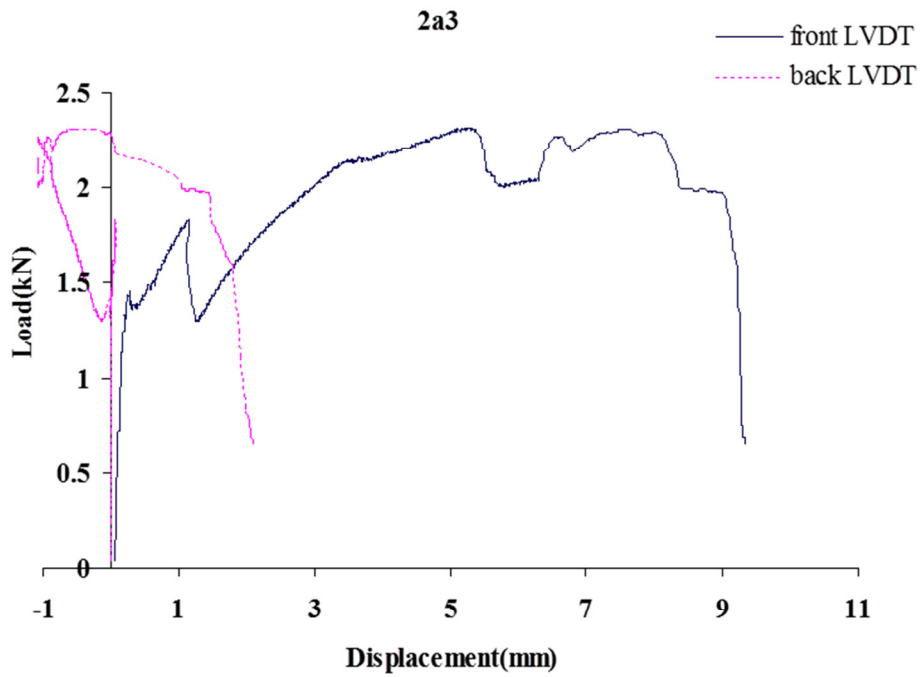Figure B.7 Load versus LVDT displacement curves for *FABcrete* with 3 layers each of SRG-45 and AR1 manually stretched

B.2 Response of *FABcrete* specimens with mechanically stretched textiles

(a) Specimen 2a2

(b) Specimen 2a3

2a4

(c) Specimen 2a4

Figure B.8 Load versus LVDT displacement curves for *FABcrete* with 2 layers of mechanically stretched SRG-45

3a1

(a) Specimen 3a1

(b) Specimen 3a3

(c) Specimen 3a8

Figure B.9 Load versus LVDT displacement curves for *FABcrete* with 3 layers of mechanically stretched SRG-45

(a) Specimen 4a1

(b) Specimen 4a2

203

(c) Specimen 4a6

(d) Specimen 4a7

4a8
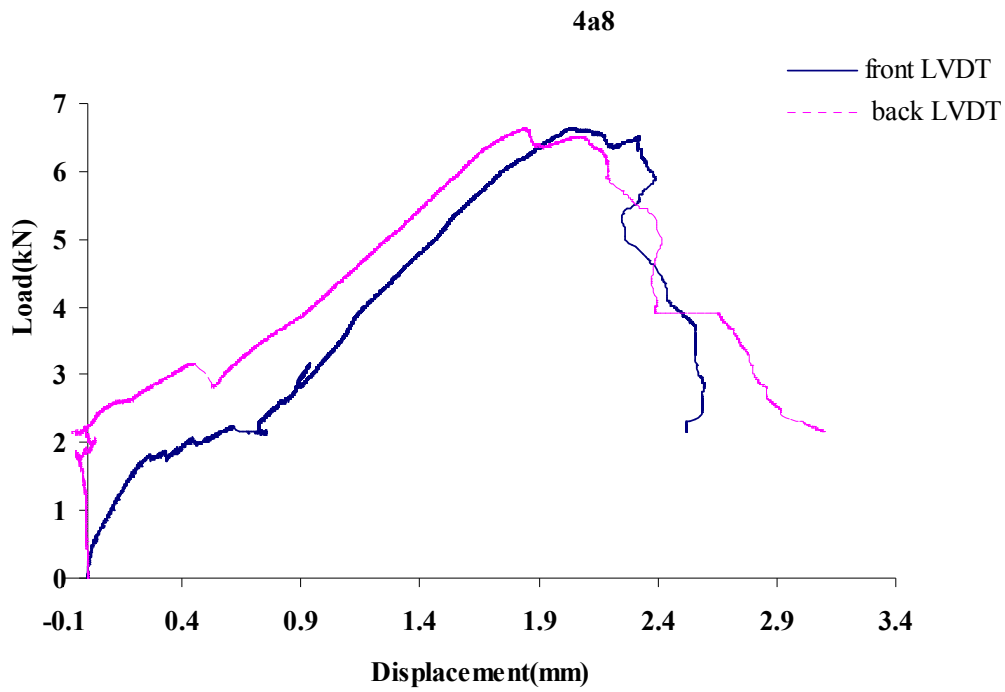
(e) Specimen 4a8

Figure B.10 Load versus LVDT displacement curves for *FABcrete* with 4 layers of mechanically stretched SRG-45

6a1

(a) Specimen 6a1

6a3

(b) Specimen 6a3

6a4

(c) Specimen 6a4

6a6
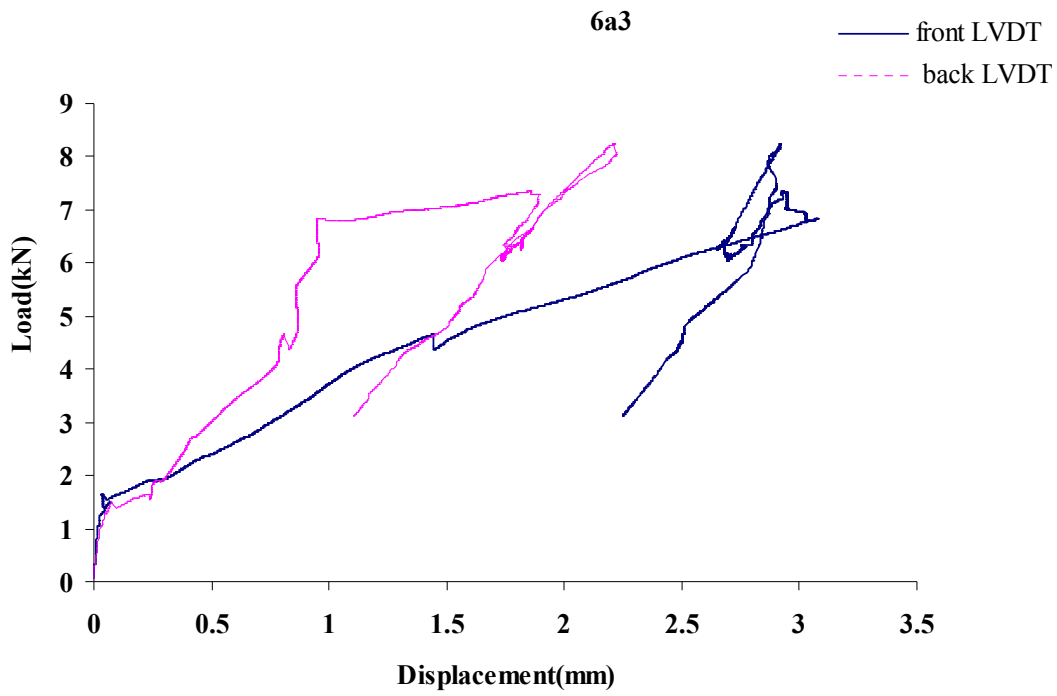
(d) Specimen 6a6

Figure B.11 Load versus LVDT displacement curves for *FABcrete* with 6 layers of mechanically stretched SRG-45

3b1
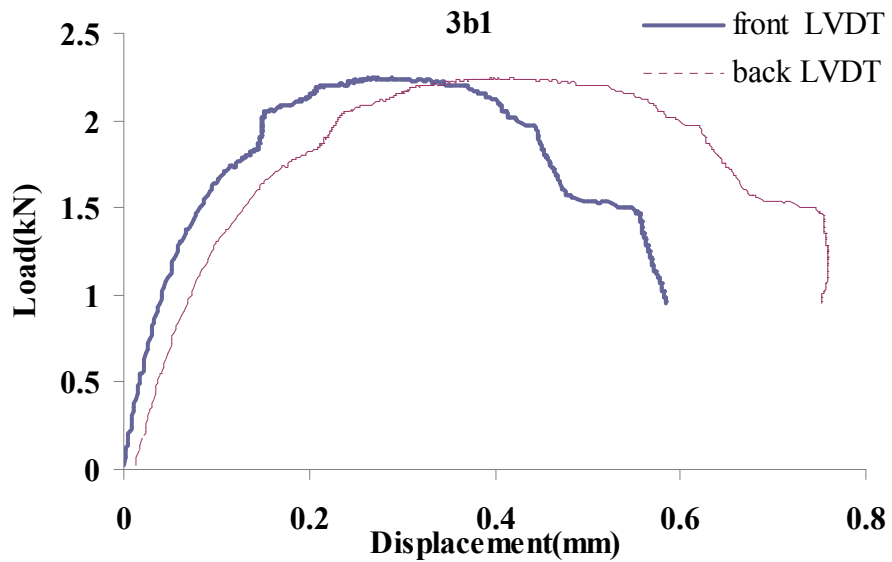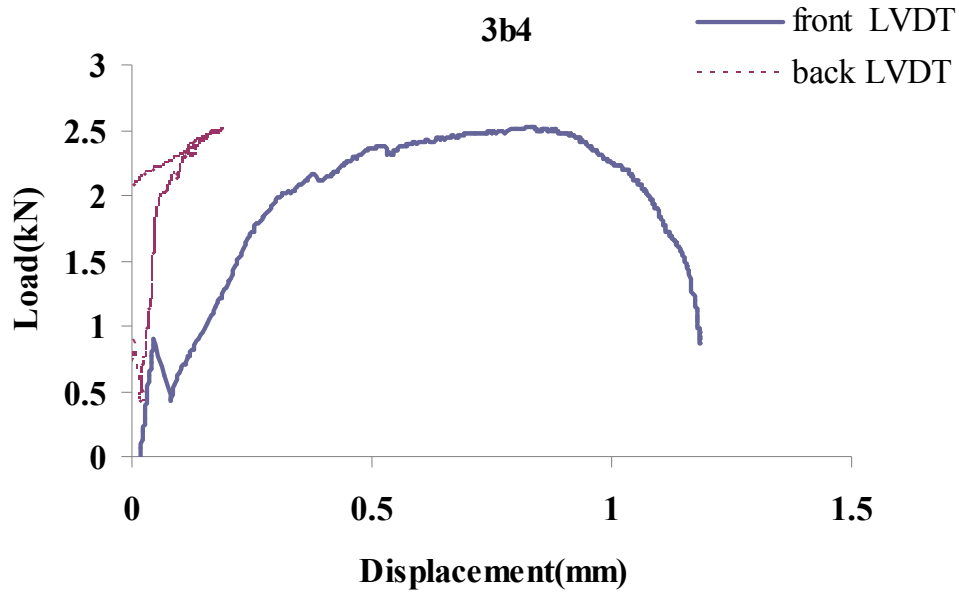
(a) Specimen 3b1
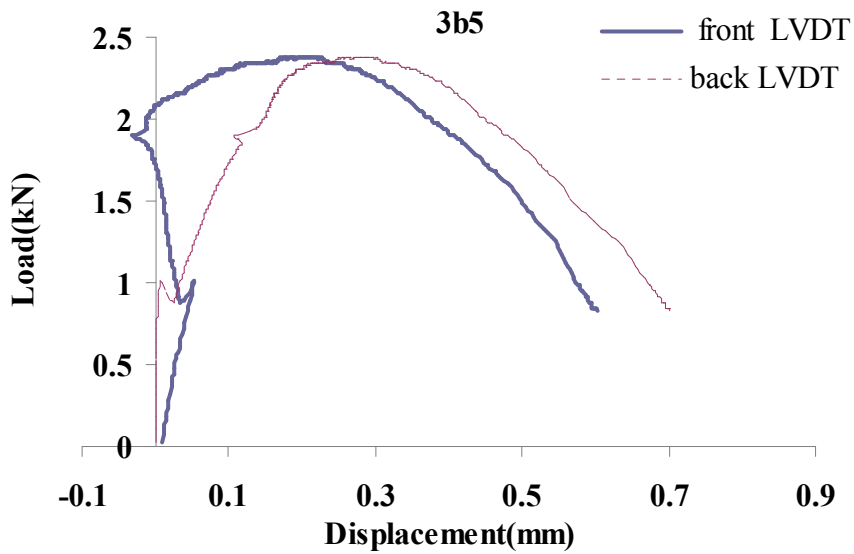
(b) Specimen 3b4

(c) Specimen 3b5

Figure B.12 Load versus LVDT displacement curves for *FABcrete* with 3 layers of mechanically stretched AR1
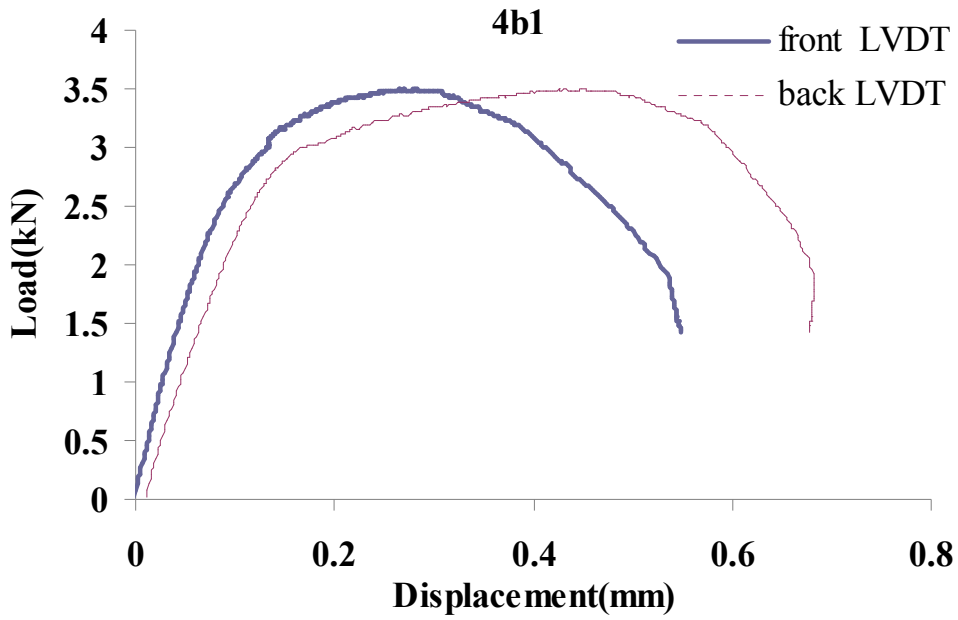
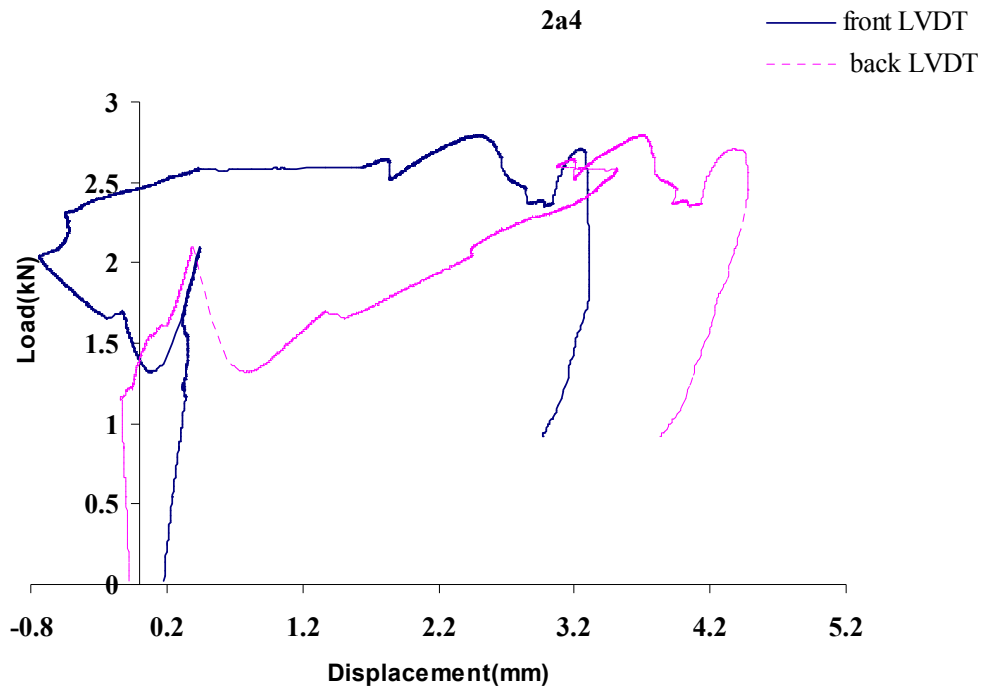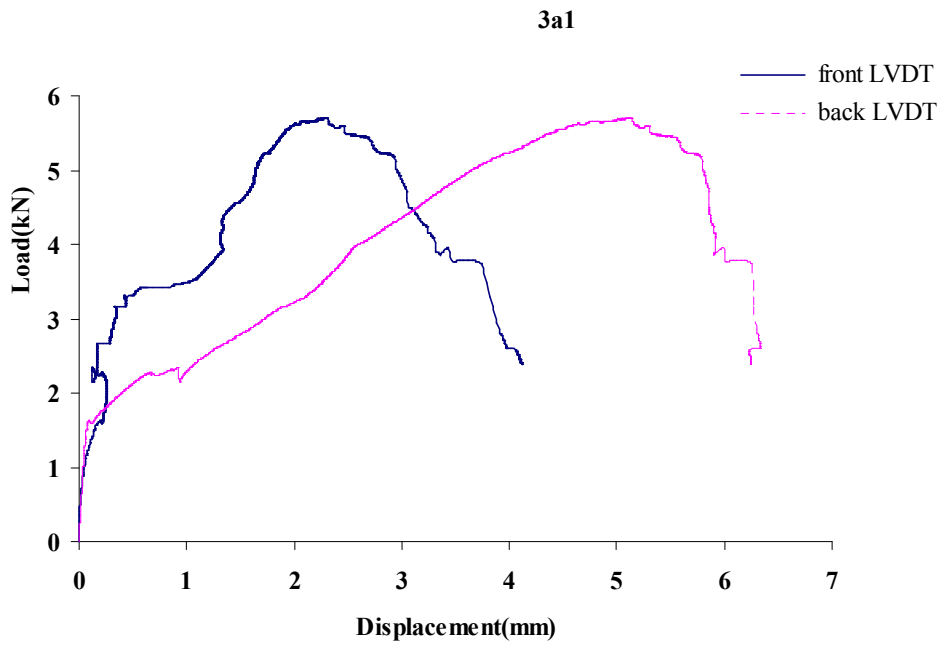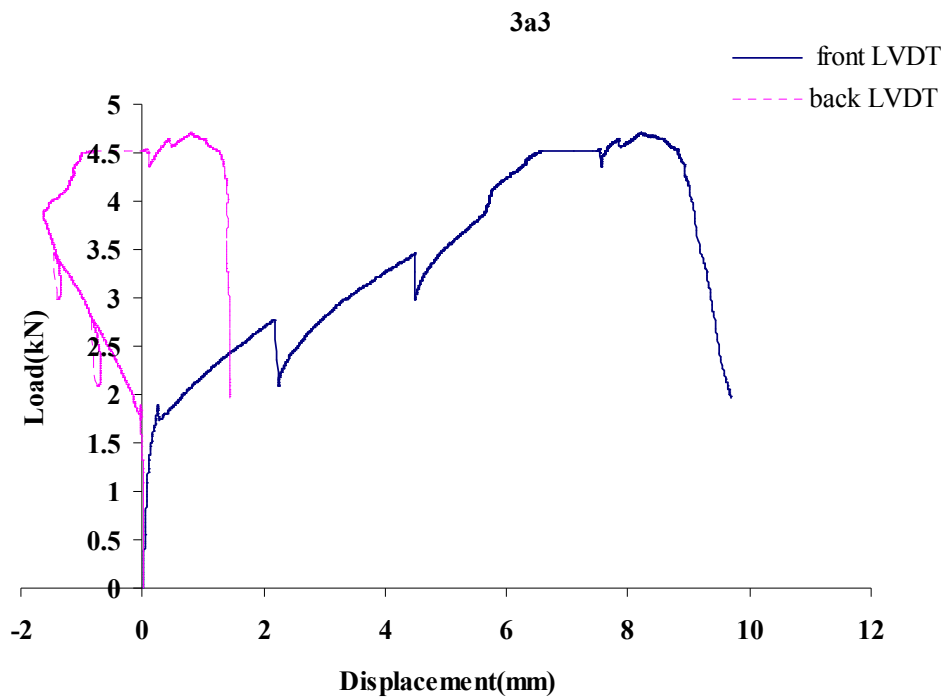(a) Specimen 4b1
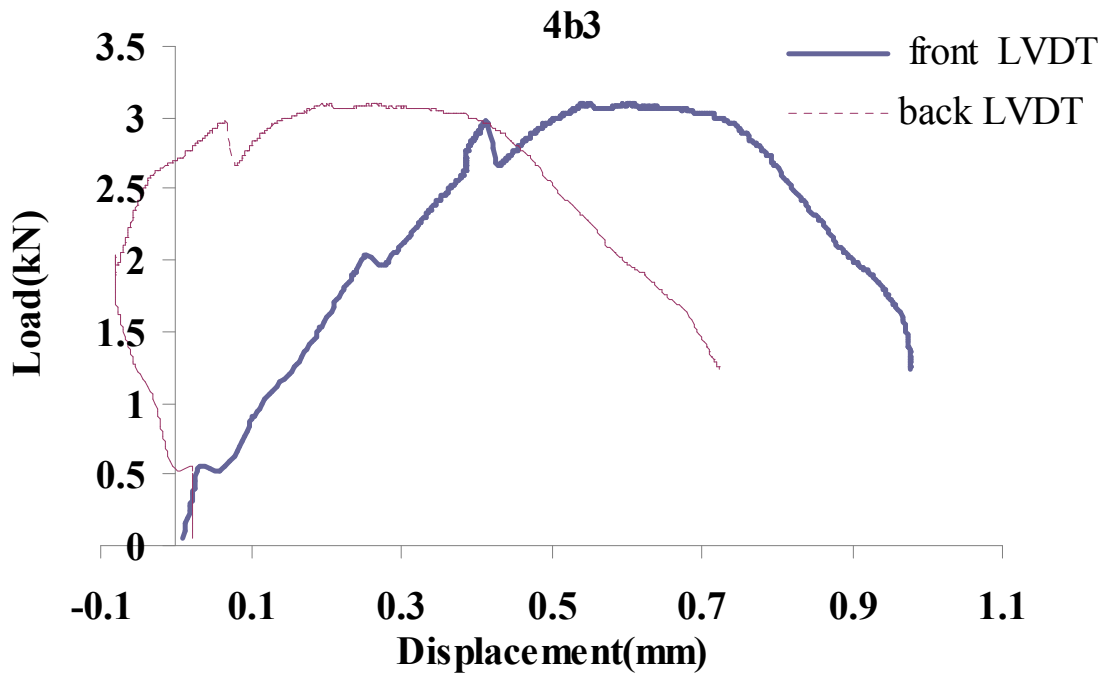
(b) Specimen 4b3
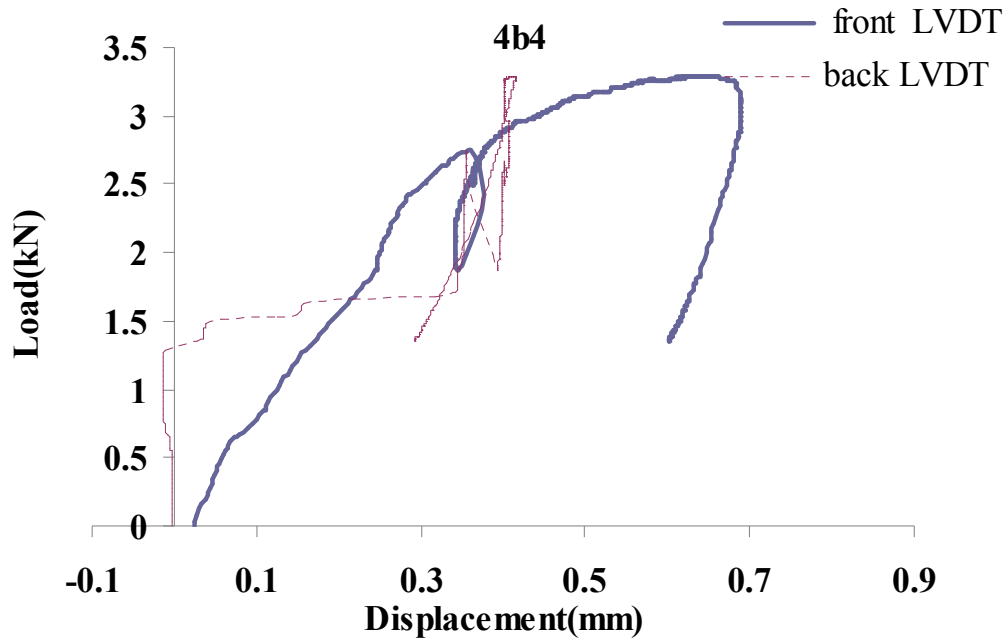
(c) Specimen 4b4

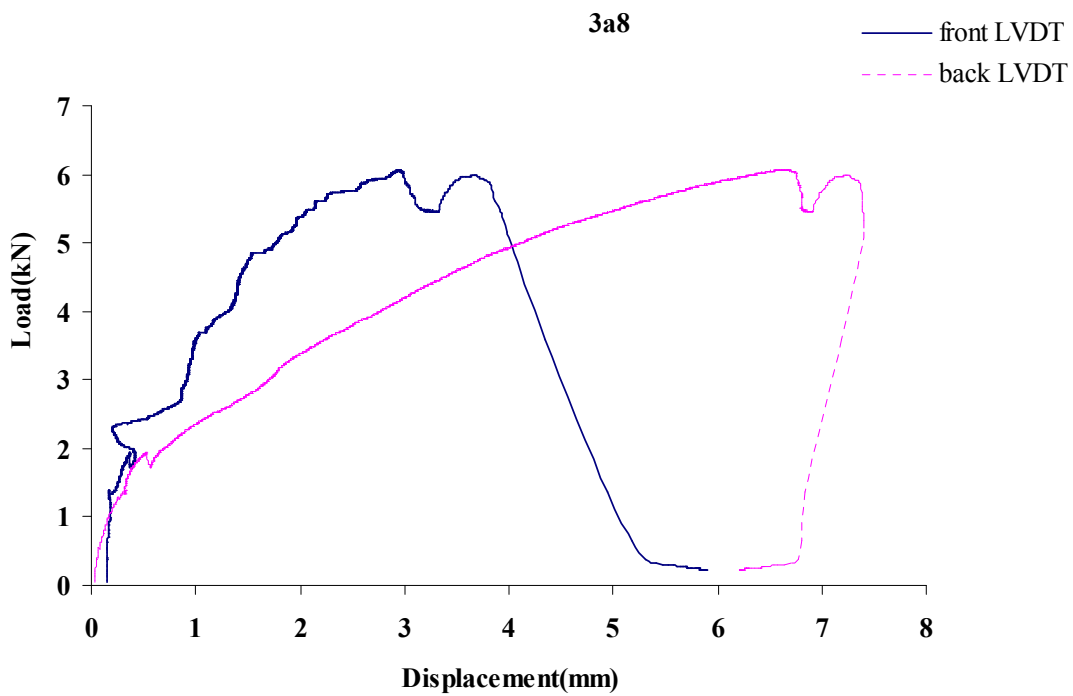Figure B.13 Load versus LVDT displacement curves for *FABcrete* with 4 layers of mechanically stretched AR1
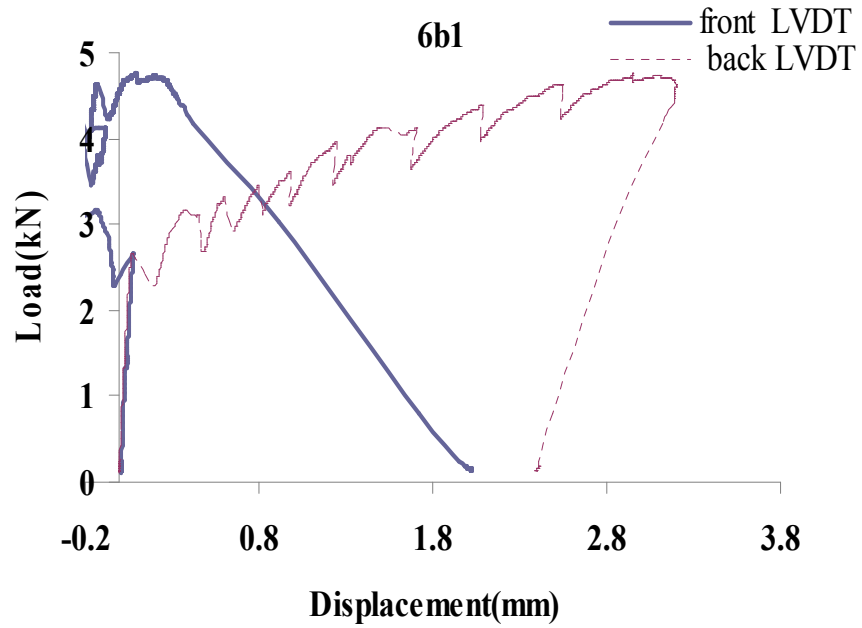
(a) Specimen 6b1
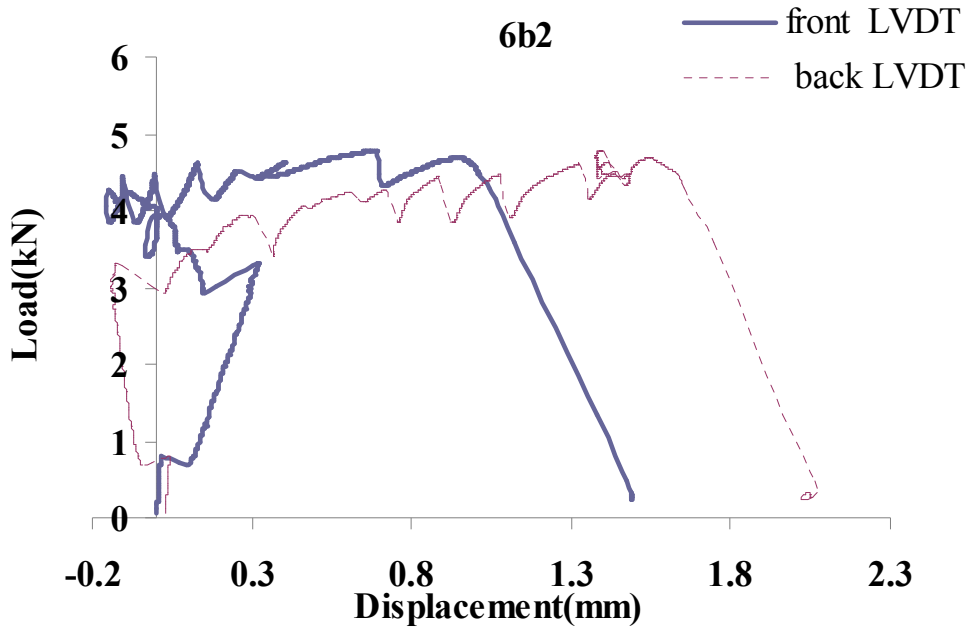
(b) Specimen 6b2
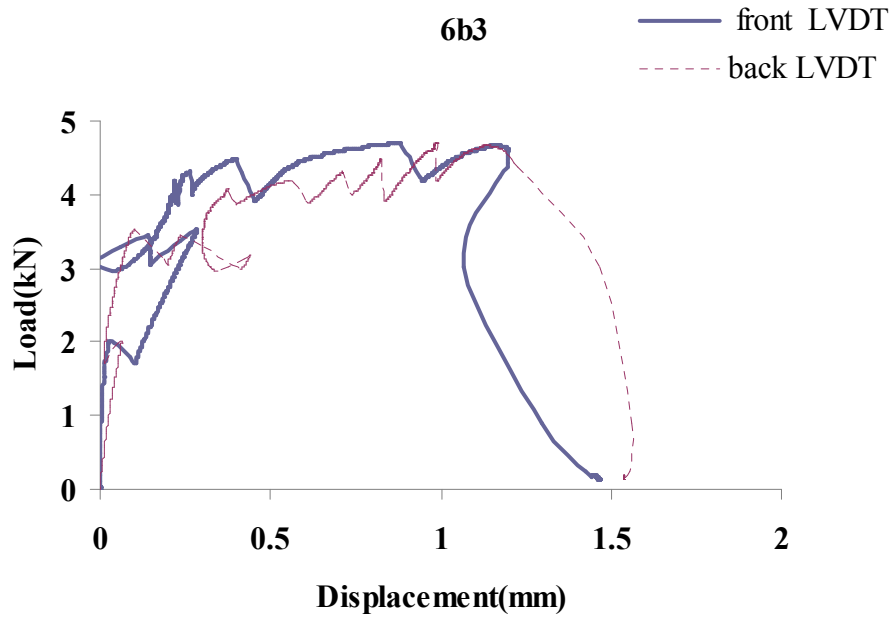
(c) Specimen 6b3
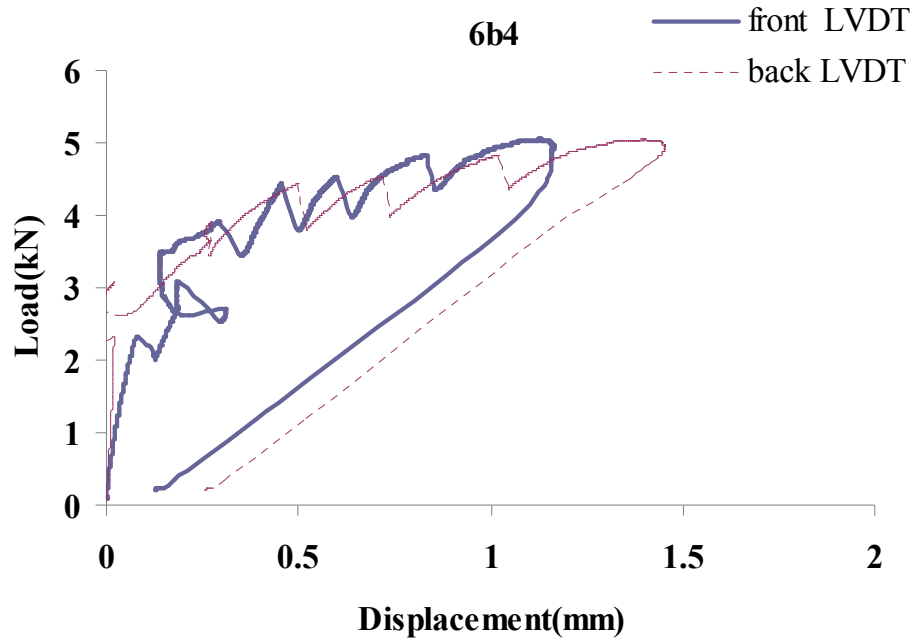
(d) Specimen 6b4
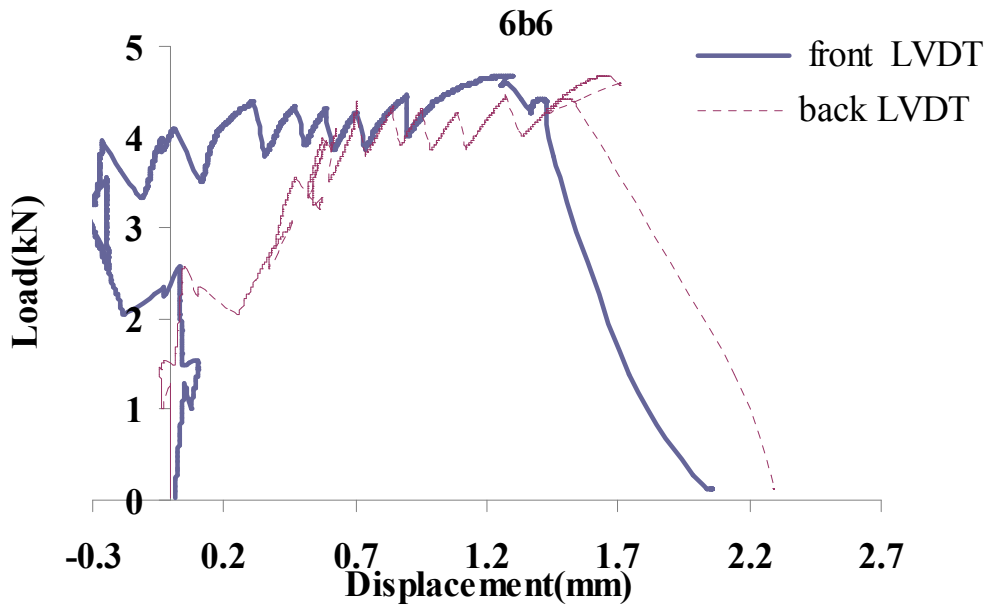
(e) Specimen 6b6

Figure B.14 Load versus LVDT displacement curves for *FABcrete* with 6ayers of mechanically stretched AR1
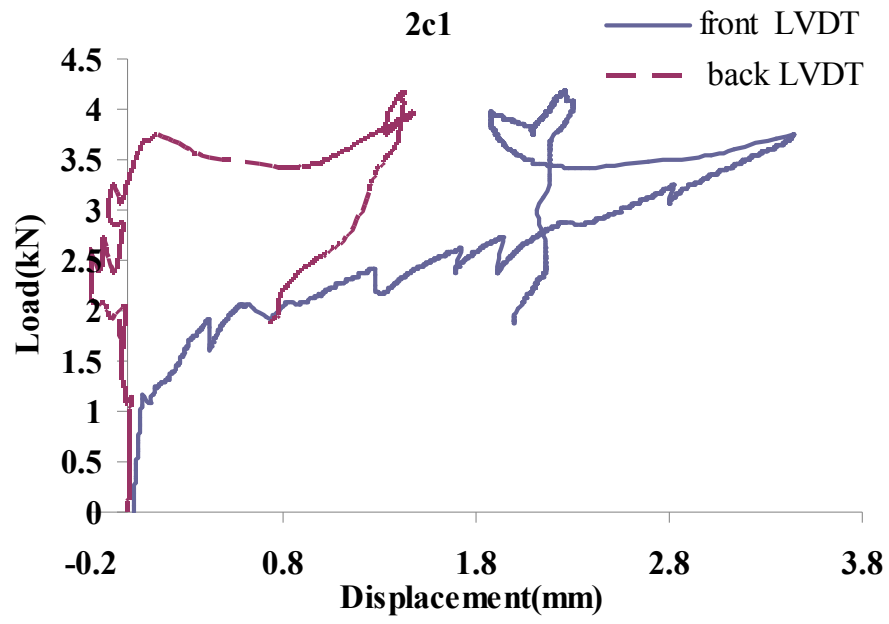
(a) Specimen 2c1
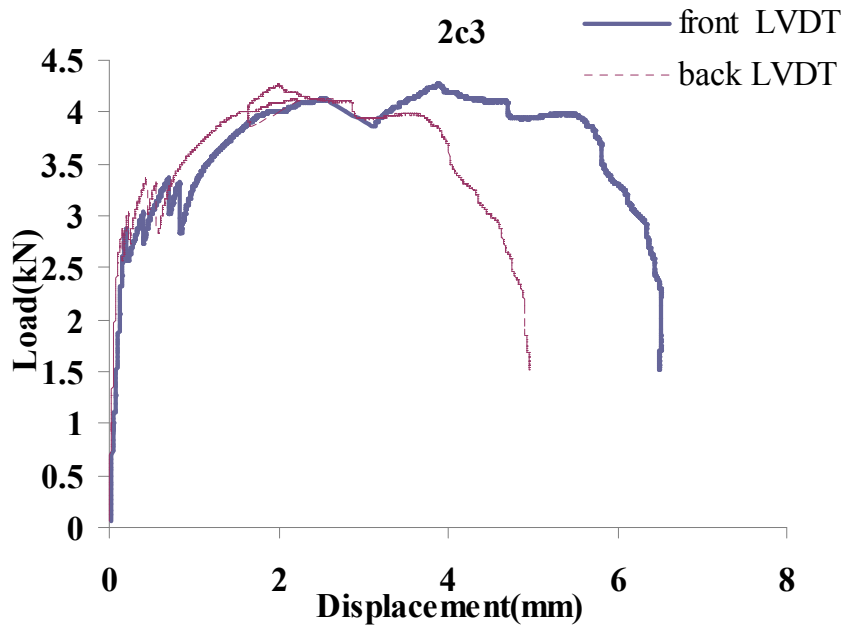
(b) Specimen 2c3
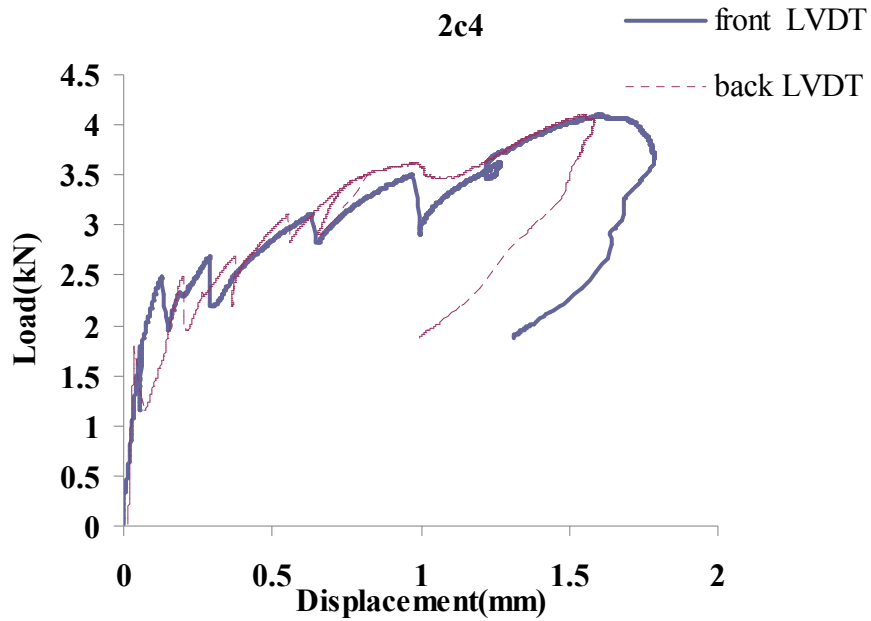
(c) Specimen 2c4
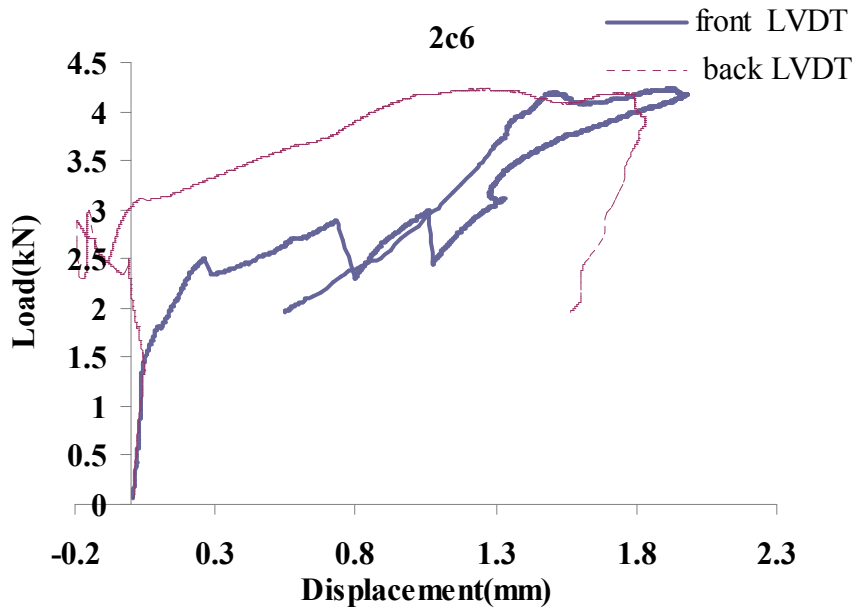
(d) Specimen 2c6

Figure B.15 Load versus LVDT displacement curves for *FABcrete* with 2 layers of mechanically stretched SRG-45 and AR1 each
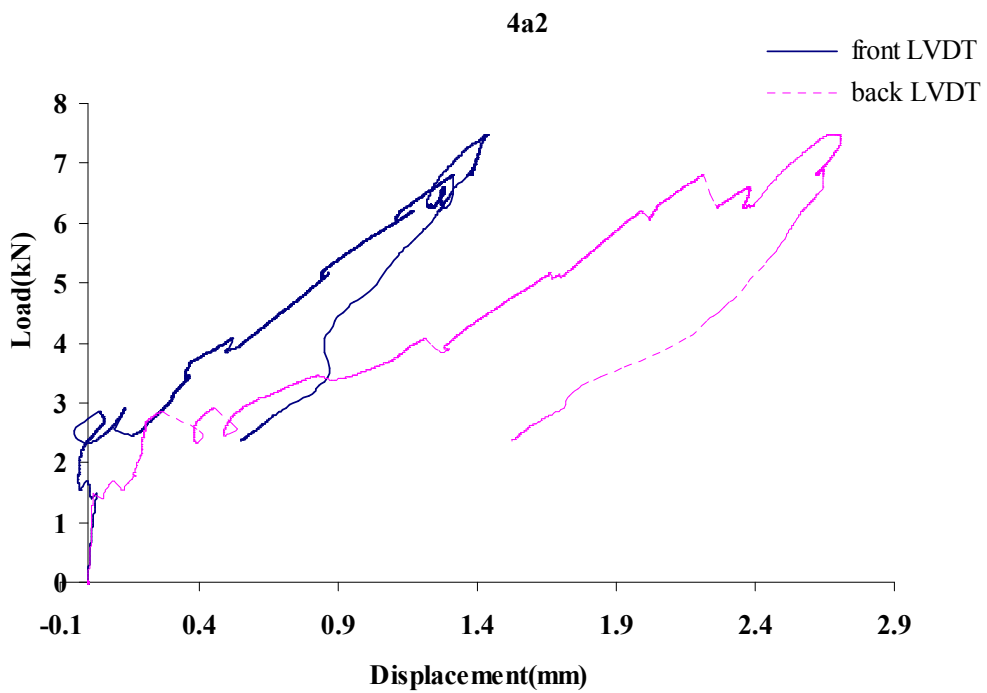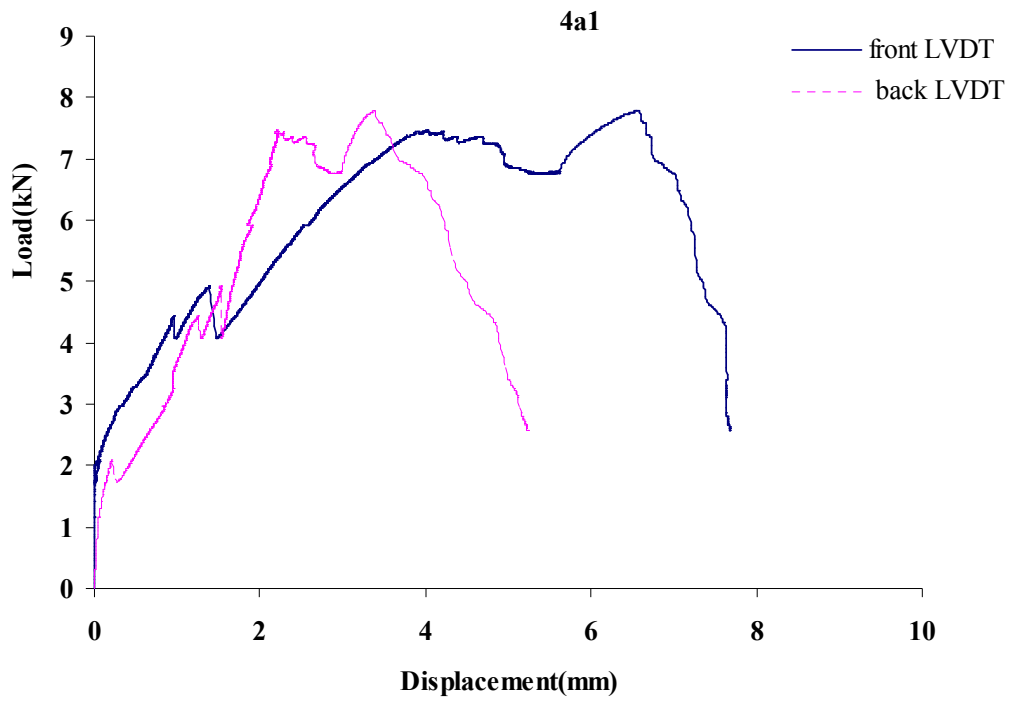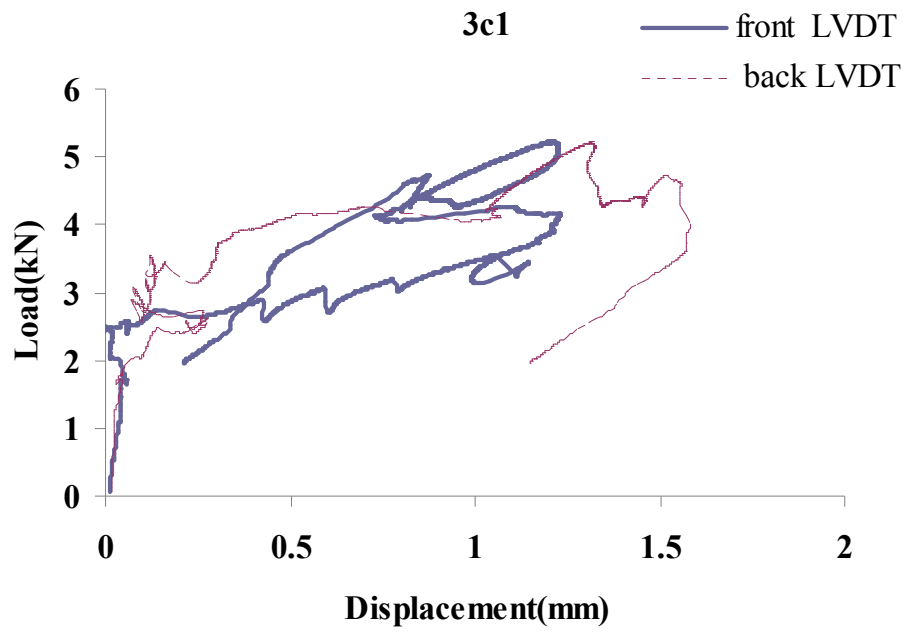
(a) Specimen 3c1
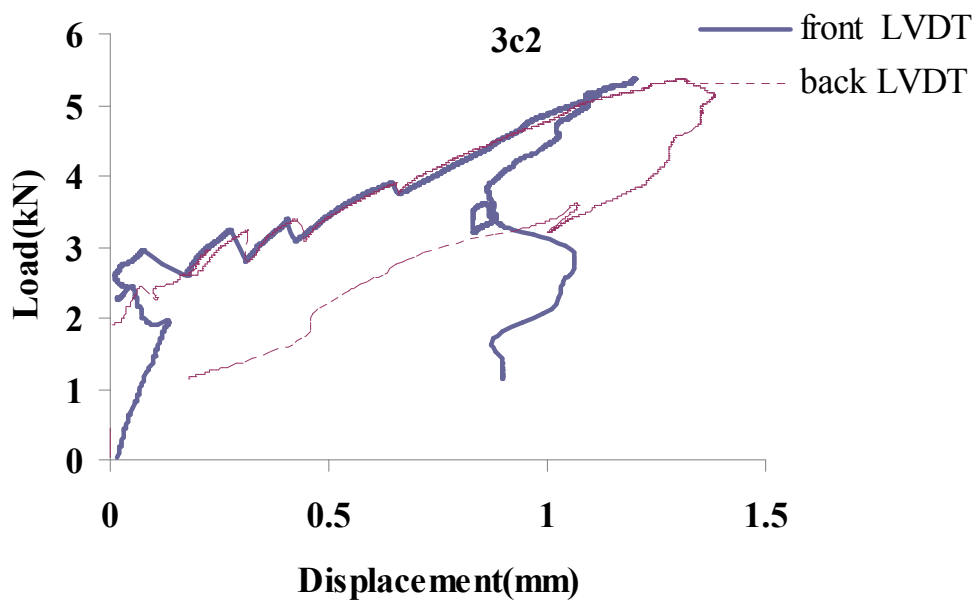
(b) Specimen 3c2
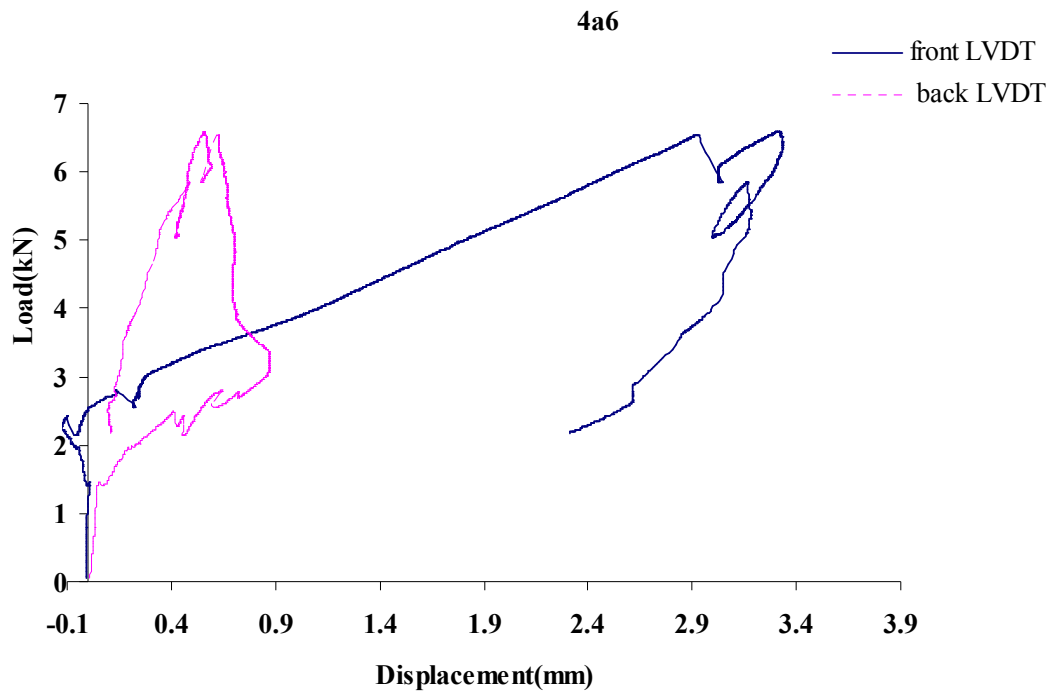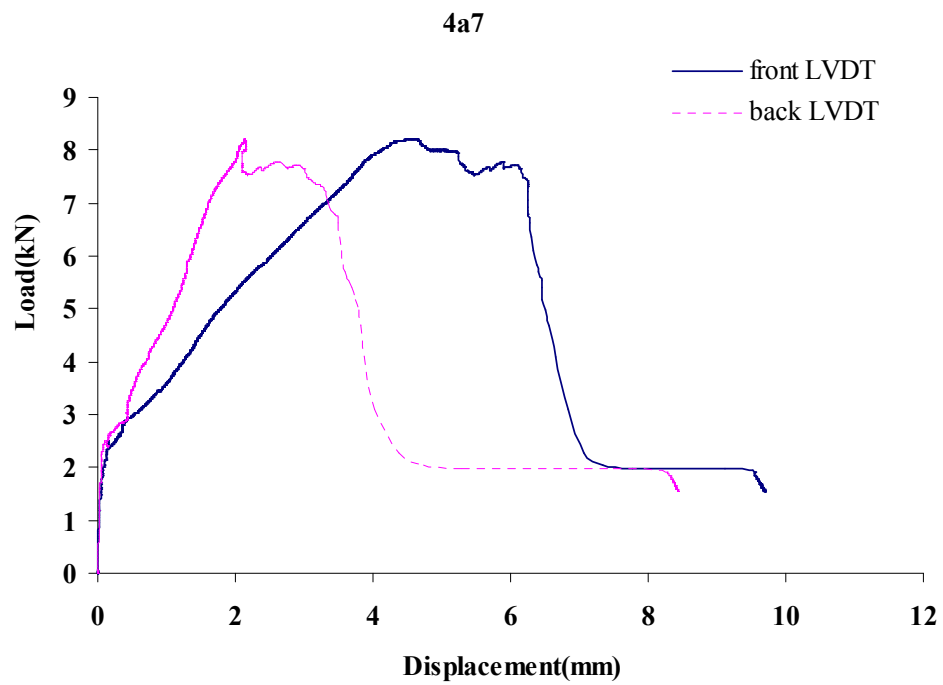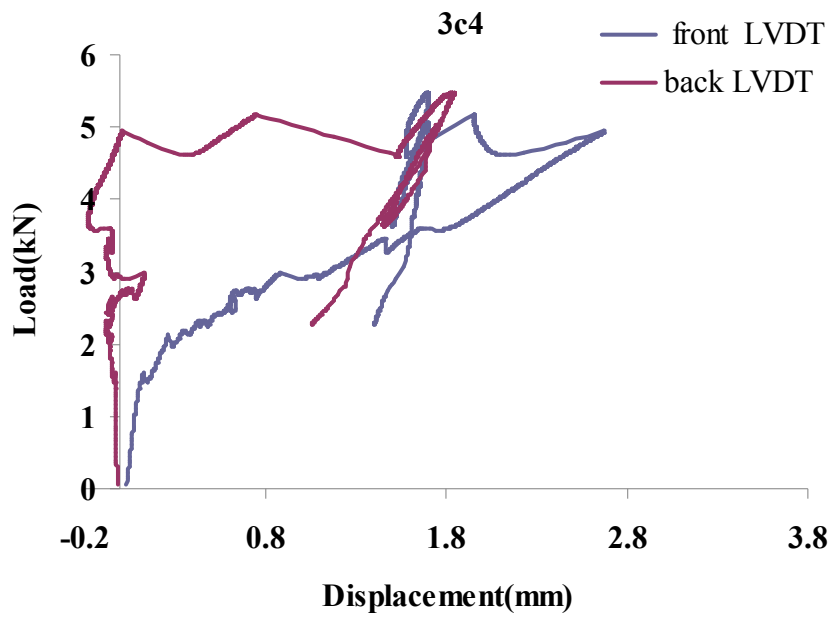
(c) Specimen 3c4
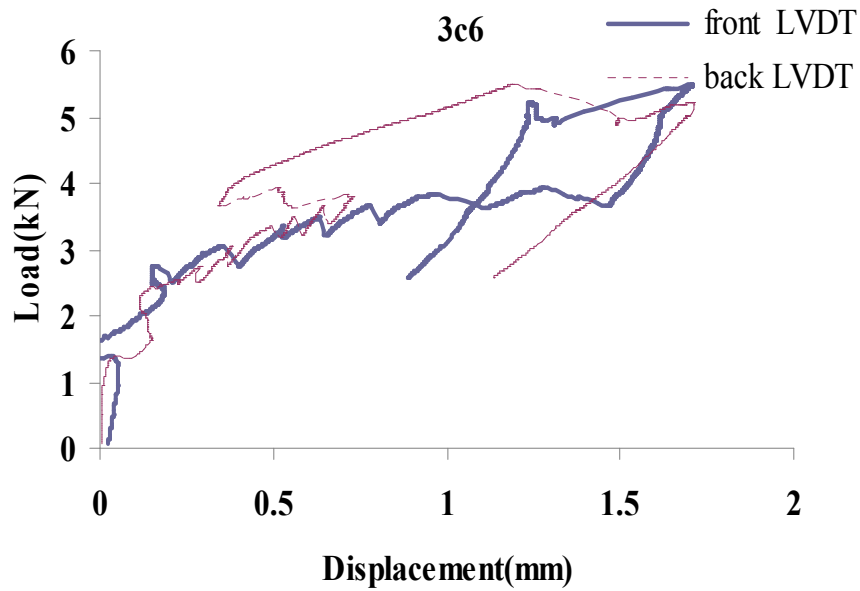
(d) Specimen 3c6

Figure B.16 Load versus LVDT displacement curves for *FABcrete* with 3 layers of mechanically stretched SRG-45 and AR1 each

B.3 Individual stress-strain curves for *FABcrete* specimens with mechanically stretched textiles
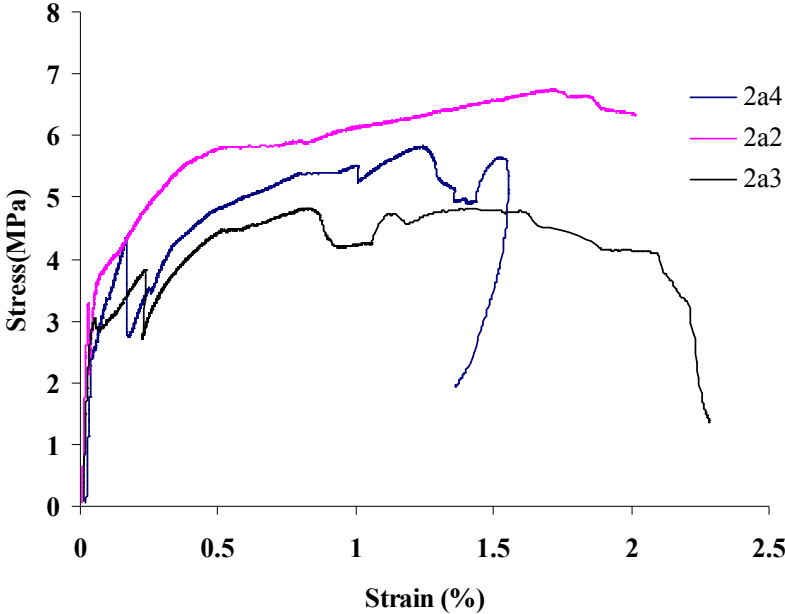
Figure B.17 Stress-strain curves for *FABcrete* with 2 layers of SRG-45
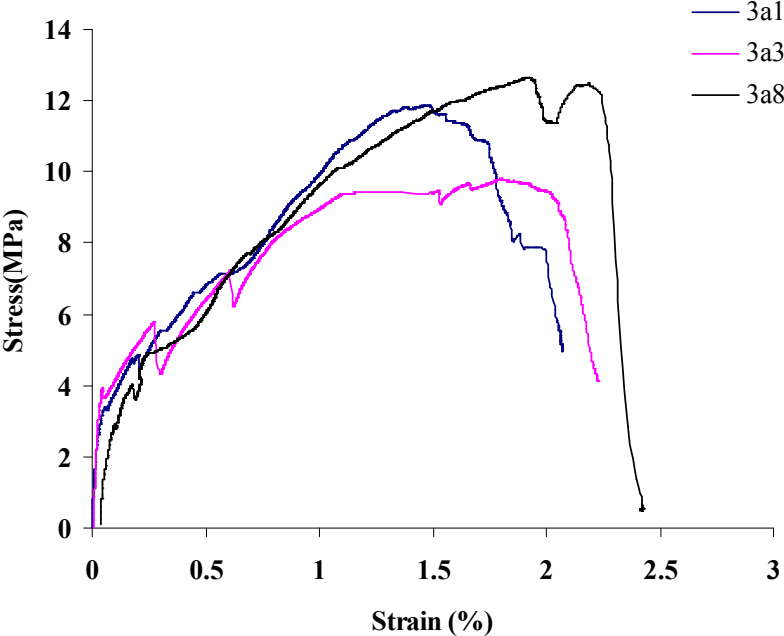
Figure B.18 Stress-strain curves for *FABcrete* with 3 layers of SRG-45
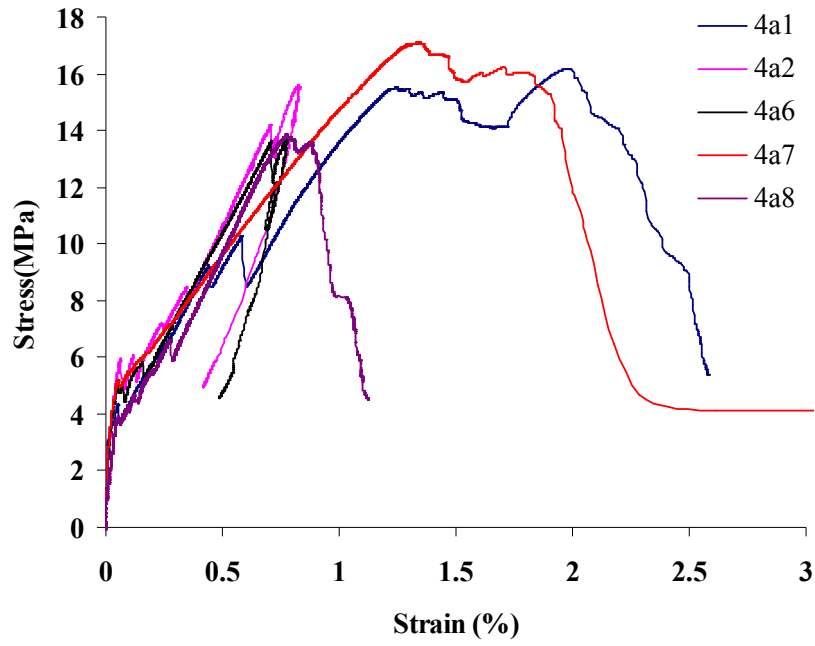
Figure B.19 Stress-strain curves for *FABcrete* with 4 layers of SRG-45
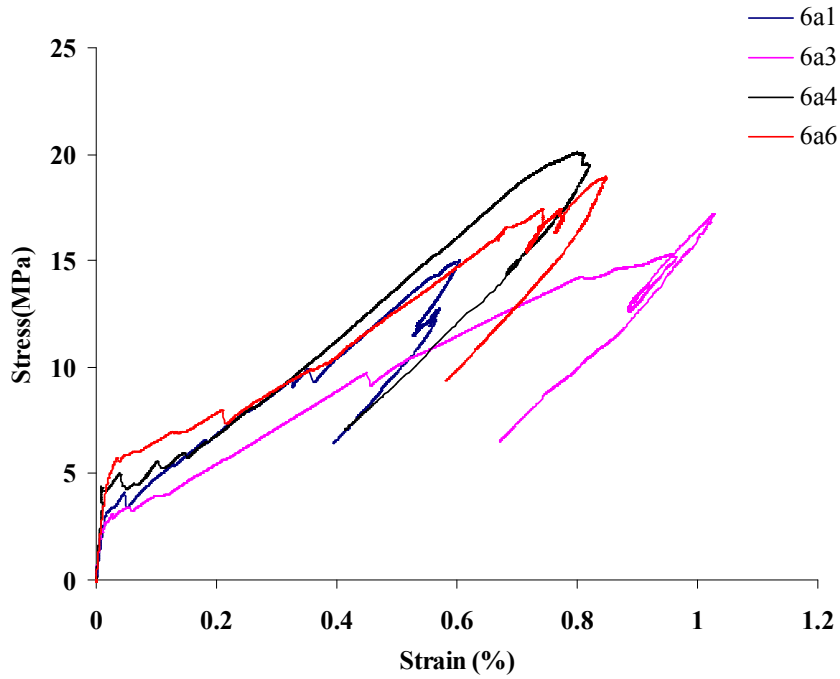
Figure B.20 Stress-strain curves for *FABcrete* with 6 layers of SRG-45

218
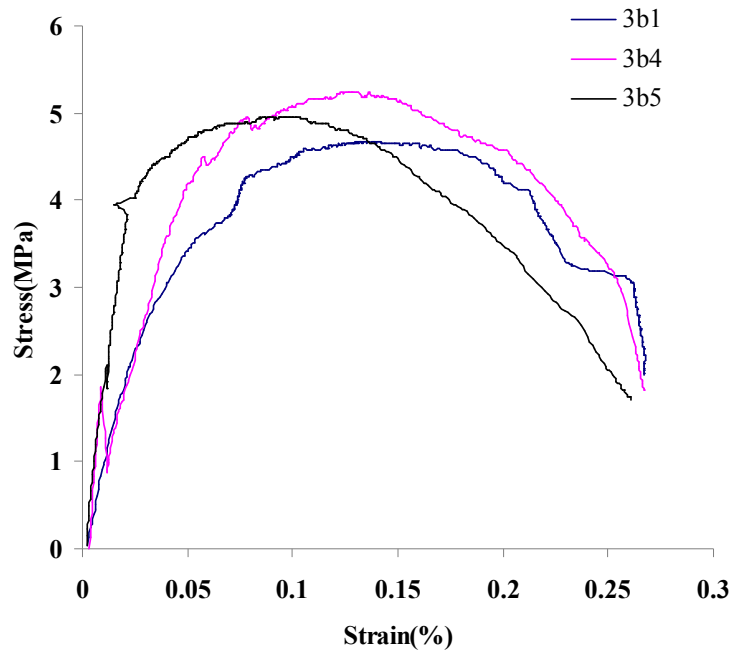
Figure B.21 Stress-strain curves for *FABcrete* with 3 layers of AR1
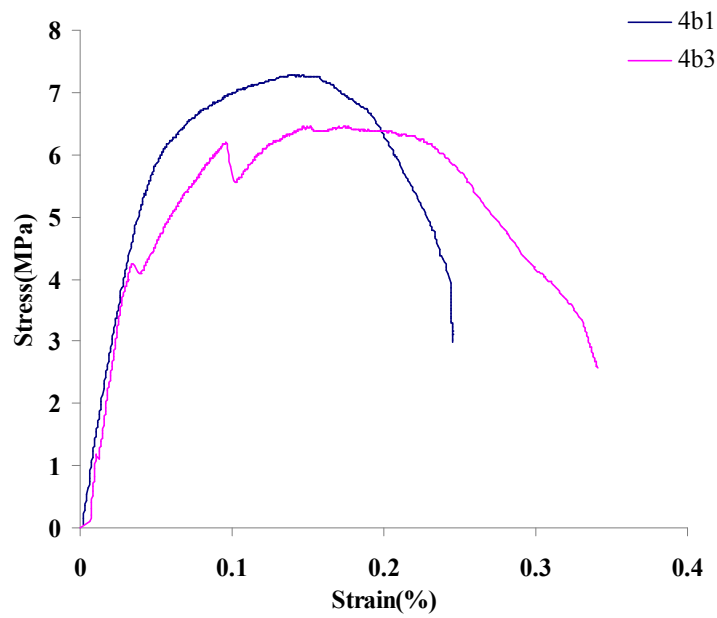
Figure B.22 Stress-strain curves for *FABcrete* with 4 layers of AR1

219
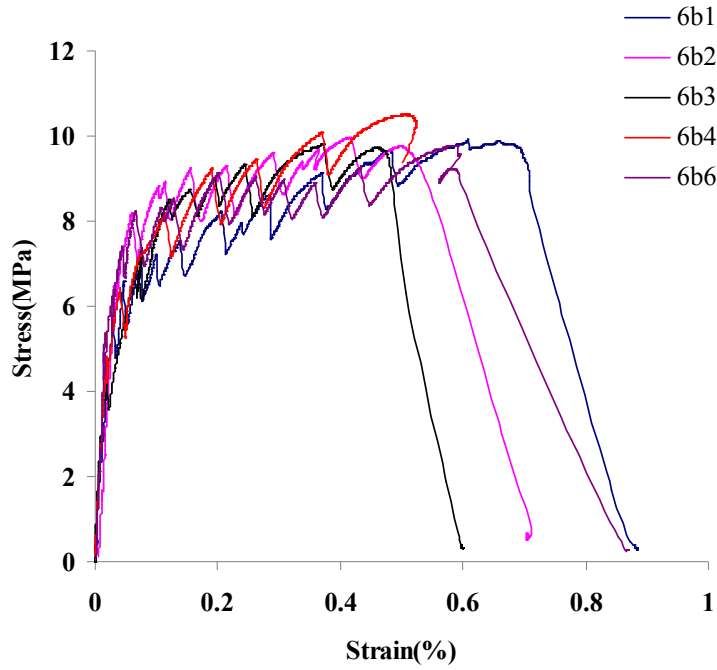
Figure B.23 Stress-strain curves for *FABcrete* with 6 layers of AR1
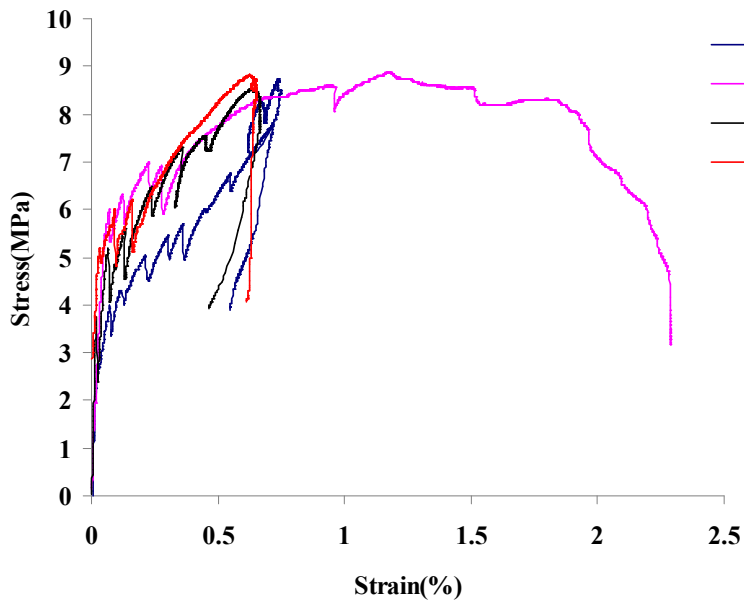
Figure B.24 Stress-strain curves for *FABcrete* with 2 layers each of SRG-45 and AR1
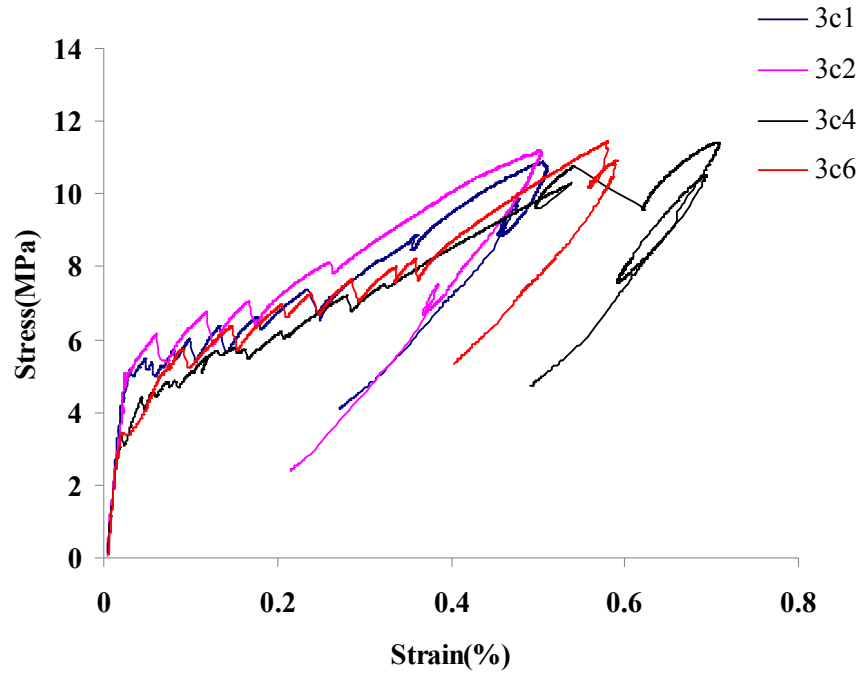
Figure B.25 Stress-strain curves for *FABcrete* with 3 layers each of SRG-45 and AR1

APPENDIX- C

C.1 WORKING PRINCIPLE OF NON-CONTACT VIDEO GAUGE

An Imetrum non-contact video gauge used in the present study for recording the movements of beam at a particular location. The data is processed thereafter to obtain the output as displacement or strain. Digital Image Correlation (DIC) principles, can provide an accuracy up to 1/500th of a pixel. It also operates in real time, processing up to 100 data points at 15Hz. The video system uses pattern recognition technology, which is capable of detecting minute changes in displacement. The pattern recognition blocks are used to identify the required measurement points, between which the changes in distance are measured. It is possible to use up to 100 blocks for real time measurements. The real time graph preview facility also allows the tracking of the displacements as the measurements are carried out. As the system uses video technology, it is possible use the recorded videos to rerun the tests offline. The field and the magnification can be increased or decreased by changing the lens on the camera. Also, it is possible to take the inputs from eight different cameras simultaneously (with all measurements synchronized, time stamped and saved to the same text limited file). Hence, it is possible to observe many individual areas of the specimen with the same system. The voltage input/output module can be used to feed load or displacement outputs from the test machine into the video gauge. Further, it is also possible to capture the strain measurements made by the video gauge by feeding it via the voltage outputs to existing data-logging equipment or into test machine for feedback control.

The data captured can also be processed off-line while using video gauge. Further, the ability to operate in real time in terms of minimal specimen preparation, simplicity, non-invasive measurements, scale insensitivity and immunity are also added advantages for the use of video-gauge measurements. Most importantly, the specimen undergoing the test will not be disturbed. The archived data from tests carried out in the past but previously unused for measurement purposes can be examined by operating the digital images.

D.1 Flowchart for the determination of load and deflection behaviour of *FABcrete* strengthened RC beams using ACI method

Specimen details (h,b,L,d)

Input

Concrete details $(f_c', E_c, \varepsilon_{cmax})$

Reinforcement details $(A_s, f_y, E_y, \varepsilon_{sy})$

Textile details $(N, A_f, E_f, f_{fe}, \varepsilon_{fe})$

Gross moment of inertia $\quad I_g = \dfrac{bh^3}{12}$

Neutral axis depth of cracked section

$$C_{cr} = \frac{0.5bh^2 + ((n-1)A_sd)}{(bh + (n-1)A_s)}$$

Cracked moment of inertia

$$I_{cr} = \frac{bh^3}{12} + (n-1)A_s(C_{cr} - d)^2$$

$$S = \frac{I_{cr}}{(h - C_{cr})}$$

$$M_{cr} = 0.62\sqrt{f_c}\, S$$

$$d_{cr} = \frac{23M_{cr}L^2}{216\, E_c\, I_{cr}}$$

$$P_{cr} = \frac{6\, M_{cr}}{L}$$

Details of load & deflection at cracking load

A

A

Assume new NA position
$$h_{new} = C_y * h$$

$$\varepsilon_{sy} = \frac{f_y}{E_s}$$

$$\varepsilon_{con} = \frac{h_{new}\, \varepsilon_{sy}}{(d - h_{new})}$$

$$\varepsilon_{fib} = \frac{(d - h_{new})\varepsilon_{sy}}{(h - h_{new})}$$

$$T_s = A_s . f_y$$

$$T_f = N_{lay}\, A_f b E_f \varepsilon_{fib}$$

$$C = \alpha_1 f_c' \beta_1 h_{new} b$$

Check $C = T_s + T_f$

$$M_s = A_s f_y \left(d - \frac{\beta_1 h_{new}}{2} \right)$$

No

$$M_f = N_{lay} A_f b E_f\ \varepsilon_{fib} \left(h - \frac{\beta_1 h_{new}}{2} \right)$$

$$M_y = M_s + M_f$$

$$d_y = \frac{23 L^2 \varepsilon_{sy}}{216\,(d - h_{new})}$$

$$P_y = \frac{6 M_y}{L}$$

B

Details of load
and deflection at
yield load

226

$$\text{B}$$

Assume $h_{new} = Cu \times h$

$$\varepsilon_{con} = \frac{h_{newu} \cdot \varepsilon_{fe}}{h - h_{new}}$$

$$\varepsilon_{nt} = \frac{(d - h_{newu}) \, \varepsilon_{fe}}{(h - h_{newu})}$$

$$ß_1 = \frac{4\varepsilon_{cmax} - \varepsilon_{con}}{6\varepsilon_{cmax} - 2\varepsilon_{con}}$$

$$\alpha 1 = \left[3\varepsilon_{cmax} \, \varepsilon_{con} - \left(\frac{\varepsilon_{con}^2}{3\beta_1 \varepsilon_{cmax}^2} \right) \right]$$

$$T_s = A_s f_y$$

$$T_f = N_{lay} \, A_f b f_{fe}$$

$$C = \alpha_1 f_c' \beta_1 h_{new} b$$

Check $C = T_s + T_f$

$$M_s = A_s f_y \left(\frac{d - \beta_1 h_{new}}{2} \right)$$

$$M_f = T_f \left(h - \frac{\beta_1 h_{new}}{2} \right)$$

$$M_u = \emptyset_m (M_s + M_f)$$

$$d_u = \frac{23L^2 \, \varepsilon_{fe}}{216(d - h_{new})}$$

$$P_u = \frac{6M_u}{L}$$

Details of load and deflection at ultimate

227

APPENDIX-E

E.1 DEVELOPMENT OF FINITE ELEMENT MODELLING METHODOLOGY

The robustness of numerical model is very much dependent on the geometrical modeling, material modeling and the interactions of various constituent ingredients. A methodology is developed to simulate the response behaviour of *FABcrete* strengthened beam by integrating various material models and implemented in a general purpose finite element software, ABAQUS.

E.1.1 Material Modelling

The constitutive relationships for material behaviour of steel reinforcing bars, concrete, cementitious matrix of *FABcrete* and textile are considered in the present study. The modelling strategies adopted for each of these materials are elaborated in the following sections.

E.1.1.1 Concrete

A possible way of defining the nonlinear behaviour of concrete under compression is through the stress versus strain behavior till crushing. Hence, a model proposed by Attard and Setunge (1996), which is applicable for concretes with compressive strength in the range of 20 to 130 MPa, is used. In this model, the parameters used to establish the stress-strain behaviour are the initial Young's Modulus (E_c), the peak compressive strength (f_{co}) and the corresponding strain (ε_{co}), and the compressive stress (f_{ci}) and compressive strain (ε_{ci}) on the descending branch of the curve. Figure E.1 shows the typical representation of stress versus strain behaviour of concrete.
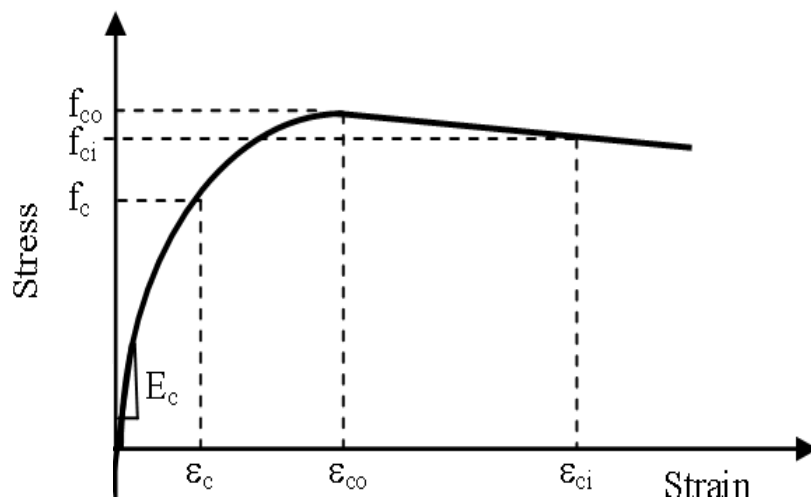
Figure E.1 Stress-strain for concrete

Under compression, the stress of concrete (σ_c) is related to strain by the Eqn. (E.1).

$$\frac{\sigma_c}{f_{co}} = \frac{A\left(\frac{\varepsilon_c}{\varepsilon_{co}}\right) + B\left(\frac{\varepsilon_c}{\varepsilon_{co}}\right)^2}{1 + (A-2)\left(\frac{\varepsilon_c}{\varepsilon_{co}}\right) + (B+1)\left(\frac{\varepsilon_c}{\varepsilon_{co}}\right)^2}$$

(E.1)

where A and B are coefficients dependent on the concrete grade and the curve is generated by using two sets of coefficients for A and B, one for the ascending branch and another for the descending branch. For the ascending branch where $\varepsilon_c \leq \varepsilon_{co}$, the coefficients A and B are given by Eqns. (E.2) and (E.3).

$$A = \frac{E_c \varepsilon_{co}}{f_{co}}$$

(E.2)

$$B = \frac{(A-1)^2}{0.55} - 1$$

(E.3)

For the descending branch, where $\varepsilon_c > \varepsilon_{co}$,

$$A = \frac{f_{ci}\left(\varepsilon_{ci} - \varepsilon_{co}\right)^2}{\varepsilon_{co}\varepsilon_{ci}\left(f_{co} - f_{ci}\right)}$$

(E.4)

$$B = 0$$

(E.5)

The parameters E_c, ε_{co}, f_{ci} and ε_{ci} are theoretically related to the value f_{co} by

$$E_c = 4370\left(f_{co}\right)^{0.52}$$

(E.6)

$$\varepsilon_{co} = 4.11\left(f_{co}\right)^{0.75}/E_c$$

(E.7)

$$f_{ci}/f_{co} = 1.41 - 0.17\ln\left(f_{co}\right)$$

(E.8)

$$\varepsilon_{ci}/\varepsilon_{co} = 2.50 - 0.30\ln\left(f_{co}\right)$$

(E.9)

E.1.1.2 Steel

To model the steel reinforcing bar, an elasto-plastic model is considered as shown in Figure E.2. To establish the behaviour, the inputs required are Young's modulus (E_s), Poisson's ratio of steel and yield strength (σ_y).
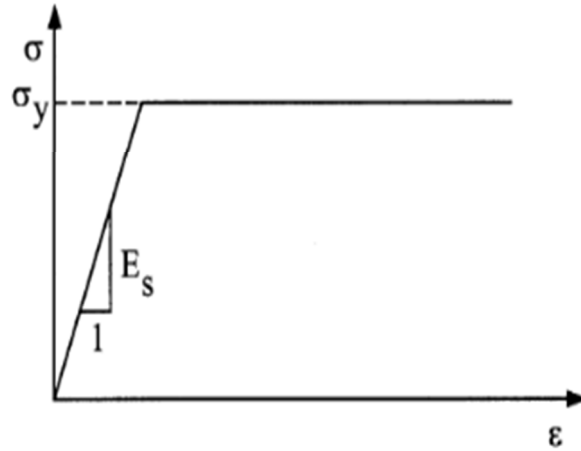
Figure E.2 Elastic- plastic model for steel reinforcing bar

E.1.1.3 Modelling of *FABcrete*

For the compressive behaviour of *FABcrete*, the Attard and Setunge (1996) model has been adopted, where the tensile behaviour of *FABcrete* is governed by multiple cracking and consequent interaction of textile with matrix, resulting in the tension stiffening effect. In the present study, a smeared model is used to represent the macro-cracking. The post failure behaviour for direct straining across the cracks is modelled, which allows to define the strain hardening for cracked concrete in *FABcrete*. During the strain hardening stage, the material is assumed to undergo damage, represented by the loss of stiffness. During the post-cracking stage, the cracked reinforced concrete can still transfer shear forces through friction or shear retention. To represent the diminishing nature of shear stiffness as the concrete cracks, a reduction in the shear modulus as a function of the opening strains across the crack has been specified. The shear retention model assumes that the shear stiffness of open cracks reduce linearly to zero as the crack opens. The shear modulus is considered as ρG for the shearing of cracks, where G is the elastic shear modulus of the uncracked concrete and ρ is a factor as given in Eqn. (E.10).

$$\rho = 1 - \frac{\varepsilon}{\varepsilon^{max}} \quad \text{for } \varepsilon < \varepsilon^{max}, \qquad \rho = 0 \quad \text{for } \varepsilon \geq \varepsilon^{max} \tag{E.10}$$

Where 'ε' is the direct strain across the crack and ε^{max} is a user-specified value obtained from the experimental characterization of *FABcrete*. A crack detection surface is the failure surface which is used to determine the cracking. The shape of failure surface is as shown in Figure E, and it mainly depends on four failure ratios: the ultimate biaxial compressive stress to the ultimate uniaxial compressive stress; the uniaxial tensile stress at failure to the ultimate uniaxial compressive stress; the ratio of plastic strain at ultimate stress in biaxial compression to that in uniaxial compression; and the tensile principal stress at cracking in-plane stress to the tensile cracking stress under uniaxial tensionwhen the other principal stress is at the ultimate compressive value.
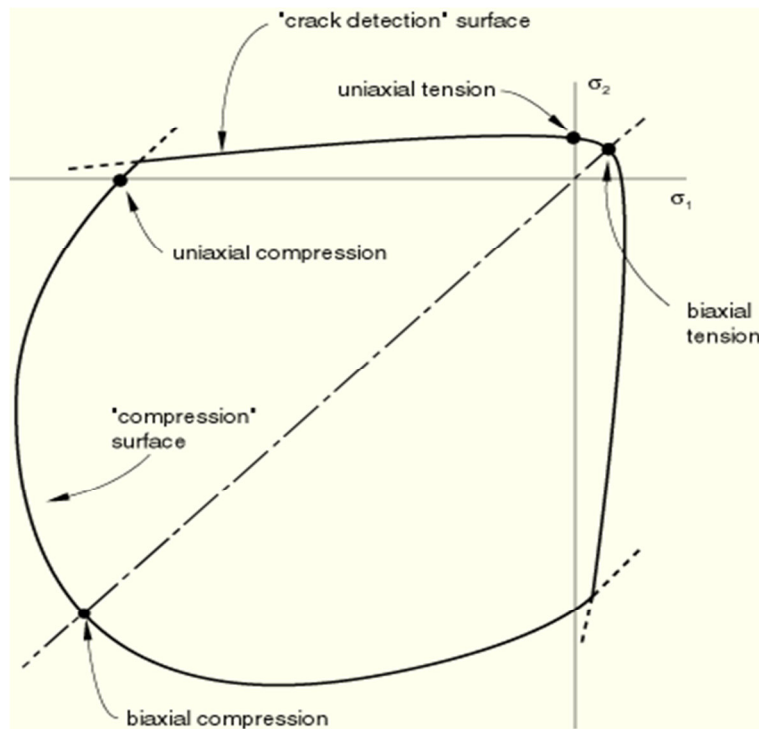
Figure E.3 Failure surface

Once FABcrete is cracked, material stiffness reduces. A model has been developed to represent load transfer occurring in the textile through the cracks. For this, the tensile stress normal to a crack is considered as a function of strain in terms of the fraction of residual stress with respect to the stress at cracking (σ/σ_{cr}) and the absolute value of the direct strain minus the direct strain

at cracking ($\varepsilon - \varepsilon_{cr}$). To develop the model, the tensile behaviour of *FABcrete* was considered from the experimental data reported in Chapter 4. Using these values, the damage in the *FABcrete* is calculated and used in subsequent calculations. The various parameters considered are volume fraction of textile (V_f), cracking stress (σ_{cr}) and cracking strain (ε_{cr}). A relationship was first established between the cracking stress and volume fraction of *FABcrete* with of SRG-45 as textile by fitting a polynomial curve (Figure E.4). The expression that can be used for predicting the cracking stress is given in Eqn.(E.11).

$$\sigma_{cr} = -6879.3\ V_f^2 + 327.67\ V_f + 0.7432 \tag{E.11}$$
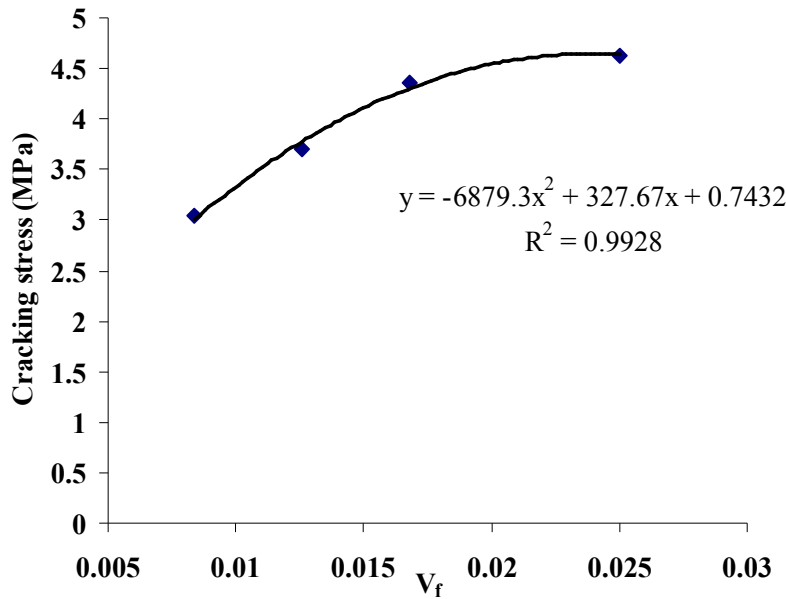
Figure E.4 Curve fit for the relation between volume fraction and cracking stress

Further, a fit was also done for the cracking strain of FABcrete with SRG-45 as textile for various volume fractions. The corresponding details about the relation is shown in Figure E.5. The expression that can be used to calculate the cracking strain of *FABcrete* is given in Eqn. (E.12).

$$\varepsilon_{cr} = 0.7932\ V_f^2 - 0.0468\ V_f + 0.0009 \tag{E.12}$$

233
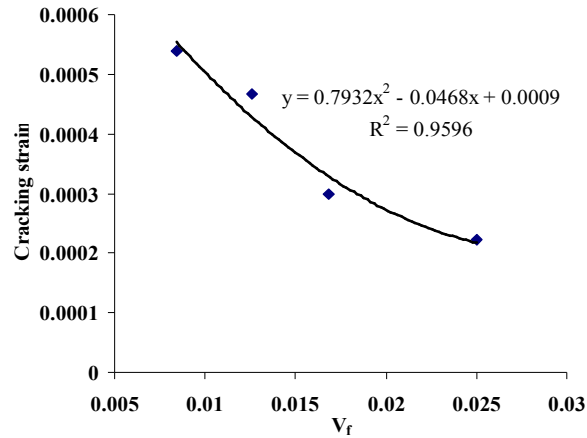
Figure E.5 Curve fit for the relation between volume fraction and cracking strain

To determine the maximum stress corresponding to a particular volume fraction, the experimental data corresponding to strain of 1.2% was considered for various cases. The maximum strain in the model is restricted to 1.2%, which is also in line with the maximum effective tensile strain level in the FRCM, reported in ACI 549, 2013. The relation between stress corresponding to strain of 1.2% with respect to volume fraction is shown in Figure E.6. The expression that can be used to calculate the maximum stress of *FABcrete* is given in Eqn.(E.13).

$$\sigma_{max} = -47700\, V_f^2 + 2389.4\, V_f - 11.319 \tag{E.13}$$
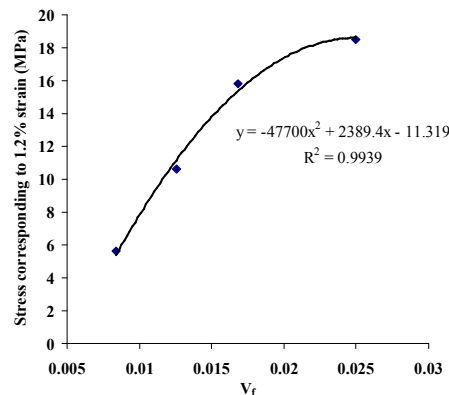
Figure E.6 Curve fit for the relation between volume fraction and stress corresponding to 1.2% strain

234

A comparison of the stress versus strain response obtained from the present model, for various volume fractions of textile in FABcrete with that of experimental behaviour is shown in Figure E.7.
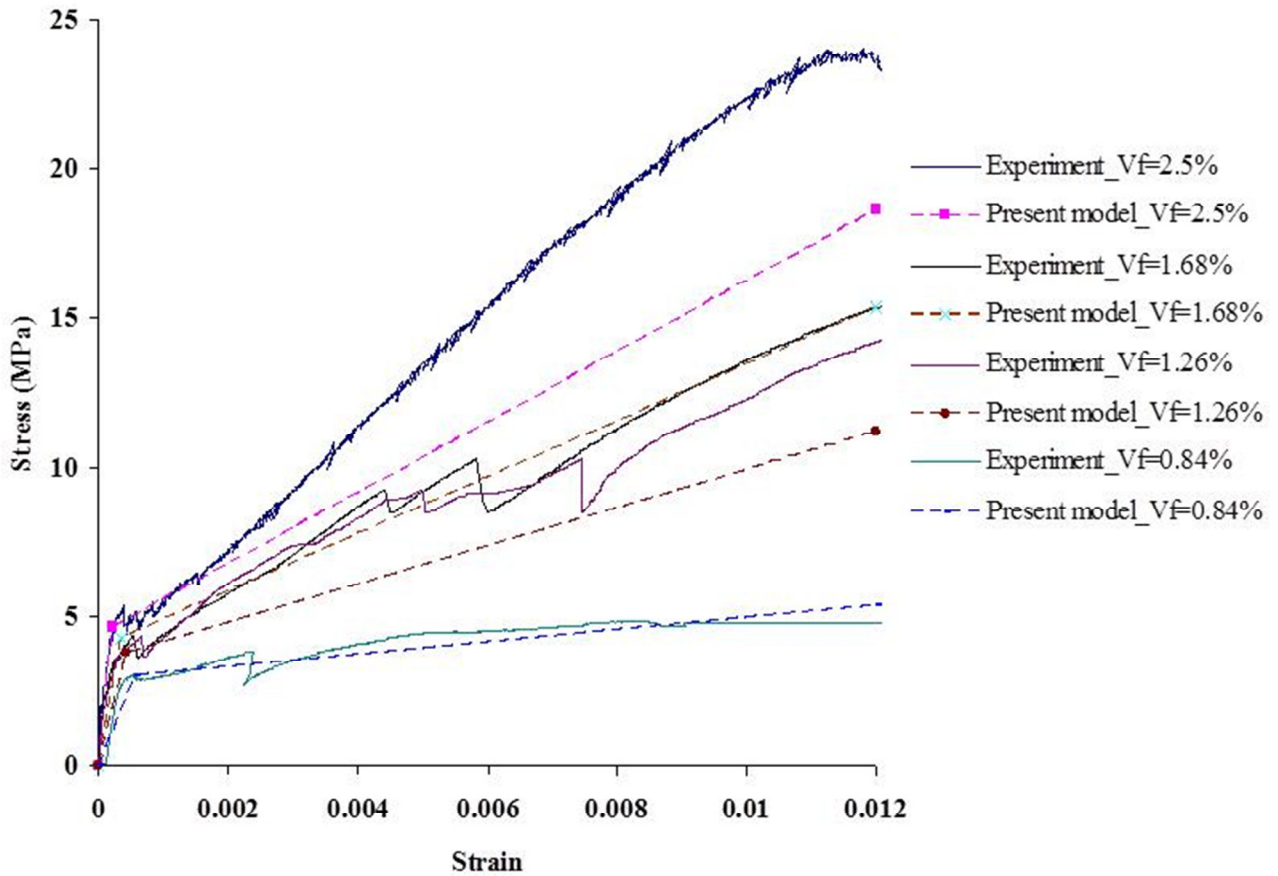
Figure E.7 Comparison of stress versus strain for the developed model and experiment

Using the Equations (E.11) to (E.13), the respective values are calculated and the ratio (σ/σ_{cr}) and the difference in maximum strain to cracking strain ($\varepsilon-\varepsilon_{cr}$) are given as input for representing the strain hardening state of *FABcrete* after cracking. Using these values, the damage to *FABcrete* in the strain hardening range is calculated and damaged elasticity model is used in subsequent calculations by ABAQUS.

E.1.1.4 Textile

The behaviour of glass textile was assumed to be linear elastic until failure with the modulus of elasticity (E_f) of the textile, Poisson's ratio and maximum tensile stress (σ_{fu}) of the textile given as the input.

E.1.1.5 Interactions between various materials in strengthened beam

The interaction modeling affects the final failure pattern in the simulation of strengthened beams. In *FABcrete* strengthening, generally four failure patterns are expected. One of the failures is by concrete crushing, in which case the full potential of textiles and steel reinforcing bars are not utilized. The second failure pattern is by yarn rupture in textile wherein the filaments in the yarn reach the maximum elongating ability and rupture. Thirdly, the steel yields and fails before the concrete crushes or textile ruptures. Finally, the failure can also occur by debonding of *FABcrete* layer from substrate concrete. All these failures, except debonding, mainly depend on the constitutive behaviour of material ingredients and the failure ratios.

E.1.2 Geometrical Modelling

In order to carry out the nonlinear finite element analysis, 8-noded linear brick elements are used for concrete as well as for the cementitious matrix of *FABcrete*. Discrete 2-noded rod elements are used to model steel reinforcement and for modeling the glass textile yarns in longitudinal and transverse directions. To model the yarns, an equivalent diameter for the number of layers of textile is calculated and a circular profile is assumed.

E.1.3 Boundary, loading and analysis details

Boundary conditions and loading information is given as input as per the experimental/practical condition. The solver capable of performing the non-linear analysis is used in finite element analysis.

E.1.4 METHODOLOGY FOR NUMERICAL ANALYSIS

A finite element modelling methodology that can be followed for strengthening of RC beams with *FABcrete* is given in Figure E.8.
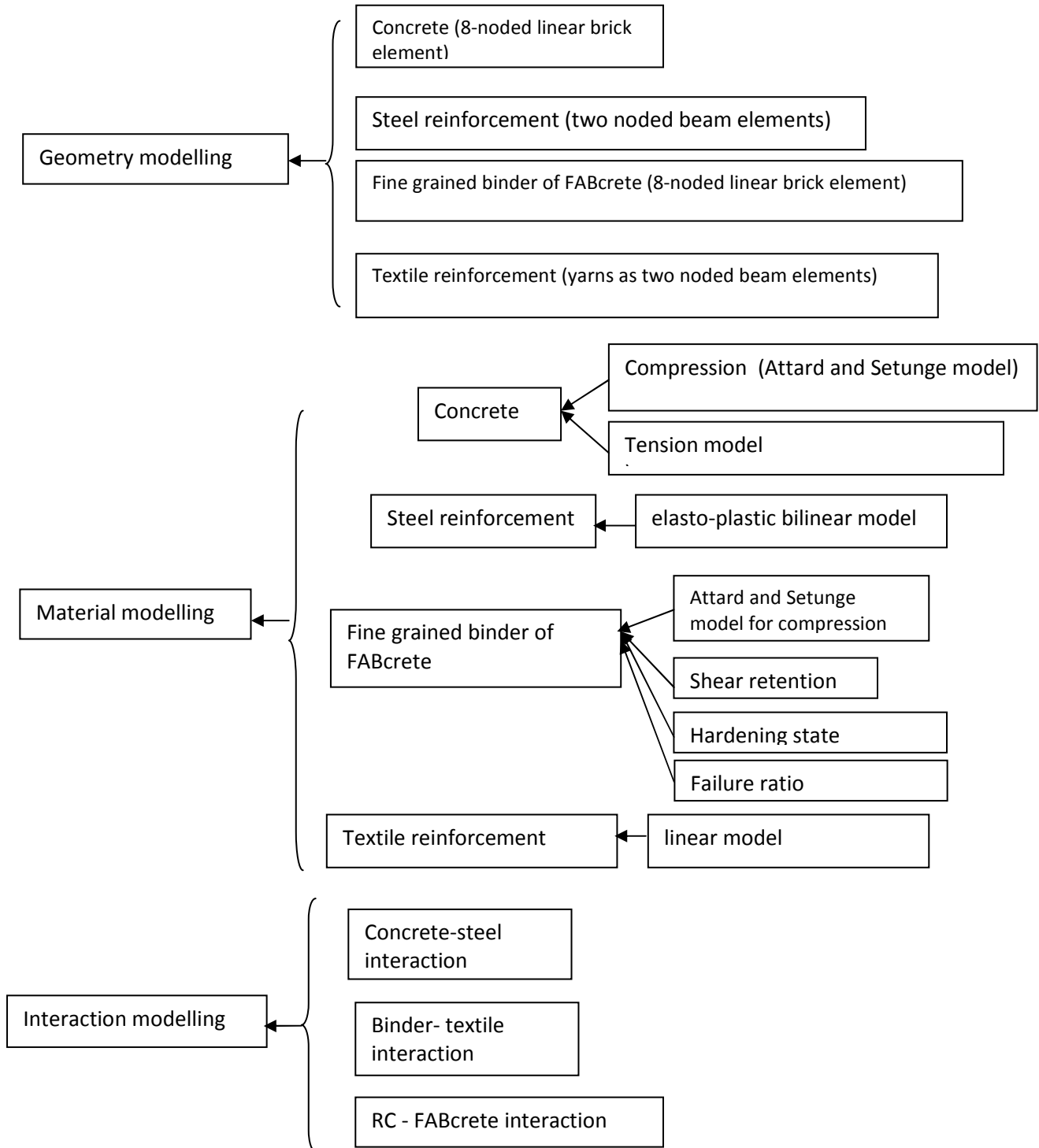
Figure E.8 Numerical simulation methodology for RC beam strengthened with *FABcrete*

E.1.5 VALIDATION STUDIES

The experimental behaviour of RC beam strengthened with *FABcrete* (refer Figure 5.14 in Chapter 5) was simulated by developing a numerical model using the finite element software ABAQUS. The element used for concrete as well as for *FABmix*, is a 8-noded linear brick element (C3D8R). The element size considered is 50mm×50mm (aspect ratio of 1), which is greater than three times the aggregate size (12×3=36mm). The element selection and the aspect ratio considered in the present study is based on the results of finite element analysis of RC beams reported in literature for handling behaviour of concrete in compression, cracking due to tension, and plastic deformations.

The steel reinforcement is modelled using a discrete approach. Respective diameters of steel bars were used to develop circular profile for the reinforcements. For modelling the glass textile yarns, a circular profile was assumed and a discrete modelling approach was followed. The equivalent diameter of each yarn, while placing 10 layers of fabric were calculated.

The nonlinear behaviour of concrete under compression was defined by making use of stress versus strain behavior till crushing. Based on the Eqn.(E.16), for a volume fraction of 3.25%, which corresponds to the volume fraction of 10 layers of textile in *FABcrete* strengthening layer was considered to arrive at the data with respect to the ratio of fraction of remaining stress to cracking stress and difference between absolute value of direct strain and direct strain at cracking, and given as a user defined input in ABAQUS software. The various input data used in the modelling is reported in Table E.1.

Table E.1 Various input parameters used

Parameter	Value
Concrete	
Young's modulus (MPa)	29500
Poisson's ratio	0.2
FABmix	
Young's modulus (MPa)	27500
Poisson's ratio	0.2
Shear retention	0.7
Failure ratio 1: ultimate biaxial compressive stress to the ultimate uniaxial compressive stress	1.26
Failure ratio 2: the absolute value of the ratio of the uniaxial tensile stress at failure to the ultimate uniaxial compressive stress	0.2
Failure ratio 3: the ratio of the magnitude of a principal component of plastic strain at ultimate stress in biaxial compression to the plastic strain at ultimate stress in uniaxial compression	1.16
Failure ratio 4: the ratio of the tensile principal stress at cracking when the other principal stress is at the ultimate compressive value to the tensile cracking stress under uniaxial tension	0.22
Steel	
Modulus of elasticity (MPa)	2×10^5
Poisson's ratio	0.3
Yield stress (MPa)	415
Textile	
Initial modulus of elasticity (GPa)	72
Poisson's ratio	0.2
Maximum tensile stress in yarn (MPa)	875
Maximum tensile strain in yarn	0.012

Perfect bond was assumed between the steel reinforcement and concrete in RC beam and also between the glass textile and *FABmix* in *FABcrete* layer. Embedded constraint was introduced in the RC beam between plain concrete, steel reinforcement and stirrups. For this, the concrete surface was chosen as the host region and the circumferential surface of the reinforcement was chosen as the embedded region. Similarly, in the case of *FABcrete* strengthening layer, *FABmix* was chosen as the host region and the textile surface was chosen as the embedded region. An image of the various constraints used in the model is given in Figure E.9.

For the interactions between *FABcrete* and substrate, a perfect bonding was assumed since no debonding of *FABcrete* from concrete surface was observed during the experiment. A surface based tie constraint with which two surfaces can be tied together was used for perfect bonding between *FABcrete* and RC beam. The bottom surface of RC beam was considered as the master surface and top surface of *FABcrete* layer was considered as the slave surface. When surfaces are in contact they usually transmit shear as well as normal forces across their interface.
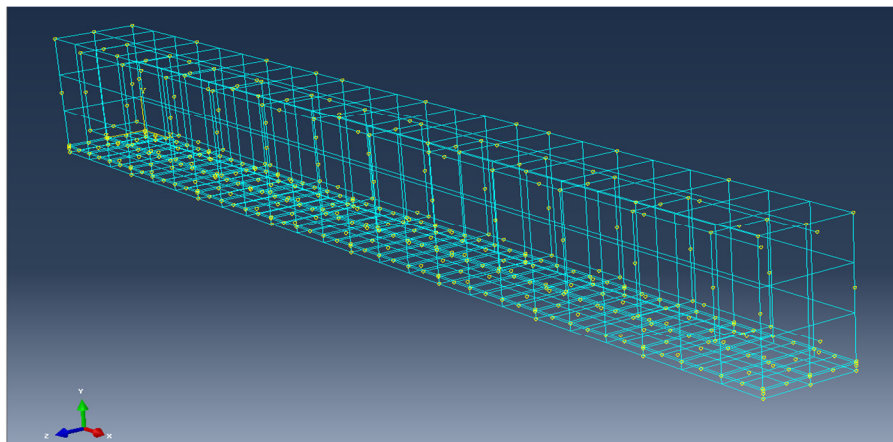
Figure E.9 Constraints used in modelling of *FABcrete* strengthened RC beam

Simply supported boundary conditions, as given in the experimental conditions, were applied to the *FABcrete* strengthened RC beam by providing a hinge at one end and a roller at the other end of the beam. As reported in Chapter 5, the experiments were carried out on RC beam strengthened with *FABcrete* under displacement controlled loading. Hence, similar type of loading was incorporated in the analysis by applying displacement boundary conditions at the loaded points of the beam to simulate the loading location in the experimental setup. The

representation of mesh, loading and boundary conditions are shown in Figure E.10. Further, Newton- Raphson's method is used to solve the nonlinear equilibrium equations.
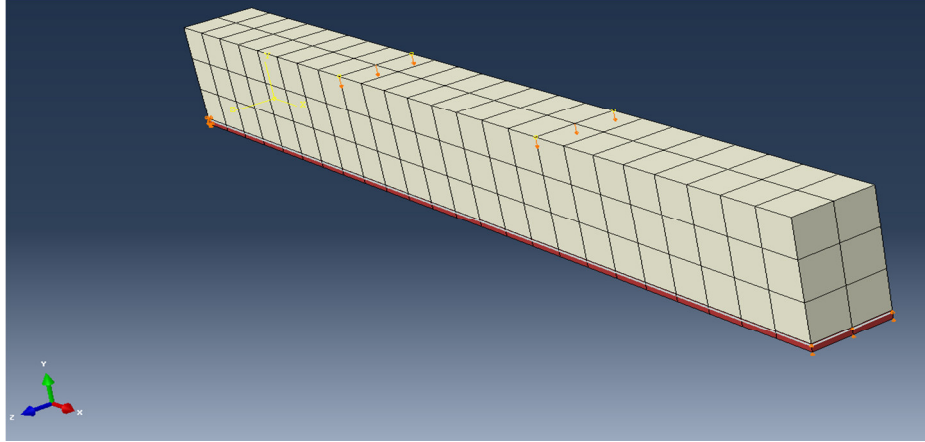
Figure E.10 FE mesh, loading and boundary conditions

E.1.5.1 Results and discussion

The load versus displacement curve obtained for the strengthened beam from numerical simulation is compared with the experimental result (refer Figure 5.14 in chapter 5) and is shown in Figure E.11. It is observed that there is a good agreement on the response between the two. In the load range of 20kN to 50kN, the numerical prediction is slightly stiffer, mainly because of the assumption of perfect bond between concrete and steel reinforcement. Near the ultimate load, both numerical and experimental values are very close, indicating the suitability of the concrete smeared model for *FABcrete*. After reaching the ultimate load, there is a drop in the load due to widening of the cracks in RC beam and also it is possible to have delamination of FABmix from textile. Figure E.12 shows the displacement contour of the deformed shape from numerical analysis.
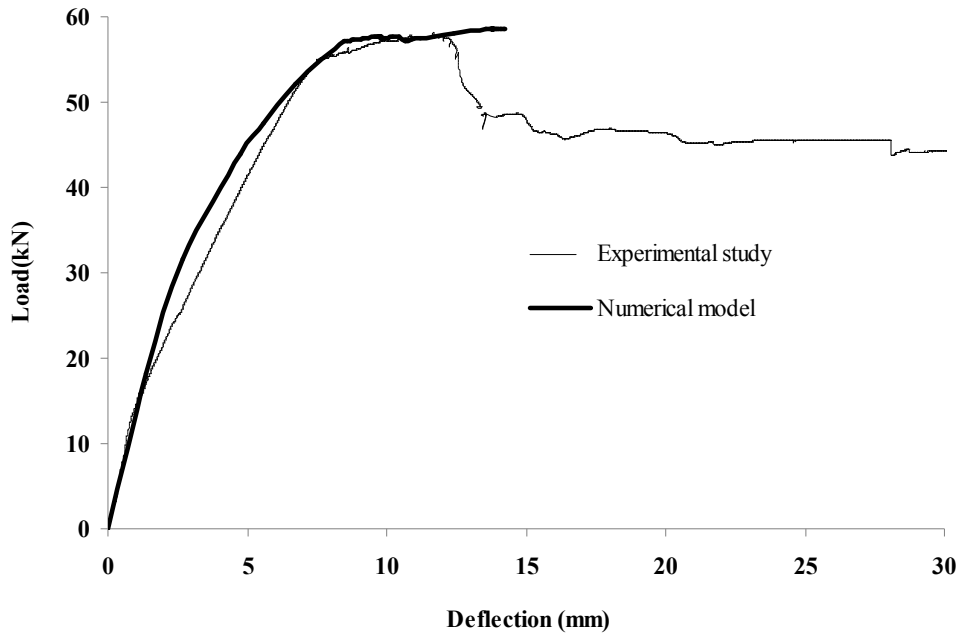
Figure E.11 Comparison of numerical and experimental results
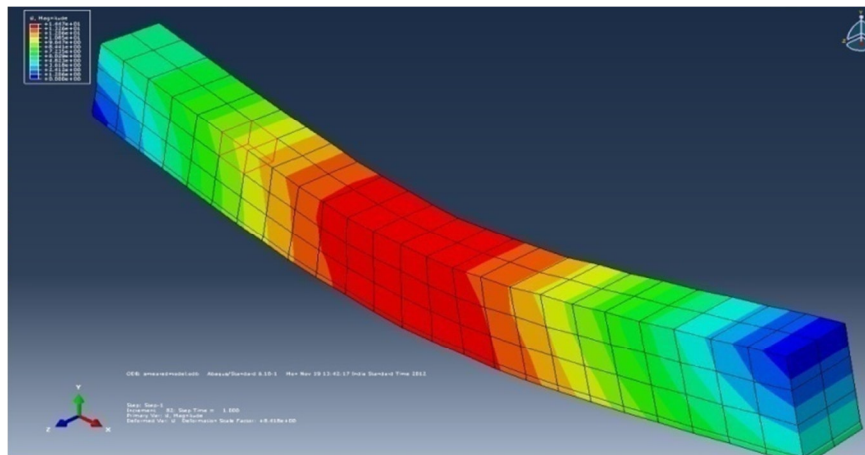
Figure E.12 Displacement contour of deformed shape

Figure E.13 shows a comparison of the strain at different load levels at mid span from the numerical and experimental studies for the top most compressive zone of concrete and bottom most tensile zone of *FABcrete* (the strain values were obtained from the experiment that are reported in Figure 5.22 in Chapter 5). It is observed that compressive strain values are in close agreement with each other for both numerical and experimental behaviour. In the case of

FABcrete under tension, the load versus strain deviates more from the experimental values. One of the main reason for this is the fact that perfect bond that was assumed between the glass textile and *FABmix* and also between steel reinforcement and concrete in RC beam, which makes the behaviour stiffer compared to actual nature. Also, the over simplification of the yarn idealization adopted for textile layers neglects the interaction between different layers of textiles. However, the strain values when cracking occurs and also at peak load are almost same.
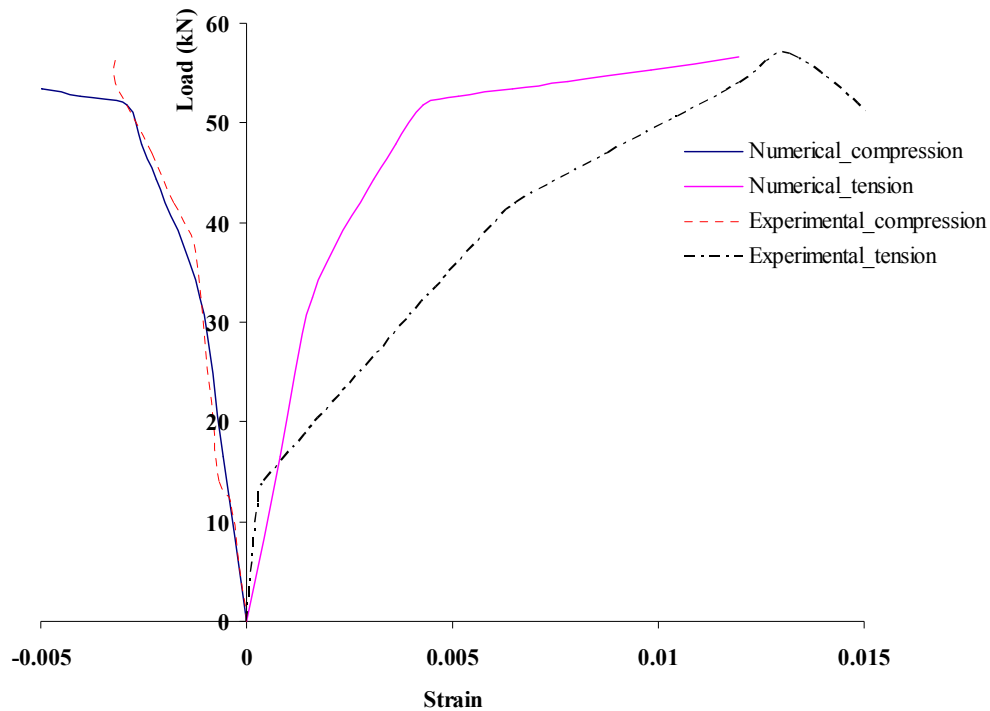
Figure E.13 Load vs strain for top compression and bottom tension

The strain at the bottom of the *FABcrete* strengthening layer along the length of the beam immediately after cracking and at peak load are shown in Figure E.14. It is observed that the strain values from the numerical study are generally close to the experimentally observed value (refer Figure 5.22 of Chapter 5) at the centre of the beam reported in Figure 5.20. Immediately after cracking, the difference in strains are not significant though near the peak load, beyond the loading points, the difference is more.
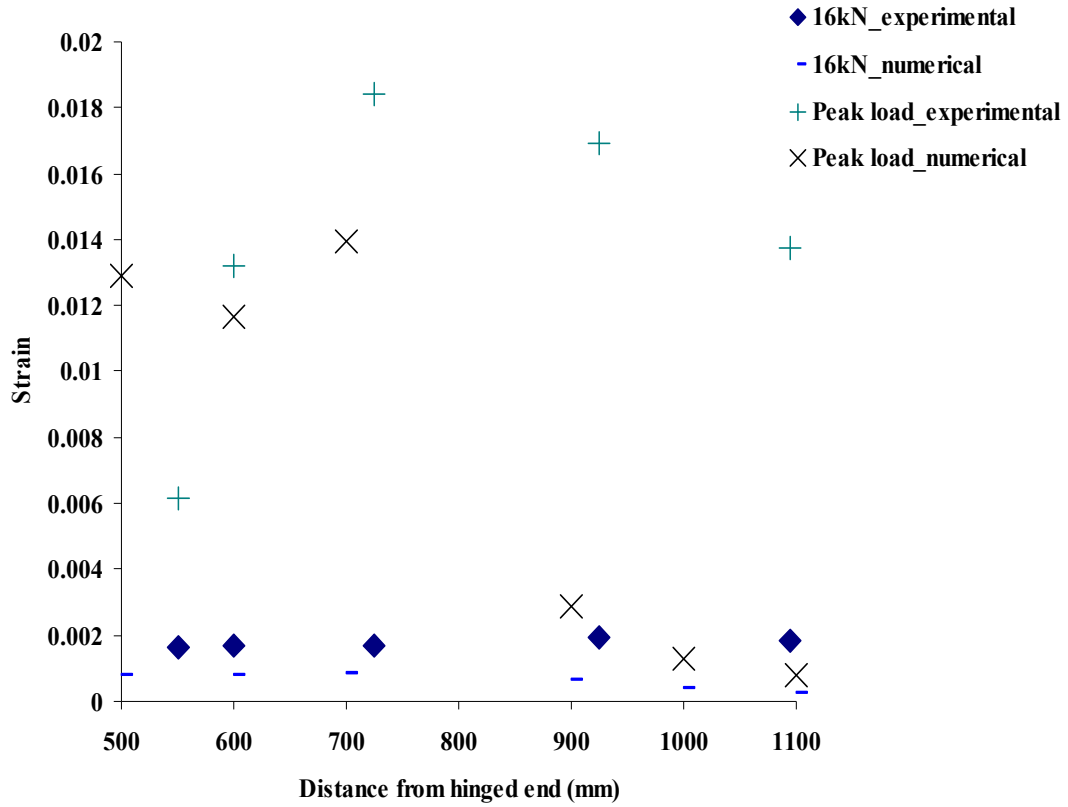
Figure E.14 Strain profile along length of beam before cracking and at peak load

REFERENCES

ACI 318 (2011) Building code requirements for structural concrete and commentary. *ACI Publication,* USA.

ACI 549 (2013) Design and construction guide of externally bonded FRCM systems for concrete and masonry repair and strengthening. *ACI Publication,* USA.

Al-Salloum, Y.A., Elsanadedy, H.M., Alsayed, S.H., Iqbal, R.A. (2012) Experimental and numerical study for the shear strengthening of RC beams using textile reinforced mortar. *Journal of Composites for Constructions*, ASCE, **16**(1), 74-90.

ASTM C 1202-97 (1997), Standard test method for electrical indication of concrete's ability to resist chloride ion penetration. *ASTM International*.

ASTM C 1437-01 (2001), Standard test method for flow of hydraulic cement mortar. *ASTM International*

ASTM C1583 (2004), Standard test method for tensile strength of concrete surfaces and the bond strength or tensile strength of concrete repair and overlay materials by direct tension (Pull-off Method), *ASTM International*

Attard, M. M., and S. Setunge, (1996) Stress-strain relationship of confined and unconfined concrete. *ACI Materials Journal,* **93**(5), 432-442.

Aveston, J., Cooper, G.A., Kelly, A. (1971) Single and multiple fracture. In: The properties of fiber composites. *IPC Science and Technology Press*: Guildford, 15 – 24.

Aveston, J., Kelly, A. (1973) Theory of multiple fracture of fibrous composites. *Journal of Materials Science*, **8**(3), 352 – 362.

Babaeidarabad, S., Loreto, G., and Nanni, A. (2014) Flexural strengthening of RC beams with an externally bonded fabric-reinforced cementitious matrix. *Journal of Composites for Construction*,**18**(5), 04014009.

Barhum, R., Mechtcherine, V. (2012) Effect of short, dispersed glass and carbon fibres on the behaviour of textile-reinforced concrete under tensile loading. *Engineering Fracture Mechanics*, **92**, 56-71.

Barhum, R., Mechtcherine, V. (2013) Influence of short dispersed and short integral glass fibres on the mechanical behaviour of textile-reinforced concrete. *Materials and Structures,* **46**, 557-572.

Banholzer, B., Brameshuber, W. and Jung, W. (2004) Analytical simulation of pull-out tests-the direct problem. *Cement and Concrete Composites,* **27**(1), 293–101.

Banholzer, B., Brockmann, T.H andBrameshuber, W. (2006) Material and bonding characteristics for dimensioning and modelling of textile reinforced concrete (TRC) elements. *Materials and Structures,* **39**(8), 749-763.

Bentur, A., Peled, A. andYankelevsky, D. (1997) Enhanced bonding of low modulus polymer fibers-cement matrix by means of crimped geometry. *Cement and Concrete Research*, **27**(7), 1099-1111.

Blanksvärd, T., Täljsten, B. and Carolin, A. (2009) Shear strengthening of concrete structures with the use of mineral based composites (MBC). *Journal of Composites for Construction*, **13**(25), 25-34.

Brameshuber W et al. (2010) Uniaxial tensile test—test method to determine the load bearing behavior of tensile specimens made of textile reinforced concrete (Proposal for a recommendation by RILEM TC 232-TDT to be published in Materials and Structures)

Brameshuber, W. Ed. (2006) Textile reinforced concrete State-of-the-art Report of RILEM Technical Committee TC 201-TRC, Report 36, *RILEM Publications.*

Brockmann, J., Raupach, M. (2002) Durability investigations on textile reinforced concrete. *9th International Conference on Durability of Building Materials and Component*, paper No. 111, Brisbane, Australia

Brockmann, T. (2007) Mechanical and fracture mechanical properties of fine grained concrete for TRC structures. *Advances in Construction Materials, Part II, 119-129, DOI: 10.*1007/978-3-540-72448-3 – 12.

Brockmann, T. and Brameshuber, W. (2005) Matrix development for the production technology of Textile Reinforced Concrete (TRC) structural elements. *Proceedings of the 3rd International Conference on Composites in Construction*, 1165-1172.

Bruckner, A., Ortlepp, R. and Curbach, M. (2006) Textile reinforced concrete for strengthening in bending and shear. *Materials and structures*, **39(8)**, 741-748.

Bruckner, A., Ortlepp, R. and Curback, M. (2008) Anchoring of shear strengthening for T-beams made of TRC. *Materials and Structures,***41**(2), 407-418.

Brückner, A., Ortlepp, R., Weiland, S. and Curbach, M. (2005) Shear strengthening with textile reinforced concrete. Proc. of Third International Conference Composites in Construction, Lyon, France, 1307-1314.

Butler, M., Mechtcherine, V., Hempel, S. (2009) Experimental investigations on the durability of fibre-matrix interfaces in textile-reinforced concrete. *Cement & Concrete Composites*, **31**(4), 221–231

Colombo, I. G., Magri, A., Zani, G., Colombo, M., & di Prisco, M. (2013). Erratum to: Textile Reinforced Concrete: experimental investigation on design parameters. *Materials and Structures*, *46*(11), 1953-1971.

Contamine, R., Si Larbi, A., Hamelin, P. (2013) Identifying the contribution of textile reinforced concrete (TRC) in the case of shear repairing damaged and reinforced concrete beams. *Engineering Structures*, **46**, 447-458.

Curbach, M., Ortlepp, R., and Triantafillou, T. C. (2006) TRC for rehabilitation, *Report of RILEM TC 201-TRC, Textile reinforced concrete—State-of-the-Art*. W. Brameshuber, Ed., Report 36, 221–236.

Cuypers, B. and Wastiels, J. (2006) Stochastic matrix-cracking model for textile reinforced cementitious composites under tensile loading. *Materials and structures,***39(8)**, 777-786.

Czymai, A. (1995) EineMethodezur Bestimmung von Tiefenprofilenankorrodierten Glasfasern. Clausthal, Technische Universität, Fakultätfür Bergbau, Hüttenwesen und

Maschinenbau, Diss.

D'Ambrisi, A., and Focacci, F. (2011) Flexural strengthening of RC beams with cement-based composites. *Journal of Composites for Construction*, ASCE, 15(5), 707-720.

D'Ambrisi. A., Focacci. F., Feo, L. (2012) Bond-slip relations for PBO-FRCM materials externally bonded to concrete. *Composites Part B: Engineering*, **43**(8), 2938-2949.

Dugas, M., Weise, S., Curbach, M., Hempel, R., Offermann, P. and Franzke, G. (1998) Force-deformation behaviour of tensile-loaded specimens made of textile reinforced concrete. In: Techtextil Symposium 1998, Lyon, 143–152.

Engberts, E. (2006) Large-size façade elements of textile reinforced concrete. Proc. of *International RILEM symposium textile reinforced concrete conference, Aachen, Germany*, Edited by J. Hegger, W. Brameshuber, and N. Will, 309-318.

Fraay, A.L.A., Bijen, J.M., De Haan, Y.M. (1989) The reaction of fly ash in concrete a critical examination. *Cement and Concrete Research,***19** (2), 235–246.

Fydro. Dinamic Creative Concrete Cladding,(2012) *http://www.dinamicccc.com/.*

Graf, W., Hoffmann,A., Möllera,B., Sickert, J.U., Steinigena, F. (2007) Shear strengthening effect by bonded composite Textiles on RC beams. *Engineering Structures,* **29**(12), 3420-3431.

Guldentops, L., Mollaert, M. and Adriaenssens, S. (2009) Fabric formed concrete shell structures. *IASS Symposium 2009*: *Evolution and trends in design, analysis and construction of shell and spatial structures,* Valencia, Spain.

Hana, A., Fiorio, B., Gallias, J. (2010) Characterization of the impregnation by a cementitious matrix of five glass multi-filament yarns. *European Journal of Environmental and Civil Engineering* , **14**(5), 529-544.

Hartig, J., F. Jesse, and U. Häußler-Combe. (2010). Evaluation of experimental setups for determining the tensile strength of Textile Reinforced Concrete. *International RILEM Conference on Material Science*, Edited by W. Brameshuber, RILEM Publications SARL, 117-127.

Hartig, J., F. Jesse, K. Schicktanz, and U. Häußler-Combe. (2012). Influence of experimental setups on the apparent uniaxial tensile load-bearing capacity of Textile Reinforced Concrete specimens. Materials and structures, **45**(3), 433-446.

Hausding, J., Engler, T., Franzke, G. and Köckritz, U. (2006) Plain Stitch-Bonded Multi-Plies for Textile Reinforced Concrete. *Autex Research Journal*, 6(2), 81-90.

Hegger J., Kulas C. (2010) TRC pedestrian bridge design, load- bearing behavior and production processes of a slender and light weight construction. *Proc. of International RILEM Conference on Material Science*, RILEM Publications, Vol. 1, 353-364.

Hegger, J. Bruckermann, O. and Sherif, A.G. (2007) Modelling Local Pressure on Inclined Rovings in Textile-Reinforced Concrete. *ACI Materials Journal,* **104**(5), 20-525.

Hegger, J. N., Will Bruckermann, O. and Voss, S. (2006) Load-bearing behaviour and simulation of textile reinforced concrete. *Materials and structures*, **39**(8), 765-776.

Hegger, J., Bruckermann, O. and Chudoba, R. (2004) A smeared bond-slip relation for multi-filament yarns embedded in fine concrete. *6th RILEM Symposium on Fiber-Reinforced Concretes (FRC), BEFIB, Varenna, Italy,* 1453-1462.

Hegger, J., Kulas, C. and Horstmann, M. (2011) Realization of TRC facades with impregnated AR-glass textiles. *Key Engineering Materials,* **466**, 121-130.

Hegger, J., Schneider, M., Kulas, C. (2010) Dimensioning of TRC with application to ventilated facade systems. *International RILEM Conference on Materials Science MATSCI,* 393-403.

Holler, S., Butenweg, C., Noh, S.Y. and Meskouris, K. (2002) Numerical simulation of Textile-Reinforced concrete structures. in B.H.V. Topping, Z. Bittnar, (Editors), *Proceedings of the Sixth International Conference on Computational Structures Technology*, Civil-Comp Press, Stirlingshire, UK, Paper 122, 287-288.

Insu-Shell-Projekt LIFE. *Life insu-Shell-Projekt • InstitutFürTextiltechnik Der Rwth Aachen* [Online]. Available: http://www.life-insushell.de/en/das-projekt.html, 2009.

IS 516 (1959) Reaffirmed 2004, Method of test for strength of concrete. Bureau of Indian Standards, New Delhi.

Jayasree, C., and Gettu, R. (2012) Choice of compatible cement-superplasticizer combinations. *ICI Journal, Special Issue on Construction Chemicals, Indian Concrete Institute*, **12**(4), 14-31.

Jesse, F. (2004) Load bearing behaviour of filament yarns in a cementitious matrix (in German). Dissertation, TU Dresden.

Konrad M. and Chudoba, R. (2004) The influence of disorder in multifilament yarns on the bond performance in textile reinforced concrete. *Acta Polytechnica,***44**(5–6), 186–193.

Kruger, M. (2004) VorgespanntertextilbewehrterBeton. *Beton‐und Stahlbetonbau*, 99(6), 472-475.

Kruger, M., Ozbolt, J. and Reinhardt, H. W. (2003) A new 3D discrete bond model to study the influence of bond on structural performance of thin reinforced and prestressed concrete plates. *Proc. of the Fourth International RILEM Workshop on High Performance Fiber Reinforced Cement Composites (HPFRCC4),* Eds. A.E., Naaman and H.W., Reindhart, Ann Arbor, 49-63.

Larbi, Si. A., Amen, A. and Patrice, H. (2013) Experimental and numerical investigations about textile-reinforced concrete and hybrid solutions for repairing and/or strengthening reinforced concrete beams, *Composite Structures,* **99**, 152-162.

Larbi, Si. A., Ferrier, E. and Hamelin, P. P. (2010) Study of reinforced concrete beams strengthened with textile reinforced concrete. Proc. International RILEM Conference on Material Science (MatSci), Aachen, Vol:I, ICTRC, 227-233.

Larbi, Si. A., Contamine, R., Ferrier, E., Hamelin, P. (2010) Shear strengthening of RC beams with textile reinforced concrete (TRC) plate. Construction and Building Materials, **24**(10),1928-1936.

Larbi, Si. A.,Contamine, R., Hamelin, P. (2012) TRC and hybrid solutions for repairing

and/or strengthening reinforced concrete beams, *Engineering Structures*, 45, 12-20.

Larrinaga, P. San-Jose, J. T. Garcia, D., Garmendia, L., Diez, J. (2010) Experimental study of the flexural behaviour of low performance RC beams strengthened with textile reinforced mortar, *MATSCI 2010,* Vol. 1, pp. 235-244

Leonard, S. and Bentur, A. (1984) Improvement of the durability of glass fiber reinforced cement using blended cement matrix. *Cement and Concrete Research*, **14**(5), 717-728

Lepenies, I.G. (2007) Zurhierarchischen und simultanen Multi-Skalen-Analysevon extilbeton. TU Dresden: Dresden, Dissertation, Inst. für Massivbau.

Lieboldt, M. (2006) Textile reinforced concrete multilayer composite pipes. *Proc. Ist Intl. conf. on Textile reinforced concrete, ICTRC, PRO-50*, 369-378.

Loreto, G., Leardini, L., Arboleda, D., and Nanni, A. (2014). Performance of RC slab-type elements strengthened with fabric-reinforced cementitious-matrix composites. *Journal of Composites for Construction,* **18**(3), SPECIAL ISSUE: 10th Anniversary of IIFC, A4013003.

Majumdar AJ, West JM, Larner LJ (1977) Properties of glass fibres in cement environment. *Journal of Material Science*, **12**(5):927–936

Mallick, P. K. (1988) Fiber reinforced composites: Manufacturing and design. New York: Marcel Dekker Inc.

Mayer, C. and Vilkner, G. (2003) Glass concrete thin sheets prestressed with aramid fiber mesh. Proceeding of the Fourth International *RILEM Workshop on High Performance Fiber Reinforced Cement Composites (HPFRCC4),* Eds. A.E., Naaman and H.W., Reindhart, Ann Arbor, Vol.1, 325-336.

Mechtcherine, V. (2012) Towards a durability framework for structural elements and structures made of or strengthened with high-performance fibre-reinforced composites. *Construction and Building Materials,* 31*,* 94-104.

Mechtcherine, V., and Lieboldt, M. (2011) Permeation of water and gases through cracked textile reinforced concrete. *Cement and Concrete Composites*, **33** (7), 725-734.

Mechtcherine, V. (2013) Novel cement based composites for the strengthening and repair of concrete structures. *Construction and Building Materials*, **41**, 365-373.

MobasherB. (2011) Mechanics of fiber and textile reinforced composites, CRC Press.

Mobasher, B. (2003) Micromechanical modeling of angle ply filament wound cement based composites. *ASCE Journal of Engineering Mechanics,* **129**(4), 373-382.

Mobasher, B., and Pivacek, A. (1998) A Filament Winding Technique for Manufacturing Cement Based Cross-Ply Laminates, *Journal of Cement and Concrete Composites*, **20(5)**, 405-415.

Mobasher, B., Mamlouk, M., and Lin, H.M. (1997) Evaluation Of Crack Propagation Properties of Asphalt Mixtures. *ASCE Journal of Transportation Engineering*, **123**(5), 405-413.

Mobasher, B., Peled, A. and Pahilajani, J. (2004b) Damage evolution in Textile-cement

composites. http://www.learningace.com/doc/4703612/.../peled-pultrusion-final.

Mobasher, B., Peled, A. and Pahilajani, J. (2004a) Pultrusion of fabricreinforced high flyash blended cement composites. *Proceedings, RILEM Technical Meeting, BEFIB*, 1473-1482.

Molter, M. (2005) ZumTragverhalten von textilbewehrtemBeton. Dissertation, RWTH Aachen, Aachen.

Mumenya S.W., Tait, R.B., and Alexander, M.G. (2008) Effect of environmental exposure on the microstructure of textile concrete. *7th RILEM International Symposium on Fibre Reinforced Concrete: Design and Applications*, September 2008, Chennai, India, Bagneux, RILEM Publications, 10 pp.

Oesch T.S. (2015) Investigation of fiber and cracking behavior for conventional and ultra high performance concrete using X-RAY computed tomography. PhD Thesis, University of Illinois at Urbana-Champaign, http://hdl.handle.net/2142/78353

Ohno, S., Hannant, D.J. (1994) Modeling the Stress-Strain Response of Continuous Fiber Reinforced Cement Composites. *ACI Materials Journal*, **91**(3), 306 – 312

Ombres L (2011) Flexural analysis of reinforced concrete beams strengthened with a cement based high strength composite material. *Composite Structures*, **94**(1), 143-155.

Orlowsky, J. and Raupach, M. (2003) Long term behaviour of textile reinforced concrete, *Proc. 13th Congress of the International Glassfiber reinforced Concrete Association*, Barcelona, Spain, 1-11.

Orlowsky, J. and Raupach, M. (2006) Modelling the loss in strength of ARglassfibres in textile-reinforced concrete. *Materials and Structures*, **39(6)**, 635– 643

Ortlepp, R. Lorenz, A. and Curbach, M., (2009) Advances in Materials Science and Engineering, Article ID 493097, 5 pages, doi:10.1155/2009/493097, 47-53.

Ortlepp, R., Hampel, U., and Curbach, M. (2006). A new approach for evaluating bond capacity of TRC strengthening. *Cement and Concrete. Composites*, 28(7), 589-597.

Padaki, N. V., Alagirusamy, R., Deopura, B. L. and Fangueiro, R. (2010) Influence of preform interlacement on the low velocity impact behavior of multilayer textile composites. *Journal of Industrial Textiles*, **40**(2), 171-185.

Papanicolaou C., Triantafillou T., and Papantoniou I. (2009) Strengthening of two-way reinforced concrete slabs with Textile Reinforced Mortars (TRM), Proc. *of the 4th Colloquium on Textile Reinforced Structures (CTRS4)*, 409-420.

Papanicolaou, C.G., Triantafillou, T.C., Karlos, K. and Papathanasiou, M. (2006) Seismic retrofitting of unreinforced masonry structures with TRM. Proc. of Ist Intl. conferenceon Textile reinforced concrete (ICTRC), PRO-50, 341-350.

Paul, A. (1977) Chemical durability of glasses: a thermo-dynamic approach. *Journal of Material Science*, **12** (11):2246–2268

Peled, A. and Bentur, A. (2000) Geometrical characteristics and efficiency of textile Textiles for reinforcing composites. *Cement and Concrete Research*, **30(5)**, 781-790.

Peled, A. and Mobasher, B. (2003) Cement based pultruded composites with Textiles. *Proceedings of the 7th International Symposium on Brittle Matrix Composites (BMC7), Warsaw, Poland*, 505-514.

Peled, A. and Mobasher, B. (2005) Pultruded fabric cement composites. *ACI Materials Journal,* **102**(1), 15-23.

Peled, A., Mobasher, B. (2010) Innovative composites-Textile reinforced concrete (TRC) for sustainable buildings.*Proceedings of the US-Israel Workshop on: Sustainable Buildings – Materials and Energy, Technion, Haifa, ISRAEL, Technion.ac.il.*

Peled, A., Bentur, A. and Mobasher, B. (2004a) Pultrusion versus casting processes for the production of Textile-cement composites Proceedings, *RILEM Conference on Fiber reinforced Concrete, BEFIB*, 1495-1504.

Peled, A., Bentur, A. and Yankelevsky, D. (1998) Effects of woven fabric geometry on the bonding performance of cementitious composites: mechanical performance. *Advanced Cement Based Materials*, **7** (1), 20–27.

Peled, A., Bentur, A. and Yankelevsky, D. (1999) Flexural performance of cementitious composites reinforced by woven textiles. *Journal of Materials in Civil Engineering (ASCE)*, **11** (4), 325-330.

Peled, A., Bentur, A. (2003) Mechanisms of fabric reinforcements of cement matrices: Effect of fabric geometry and yarn properties. 2nd Colloquim on textile reinforced structures (CTRS2), Dresden Germany, Sept 29-Oct 1, 2003, Vol. 9.

Peled, A., Cohenb,Z., Pasderb,Y., Royec, A., and Thomas, G. (2008) Shear strengthening of RC beams with textile reinforced concrete (TRC) plate. *Cement and Concrete Composites,* **30** (3), 174-183.

Peled, A., Mobasher, B. andZviCohenc. (2009) Cement and Concrete Composites Mechanical properties of hybrid Textiles in pultruded. C*ement Composites,* **31**(9), 647- 657.

Peled, A., Mobasher, B. and Sueki, S. (2004b) Technology methods in textile cement-based composites" Concrete Science and Engineering, A Tribute to ArnonBentur, Eds. K. Kovler, J. Marchand, S. Mindess, and J. Weiss, *RILEM Proceedings PRO- 36*, 187-202.

Peled, A., Sueki, S. andMobasher, B. (2006) Bonding in Textile-cement systems: effects of fabrication methods. *Cement and Concrete Research,* **36** (9), 1661–1671.

Peled, A., Zhu, D. and Mobasher, B. (2012) Impact behavior of 3D fabric reinforced cementitious composites. *Conference on High Performance Fiber Reinforced Cement Composites 6*, Springer Netherlands, 543-550.

Ramachandran, V. S., Malhotra, V. M., Jolicoeur, C., & Spiratos, N. (1998). Superplasticizers: properties and applications in concrete.

Ramm, E., Schunck, E. (2002) Heinz Ilser Schalen: Katalog zur Austellung Vdf Hochschulverlag Ag Publishers.

Raupach, M., Brockmann, J. (2001) Development of a Test Method to Investigate the Change between the Bond Behaviour of Glass Filament-Yarns and Concrete. Porto: 2001. – In: Porto CCC2001 Composites in Construction International Conference in Porto. Erscheint

in Kürze

Reinhardt, H. W. and Kruger, M. (2004) Prestressed concrete plates with high strength Textile. *Proceedings, RILEM Conference on Fiber reinforced Concrete,* BEFIB, 187-196.

Richter, M. (2005) EntwicklungmechanischerModellezuranalytischenBeschreibungder Materialeigenschaften von textilbewehrtemFeinbeton. TU Dresden: Dresden, Dissertation

Rixom, T. and Mailvaganam, N. (1999) Chemical Admixtures for Concrete. *E&FN Spon, London*.

Rocco, C., Guinea, G. V., Planas, J., Elices, M. (1999), Size effect and boundary conditions in the Brazilian test: Experimental verification. *Materials and Structures*, **32**, 210-217.

Rocco, C., Guinea, G. V., Planas, J., Elices, M. (1999), Size effect and boundary conditions in the Brazilian test: Theoretical analysis. *Materials and Structures*, **32**, 437-444.

Roncero, J., Gettu, R., Agulló, L. andVázquez, E. (2002) Flow behaviour of super plasticised cement pastes: influence of silica fume. *Indian Concrete Journal,***76** (1), 31-35.

Schatzke, C. Joachin, T. Schneider, H. N. (2010) Single and Double curved structures made of TRC. International RILEM Conference on Materials Science, MATSCI, 367-379.

Schefflera, C., Gaoa, S. L., Plonkaa, R., Mädera, E., Hempelb, S., Butlerb, M. and Mechtcherineb, V. (2009) Inter phase modification of alkali-resistant glass fibers and carbon fibers for textile reinforced concrete I: Fiber properties and durability. *Composites Science and Technology,***69**(3), 531-538.

Schladitz, F., Frenzel, M., Ehlig, D., and Curbach, M. (2012) Bending load capacity of reinforced concrete slabs strengthened with textile reinforced concrete. *Engineering Structures,* **40**, 317-326.

Schleser, M., Walk-Lauffer, B., Raupach, M. and Dilthey, U. (2006) Application of Polymers to Textile-Reinforced Concrete. *Journal of Materials in Civil Engineering,* **18**(5), 670-676

Schneider, H.N. and Bergmann, I. (2008) The Application Potential of Textile-Reinforced Concrete. *ACI Publication SP-250-1*, 7-22.

Schneider, H.N., Schatzke, C., Bergmann, I, (2006), Textile Reinforced Concrete-Applications and Prototypes, Proc. of Ist Intl. conference Textile reinforced concrete (ICTRC), PRO-50, 297-308.

Sueki, S., Peled, A. and Mobasher, B. (2007) Pullout-slip response of Fabrics embedded in a cement paste matrix. *Journal of Materials in Civil Engineering,* **19**(9), 718-727.

Tommaso Di. A, Focacci, F., Mantegazza, G., Gatti, A. (2007) FRCM versus FRP composites to strengthen RC beams: a comparative analysis. *Proceedings of the International Symposium on Fibre Reinforced Polymers for Reinforced Concrete Structures (FRPRCS8)*, Triantafillou TC Ed., Patras, Greece.

Tomoscheit, S., Gries, T., Horstmann, M. (2011) Project Life INSUSHELL: Reducing the Carbon Footprint in Concrete Construction, *International Journal of Sustainable Building Technology and Urban Development,* **2**(2), 162-169.

Triantafillou, T. C. and Papanicolaou, C. G. (2005) Fiber reinforced polymers (FRP) as strengthening materials of concrete structures versus Textile reinforced mortars (TRM). SP-230, FRPRCS-7, 99-118.

Triantafillou, T.C., Papanicolau, C.G., Zisimopoulos, P. and Laourdekis, T. (2006) Concrete confinement with textile reinforced mortar jackets. *ACI Structural Journal,* **103** (1), 28-37.

Triantafillou, **T.** (2010) Innovative Textile-based Composites for Strengthening and Seismic Retrofitting of Concrete and Masonry Structures. *The 5th International Conference on FRP Composites in Civil Engineering*, September 27-29, CICE 2010 Beijing, China .

Trtik, P. and Bartos, P. J. M. (1999) Assessment of glass fiber reinforced cement by in-situ SEM bending test. *Materials and Structure,* **32** (2), 140-143.

Vecchio, Frank J., and Michael P. Collins. (1993) Compression response of cracked reinforced concrete. *Journal of Structural Engineering,* **119** (12), 3590-3610.

Verbruggen, S. Remy, O. Wastiels, J. and Tysmans, T. (2013) Stay-in-place formwork of TRC designed as shear reinforcement for concrete beams. *Advances in Materials Science and Engineering*, http://dx.doi.org/10.1155/2013/648943

Zhu, D. Gencoglu, M. and Mobasher, B. (2009) Low velocity flexural impact behavior of AR glass fabric reinforced cement composites. *Cement & Concrete Composites*, **31**(6), 379–387.

Zhu, W. and Bartos, P. J. M. (1997) Assessment of interfacial microstructure and bond properties in aged GRC using a novel micro indentation method. *Cement and Concrete Research*, **27**(11), 1701-1711.

PATENT AND PUBLICATIONS BASED ON THE THESIS WORK

PATENT FILED

1. **Smitha Gopinath**, **Nagesh R. Iyer**, An Apparatus For Cast-In-Place Strengthening Of Structural Members Using Textile Reinforced Concrete and method thereof, Indian Patent application: 2339DEL2015.

PUBLICATIONS

1. **Smitha, Gopinath., Nagesh, R. Iyer., Ravindra, Gettu.** (2017) Finite element analysis of RC beams strengthened with textile reinforced concrete. *Journal of Structural engineering (JoSE)*, CSIR-SERC, **43**(5), 454-460.

2. Wolfgang BRAMESHUBER; M. Hinzen, A. Dubey, A. Peled, B. Mobasher, A. Bentur, C. Aldea, F. Silva, J. Hegger, T. Gries, J. Wastiels, K. Malaga, C. Papanicolaou, L. Taerwe, M. Curbach, V. Mechtcherine, A. Naaman, J. Orlowsky, P. Hamelin, H.-W. Reinhardt, S. Shah, R. Toledo, T Triantafillou, A. Larbi, D. Garcia, L. Garmendia, S. Gopinath, F. Jesse, **(2016)** Recommendation of RILEM TC 232-TDT: Test methods and design of textile reinforced concrete, *Materials and structures*, 49 **(12), 4923–4927.**

3. **Smitha, Gopinath., Nagesh, R. Iyer,, Ravindra Gettu.** (2013) Flexural strengthening of RC beams using fabric reinforced concrete, *Proc. of Intl. Conf. on Rehabilitation and Restoration of Structures,* IIT Madras, Chennai, February 13-16, 449-456.

JOURNAL PAPER UNDER REVIEW

1 **Smitha, Gopinath.**, **Ravindra, Gettu., Nagesh, R, Iyer.** Influence of the Stretching of the textiles on the tensile behaviour of textile reinforced concrete, (*Submitted to Materials and Structures*).

JOURNAL PAPERS TO BE COMMUNICATED

1. **Smitha Gopinath, Ravindra Gettu, Nagesh R. Iyer**, Textile Reinforced Concrete- A Review.
2. **Smitha Gopinath, Ravindra Gettu, Nagesh R. Iyer,** Tensile characterization of glass textiles as reinforcement for textile reinforced concrete.
3. **Smitha Gopinath, Nagesh R. Iyer**, **Ravindra Gettu,** Experimental and analytical investigations on flexural strengthening of RC beams using textile reinforced concrete.
4. **Smitha Gopinath, Nagesh R. Iyer**, **Ravindra Gettu,** On-site approach for cast-in-place strengthening of reinforced concrete beams using textile reinforced concrete.
5. **Smitha Gopinath, Ravindra Gettu, Nagesh R. Iyer**, Design parameters for tensile behavior of textile reinforced concrete

CURRICULAM VITAE

NAME		**:**	**SMITHA GOPINATH**
DATE OF BIRTH		**:**	**31-05-1977**

EDUCATIONAL QUALIFICATIONS

1999   **Bachelor of Technology (B.Tech)**

Specialization	:	Civil Engineering
Institution	:	Govt. Engineering College Thrissur, Kerala

2001   **Master of Engineering (M.E)**

Specialization	:	Structural Engineering
Institution	:	PSG College of Technology, Coimbatore

Doctor of Philosophy (Ph.D.)

Institution	:	Indian Institute of Technology Madras, Chennai
Registration	:	17-07-2009

DOCTORAL COMMITTEE

CHAIR PERSON	:	**Dr. K. Ramamurthy** Professor and Head, Department of Civil Engineering, IIT Madras, Chennai
GUIDE(S)	:	**Dr. Ravindra Gettu** Professor, Department of Civil Engineering, IIT Madras, Chennai
	:	**Dr. Nagesh R. Iyer** Former Director, CSIR-Structural Engineering Research Centre & Distinguished Emeritus Professor, AcSIR, Chennai
MEMBERS	:	**Dr. Alagasundaramoorthy** Professor, Department of Civil Engineering, IIT Madras, Chennai
	:	**Dr. Amlan K. Sengupta** Professor, Department of Civil Engineering, IIT Madras, Chennai
	:	**Dr. M. S. Sivakumar** Professor, Department of Applied Mechanics, IIT Madras, Chennai
	:	**Dr. K. Ramanjaneyulu** Chief Scientist, CSIR-Structural Engineering Research Centre, Chennai